Constant Modulus Based Blind Adaptive Multiuser Detection

James Bruce Whitehead

November 2004

Submitted in fulfilment of the academic requirements for the degree of PhD in the School of Electrical, Electronic, and Computer Engineering, University of KwaZulu-Natal.

Abstract

Signal processing techniques such as multiuser detection (MUD) have the capability of greatly enhancing the performance and capacity of future generation wireless communications systems. Blind adaptive MUD's have many favourable qualities and their application to DS-CDMA systems has attracted a lot of attention. The constant modulus algorithm is widely deployed in blind channel equalizations applications. The central premise of this thesis is that the constant modulus cost function is very suitable for the purposes of blind adaptive MUD for future generation wireless communications systems. To prove this point, the adaptive performance of blind (and non-blind) adaptive MUD's is derived analytically for all the schemes that can be made to fit the same generic structure as the constant modulus scheme. For the first time, both the relative and absolute performance levels of the different adaptive algorithms are computed, which gives insights into the performance levels of the different blind adaptive MUD schemes, and demonstrates the merit of the constant modulus based schemes. The adaptive performance of the blind adaptive MUD's is quantified using the excess mean square error (EMSE) as a metric, and is derived for the steady-state, tracking, and transient stages of the adaptive algorithms.

If constant modulus based MUD's are suitable for future generation wireless communications systems, then they should also be capable of suppressing multi-rate DS-CDMA interference and also demonstrate the ability to suppress narrow band interference (NBI) that arises in overlay systems. Multi-rate DS-CDMA provides the capability of transmitting at various bit rates and quality of service levels over the same air interface. Limited spectrum availability may lead to the implementation of overlay systems whereby wide-band CDMA signal are collocated with existing narrow band services. Both overlay systems and multi-rate DS-CDMA are important features of future generation wireless communications systems. The interference patterns generated by both multi-rate DS-CDMA and digital NBI are cyclostationary (or periodically time varying) and traditional MUD techniques do not take this into account and are thus suboptimal. Cyclic MUD's, although suboptimal, do however take the cyclostationarity of the interference into account, but to date there have been no cyclic MUD's based on the constant modulus cost function proposed.

This thesis thus derives novel, blind adaptive, cyclic MUD's based on the constant modulus cost function, for direct implementation on the FREquency SHift (FRESH) filter architecture. The FRESH architecture provides a modular and thus flexible implementation (in terms of computational complexity) of a periodically time varying filter. The operation of the blind adaptive MUD on these reduced complexity architectures is also explored. The robustness of the new cyclic MUD is proven via a rigorous mathematical proof. An alternate architecture to

the FRESH filter is the filter bank. Using the previously derived analytical framework for the adaptive performance of MUD's, the relative performance of the adaptive algorithms on the FRESH and filter bank architectures is examined. Prior to this thesis, no conclusions could be drawn as to which architecture would yield superior performance. The performance analysis of the adaptive algorithms is also extended in this thesis in order to consider the effects of timing jitter at the receiver, signature waveform mismatch, and other pertinent issues that arise in realistic implementation scenarios. Thus, through a careful analytical approach, which is verfied by computer simulation results, the suitability of constant modulus based MUD's is established in this thesis.

Acknowledgements

I wish to thank my supervisor, Prof. Takawira, for his valuable help and advice provided during my postgraduate studies. It is much appreciated.

Thanks are also owed to Telkom, Alcatel and the South African Department of Labour for providing financial support and equipment for the completion of this degree.

Thank you to my family for your support and encouragement.

Finally, I wish to thank Shelley for her time spent proof reading parts of this document. Her support and encouragement, is greatly appreciated.

Preface

The work presented in this thesis was performed by Mr. James Whitehead, under the supervision of Prof. F. Takawira, at the University of KwaZulu-Natal's School of Electrical, Electronic and Computer Engineering Centre for Radio Access Technologies, which is sponsored by Telkom SA and Alcatel.

This thesis has been presented in part by the student at the 2002, 2003, and 2004 Southern African Telecommunication Networks and Applications Conference (SATNAC'02, SATNAC'03, SATNAC'04), the 2004 IEEE International Conference on Communications (IEEE ICC'04), and the 2004 IEEE Africon conference. This thesis has also been published in part in the IEEE Transactions on Signal Processing.

This thesis is completely the student's own work, unless otherwise stated in the text. It has not been submitted in part, or in its entirety, to any other university.

The financial assistance of the Department of Labour (DoL) towards this research is hereby acknowledged. Opinions expressed and conclusions arrived at, are those of the author and are not necessarily to be attributed to the DoL.

Contents

List of Figures

List of Tables

List of Acronyms

2G	second generation
3G	third generation
4G	fourth generation
AAA	adaptive antenna array
AMPS	Advanced Mobile Phone Service
AWGN	additive white Gaussian noise
BER	bit error rate
CM	constant modulus
CMA	constant modulus algorithm
D-AMPS	digital AMPS
DD-LMS	decision directed LMS
DS-CDMA	direct sequence code division multiple access
EDGE	Enhanced Data Rates for Global Evolution
EMSE	excess mean square error
FDMA	frequency division multiple access
FEC	forward error correction
FIR	finite impulse response
FRESH	frequency shift
FSR	Fourier series representation
GPRS	General Packet Radio Services
GSM	Global System for Mobile Communications
HR	high rate
HSCSD	high-speed circuit switched data
i.i.d.	independent and identically distributed
IIR	infinite impulse response
IS-95	interim standard 95
ISI	intersymbol interference
kbs	kilobits per second
LCCMA	linearly constrained constant modulus algorithm
LCDCMA	linearly constrained differential constant modulus algorithm
LMS	least mean square
LR	low rate
MAI	multiple access interference
Mbps	megabits per second
MBER	minimum bit error rate
MC-CDMA	multicarrier CDMA
MIMO	multiple input multiple output
MMSE	minimum mean square error
MOE	minimum output energy
MSE	mean square error
MUD	multiuser detector/detection
NMT	Nordic Mobile Telephone
ODE	ordinary differential equation
OFDM	orthogonal frequency division multiplexing
PBE	perfectly blind equalizability
PDC	Personal Digital Cellular
PDF	probability distribution function

PIC	parallel interference canceller
PLL	phase locked loop
PTV	periodically time varying
QoS	quality of service
RF	radio frequency
RLS	recursive least squares
rms	root mean square
SGD	stochastic gradient descent
SIC	successive interference canceller
SINR	signal to interference plus noise ratio
SMS	short message service
SNR	signal to noise ratio
TACS	Total Access Communications System
TDMA	time division multiple access
VCR	variable chip rate
VCRFS	variable chip rate with frequency shift
VSL	variable spread length
W-CDMA	wideband CDMA

Mathematical Notation and Common Parameters

BOLD CAPITAL	matrix
bold	column vector
CAPITAL	constant
lower case	scalar (complex or real valued)
$(.)^*$	complex conjugate
$(.)^T$	transpose
$(.)^H$	Hermitian (or complex conjugate) transpose
$Z[.]$	z-transform
$*$	convolution
$\otimes$	Kronecker tensor product
$\mathrm{diag}(.)$	extracts the main diagonal of a matrix
$\mathrm{Tr}(.)$	trace of a matrix/ sum of diagonal elements
$E\{.\}$	expectation
$\not\equiv$	not identical with
$\lfloor . \rfloor$	floor operator
$\mathbf{I}_N$	identity matrix of dimension $N \times N$
$\mathbf{C}^x$	matrix $\mathbf{C}$ raised to the (matrix) power x
$\mathcal{O}(.)$	complexity order
$\perp$	orthogonality: if $\mathbf{x} \perp \mathbf{y}$, then $\mathbf{x}^T\mathbf{y} = 0$
$\lvert x \rvert$	absolute value of x
$\lVert \mathbf{x} \rVert$	Euclidean norm of vector: $\sqrt{\mathbf{x}^H\mathbf{x}}$
$\lVert \mathbf{x} \rVert_2^{\mathbf{A}}$	weighted squared Euclidian norm: $\mathbf{x}^H\mathbf{A}\mathbf{x}$ defined for positive definite Hermitian matrix $\mathbf{A}$
N	processing gain
K	number of users

Chapter 1

Introduction

Future generation wireless personal communications systems require advanced signal processing techniques to fully exploit the limited radio resources. The central premise of this thesis is that constant modulus based blind adaptive multiuser detectors provide low complexity, robust and reliable signal processing techniques for the enhancement of future generation personal communications systems that are based on DS-CDMA. These properties and capabilities are proved and expounded in this thesis via the derivation of novel algorithms as well as performance analyses which consider the constraints of realistic operating conditions. The rest of this chapter details some of the relevant characteristics of future generation wireless personal communications systems to better illustrate why such signal processing techniques are required, and why the analyses and algorithms presented in this thesis are significant.

1.1 Wireless personal communications systems

1.1.1 An evolution in performance, a revolution in uptake

First generation mobile cellular telephony systems were first introduced in the 1980's. The cellular concept breaks the coverage area into smaller cells and reuses frequency spectrum that is not used in adjacent cells. The cellular concept greatly enhanced system capacity and thereby made a cost effective use of available spectrum which in turn made wireless personal communications viable for the first time. First generation systems were based on analogue technology such as frequency division multiple access (FDMA) and predominantly only supported voice services. The most popular first generation standards were Advanced Mobile Phone Service (AMPS), Total Access Communications System (TACS), and Nordic Mobile Telephone (NMT). Each standard found favour in different parts of the world, a break down of which may be found in [1]. Without the dominance of a single standard, as well as a lack of interoperability between first generation standards, international roaming was not feasible during the era of first generation networks. First generation standards are still in use around the world but are being phased out as they offer relatively low spectral efficiencies and a poorer quality of service relative to modern standards, and are thus no longer in favour.

The move to second generation (2G) wireless personal communications systems is marked by the occurrence of digital technology. This move to digital technology enabled such techniques as forward error correction (FEC) to improve performance as well as the implementation of the multiple access techniques: time division multiple access (TDMA) and code division multiple access (CDMA), to greatly improve the spectral efficiency of 2G systems relative to the first

generation systems. The most popular 2G standard by far is the Global System for Mobile Communications (GSM), as it has captured 73% of the digital market and 72% of the wireless market, as shown in Table 1.1 and Table 1.2. Other 2G standards that exist are: digital AMPS (D-AMPS), CDMA IS-95, and Personal Digital Cellular (PDC). GSM arose out of the requirement to provide international roaming across Europe, but has been rapidly adopted all over the world. 2G standards are also marked by the emergence of data services, for example: the GSM network offers the short message service (SMS) and the ability to make data connections at either 9.6 or 14.4kbs.

The inception of GSM technology in 1992 saw the start of the global wave of the uptake of mobile telephony. In 2003 mobile subscribers outnumbered the number of fixed line connections in the world [2]. The steady refinement of this technology along with the size of the market for cellular telephony has made wireless personal communications almost ubiquitous. In February this year (2004) the total number of GSM subscribers exceeded 1 billion [3]. This is most impressive considering that the world's population is estimated at roughly 6 billion people. The GSM standard has also been adopted by more than 200 countries and territories [3].

Table 1.1. Wireless subscriber statistics (all figures in millions). Source: EMC world cellular database.

	Jan-03	Apr-03	Jul-03	Oct-03	Jan-04	Feb-04	Mar-04
Total digital subscribers	1123.7	1177.7	1232.8	1278.8	1388.0	1411.6	1440.0
Total analogue subscribers	28.1	25.1	23.2	20.7	19.0	18.3	16.5
Total wireless subscribers	1151.8	1202.8	1256.0	1299.5	1407.0	1429.9	1456.5

Table 1.2. Breakdown of Digital subscribers (all figures in millions). Source: EMC world cellular database.

	Jan-03	Apr-03	Jul-03	Oct-03	Jan-04	Feb-04	Mar-04
GSM	805.8	847.3	895.2	935.2	1006.5	1024.3	1046.8
W-CDMA	0.2	0.4	1.4	1.9	3.0	3.4	4.3
CDMA	148.3	157.9	162.3	174.1	190.2	194.4	199.1
PDC	60.3	61.7	62.3	62.5	62.0	62.2	62.4
US TDMA	108.4	110.4	112.2	109.2	109.4	110.2	111.2

As the market for mobile voice calls becomes saturated, growth is expected to come from mobile data applications which require broadband access [4]. In the future, it is expected that the most common method that will be used to access the internet will be wireless communications devices like the so called "smart phone". In fact, approximately half a billion GSM cellular telephones were manufactured in 2003 [5], and of those 10 million were "smart phones". Various additions to the 2G standards have been implemented to satisfy the growing wireless data market. These include high-speed circuit switched data (HSCSD), General Packet Radio Services (GPRS) and Enhanced Data Rates for Global Evolution (EDGE), and are generally referred to as 2.5G services.

This drive towards broadband wireless data has largely determined the characteristics of third generation (3G) systems that are either in development or are now being deployed around the world [6], [7]. Third generation wireless communications systems are therefore characterised by high data rates: typically 144-384kbps, and up to 2Mbps under ideal conditions. These high data rates lead to the requirement that 3G systems have even higher spectral efficiencies compared to 2G technologies. The air-interface for 3G systems is predominantly based on wideband code division multiple access (W-CDMA) [8], the steady uptake of which can be seen in Table 1.2, but still constitutes less than 0.3% of the number of total wireless subscribers. W-CDMA is therefore still just a niche market. Various other standards have been proposed that fall under the ITU's IMT-2000 umbrella of 3G standards, but the differences are largely determined by the state of a particular country's spectrum allocation and the requirement for backward compatibility to standards other than GSM, for example: CDMA2000 in the USA. This thesis is primarily concerned with technologies applicable to the DS-CDMA multiple access technique, such as W-CDMA. Further technological advances in this regard will advance the capabilities of 3G services making them even more cost effective and therefore enabling their widespread uptake.

Research has already begun on fourth generation (4G) wireless communications systems [9], [10]. These systems are characterised by even higher data rates, as can be seen in Table 1.3 where a comparison between the key parameters of 3G and 4G systems is made. 4G systems are expected to make use of multicarrier techniques such as orthogonal frequency division multiplexing (OFDM) or multicarrier (MC-) CDMA in the air interface to provide these high data rates. OFDM type signalling however suffers from a high peak-to-average power ratio and therefore does not make efficient use of the non-linear power amplifiers that are typically used in the RF stages of the mobile handsets. W-CDMA may thus still be used for quite some time in the uplink of future personal wireless communications systems. To achieve such high bandwidths economically, massive increases in spectral efficiencies are required. Some services may also have to be offered, or operate in, unregulated spectrum like the ISM band. These overlay systems thus need to combat the effects of narrow band interference (NBI).

Table 1.3. Key Parameters of 3G and 4 G Systems. Source: [11].

	3G	4G
Frequency band	1.8 - 2.5 GHz	2 - 8 GHz
Bandwidth	5 - 20 MHz	20 MHz
Data rate	Up to 2 Mbps (384 kbps deployed)	Up to 20 Mbps
Access	W-CDMA	MC-CDMA or OFDM (TDMA)
Forward error correction	Convolutional rate 1/2, 1/3	Concatenated coding scheme
Switching	Circuit/packet	Packet
Mobile top speeds	200 km/h	200 km/h

1.1.2 Enabling technologies for 3G and future generation systems

The characteristics of the communications channel and multiple access system need to be taken into account and exploited to the full to achieve the high spectral efficiencies necessary to ensure the viability of 3G and future generation wireless communications systems. There are many ways to improve the spectral efficiency, for example:

- Modulation format
- Coding
- Diversity techniques
    - Time (RAKE receiver)
    - Space (antenna array)
    - Frequency (multicarrier communications)

Advanced combinations of diversity and coding have already been proposed such as space-time trellis codes [12] that offer exceptional spectral efficiencies in terms of bps/Hz. Diversity techniques are chiefly employed to counteract the negative phenomena associated with the propagation medium, such as fading. Fading selectivity in the time, frequency, or space dimensions is actually a source of diversity that may be exploited.

The fundamental limitation, however, of CDMA communications systems is the amount of multiple access interference (MAI) that arises from the presence of other co-users. The near-far problem, whereby a single strong transmitter close to the receiver swamps out all the other weaker CDMA signals, is a serious design issue in DS-CDMA networks. NBI that arises in overlay systems similarly inhibits system performance. Suppressing these types of interference is the focus of this thesis. Two categories of techniques that exist for the suppression of MAI and NBI are:

- Adaptive antenna arrays (AAA)
- Multiuser detection (MUD)

AAA's have the capability to vary their sensitivity as a function of the angle of arrival of impinging signals. They suppress interference via various adaptive beamforming techniques which create nulls in the AAA response that correspond to the angle of arrival of interference sources. Multiuser detectors attempt to directly suppress the interference via exploiting the structure of the interference. Various combinations of AAA's and MUD's have also been proposed [13], [14], and these are referred to as space-time multiuser detectors (ST-MUD's).

MUD is the core topic of this thesis, as MUD has been identified as one of the enabling technologies for 3G and future generation personal wireless communications systems.

> *"Multiuser detection techniques are essential for achieving near-optimal performance in communications systems where signals conveying the desired information are received in the presence of ambient noise plus multiple-access interference. With the exploding interest from both the research community and industry in wireless code-division multiple-access (CDMA) systems, the application of multiuser detection techniques to wireless systems is becoming increasingly important."*
>
> —H. Vincent Poor
> *Guest Editorial for IEEE JSAC, Aug. 2001, Special Issue on:*
> *"Multiuser detection techniques with application to wired and wireless communications systems"*

1.2 The argument for constant modulus signal restoration

There is consensus within the research community that MUD is one of the enabling technologies for future generation wireless communications systems. However, any device, especially those situated in the mobile terminal, employed to enhance the performance or capacity of the radio link has to operate under constraints as there is: finite processing power, finite memory, and a finite power supply. If such a device is to be implemented then its performance levels should be both predictable and robust. The benefits of implementation must exceed the cost, and therefore high performance is expected from as low a complexity level as possible.

When considering the choice of interference suppression/MUD technique, the fundamental trade-off between performance and cost must thus be made. In this context, performance is defined as the gain in the number of users that can be accommodated simultaneously or the improvement of the bit error rate (BER) of the air interface. The cost is measured in terms of the system and algorithm complexity which directly translates to the cost of the hardware required. The plethora of MUD's that have been explicitly developed for DS-CDMA systems by numerous researches over the last 18 years span the full dynamic range of complexity: from the optimal detector of complexity order 2^K to the linear detector of complexity order N, where K is the number of users and N is the processing gain.

The performance margin between the optimal (in terms of BER) MUD and minimum mean square error (MMSE) linear MUD is not large in most systems of interest; however, the difference in complexity is so large that optimal MUD is not practical in all but the simplest of systems. Many non-linear MUD's that attempt to approach the optimal MUD performance level have been suggested. Non-linear MUD's have been proposed based on the following techniques: genetic algorithms [15], neural networks [16], probabilistic data association [17], and evolutionary programming [18] to name a few. These schemes generally still have a very high computational complexity compared to linear MUD and it is yet to be determined if the higher cost is worth the extra performance gain. The lack of analytical tools available to fully analyse their performance levels does not work in their favour either, as it is hard to prove the robustness of non-linear MUD schemes in general.

The parallel and successive interference cancelling structures (PIC and SIC) show promise [19] as they have a relatively lower computational complexity than the other non-linear techniques mentioned; however, they are true MUD's in the sense that all the interfering users need to be decoded in order for the algorithms to work. This is appropriate for base station receivers where all the users need to be received but is not desirable for single user receivers. Also, if there were significant intercellular interferers present (whose spreading codes were not known at the receiver) then the interference cancellation systems would fail. This phenomenon has been recognised and has prompted the development of group blind MUD's [20], where it is understood that at the receiver some interferers' spreading codes are known and other are not. Due to the non-linear nature of the algorithms involved in PIC and SIC, their analysis is difficult and thus performance and robustness is difficult to prove. Performance levels are generally explored via simulation.

The performance characteristics of linear MUD's have been extensively studied [21]. The two most widely studied linear MUD's are the MMSE and decorrelating detectors. These two detectors are related as they become equivalent at high signal to noise ratios (SNR's), but the MMSE detector avoids the noise enhancement problem of the decorrelating detector at lower SNR's, so the MMSE detector is always preferable. In addition to the MMSE and decorrelating detectors, there has recently been interest in linear minimum bit error rate (MBER) detectors [22]. The performance gain versus the extra system complexity is not clear at this point. Another advantage of linear MUD is that it may be implemented using a (linear transversal) adaptive filter, thus incurring a particularly low computational complexity. The convergence of most adaptive schemes can also be analysed to ensure some measures of robustness and stability. The MMSE receiver also has the ability to be implemented blindly, which is a very desirable quality, as it circumvents the need for pilot channels, thereby increasing the spectral efficiency, and also provides for procedural convenience. In this thesis, blind indicates that only the timing and spreading code information of the desired user is known at the receiver. It is concluded then, that linear blind adaptive multiuser detectors offer some of the best cost to performance ratios, and are therefore the focus of this thesis.

Blind adaptive MUD has rightly been extensively studied by numerous researchers (see [23] and [24] for a review). Seminal work in the field of blind adaptive MUD was presented in [25] where it was shown that by minimising the output energy of the adaptive filter subject to a linear constraint, the filter will always converge towards the MMSE receiver. This linear constraint is the spreading code, or signature sequence of the desired user, and is used to prevent the receiver from suppressing energy associated with the desired user, which would of course result in the failure of the receiver. This use of only the knowledge of the timing and spreading code of the desired user to perform blind adaptive MUD has led to the use of the terminology: code-aided or code-constrained blind adaptive MUD's.

This thesis's central premise is that the constant modulus algorithm (CMA) provides a very suitable cost function to perform code-aided blind adaptive MUD. The CMA was developed in the late 1970s and disclosed in 1980 in [26] as a technique to perform blind channel equalization. The CMA is now in widespread use:

> *"Just as the LMS algorithm has established itself as the workhorse for supervised linear adaptive filtering, the CMA has become the workhorse for blind channel equalization."*
>
> —S. Haykin
> *Unsupervised Adaptive Filtering, vol. II*

Such widespread use of the CMA is in no doubt due to the impressive performance of the algorithm relative to its computational complexity. The research community has recognized that the task of suppressing MAI is sufficiently similar to that of suppressing intersymbol interference (the task of blind channel equalization) that there has been a multitude of schemes proposed whereby the CMA is adapted to perform the task of blind adaptive MUD [27]–[48]. Such widespread use of the CMA in actual blind channel equalizer implementations also lends the algorithm much credibility as it has a proven implementation track record. The basic theory behind the operation of the CMA in the context of blind fractionally spaced equalizers (FSE) has been developed extensively over the last 20 years, and its operation in this context is now well understood. The most comprehensive and significant treatment of this theory is contained in [49].

The CMA falls into the Bussgang family of unsupervised (or blind) adaptive filters. Other algorithms that also fall into this category include the decision-directed least mean squares (DD-LMS) [50], and the Sato algorithm [51]. The CMA employs a stochastic gradient descent algorithm (SGD) to minimize a cost function that penalises any deviation of the received signal away from a constant modulus (CM). Any deviation in the received signal away from a CM is deemed to have come from intersymbol interference and thus restoring the CM property of the received signal removes the intersymbol interference and thus performs channel equalization. In the case of MUD, deviation from a CM is brought about by MAI, and so restoring the CM property is tantamount to suppressing MAI. The CMA only makes use of the higher order statistics of the received signal implicitly, as opposed to higher order statistical methods which do so explicitly and which also have a significantly higher computational complexity as a result.

For the reasons outlined above, it is concluded that blind adaptive MUD based on the constant modulus algorithm provides an excellent performance versus complexity trade off and is thus the focus of this thesis.

1.3 Problem formulation

The first problem that this thesis tackles is the performance of the SGD algorithm associated with constant modulus based blind adaptive MUD. The adaptive performance of the CMA has only been analysed in the context of the FSE application and under the limiting assumption of

the complete absence of additive noise. The analysis performed in this thesis, of the linearly constrained (LC-) CMA [27]–[30], [48] applied to blind adaptive MUD in a DS-CDMA communications system, is significantly different. DS-CDMA specific issues, such as the near-far problem and the (not insignificant) additive noise, are taken into account in this thesis. The task then is to quantify the adaptive performance of LCCMA in the steady-state, tracking, and transient phases of the adaptive algorithm. This is a worthwhile research problem as this information is vital for the effective implementation of the MUD. The analysis also enables the computation of the exact reduction in performance that the adaptive algorithm incurs relative to the optimal MMSE detector. No similar analyses exist for other blind adaptive MUD cost functions either, to the best of the author's knowledge. This thesis, therefore, also analyses the adaptive performance of alternate cost functions, yielding new results, and also enabling a comparative study between the cost functions. This comparative study is crucial to enable conclusions to be drawn about the suitability of the CMA applied to blind adaptive MUD.

It is put forward by this thesis that MUD's based on the constant modulus cost function are suitable for future generation PCS. They should therefore also be suitable for the suppression of periodically time varying (PTV) interference. There are, however, no schemes in existence that are based on the CMA that have been designed explicitly for the suppression of PTV interference. The problem therefore is to derive such schemes and quantify their performance. The good performance-versus-complexity characteristic of the new algorithms should be demonstrated via direct comparisons to existing blind adaptive MUD's that have been explicitly developed to suppress PTV interference sources. The reliability of these new algorithms needs to be ensured through a rigorous analytical proof of their convergence. The adaptive performance of these new algorithms may also be quantified using the analytical framework that was devised for the analysis of the LCCMA, as described above. PTV interference arises in 3G and future generation communications systems due to the heterogeneous nature of the services that will be offered over the same air-interface (e.g. voice or video). These different services require different data rates that are in turn made possible by multi-rate DS-CDMA [8]. The resulting MAI is PTV (or cyclostationary) and the effective suppression of this type of MAI is therefore a very important element necessary for the successful implementation of 3G and future generation personal communications systems. PTV interference suppression is also very important for the effective implementation of DS-CDMA overlay systems. Overlay systems have been proposed for situations where large contiguous blocks of free spectrum are not available, and therefore DS-CDMA communications systems are collocated with pre-existing narrow band services. The resulting narrow band interference (NBI) can be effectively suppressed if the PTV nature of the NBI is taken into account at the design stage of the MUD algorithm.

This thesis is concerned with the derivation of the adaptive performance of certain types of blind adaptive MUD's as this information is vital to their effective implementation. Aligned to

that research question is: what impact will channel effects and implementation issues have on the adaptive performance of these algorithms? Thus the effects of mismatch at the receiver between the nominal and received spreading code of the desired user, receiver timing jitter, asynchronous DS-CDMA transmissions, Rayleigh fading and other implementation issues are studied in the context of the adaptive algorithm performance. There exists no prior analytical work that takes into account the effects mentioned above, on the adaptive performance of the algorithms, and such work thus provides greater insight into the performance of blind adaptive MUD's.

1.4 Outline of thesis

In Chapter 1 a brief overview of the evolution of personal wireless communications systems was presented to illustrate what technological solutions will be required for the successful implementation of 3G and future generation communications systems. In this context, it was shown why blind adaptive MUD, based on the CMA, is an appropriate research topic. This led on to a discussion of the unsolved problems associated with CMA based MUD which this thesis tackles as well as the relevance and importance of solving these problems.

The performance analysis of the LCCMA is given in Chapter 2. The adaptive performance is quantified in the steady-state, tracking, and transient stages of the adaptive algorithm using the excess mean square error (EMSE) as a metric. This is achieved by using the *feedback approach* [52]–[54], and related technique given in [57], [58]. The feedback approach provides a unified approach to studying the performance of a class of adaptive algorithms. After a preliminary review of how the performance of adaptive filters is quantified, and the necessary elements of the feedback theory, the rest of the chapter is comprised of original work. The steady-state analysis of LCCMA is derived first and constitutes the first major original contribution of the thesis. Computer simulations are used to verify the accuracy of the analysis. The tracking and transient analyses are then carried out, the results of which also constitute an original contribution. The accuracy of these analyses is again demonstrated via computer simulation. Original formulas for the computation of the adaptive performance of the minimum output energy (MOE) [25], DD-LMS [50], LCCMA (CMA1-2), Sato [59], and LCDCMA [45] blind adaptive MUD's are also derived in this chapter. These new formulas are subsequently used in a study of the relative adaptive performance of these different MUD's. Using this study, Chapter 2 demonstrates the suitability of the CMA based MUD's.

The focus of Chapter 3 is the development and analysis of new cyclic MUD's based on the CMA. A preliminary discussion on cyclostationarity and then the link between two competing PTV filter implementations, the filter bank and the FREquency SHift (FRESH) filter, is shown. Multi-rate DS-CDMA systems are briefly reviewed and a model is presented based on a variable spread length scheme (VSL). The model has the added utility of being able to represent NBI. The optimal cyclic MMSE MUD's on the filter bank and FRESH architectures for such

systems are then presented. After this foundation has been established, the rest of the chapter is concerned with original work, starting with a novel investigation into the different suboptimal FRESH filtering schemes that are possible. The modifications to the LCCMA are then made in order for it to operate directly on the FRESH architecture. This new algorithm is referred to as FRESH-LCCMA. The proof of the global convergence of FRESH-LCCMA and suboptimal FRESH-LCCMA is then carried out. The adaptive performance of these algorithms is then analysed by making use of the methodology given in Chapter 2. For the first time, a direct comparison between the performance levels of the filter bank implementation and the FRESH filter implementation is possible. Following said comparison, the performance of the newly proposed algorithms is compared to existing cyclic MUD schemes. A new higher performance FRESH-LCCMA option is then presented which makes use of the recursive least squares (RLS) procedure instead of stochastic gradient techniques. Its higher performance comes with a higher computational complexity. However, this new algorithm vastly outperforms the recently proposed cyclic RLS-MOE algorithm [60] to which it has an equivalent computational complexity level.

In Chapter 4 the impact of realistic implementation and channel effects on the adaptive performance on the blind adaptive MUD's are considered. The effects of amplitude estimation error, mismatch, timing jitter at the receiver, Rayleigh fading, operation in an asynchronous DS-CDMA system, and the ability to suppress NBI with non-PTV techniques, are analysed. The accuracy of these analyses are confirmed via computer simulation and are once again used to show the applicability of the constant modulus cost function to blind adaptive MUD.

Concluding remarks are made in Chapter 5 together with a summary of the thesis, and several ideas for future work.

1.5 Original contribution

The major original contributions made by this thesis may be summarised as follows:-

- The steady-state, tracking and transient performance of code-constrained blind adaptive MUD's.
- The derivation of the optimal and suboptimal FRESH-LCCMA algorithms for PTV interference suppression and the associated proof of convergence.
- The performance analysis of blind adaptive MUD's considering mismatch and timing jitter at the receiver.
- The analytical performance comparison between the filter bank and FRESH implementations of PTV filters.

The following six publications have resulted from the work done in this thesis (with another two under review):

Accredited journals

J. Whitehead, F. Takawira, "Performance analysis of the linearly constrained constant modulus algorithm based multiuser detector," *Accepted for publication in the IEEE Trans. on Signal Process.*

Conference proceedings

J. Whitehead, F. Takawira, "Tracking and transient performance of code-constrained blind adaptive MUD's," *Proceedings of IEEE International Conference on Communications (ICC)*, Paris, France, vol. 5, pp. 2600–2605, June 2004.

J. Whitehead, F. Takawira, "Blind MUD of DS-CDMA using the linearly constrained constant modulus algorithm," *Proceedings of Southern African Telecommunication Networks and Applications Conference (SATNAC)*, Drakensberg, South Africa, pp. 115–119, Sept. 2002.

J. Whitehead, F. Takawira, "Convergence analysis of the LCCMA in an asynchronous DS-CDMA system," *Proceedings of Southern African Telecommunications Networks and Applications Conference (SATNAC)*, George, South Africa, Sept. 2003.

J. Whitehead, F. Takawira, "Code-aided blind adaptive cyclic multiuser detection," *Proceedings of South African Telecommunication Networks and Applications Conference (SATNAC)*, Spier Wine Estate, South Western Cape, South Africa, Sept. 2004.

J. Whitehead, F. Takawira, "Low complexity constant modulus based cyclic blind adaptive multiuser detection," *Proceedings of IEEE Africon Conference*, Gaborone, Botswana, vol. 1, pp. 115–120, Sept. 2004.

Under review (accredited journal and conference)

J. Whitehead, F. Takawira, "Constant modulus based cyclic blind adaptive multiuser detection," *Submitted to IEEE Trans. Veh. Technol.*

J. Whitehead, F. Takawira, "Blind adaptive multiuser detection for periodically time varying interference suppression," *Submitted to Proc. IEEE Wireless Communications and Networking Conference*, New Orleans, March 2005.

Chapter 2

Performance Analysis of the LCCMA

2.1 Introduction

It was established in Chapter 1 that the performance of personal wireless communications systems using direct sequence code division multiple access (DS-CDMA) can be greatly enhanced through the use of signal processing techniques, such as multiuser detection (MUD) [21]. This chapter's primary focus is on the performance analysis of blind adaptive MUD's that employ stochastic gradient descent (SGD) algorithms, and in particular the linearly constrained constant modulus algorithm (LCCMA), as it is an important blind adaptive MUD which is based on the constant modulus algorithm (CMA).

The performance of blind adaptive MUD's has to date mostly been quantified via the performance of their optimum tap weight vectors and through computer simulations, such as in [61] and [44]. The reduction in performance incurred by the adaptive algorithm measured in terms of convergence speed, tracking ability and steady-state performance has not (in general) been studied analytically in the open literature due to the difficulties associated with the analysis. The adaptive performance is quantified using the excess mean square error (EMSE) as a metric and it should be defined for the steady-state, tracking and transient modes of the adaptive algorithm. These aspects of adaptive algorithm performance are dealt with in more detail in Section 2.2.

The constant modulus algorithm (CMA) [26] has recently been applied to the blind adaptive MUD problem, where the various versions: linearly constrained (LC-) CMA [27], [30], multiuser (MU-) CMA [42], cross correlation (CC-) CMA [43], and linearly constrained differential (LCD-) CMA [45] have modified the CMA cost function to ensure that the desired user is captured. The CMA was originally intended for blind equalization applications that consider the problem of suppressing the intersymbol interference (ISI) associated with the reception of a single digital source. DS-CDMA communications systems, however, are characterised by the presence of multiple digital sources as there are generally multiple users transmitting at any one time. The conventional CMA could potentially lock onto any one of these digital sources and thus a mechanism is required to ensure the capture of a particular user, who is referred to as the desired user.

The performance analysis of LCCMA is the primary focus of this chapter because of its relative simplicity and proven resilience under mismatch conditions [27]. The LCCMA ensures the capture of the desired user through its knowledge of the spreading code of the desired user, and thus is a member of the code-aided or code-constrained family of blind adaptive MUD's. To

properly evaluate the performance of LCCMA, the other members of this family of MUD are also computed to enable a comparative study. These other algorithms include the LCDCMA, minimum output energy (MOE), and Sato cost functions. Other adaptive MUD's included for comparison are the least mean squares (LMS) and decision-directed (DD-) LMS. Global convergence in the mean of the LCCMA was proven in [30], but the adaptive performance was not considered therein. The actual tracking and steady-state performance analyses have largely been left undone due to the complexity of analyzing the time evolution of the weight error covariance matrix that arises from the non-linear update steps of the adaptive algorithms.

The theory of the operation of fractionally spaced equalizers (FSE's) based on the CMA is comprehensively treated in [49]. The adaptive performance of the CMA is dealt with in [49] in terms of convergence and the location of stationary points on the cost surface, the EMSE, and transient behaviour of the SGD algorithm when nearby a local minimum on the cost surface. Originally published in [62], the relationship between the minima of the CMA and those of the MMSE cost function is derived using the "exact analysis" which employs the Weierstrass maximum theorem [63] to define a region around the MMSE minimum in which a CMA minimum will be found. In so doing Godard's conjecture about the proximity of the CMA and MMSE minima is confirmed. This is an important point as noise is a significant issue in wireless communications systems, and the presence of noise violates one of the perfectly blind equalizability (PBE) conditions laid out in [49]. When one of the PBE conditions are violated, the constant modulus minima no longer correspond to the MMSE minimum, which in turn indicates that the constant modulus receiver no longer corresponds to the MMSE receiver. The "exact analysis" is thus important in the context of this thesis as it lends credibility to the approximation that the proximity of the CM and MMSE minima are such that they may be assumed to be the same.

The theory outlined to quantify the steady-state EMSE in [49], which was first published in [64], only considers the EMSE that arises from a non-CM source. This was achieved using an approximation of the weight error covariance matrix. The effects of noise and other PBE violations are not considered, as the authors of [49] conclude that a method of quantifying the EMSE of the CMA under arbitrary violations of the PBE conditions remains an open problem. Few studies exist on the transient behaviour of the CMA. In [65] (also outlined in [49]) the convergence behaviour of the CMA was analysed in the absence of noise and only applies for the close vicinity around a CMA minimum. The analysis approximates the operation of the SGD algorithm with an ordinary differential equation (ODE). Solutions to the ODE describe the trajectory of the adaptive algorithm. Mean convergence times were then computed using the gradient along the trajectory, where the exact gradient was approximated by the first term of its Taylor series expansion.

The feedback approach [52]–[56] is a relatively new technique to study the steady-state and tracking performance of adaptive algorithms. The feedback approach was explicitly applied to the steady-state analysis of FSE using CMA in [53] where it was shown to produce a far more accurate estimate of the steady-state EMSE compared to the technique published in [64]. The feedback approach also enables an extension of the steady-state analysis to include a non-stationary system, thereby computing the tracking performance. References [52]–[56] make some crucial approximations and assumptions: zero noise and that the EMSE is very small, in order to simplify the process of deriving the steady-state EMSE for the CMA. They therefore only consider the EMSE that arises from a non-CM source when using the CMA.

This chapter makes two major contributions, the first of which is the derivation of the steady-state and tracking performance of the LCCMA, using the feedback approach [52]–[56]. This chapter quantifies the actual performance with closed form expressions for both the EMSE and output signal to interference plus noise ratio (SINR) in the steady-state and tracking phases of the adaptive algorithm. Similar expressions for the EMSE of other blind adaptive MUD's do not exist in the literature to the best of the author's knowledge, with the exception of the steady-state EMSE of the MOE detector derived in [25]. This chapter derives a new more accurate expression of the EMSE of the MOE detector, and in a much simpler manner than was done in [25], through the use of the feedback approach. The emphasis of this chapter is on DS-CDMA specific issues which affect the adaptive performance of LCCMA. These issues are specifically the effect of multiple users and thus multiple access interference (MAI), as well as additive noise which can also be significant in wireless communications systems. Since only constant modulus signals are considered in this chapter, the results of [52]–[56] are not useful for comparative purposes, as they predict zero steady-state EMSE under these conditions.

The second major contribution is the transient analysis of the LCCMA. The transient behaviour is usually described in terms of a performance metric which makes use of the eigen-spread of the input covariance matrix [49], [65], [66]. This chapter shows that the exact time evolution of the output SINR can be predicted for the LCCMA and other SGD based blind adaptive MUD's, from initialization to steady-state. The transient analysis is performed using the technique presented in [58], where non-linear cost functions are explicitly considered. The transient analysis technique is based on the same energy conservation arguments first developed in [52]–[56], and is therefore related to the preceding steady-state and tracking analysis. The computation of the reduction in performance that the adaptive algorithm incurs relative to the optimal minimum mean square error (MMSE) receiver is thus possible, which this chapter shows may be significant.

This chapter is organized as follows: Section 2.2 explains the rationale behind the adaptive filter performance metrics, Section 2.3 outlines important energy conservation concepts from the feedback theory, and Section 2.4 presents the system model and the operation of the LCCMA.

The steady-state, tracking, and transient analyses of LCCMA are performed in Sections 2.5, 2.6, and 2.7 respectively. The steady-state, tracking and transient performance of various other blind adaptive MUD's are derived in Section 2.8 for comparative purposes. Results of the analyses are given in Section 2.9 where the suitability of constant modulus based blind adaptive MUD's is shown. A summary of the chapter as well as important contributions are highlighted in Section 2.10.

2.2 Quantifying the performance of adaptive filters

Digital filters with fixed coefficients are not suitable for situations when either the desired response of the filter is unknown or the desired response of the filter is time-varying. Adaptive filters, which are self designing, are necessary for these situations. Adaptive filters have been exploited for many diverse applications such as: echo cancellation, equalization of dispersive channels, system identification, signal enhancement, adaptive beamforming, noise cancelling, and control [67]–[69].

The basic operation of an adaptive filter is to adjust its filter coefficients such that its output tries to minimize some objective function. The objective function is chosen such that its minimum coincides with the optimal choice of filter coefficients. The objective function (also known as the cost function) may make use of a known reference signal (e.g. training symbols) or some known property of the received signal (e.g. constant modulus), in order to penalize any deviation in the output of the filter away from its optimal value. The technique used to minimize the cost function affects the computational complexity and speed of convergence of the adaptive filter. An adaptive filter is then essentially characterised by its cost function, the associated input arguments to the cost function, and the technique used to minimise the cost function.

This thesis is primarily concerned with the use of stochastic gradient descent (SGD) techniques for the minimisation of the cost functions and computing the relative effect that the different cost functions have on system performance. Reliability is an important aspect of an adaptive filter's performance. The reliability of an adaptive filter is guaranteed by an assurance that the adaptive filter will always converge towards the optimal choice of filter coefficients. This assurance is usually garnered from a rigorous mathematical proof of the convergence in the mean and the mean square sense of the adaptive filter. A robust adaptive filter should also remain stable for all possible inputs.

The performance of an adaptive filter may be quantified using numerous metrics or qualities which encompass various aspects of its operation, but they generally involve quantifying the inevitable trade-off between the *speed* and *quality* of adaptation. The accuracy of the adaptation can be measured by noting the deviation of the adaptive filter's coefficients from that of the optimal filter. A quantity, referred to as the mean square deviation (MSD), performs this task, however MSD is not measurable in practice, and other performance metrics are therefore

normally used. The most common objective function in adaptive filtering is the mean square error (MSE) where the error is defined as the difference between the desired response of the filter and the adaptive filter's output. The minimum mean square error (MMSE) would be observed if the optimal filter was used. When the adaptive filter is used the difference between the MMSE and the measured MSE is referred to as the excess MSE (EMSE). The ratio between the EMSE and the MMSE is referred to as the misadjustment. Since the MSE is more easily measured in real systems, the EMSE is the most common metric employed to quantify the quality of adaptation.

The three general modes of operation that an adaptive filter can find itself in are the steady-state, tracking, and transient modes. It is important to quantify the performance of the adaptive filter in all three of these modes:

Steady-state performance

A non-vanishing step size is usually employed in adaptive filters to enable it to track a time-varying channel, and also for stability reasons. This finite step size will usually cause a small jitter in the filter coefficients around their optimal value even after convergence has been achieved and the filter is operating in the steady-state mode. This usually small but not insignificant amount of jitter in the values of the adaptive filter's coefficients is quantified using the EMSE.

Tracking performance

In a non-stationary channel the adaptive filter must track a constantly time-varying set of optimal filter coefficients. The step size determines the tracking ability of the adaptive filter and trades-off tracking error with gradient approximation error (misadjustment). The EMSE is once again the most useful metric for quantifying the tracking performance of an adaptive filter as every cost function will have a unique minimum EMSE value attainable when using its optimal step size value. The algorithm with the lowest EMSE attainable in a non-stationary channel could be said to offer the best adaptive performance.

Transient performance

The transient performance of an adaptive algorithm is measured in terms of the convergence speed and final misadjustment level. Faster convergence is attainable by using a larger step size, however this is at the cost of higher misadjustment or EMSE at steady-state. The speed with which a particular adaptive algorithm can drive the EMSE below a particular threshold is a measure of the quality of that adaptive algorithm. Speed of convergence is usually predicted using a function of the eigen-spread of the covariance matrix of the input signal [67]. Recently however, techniques have been derived to quantify the exact time evolution of the EMSE from initialization through to steady-state [57], [58].

In the context of MUD, the computation of the EMSE is important as it enables the computation in the reduction in SINR that the adaptive filter incurs relative to the optimal MMSE filter using the relation,

$$\text{SINR} = \frac{\text{desired user's power}}{(\text{interference} + \text{noise power}) + \text{EMSE}} \tag{2.1}$$

The SINR is in turn a very important metric, especially in the case of linear MMSE MUD's, as it enables a very accurate estimate of the BER that a particular user is likely to experience [21]. The reduction in SINR and subsequent increase in the BER that the adaptive algorithm incurs relative to the MMSE receiver may not be insignificant as this thesis will show, and thus the derivation of the adaptive performance is very important to fully quantify the MUD's performance.

Other important metrics used to quantify the performance of MUD's are asymptotic multiuser efficiency, and near-far resistance. The asymptotic multiuser efficiency and near-far resistance of the adaptive filter will be the same as that of its optimal set of filter coefficients, for example the MMSE filter. These metrics have already been defined for the linear MMSE detector [21].

2.3 Feedback theory

2.3.1 Steady-state and tracking analysis

The *feedback approach* [52]–[56] provides a unified approach to studying the steady-state and tracking performance of any adaptive algorithm whose update step takes the form,

$$\mathbf{w}(i+1) = \mathbf{w}(i) + \mu \mathbf{u}(i) F_c(i) \tag{2.2}$$

where $\mathbf{w}(i)$ is the vector of filter coefficients at time step i, μ is a small constant referred to as the step size, $\mathbf{u}(i)$ is the regression or input vector, and $F_c(i)$ is the instantaneous error characteristic of the particular cost function under consideration. The EMSE is related to the error in the filter coefficients, $\Delta\mathbf{w}(i)$, via the *a priori* estimation error, defined as

$$e_a(i) \triangleq \Delta\mathbf{w}(i)^T \mathbf{u}(i) \tag{2.3}$$

where $\Delta\mathbf{w}(i) = \mathbf{w}_{opt} - \mathbf{w}(i)$, and $\mathbf{w}_{opt}$ is the optimum filter tap vector of the adaptive algorithm. The steady-state EMSE is then defined as

$$\zeta \triangleq \lim_{i\to\infty} E\{e_a^2(i)\}. \tag{2.4}$$

The feedback approach is based on an energy conservation relationship that holds exactly for any adaptive algorithm of the form (2.2). This relationship is given by,

$$\|\Delta\mathbf{w}(i+1)\|^2 + \frac{|e_a(i)|^2}{\|\mathbf{u}(i)\|^2} = \|\Delta\mathbf{w}(i)\|^2 + \frac{|e_p(i)|^2}{\|\mathbf{u}(i)\|^2} \tag{2.5}$$

where,

$$e_p(i) \triangleq \Delta\mathbf{w}(i+1)^T \mathbf{u}(i) \tag{2.6}$$

and is the *a posteriori* estimation error. It is shown [52]–[54] that $e_p(i)$ is related to $e_a(i)$ via the relation,

$$e_p(i) = e_a(i) - \mu\|\mathbf{u}(i)\|^2 F_e(i). \tag{2.7}$$

The feedback approach derives its name from the feedback loop which may be used to describe the lossless mapping from the left hand side of (2.5) to the right hand side of (2.5). This feedback loop is reproduced in Fig. 2.1 where $\mathcal{T}$ represents the mapping function, and the relationship in (2.7) has been used to relate $e_a(i)/\|\mathbf{u}(i)\|$ to $e_p(i)/\|\mathbf{u}(i)\|$ (this can be seen if one divides both sides of (2.7) by $\|\mathbf{u}(i)\|$). The feedback loop was first studied in [70]–[74] to enable a robustness and l_2-stability analysis of adaptive filters within a deterministic framework.

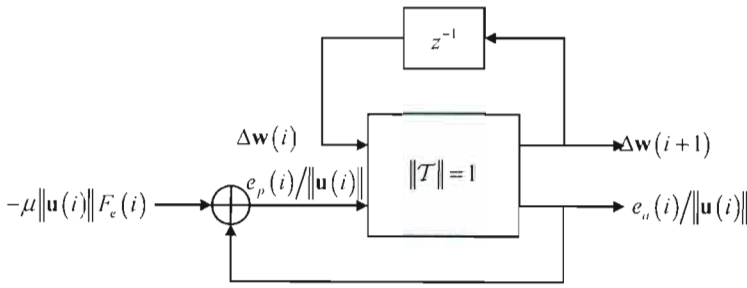

Fig. 2.1. The feedback loop relating left and right hand side of (2.5) by making use of (2.7), where z^{-1} denotes the unit delay operator. (Similar figures have appeared in [52] and [53].)

By taking the expectation of both sides of (2.5), expressing $e_p(i)$ using the right hand side of (2.7), and exploiting the fact that at steady-state,

$$E\left\{\|\Delta\mathbf{w}(i+1)\|^2\right\} = E\left\{\|\Delta\mathbf{w}(i)\|^2\right\} \tag{2.8}$$

it is possible (as shown in to [52]–[54]) to arrive at the *fundamental energy preserving equation*, given by

$$E\left\{\bar{\mu}(i)e_a^2\right\} = E\left\{\bar{\mu}(i)\left(e_a(i) - \frac{\mu}{\bar{\mu}(i)}F_e(i)\right)^2\right\} \tag{2.9}$$

where $\bar{\mu} = 1/\|\mathbf{u}\|^2$. Equation (2.9) is the major result of the feedback approach as it relates the *a priori* estimation error to the error function $F_e(i)$, and the driving vector, $\mathbf{u}$, once the algorithm has reached the steady-state. The steady-state EMSE is thus computed by directly solving (2.9) for $E\left\{e_a^2(i)\right\}$. This task is easier than conventional methods of computing the EMSE since the effect of the weight error vector has been removed.

The extension of the steady-state analysis presented above to include the effects of a non-stationary channel, in other words, to perform the tracking analysis, is detailed in [52] and [54].

2.3.2 Transient analysis

The transient analysis as described in [57], [58] computes the dynamical behaviour of the weight error vector by exploiting the weighted energy conservation relationship,

$$\left\|\Delta\mathbf{w}(i+1)\right\|_{\Sigma}^{2}+\frac{\left|e_{a}^{\Sigma}(i)\right|^{2}}{\left\|\mathbf{u}(i)\right\|_{\Sigma}^{2}}=\left\|\Delta\mathbf{w}(i)\right\|_{\Sigma}^{2}+\frac{\left|e_{p}^{\Sigma}(i)\right|^{2}}{\left\|\mathbf{u}(i)\right\|_{\Sigma}^{2}} \tag{2.10}$$

which corresponds to the same relationship as (2.5) if $\mathbf{\Sigma}=\mathbf{I}$. In the above equation the weighted norm notation has been used where $\left\|\mathbf{w}\right\|_{\Sigma}^{2}$ is used to indicate the weighted squared Euclidian norm $\mathbf{w}^{H}\mathbf{\Sigma}\mathbf{w}$, where $\mathbf{\Sigma}$ is some symmetric positive definite weighting matrix. In a similar fashion to [52]–[54], the expected value of both sides of (2.10) is taken, where the substitution,

$$e_{p}^{\Sigma}(i)=e_{a}^{\Sigma}(i)-\mu\left\|\mathbf{u}(i)\right\|_{\Sigma}^{2}F_{e}(i) \tag{2.11}$$

is made. It is then shown in [58] how the resulting expression may be simplified to arrive at the recursive formula that describes the time evolution of the weighted weight error variance $E\left\{\left\|\Delta\mathbf{w}(i)\right\|_{\Sigma}^{2}\right\}$:

$$\begin{aligned}E\left\{\left\|\Delta\mathbf{w}(i)\right\|_{\Sigma}^{2}\right\}=E\left\{\left\|\Delta\mathbf{w}(i-1)\right\|_{\Sigma}^{2}\right\}-2\mu h_{G}\left(E\left\{\left\|\Delta\mathbf{w}(i-1)\right\|_{\mathbf{R}}^{2}\right\}\right)\left(E\left\{\left\|\Delta\mathbf{w}(i-1)\right\|_{\Sigma\mathbf{R}}^{2}\right\}\right)\\+\mu^{2}E\left\{\left\|\mathbf{u}(i)\right\|_{\Sigma}^{2}\right\}h_{U}\left(E\left\{\left\|\Delta\mathbf{w}(i-1)\right\|_{\mathbf{R}}^{2}\right\}\right)\end{aligned} \tag{2.12}$$

where

$$h_{G}\triangleq\frac{E\left\{e_{a}(i)F_{e}(i)\right\}}{E\left\{e_{a}^{2}(i)\right\}}\qquad\qquad h_{U}\triangleq E\left\{F_{e}^{2}(i)\right\} \tag{2.13}$$

and

$$\mathbf{R}=E\left\{\mathbf{u}(i)\mathbf{u}^{H}(i)\right\}. \tag{2.14}$$

It is noted at this point that in both [57] and [58] the function $F_{e}(i)$ was constrained to be a scalar function of $\mathbf{u}(i)$ and the error $e(i)$ term where

$$e(i)\triangleq d(i)-\mathbf{w}^{T}(i)\mathbf{u}(i) \tag{2.15}$$

and $d(i)$ is the desired output of the filter. This constraint is relaxed in this thesis since blind algorithms are the focus, and blind indicates that $d(i)$ is not available at the receiver, and therefore $e(i)$ is not computable at the receiver either.

Equation (2.12) together with the recursive technique that is used to solve it, are the major contributions of [58]. The steady-state performance is also computed in [58] by noting that in steady-state,

$$\lim_{i\to\infty}E\left\{\left\|\Delta\mathbf{w}(i+1)_{\Sigma}^{2}\right\|\right\}=\lim_{i\to\infty}E\left\{\left\|\Delta\mathbf{w}(i)_{\Sigma}^{2}\right\|\right\} \tag{2.16}$$

and so (2.12) may be simplified by removing the effect of weight error vector from each side. It is then shown in [58] that the steady-state EMSE, denoted by ζ, is a fixed point of the function

$$\zeta = \tfrac{\mu}{2}\mathrm{Tr}(\mathbf{R})\frac{E\{F_c^2(i)\}\zeta}{E\{e_a(i)F_c(i)\}}. \tag{2.17}$$

It is shown below that this formula is the same result arrived at in [52]–[54] through simplifying (2.9):

$$E\{\bar{\mu}(i)e_a^2(i)\} = E\left\{\bar{\mu}(i)\left(e_a(i)-\frac{\mu}{\bar{\mu}(i)}F_c(i)\right)^2\right\}$$

$$\mathrm{Tr}(\mathbf{R})E\{e_a^2(i)\} = \mathrm{Tr}(\mathbf{R})E\{e_a^2(i)\} - 2E\left\{\bar{\mu}(i)e_a(i)\frac{\mu}{\bar{\mu}(i)}F_c(i)\right\} + \mu^2\mathrm{Tr}(\mathbf{R})E\{F_c^2(i)\} \tag{2.18}$$

$$E\{e_a(i)F_c(i)\} = \tfrac{\mu}{2}\mathrm{Tr}(\mathbf{R})E\{F_c^2(i)\}$$

and then manipulating (2.17):

$$\zeta = \tfrac{\mu}{2}\mathrm{Tr}(\mathbf{R})\frac{E\{F_c^2(i)\}\zeta}{E\{e_a(i)F_c(i)\}}$$

$$1 = \tfrac{\mu}{2}\mathrm{Tr}(\mathbf{R})\frac{E\{F_c^2(i)\}}{E\{e_a(i)F_c(i)\}} \tag{2.19}$$

$$E\{e_a(i)F_c(i)\} = \tfrac{\mu}{2}\mathrm{Tr}(\mathbf{R})E\{F_c^2(i)\}.$$

It was not detailed in [57] and [58] how the relation in (2.12) is extended to include the effects of a non-stationary channel.

2.4 System model

2.4.1 Transmitter and receiver models

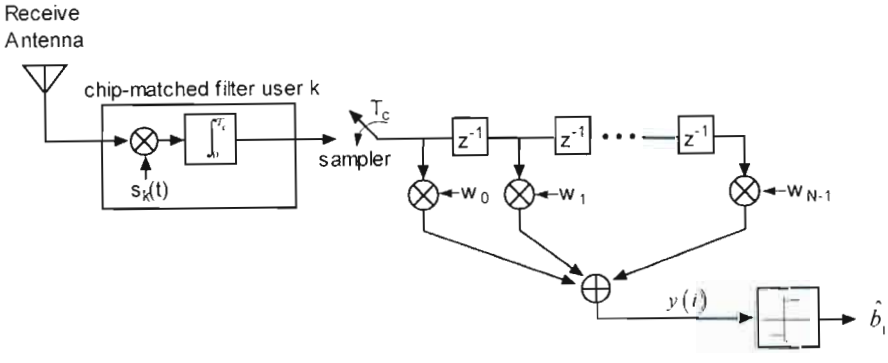

Fig. 2.2. Receiver Model.

A synchronous DS-CDMA transmitter model for the uplink of a mobile radio network is considered. The synchronous system provides ease of notation and applies without loss of generality for an asynchronous system [21].

The received signal is passed through a chip-matched filter and sampled at the chip-rate. These samples are concatenated into a length N vector of received samples:

$$\mathbf{r}(i) = \mathbf{SAb}(i) + \mathbf{n}(i) \tag{2.20}$$

where

$\mathbf{s}_k = \left[c_k(1),\ldots,c_k(N)\right]^T$,

$\mathbf{b}(i) = \left[b_1(i),\ldots,b_K(i)\right]^T$,

$\mathbf{S} = \left[\mathbf{s}_1,\ldots,\mathbf{s}_K\right]^T$,

$\mathbf{A} = \mathrm{diag}\left(\left[A_1,\ldots,A_K\right]\right)$,

and A_k, $\mathbf{s}_k$ denote the amplitude and normalised spreading waveform of the kth user respectively. The transmitted symbols $b_k(i)$, at time index i, take on the values $\{+1,-1\}$ with equal probability and have a constant modulus; diag(.) constructs a diagonal matrix. The additive white Gaussian noise (AWGN) vector $\mathbf{n}(i)$ has covariance matrix $\sigma^2\mathbf{I}_N$. The vector $\mathbf{r}(i)$ is filtered by a finite impulse response (FIR) filter structure, whose coefficients form the vector $\mathbf{w}(i) = \left[w_1(i),\ldots,w_N(i)\right]^T$. Without loss of generality, the desired user from here on will be user 1. The output of the filter, which constitutes the decision statistic, is given by

$$y(i) = \mathbf{w}(i)^T\,\mathbf{r}(i). \tag{2.21}$$

This receiver structure is depicted in Fig. 2.2 where $\hat{b}_1(i) = \mathrm{sign}\left(y(i)\right)$ and represents the output of the hard decision device which is the receiver's guess at the value of the desired user's transmitted bit.

2.4.2 LCCMA

The canonically constrained LCCMA is based on the CMA2-2 algorithm [26], and attempts to minimize the cost function,

$$J\left(\mathbf{w}(i)\right) = E\left\{\left(\left(\mathbf{w}(i)^T\,\mathbf{r}(i)\right)^2 - R_2\right)^2\right\} \tag{2.22}$$

subject to the linear (canonical) constraint $\mathbf{w}^T\mathbf{s}_1 = 1$, where R_2 is the dispersion factor defined as $E\left\{(A_1b_1)^4\right\}/E\left\{(A_1b_1)^2\right\}$ which is equal to A_1^2 in this case. The LCCMA uses its estimate of the desired user's signature sequence, $\mathbf{s}_1$, to prevent the capture of unwanted users. The cost function, as it stands, is not amenable to conventional stochastic gradient techniques due to the constraint, but by making use of the canonical representation of the MMSE filter [25] it is possible to split the filter coefficients into two orthogonal components: a fixed (or non-adaptive) part, and an adaptive part, given by

$$\mathbf{w}(i) = \mathbf{s}_1 + \mathbf{w}_\perp(i). \tag{2.23}$$

The filter component orthogonal to the spreading code, $\mathbf{w}_\perp$, is adapted without constraint. The update step of the adaptive algorithm is given by,

$$\mathbf{w}_\perp(i+1) = \mathbf{w}_\perp(i) + \mu y(i)\left(R_2 - \left|y(i)\right|^2\right)\mathbf{r}_\perp(i) \tag{2.24}$$

Table 2.1.Outline of LCCMA Algorithm.

Parameters:	
$\mathbf{r}(i)$	received (input) signal
$\mathbf{w}(i)$	filter coefficients
$\mathbf{s}_1$	signature sequence of desired user
R_2	dispersion factor
Initialisation:	
$i=1$	time index
$\mathbf{w}_\perp(1)=\mathbf{0}$	adaptive part of filter coefficients
For n = 1, 2, 3..., compute:	
$\mathbf{w}=\mathbf{s}_1+\mathbf{w}_\perp(i)$	filter coefficients
$y(i)=\mathbf{w}^T(i)\mathbf{r}(i)$	output of filter
$F_c(i)=y(i)\left(R_2-\lvert y(i)\rvert^2\right)$	error term
$y_{MF}=\mathbf{s}_1^T\mathbf{r}(i)$	(bit-) matched filter output
$\mathbf{r}_\perp(i)=\mathbf{r}(i)-y_{MF}\mathbf{s}_1$	component of $\mathbf{r}(i)\perp\mathbf{s}_1$
$\mathbf{w}_\perp(i+1)=\mathbf{w}_\perp(i)+\mu F_c(i)\mathbf{r}_\perp(i)$	new adaptive component of filter coefficients

where μ is a small positive constant (step size). The orthogonal projection of the received vector,

$$\mathbf{r}_\perp(i)=\mathbf{r}(i)-\mathbf{s}_1^T\mathbf{r}(i)\mathbf{s}_1, \tag{2.25}$$

is used in (2.24) to ensure that $\mathbf{w}_\perp$ remains orthogonal to $\mathbf{s}_1$, this in turn ensures that the constraint, $\mathbf{w}^T\mathbf{s}_1=1$ is always met. An outline of LCCMA is given in Table 2.1.

The non-canonically constrained LCCMA was proposed in [31] and further analysed in [30]. This variation sets $R_2=1$ and the filter coefficients are decomposed into

$$\mathbf{w}(i)=d\mathbf{s}_1+\mathbf{w}_\perp(i). \tag{2.26}$$

subject to the linear constraint $\mathbf{w}^T\mathbf{s}_1=d$, and has the stability constraint $3d^2A_1^2-1\geq 0$. It is important to note that the cost functions of the non-canonically constrained LCCMA and canonically constrained LCCMA are equivalent when $d=1/A_1$, [37]. Stability garnered by varying d in the non-canonically constrained case can equivalently be achieved by varying R_2 in the canonically constrained case.

The EMSE analysis performed in this thesis relies on the assumption that the LCCMA converges to within a positive scalar multiple of the actual MMSE filter. This assumption makes the analysis tractable, as well as enables the assumption that the residual MAI at the output of the LCCMA receiver has a Gaussian distribution [75]. It is reasonable to assume convergence to the (scaled) MMSE receiver as is further explained in this section. It was conjectured (with strong arguments) in [30] that by properly selecting d, the LCCMA cost function is convex in

the presence of AWGN. Godard conjectured in [26] that the optimal CMA minima roughly correspond to the MMSE minima; this has been thoroughly scrutinized in [62], and shown to hold well under the constraint imposed on d, A_1. As only one LCCMA minimum exists, then that minimum very closely approximates the actual MMSE solution (simulation results to date support this conjecture). Since the LCCMA filter is anchored by $\mathbf{s}_1$, and thus assuming convergence to the (scaled) MMSE receiver, the LCCMA solution is the same as the MOE receiver [25], and is given by:

$$\mathbf{w}_{opt} = \frac{\mathbf{C}^{-1}\mathbf{s}_1}{\mathbf{s}_1^T\mathbf{C}^{-1}\mathbf{s}_1} \tag{2.27}$$

$$\mathbf{C} = E\left\{\mathbf{r}(i)\mathbf{r}^T(i)\right\} = \mathbf{S}\mathbf{A}\mathbf{A}^T\mathbf{S}^T + \sigma^2\mathbf{I}. \tag{2.28}$$

The optimal non-canonically constrained LCCMA filter $\mathbf{w}_{opt,N}$ is related to optimal canonical filter via

$$\mathbf{w}_{opt,N} = (1/A_1)\mathbf{w}_{opt}. \tag{2.29}$$

The canonical and non-canonical formulations have different tracking performances, as will be investigated in Section 2.6.2, and thus their distinction is made.

2.5 Steady-state analysis

EMSE arises due to the presence of MAI and AWGN, as the MMSE receiver can never completely suppress MAI when there is additive noise present. The adaptive algorithm's finite step size thus continuously perturbs the filter coefficients around their mean, even when convergence has been achieved. If the AWGN was discounted in this thesis, then the LCCMA would converge towards the decorrelating detector. There would then be zero residual MAI at the output of the receiver, and thus the EMSE would be zero as predicted in [54] and [53], as only constant modulus data is considered in this thesis. The zero noise assumption made by previous researchers is stressed here, as AWGN is not insignificant in wireless communications systems and the resulting EMSE can be very significant, which this section proves.

2.5.1 Solving the energy preserving equation

The first contribution of this thesis is the derivation of steady-state EMSE expressions for the canonically constrained LCCMA using the fundamental energy preserving equation in (2.9). This derivation differs from the work done in [53] and [54] as those papers did not consider the effects of AWGN on the constant modulus cost function. The system model also differs from that in this thesis as a DS-CDMA system model that has multiple users is introduced in this thesis, and thus MAI affects the dynamics of the adaptive algorithm. The orthogonal projection operation and the combination of adaptive and non-adaptive filter components also differentiate LCCMA from CMA.

The first step is to compare the update step of the LCCMA in (2.24) to the general formula in (2.2). Clearly the LCCMA has the correct general structure. Its error function is given by

$$F_e(i) = y(i)\left(\left(y(i)\right)^2 - R_2\right) \tag{2.30}$$

and the driving vector is $\mathbf{r}_\perp$, so $\bar{\mu} = 1/\|\mathbf{r}_\perp\|^2$. The next step is to express $F_e(i)$ in terms of the *a priori* estimation error, $e_a(i)$. This is achieved by expressing the output of the filter in terms of the optimal filter output $\mathbf{w}_{opt}$ (given in (2.27)) and the definition of $e_a(i)$ (see section 2.3):

$$\begin{aligned} y(i) &= \left(\mathbf{w}_{opt} - \Delta\mathbf{w}(i)\right)^T \mathbf{r}(i) \\ &= \mathbf{w}_{opt}^T \mathbf{r}(i) - e_a(i) \\ &= A_1 b_1 + M(i) + v(i) - e_a(i) \end{aligned} \tag{2.31}$$

where $M(i) = \sum_{k=2}^{K} \mathbf{w}_{opt}^T \left(A_k b_k(i)\mathbf{s}_k\right)$ is the residual MAI at the output of the optimum filter, and $v(i) = \mathbf{w}_{opt}^T \mathbf{n}(i)$ is the filtered AWGN. This expression for $y(i)$ can now be substituted into (2.30), which can in turn be substituted into the fundamental energy preserving equation (2.9), which can be directly solved for the steady-state EMSE, ζ. This task can be greatly simplified by making use of some of the properties, assumptions, and simplifications of the random variables $\{b_1(i), M(i), v(i), e_a(i)\}$. From here onwards, time index (i) will be dropped for ease of notation.

Properties:

Firstly, $\{b_1, M, v, e_a\}$ are zero-mean random variables, and $\{b_1, M, v\}$ are mutually independent. It is also known that e_a and b_1 are independent, since the adaptive algorithm is adapted in the space orthogonal to $\mathbf{s}_1$, which is the space that contains the energy from b_1, also $E\{b_k^{2m}\} = 1$, for any positive integer m.

The filtered noise term v is a Gaussian random variable.

Approximations:

The residual MAI, M, is Gaussian. This is a well studied approximation, and has been shown to hold well [21], [75].

The *a priori* estimation error is Gaussian. This is confirmed via simulation; its Gaussianity is understandable considering central limit theorem arguments: there are a number of independent random sources that constitute the MAI, there is AWGN present, and the filter length is long (of the order of the spreading code).

Assumptions:

i. In steady-state $\|\mathbf{r}_\perp\|^2$ and F_e^2 are uncorrelated. This assumption was made in [54], and becomes more accurate as the length of the filter increases, and thus applies in this case.

ii. The noise sequence v is independent of regressor sequence $\mathbf{r}_\perp$ [54]. This assumption forces e_a and v to be independent since: $E\{e_a v\} = E\{\Delta\mathbf{w}^T\mathbf{r}_\perp\}E\{v\} = 0$ and v is a zero mean random variable. This, often realistic, assumption that the noise sequence is independent of the regressor sequence has been well studied (see e.g. [67]).

iii. M is independent of e_a in the steady-state. This is analogous to the assumption that a blind equalizer operates independently of the transmitted signals [53]; it may not hold in general, but leads to a good fit between the theoretical and simulation results.

2.5.2 Simplifying the energy preserving equation

Expanding the right hand side of (2.9), the energy preserving equation may be simplified to

$$2\mu E\{e_a F_c\} = \mu^2 \mathrm{E}\left\{\frac{F_c^2}{\bar{\mu}}\right\}. \tag{2.32}$$

Using assumption (i) this may be further simplified to,

$$E\{e_a F_c\} = T.E\{F_c^2\} \tag{2.33}$$

where $T = \frac{\mu}{2}\mathrm{Tr}(\mathbf{C}_\perp)$, and $E\{1/\bar{\mu}\} = E\left\{\|\mathbf{r}_\perp(i)\|^2\right\} = \mathrm{Tr}(\mathbf{C}_\perp)$, and $\mathbf{C}_\perp$ is the covariance matrix of the driving vector, $\mathbf{r}_\perp$. Equation (2.33) may now be expanded using (2.30) and the new definition of y given in (2.31). As a direct result of assumptions (ii) and (iii), the random variables $\{b_1, M, v, e_a\}$ are now mutually independent, which in turn causes any term with an odd power of $\{b_1, M, v, e_a\}$ to drop out of this new expression, after applying the expectation operation. This new expression for the energy preserving equation is given in (2.34),

$$J_2 E\left\{(e_a)^2\right\}^2 + J_1 E\left\{(e_a)^2\right\} = T.\left(K_3 E\left\{(e_a)^2\right\}^3 + K_2 E\left\{(e_a)^2\right\}^2 + K_1 E\left\{(e_a)^2\right\} + K_0\right) \tag{2.34}$$

where the Gaussian approximation for e_a has been used. The coefficients $\{J_2, J_1, K_3, K_2, K_1, K_0\}$ are given in Table 2.2. (The Gaussian approximation for e_a relates the higher order moments of e_a to the second moment of e_a via the Gaussian moment generating function.) The energy preserving equation is now a third order polynomial function of $E\{e_a^2\}$, or equivalently ζ. This new function has deterministic coefficients (Table 2.2), and is thus now trivial to solve for the EMSE, ζ.

The noise term at the output of the filter is a Gaussian random variable of type $v \sim \mathcal{N}(0, \sigma_n)$ where $\sigma_n = \|\mathbf{w}_{opt}\|\sigma$. When the power levels of all the interfering users are equal then a valid approximation is that $M \sim \mathcal{N}(0, \eta)$ where $\eta = \sqrt{K-1}\mathbf{w}_{opt}^T(A_k\mathbf{s}_k)$ for $k \neq 1$. Also,

$$\mathrm{Tr}(\mathbf{C}_\perp) = \sum_{k=2}^{K} A_k^2\left(1-\rho_{1k}^2\right) + \sigma^2(N-1) \tag{2.35}$$

Table 2.2. Coefficients for LCCMA EMSE Expressions.

Coefficient	Value
J_2	3
J_1	$3\sigma_n^2 + 3\eta^2 + 3A_1^2 - R_2$
K_3	15
K_2	$45\sigma_n^2 + 45\eta^2 + 45A_1^2 - 6R_2$
K_1	$90A_1^2\eta^2 + 45\eta^4 - 12R_2\eta^2 + 90\eta^2\sigma_n^2 + 90A_1^2\sigma_n^2 - 12R_2A_1^2 + 45\sigma_n^4 + 15A_1^4 - 12R_2\sigma_n^2 + R_2^2$
K_0	$90A_1^2\eta^2\sigma_n^2 - 12A_1^2R_2\eta^2 + 15\eta^6 + 15\sigma_n^6 - 12A_1^2R_2\sigma_n^2 + 15A_1^4\eta^2 + 15A_1^4\sigma_n^2 + A_1^2R_2^2 + 45A_1^2\eta^4 + 45A_1^2\sigma_n^4$ $-2A_1^4R_2 - 12\eta^2R_2\sigma_n^2 + A_1^6 + 45\eta^4\sigma_n^2 + \eta^2R_2^2 - 6\eta^6R_2 + 45\eta^2\sigma_n^4 + \sigma_n^2R_2^2 - 6\sigma_n^4R_2$

Filtered noise variance: $\sigma_n^2 = E\{v^2\}$, Residual MAI variance: $\eta^2 = E\{M^2\}$.

where $\rho_{1k} = \mathbf{s}_1^T\mathbf{s}_k$.

2.5.3 Further simplifications

The higher powers of ζ may be neglected in (2.34), if it is assumed that ζ is very small. A first order approximation for (2.34) then describes the EMSE, and is given by

$$\zeta_1^{LCCMA} = \frac{T.K_0}{J_1 - TK_1}. \tag{2.36}$$

This expression is expanded fully in (2.37), where the substitution $A_1 = R_2 = 1$ has been made.

$$\zeta_1^{LCCMA} = T\left(\frac{15\sigma_n^6 + 45\eta^2\sigma_n^4 + 39\sigma_n^4 + 78\eta^2\sigma_n^2 + 4\sigma_n^2 + 45\eta^4\sigma_n^2 + 4\eta^2 + 39\eta^4 + 15\eta^6}{3\sigma_n^2 + 2 + 3\eta^2 - T\left(4 + 78\sigma_n^2 + 78\eta^2 + 45\sigma_n^4 + 45\eta^4 + 90\eta^2\sigma_n^2\right)}\right) \tag{2.37}$$

In DS-CDMA communications systems the combination of MAI, and the possibility of lower SNR's could cause a significant level of EMSE. Employing a large step-size to increase tracking and convergence performance also increases the EMSE level. These conditions limit the accuracy of the first order solution and therefore the full (third order) solution is also considered in this chapter. It is the Gaussian assumption for e_a, that enables the higher order moments of e_a to be considered in this thesis, in contrast to [52]–[54] which do not consider them when analysing CMA. These higher moments are considered by [58], although in a non-CMA context. The roots of the higher order polynomial of ζ are trivial to compute using Table 2.2 and are omitted for brevity. Simulations show that when more than one root exists, only the smallest positive root is of interest. Also note, that studying the steady-state behaviour of the non-canonically constrained LCCMA as a function d can be equivalently studied by the canonical case by varying R_2.

The coefficients of Table 2.2 can be greatly simplified if the substitution is made: $A_1 = 1$, and $R_2 = 1$. In most cases the residual MAI power η^2 at the output is significantly lower than the output noise power σ_n^2, and thus an even simpler expression can be derived if all the terms that contain η are removed. The simplified first order solution is then given by

$$\zeta_1^{LCCMA} = \frac{T\left(4\sigma_n^2 + 39\sigma_n^4 + 15\sigma_n^6\right)}{2 + 3\sigma_n^2 - T\left(4 + 78\sigma_n^2 + 45\sigma_n^4\right)}. \tag{2.38}$$

The accuracy of this approximation is analysed via simulation. This is not to say that the MAI is not important, as the amount of MAI determines the exact value of the filter coefficients which in turn affect σ_n.

2.5.4 Validation of steady-state analysis

A computer simulation is used to validate the accuracy of the preceding steady-state analysis. All the results were generated using length 31 Gold codes. The MAI ratio is defined as A_k/A_1, $k \neq 1$, where all the interfering users transmit at the same amplitude. The EMSE was obtained from Monte Carlo simulations of the received vector of samples in (2.20) and implementing the LCCMA as given in (2.24). Once the algorithm had reached steady-state the EMSE was calculated as the mean square value of $e_a \triangleq \Delta\mathbf{w}^T\mathbf{r}$ over 100000 transmitted bits. The third order, or full solution, in the steady-state results is computed as the smallest positive root of (2.34).

The first aspect of the analysis that is tested is the Gaussian approximation that is used for the *a priori* estimation error. A histogram of e_a from a simulation of the LCCMA operating in the steady-state, is plotted in Fig. 2.3. A sample size of 60000 was used. A situation is considered where there is a 20dB SNR, MAI level of 0dB's, and there are 20 users in the system (66% loading). The Gaussian probability distribution function (PDF), having the same variance as the histogram data, is superimposed. The validity of the Gaussian approximation of e_a is clearly evident.

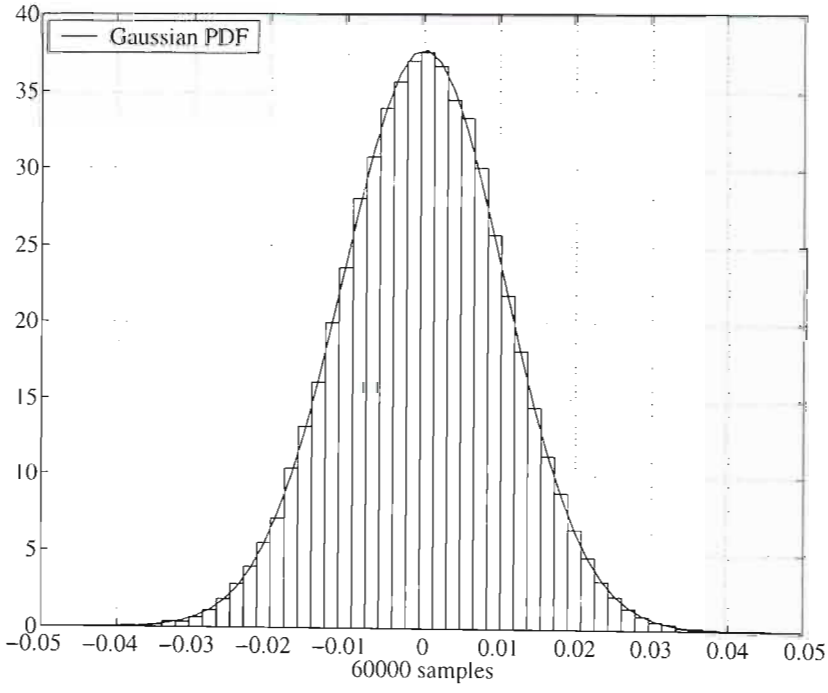

Fig. 2.3. Histogram of $e_a(i)$ for the LCCMA algorithm in steady-state, with 20 users, 20dB SNR, 0dB MAI ratio, and $\mu = 10^{-4}$.

Fig. 2.4–Fig. 2.7 compare the LCCMA steady-state analysis (2.34) with simulation results, which concur, and thus validate the analytical formulas and the assumptions used to attain them. In all the results, it is observed that the first order analytical solution only starts losing accuracy (compared to the higher order solutions) when the EMSE becomes large. It otherwise correctly captures the steady-state behaviour of the adaptive algorithm over a very wide range of operating conditions. Fig. 2.4 shows the effect that SNR has on the EMSE in a 25 user system, 10dB MAI ratio, and $\mu = 3\times10^{-5}$. The simulation confirms the analysis result that the EMSE decreases monotonically with SNR. This is because as the SNR increases the MUD approaches the decorrelating detector and the amount of residual MAI approaches zero. As this occurs the cost function approaches zero at convergence, and thus the steady-state EMSE approaches zero. It is observed that both the first order and simplified first order solutions hold closely when the SNR is above 5dB as the EMSE is small in this region. Below this point (which is possible in a wireless communications system) it becomes necessary to consider the higher order solutions.

The effects of increasing the step size in a 15 user system with a 20dB SNR and MAI ratio of 5dB are illustrated in Fig. 2.5. As the step size increases, the filter coefficients oscillate with greater amplitude around the optimum solution because of the increased value of each filter update, and thus the misadjustment increases with step size. It is noted that the analysis correctly predicts the rapid rise in EMSE when μ increases above 10^{-3}.

The accuracy of the steady-state analysis is explored over a wide dynamic range of MAI ratio of Fig. 2.6. Each data point is the average of 2×10^{5} iterations. A small step size of 10^{-5} was used to ensure stability as the low SNR of 5dB combined high MAI ratios creates large EMSE values. It is evident in Fig. 2.6 that as the EMSE level increases the first order approximation looses accuracy compared to the second and third order solutions which accurately predict the EMSE level.

The importance of including the higher order solutions is most evident in Fig. 2.7 where the first order solution tends to underestimate the EMSE. The higher order solutions are observed to accurately predict the EMSE. Each data point is once again the average of 2×10^{5} iterations. The trend in the increase in EMSE as a function of the number of users is also evident, this relationship is important as it enables the scaling of the network to be computed.

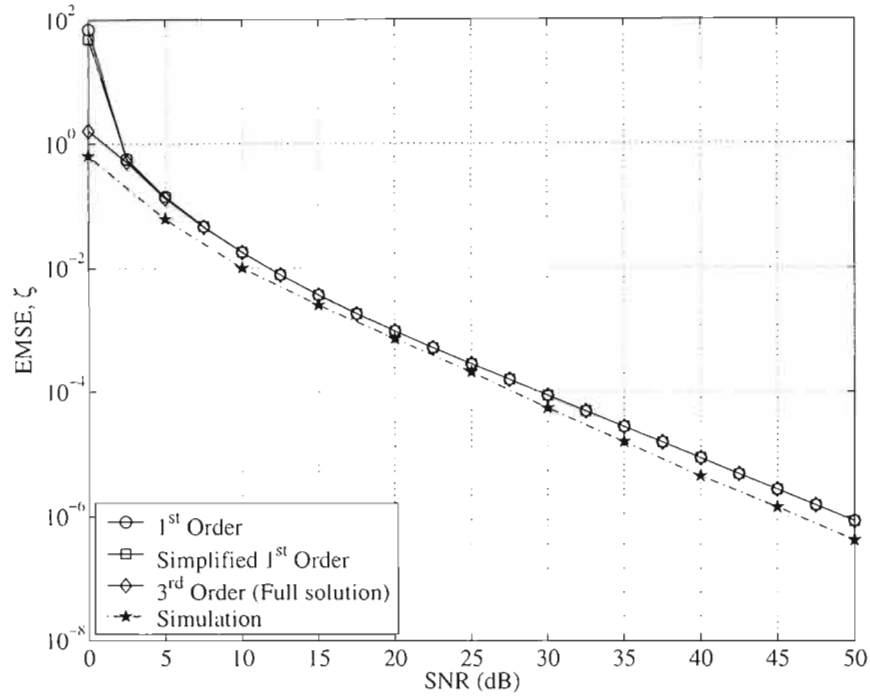

Fig. 2.4. Theoretical and simulated steady-state EMSE values for LCCMA as a function of SNR for a 25 user system. A 10dB MAI ratio and a step size of 3×10^{-5} was considered.

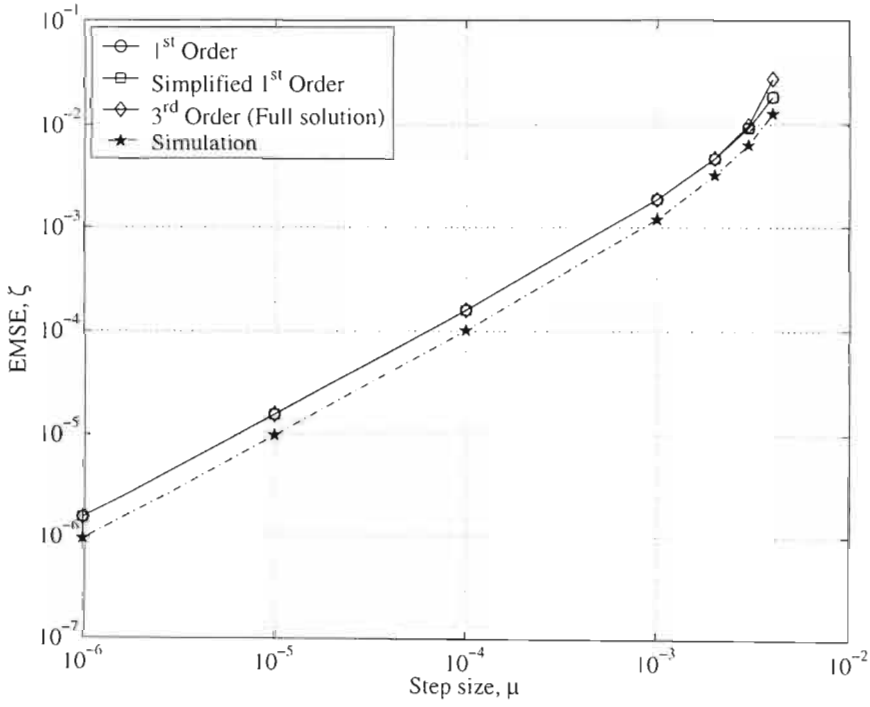

Fig. 2.5. Theoretical and simulated steady-state EMSE values for LCCMA as a function of step size for a 15 user system. A 20dB SNR and a MAI ratio of 5dB was considered.

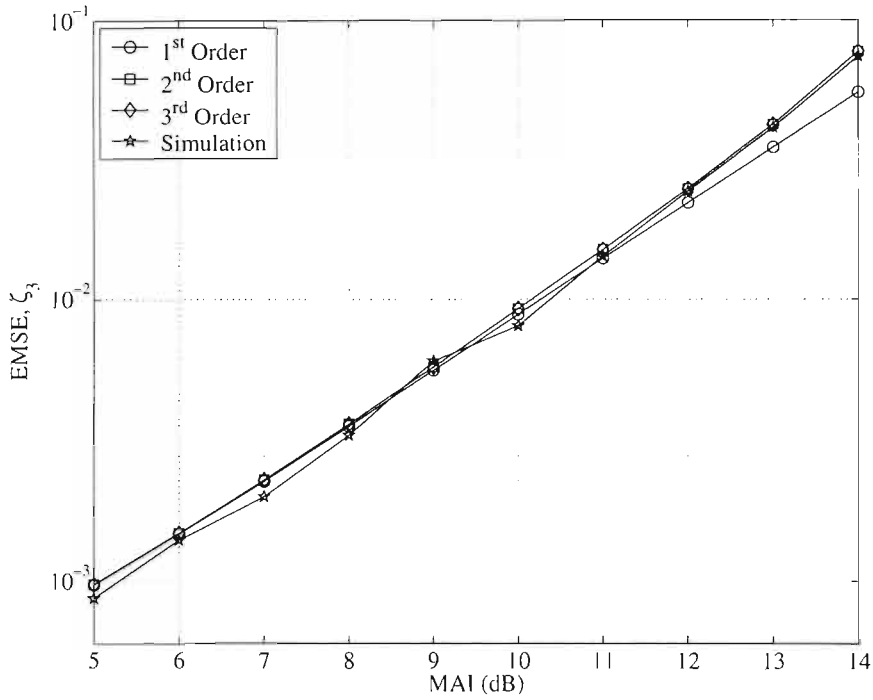

Fig. 2.6. Theoretical and simulated steady-state EMSE values for LCCMA as a function of MAI ratio for 10 user system, 5dB SNR and step size set to $\mu = 10^{-5}$.

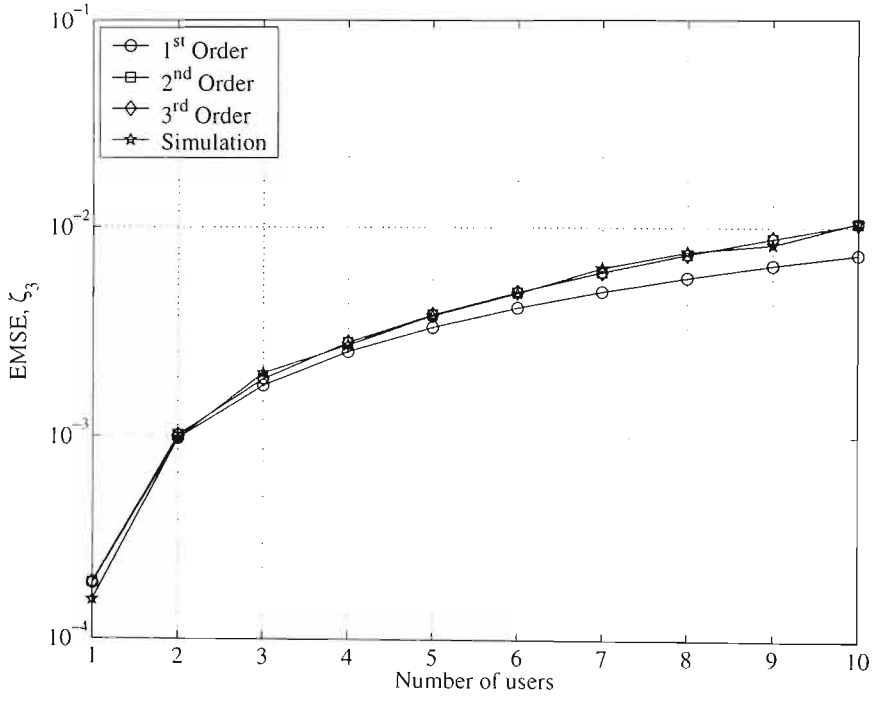

Fig. 2.7. Theoretical and simulated steady-state EMSE values for LCCMA as a function of the number of users in the system. A MAI ratio of 3dB and SNR of 15dB was considered. The step size was fixed at 5×10^{-3}.

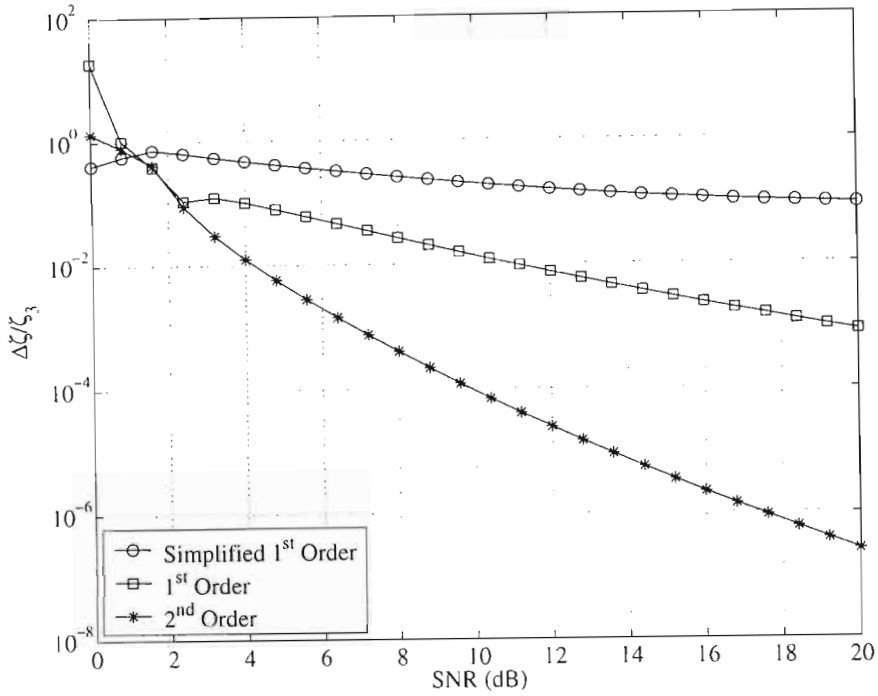

Fig. 2.8. Relative error between the (full) 3rd order solution and the simplified expressions for the EMSE of the LCCMA as a function of SNR.

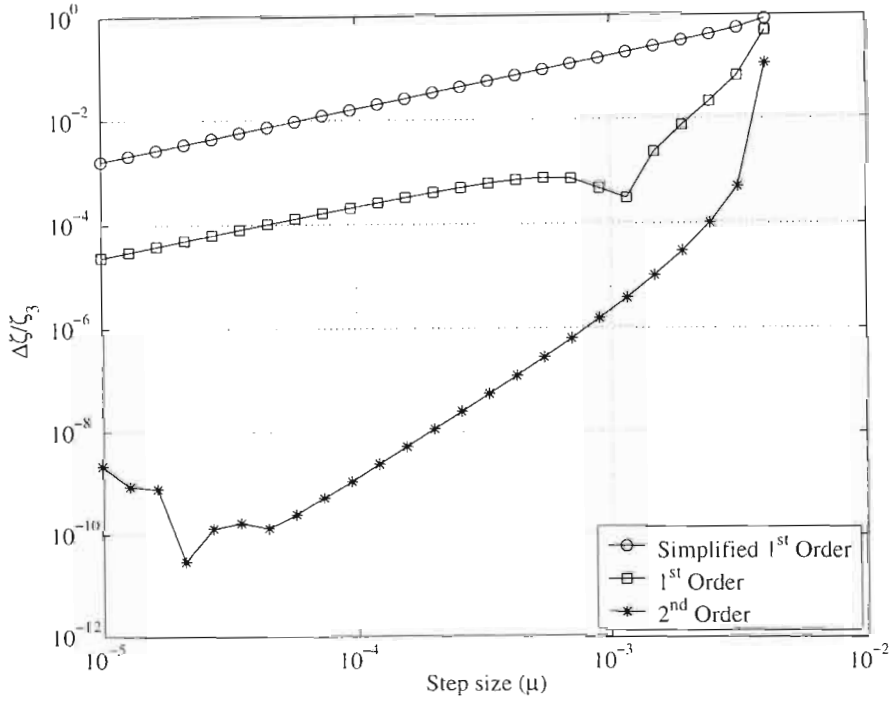

Fig. 2.9. Relative error between the (full) 3rd order solution and the simplified expressions for the EMSE of the LCCMA as a function of step size.

The difference between the different order solutions in Fig. 2.4 and Fig. 2.5 is examined more closely in Fig. 2.8 and Fig. 2.9 respectively. The exact difference $\Delta\zeta$ is given by $|\zeta_3 - \zeta|$ where ζ_3 is the full 3rd order solution to (2.34) and ζ represents the lower order approximations. This value is then normalised with respect to ζ_3 to measure the relative error.

The preceding validation of the steady-state analysis showed that the 3rd order solution most accurately captures the behaviour of the adaptive algorithm and is thus used as the reference point. The curves in Fig. 2.8 and Fig. 2.9 illustrate that the 2nd order solution is more accurate than the 1st order solutions since the error is lower. Fig. 2.8 and Fig. 2.9 also reflect the decreasing accuracy of the lower order approximations as the EMSE increases. This is expected since the lower order approximations arise through the assumption that the EMSE is small. These curves are thus also useful as they show over which range the simplified EMSE expressions are valid.

2.6 Tracking analysis

2.6.1 Canonical LCCMA

The feedback approach provides a convenient mechanism to extend the steady-state analysis to the tracking analysis, as shown in [52] and [54]. EMSE expressions for the tracking performance of the CMA were published in [52] and [54]. The derivation of EMSE in this section has not been done in the literature for any other blind adaptive MUD. It requires further assumptions and yields different results to [52] and [54]; this is due again to the different system model, application, and the difference between LCCMA and CMA.

In the time varying channel, the optimum filter coefficients are assumed to vary according to the model $\mathbf{w}_{opt}(i+1) = \mathbf{w}_{opt}(i) + \mathbf{q}(i)$, where $\mathbf{q}(i)$ denotes a random perturbation. This is typical in the context of tracking analyses of adaptive filters [54]. This perturbation is brought about by the random perturbation of all the users' spreading codes, where it is assumed that variations in the desired user's spreading code are tracked perfectly (no mismatch). The model for the non-stationary component of the optimal filter coefficients tracked by the LCCMA therefore simplifies to,

$$\mathbf{w}_{\perp}^{opt}(i+1) = \mathbf{w}_{\perp}^{opt}(i) + \mathbf{q}_{\perp}(i). \tag{2.39}$$

The weight error vector is redefined as $\Delta\mathbf{w}(i) = \mathbf{w}_{opt}(i) - \mathbf{w}(i)$. The feedback approach theory derived the modification to the fundamental energy preserving equation to take into account a time varying (non-stationary) channel. The fundamental steady-state energy preserving equation in the non-stationary channel, as shown in [52] and [54], is

$$E\{\bar{\mu}(i)e_a^2\} = \mathrm{Tr}(\mathbf{Q}_{\perp}) + E\left\{\bar{\mu}(i)\left(e_a(i) - \frac{\mu}{\bar{\mu}(i)}F_c(i)\right)^2\right\} \tag{2.40}$$

and relies on the following assumptions:

iv. Sequence $\{\mathbf{q}_{\perp}(i)\}$ is stationary, independent, zero mean, with positive definite covariance matrix, $\mathbf{Q}_{\perp}$.

v. The sequences $\{\mathbf{q}_\perp(i)\}$, $\{\mathbf{r}_\perp(i)\}$, and $\{v(i)\}$ are mutually independent.

These assumptions are reasonable under the given conditions, as the accuracy of the simulations illustrate. Expanding the right hand side of (2.40), the fundamental energy preserving equation can be simplified to

$$E\{e_a F_c\} = G + T.E\{F_c^2\} \tag{2.41}$$

where $T = \frac{\mu}{2}\mathrm{Tr}(\mathbf{C}_\perp)$, and $G = \frac{\mathrm{Tr}(\mathbf{Q}_\perp)}{2\mu}$. Equation (2.41) is then expanded using the same set of assumptions and approximations as before in Section 2.5 to obtain:

$$J_2 E\{e_a^2\}^2 + J_1 E\{e_a^2\} = G + T.\left(K_3 E\{e_a^2\}^3 + K_2 E\{e_a^2\}^2 + K_1 E\{e_a^2\} + K_0\right) \tag{2.42}$$

where it is assumed that $\mathbf{q}_\perp(i)$ is independent of $\{b_1, M, v, e_a\}$ and the higher moments of $\{b_1, M, v, e_a\}$ are not affected by the non-stationary channel. Neglecting the terms with the higher order powers of e_a, the first order solution for the EMSE in a non-stationary channel is given by

$$\zeta_{\mathrm{LCCMA}} = \frac{G + TK_0}{J_1 - TK_1}. \tag{2.43}$$

The EMSE expression in a non-stationary channel may be derived using the assumption from [54] that there is no AWGN, for comparative purposes. Constant modulus data symbols are assumed, and thus the EMSE in the resulting expression is solely derived from the system non-stationarity $\mathrm{Tr}(\mathbf{Q}_\perp)$. This expression is given by,

$$\zeta'_{\mathrm{LCCMA}} = \frac{\mathrm{Tr}(\mathbf{Q}_\perp)}{4\mu}, \tag{2.44}$$

and is computed by simplifying (2.43) using the fact that $\sigma_n = \eta = 0$, by assuming TK_1 is negligibly small compared to J_1, and that $R_2 = A_1^2 = 1$. This new expression is a monotonically decreasing function of step size and as such is clearly inaccurate.

Optimum μ:

For simplicity consider a simplified expression for the first order approximation of the EMSE, where it is assumed that the optimum choice for μ is small and thus $TK_1 \ll J_1$. The TK_1 term can then be removed from the denominator of (2.43), and then the optimum value for μ is

$$\mu_o = \sqrt{\frac{\mathrm{Tr}(\mathbf{Q}_\perp)}{\mathrm{Tr}(\mathbf{C}_\perp)K_0}}. \tag{2.45}$$

Substituting this value into (2.43), the lowest attainable EMSE in a non-stationary channel can be computed.

2.6.2 Non-canonical LCCMA

The non-canonically constrained receiver converges to a scaled set of filter coefficients related to the canonically constrained detector in (2.29). If one considers the operation of both receivers in the same fading channel, it becomes apparent that the value of $\mathrm{Tr}(\mathbf{Q}_\perp)$ will be higher for the non-canonically constrained LCCMA compared to canonical LCCMA. This will lead to differing values of μ_o as shown in (2.45) which will in turn lead to differing optimal EMSE levels, in the same channel. This can be explained by noting that the majority of the energy of the MMSE filter coefficients lies in the $\mathbf{s}_1$ direction [25], which is fixed in the canonically constrained case. The non-canonically constrained detector is anchored by $d\mathbf{s}_1$, where d is a function of the desired user's amplitude, which varies due to fading. It can be seen then that the magnitude of the orthogonal (adaptive) component for the non-canonically constrained detector requires a much larger dynamic range than the canonically constrained detector, which increases the tracking requirements of the adaptive algorithm. With the increase in tracking requirements, the non-canonically constrained detector will have inferior performance in a fading channel.

2.6.3 Validation of tracking analysis

The time varying channel was induced by perturbing each users' spreading code at each bit epoch by a small Gaussian random vector $\mathbf{n}_s(i)$ (with covariance matrix $\sigma_s^2\mathbf{I}$) and then normalizing the new spreading codes to give,

$$\mathbf{s}_k(i) = \frac{\mathbf{s}_k + \mathbf{n}_s(i)}{\left\|\mathbf{s}_k + \mathbf{n}_s(i)\right\|}. \tag{2.46}$$

This models the time varying channel distortions inherent to a wireless communications channel. The average value of $\mathrm{Tr}(\mathbf{Q}_\perp)$ was calculated from the simulation using the definition $\mathbf{q}_\perp(i) \triangleq \mathbf{w}_\perp^{opt}(i+1) - \mathbf{w}_\perp^{opt}(i)$.

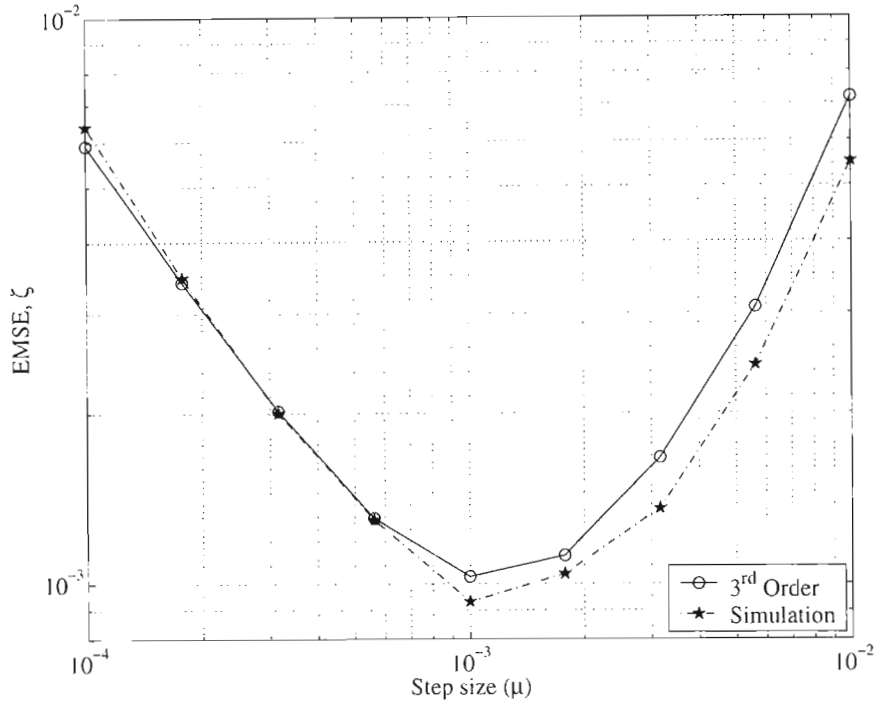

Fig. 2.10. Theoretical and simulated EMSE values for LCCMA as a function of step size, in a non-stationary channel.

The EMSE of canonically constrained LCCMA is plotted in Fig. 2.10 as a function of step size. A 10 user system with 20dB SNR and MAI level of 3dB's was considered, where $\mathrm{Tr}(\mathbf{Q}_\perp) = 2.4\times10^{-6}$. It is immediately evident that the EMSE is no longer a monotonically increasing function of step size, but rather an optimum value exists that trades off lag error and misadjustment. The optimum value for μ is correctly predicted by the analysis.

2.7 Transient analysis

2.7.1 LCCMA

The transient analysis is performed using the generic analysis technique proposed in [58] which is conveniently based on energy arguments, much like the preceding steady-state and tracking analyses. This is convenient as the formulas derived for the steady-state and tracking analysis are exploited in this section to derive the transient performance of the LCCMA. The transient analysis computes the expected value of the EMSE of the adaptive filter at each time instant from initialization to steady-state. The EMSE at time instant *i* is defined as,

$$\begin{aligned} E\left\{e_a^2(i)\right\} &= E\left\{\left\|\Delta\mathbf{w}_\perp(i)\right\|_{\mathbf{C}_\perp}^2\right\} \\ &= \zeta_i. \end{aligned} \tag{2.47}$$

The *recursion data* is in this case the projected received vector $\mathbf{r}_\perp$, which has the covariance matrix,

$$\mathbf{C}_\perp = \sum_{k=2}^{K} A_k^2\left(\mathbf{s}_k\mathbf{s}_k^T + \rho_{1k}\left(\rho_{1k}\mathbf{s}_1\mathbf{s}_1^T - \mathbf{s}_1\mathbf{s}_k^T - \mathbf{s}_k\mathbf{s}_1^T\right)\right) + \sigma^2\left(\mathbf{I} - \mathbf{s}_1\mathbf{s}_1^T\right) \tag{2.48}$$

where $\rho_{1k} = \mathbf{s}_1^T \mathbf{s}_k$. This covariance matrix is not diagonal, and thus a state space model, using the first $N-1$ weighted norms of the weight error vector $\Delta\mathbf{w}_\perp(i)$ is required to compute the time evolution of the EMSE, as shown in [58]. The transient analysis assumes $e_a(i)$ is Gaussian (which has already been assumed in Section 2.5), and that the weighted norm of the input regressor $\mathbf{r}_\perp$ is uncorrelated with $F_e^2(i)$, which is similar to assumption (i). These assumptions are realistic during the early stages of adaptation [58]. The methodology which this thesis utilises for computing the transient analysis is presented in [58]. The state-space recursion used to compute ζ_i is given in [58] as,

$$\mathcal{W}_{i+1} = \mathcal{A}\mathcal{W}_i + \mu^2 \mathcal{Y} \tag{2.49}$$

where the state-space recursion is defined using,

$$\mathcal{W}_i = \begin{bmatrix} E\left\{\left\|\tilde{\mathbf{w}}_\perp(i)\right\|^2\right\} \\ E\left\{\left\|\tilde{\mathbf{w}}_\perp(i)\right\|^2_{\mathbf{C}_\perp}\right\} \\ \vdots \\ E\left\{\left\|\tilde{\mathbf{w}}_\perp(i)\right\|^2_{\mathbf{C}_\perp^{N-1}}\right\} \end{bmatrix}, \quad \mathcal{Y} = h_{ij} \cdot \begin{bmatrix} E\left\{\left\|\mathbf{r}_\perp(i)\right\|^2\right\} \\ E\left\{\left\|\mathbf{r}_\perp(i)\right\|^2_{\mathbf{C}_\perp}\right\} \\ \vdots \\ E\left\{\left\|\mathbf{r}_\perp(i)\right\|^2_{\mathbf{C}_\perp^{N-1}}\right\} \end{bmatrix}, \tag{2.50}$$

$$\mathcal{A} = \begin{bmatrix} 1 & -2\mu h_{ij} & 0 & \dots & 0 & 0 \\ 0 & 1 & -2\mu h_{ij} & \dots & 0 & 0 \\ \vdots & \vdots & \vdots & \ddots & \vdots & \vdots \\ 0 & 0 & 0 & \dots & 1 & -2\mu h_{ij} \\ 2p_0\mu h_{ij} & 2p_1\mu h_{ij} & 2p_2\mu h_{ij} & \dots & 2p_{N-2}\mu h_{ij} & 1+2p_{N-1}\mu h_{ij} \end{bmatrix}. \tag{2.51}$$

The elements of $\mathcal{Y}$ may be computed using the relation,

$$E\left\{\left\|\mathbf{r}_\perp(i)\right\|^2_{\mathbf{C}_\perp^x}\right\} = \mathrm{Tr}\left(\mathbf{C}_\perp^* \mathbf{C}_\perp^x\right), \tag{2.52}$$

where $x \in \{0,\dots,N-1\}$. The elements of $\mathcal{W}_0$ may be similarly computed. The characteristic polynomial of $\mathbf{C}_\perp$ is $p(x) \triangleq \det(x\mathbf{I} - \mathbf{C}_\perp) = p_0 + p_1 + \dots + p_{M-1}x^{M-1} + x^M$. The entries of matrices $\mathcal{A}$ and $\mathcal{Y}$ are functions of $\{h_{ij}, h_{ij}\}$ which are in turn functions of ζ_i, given by

$$h_{ij} = E\left\{F_e^2(i)\right\}, \quad h_{ij} = \frac{E\left\{e_a(i)F_e(i)\right\}}{E\left\{e_a^2(i)\right\}}. \tag{2.53}$$

Section 2.5.2 showed how to express $F_e(i)$ in terms of $e_a(i)$ and other deterministic quantities for the LCCMA. It is possible to simplify $\{h_{ij}, h_{ij}\}$ using the same set of assumptions and simplifications given in Section 2.5, which gives,

$$h_{ij} = K_3\zeta_i^3 + K_2\zeta_i^2 + K_1\zeta_i + K_0 \tag{2.54}$$

$$h_{ij} = 3\zeta_i + J_1 \tag{2.55}$$

and the coefficients $\{K_3, K_2, K_1, K_0, J_1\}$ are given in Table 2.2. Note that h_{ij} is contained in the right hand side of (2.34), and the numerator of h_{ij} is given in the left hand side of (2.34).

Closed form expressions have been given for $\{\mathbf{C}_\perp, h_{ci}, h_{ij}\}$, and thus the transient performance may be computed using (2.49). The first entry of the vector $\mathcal{W}_i$ characterizes the mean square deviation (MSD) of the filter coefficients, and the second entry characterizes the EMSE, which may then be used to plot the time evolution (or learning curve) of the EMSE. The EMSE is assumed to be Gaussian and thus the learning curve for the output SINR may be constructed using

$$SINR(i) = \frac{A_1^2}{\sigma_n^2 + \eta^2 + \zeta_i}. \tag{2.56}$$

It is assumed that the receiver is correctly initialised to the single user matched filter, and so the starting point of the state-space recursion is deterministic, with $\mathcal{W}_0$ computed using $\Delta\mathbf{w}_\perp(0) = \mathbf{w}_{opt} - \mathbf{s}_1$.

2.7.2 Validation of transient analysis

The accuracy of the transient analysis is verified in Fig. 2.11 using the ensemble average of 100 independent simulation runs of the LCCMA using different choices of step size. A 15 user system was considered where the MAI ratio was 0dB's, SNR was 20dB's, and all the users transmitted synchronously using length 31 Gold codes. The learning curves, or time evolution, of the EMSE is plotted in Fig. 2.11, where the receiver is initialised to the single user matched filter and converges towards the MMSE MUD. For the set of different step sizes in the figure sequence, the transient analysis is observed to hold closely. The effects of reducing the step size are illustrated in the sequence Fig. 2.11 (a)–(c), where the step size sequence 1×10^{-2}, 5×10^{-3}, and 1×10^{-3} is used. These effects are: the slower convergence rate as the step size decreases, and the lowering of the steady-state EMSE levels as the step size decreases. This is due to the higher accuracy of gradient approximation associated with a smaller step size. The steady-state EMSE level, as predicted by the preceding steady-state analysis, is also superimposed in each plot in Fig. 2.11. This level is observed to correspond to the steady-state EMSE level predicted by the transient analysis, which is expected since the equivalence between the theoretical levels predicted by both theories was shown in Section 2.3.2. The theoretical steady-state EMSE levels are (again) observed to correspond closely with the simulation data.

The EMSE levels in isolation do not provide a direct measure of the performance cost incurred by the adaptive algorithm relative to the exact MMSE MUD. A more useful metric is the SINR of the desired user at the output of the adaptive filter. It is shown in Fig. 2.12 how the transient analysis may be used to compute the learning curves of the output SINR as the adaptive algorithm converges towards the MMSE MUD, after being initialized with the single user matched filter. The same set of operating conditions as per Fig. 2.11 (a)–(c) are used in Fig. 2.12 (a)–(c) where the theoretical SINR learning curves are computed using (2.56) and the SINR level at time step *i* of the simulation are computed using,

$$SINR(i) = \frac{\left(\mathbf{w}^T(i)(A_1\mathbf{s}_1)\right)^2}{\mathbf{w}^T(i)\left(\mathbf{C} - A_1^2\mathbf{s}_1\mathbf{s}_1^T\right)\mathbf{w}(i)}. \tag{2.57}$$

The simulation results are again the average of 100 independent simulation runs. The simulation and theoretical results are observed to tie-up closely. The trade-off between misadjustment levels and rate of convergence is clearly evident in the sequence Fig. 2.12 (a)–(c). The difference in dB's between the MMSE and adaptive algorithm in steady-state is accurately predicted as well as the transient curve taken to reach steady-state. This is vital information as the time it takes to reach steady-state as well as the subsequent drop in SINR incurred by the adaptive algorithm is significant. The optimization of the step size parameter is now possible as the exact adaptive performance of LCCMA has now been computed.

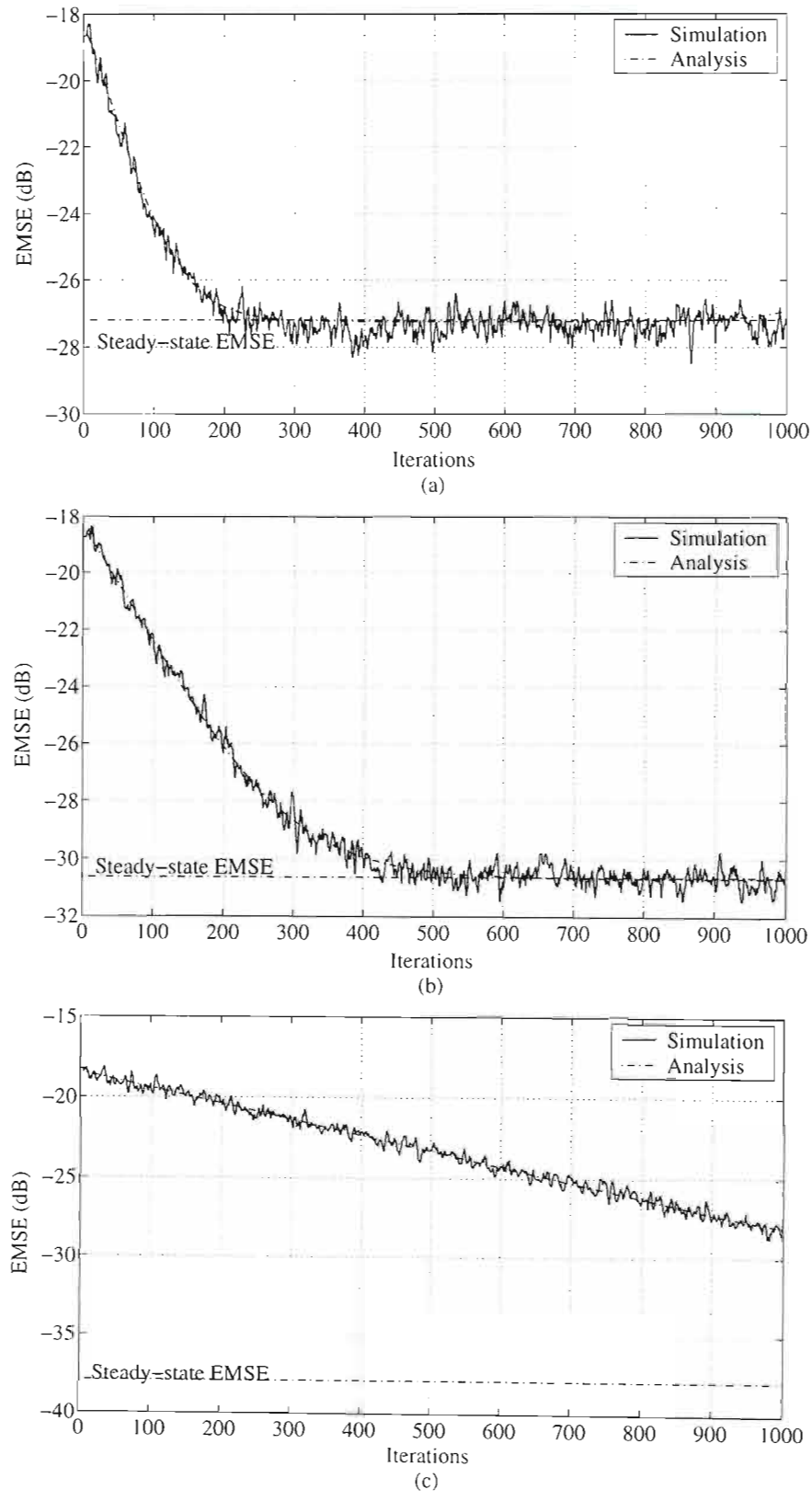

Fig. 2.11. Comparison between EMSE learning curves predicted by theory and from simulation, for various choices of step size (figs. (a), (b) and (c) correspond to step sizes of 10^{-2}, 5×10^{-3}, and 10^{-3} respectively).

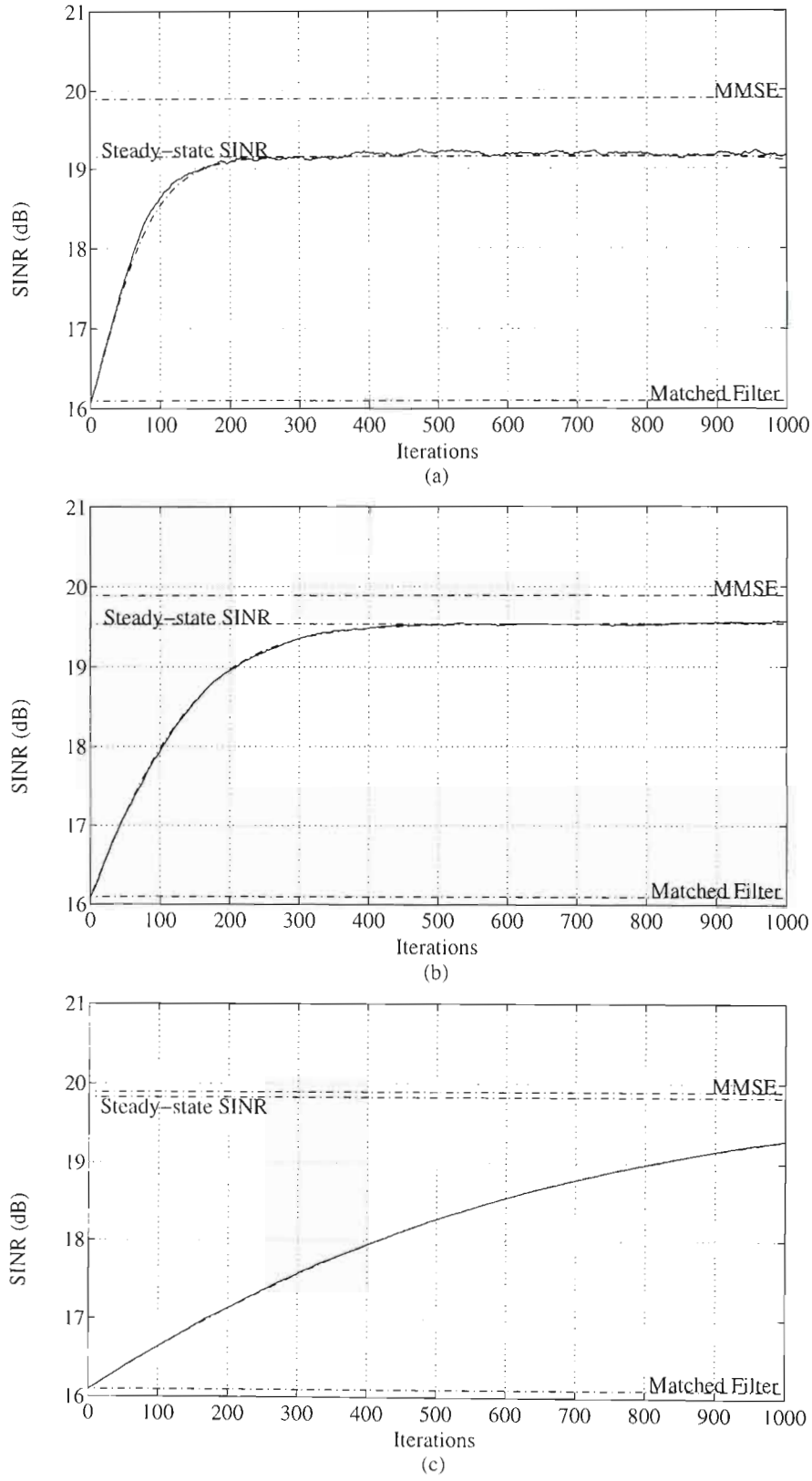

Fig. 2.12. Comparison between SINR learning curves predicted by theory and from simulation, for various choices of step size (figs. (a), (b) and (c) correspond to step sizes of 10^{-2}, 5×10^{-3}, and 10^{-3} respectively).

2.8 Derivation of alternate blind adaptive MUD's

The steady-state and tracking analyses are derived below for various adaptive MUD's where the general technique is to start with the simplified energy preserving equation for a non-stationary channel, given in Section 2.6, and repeated here for convenience:

$$E\{e_a F_c\} = G + T.E\{F_c^2\} \tag{2.58}$$

The driving vector is then identified in order to specify $T = \frac{\mu}{2}\mathrm{Tr}(\mathbf{R})$. F_c is then expressed in terms of y using,

$$\begin{aligned} y(i) &= \left(\mathbf{w}_{opt}(i) - \Delta\mathbf{w}(i)\right)^T \mathbf{r}(i) \\ &= \theta b_1(i) + M(i) + v(i) - e_a(i) \end{aligned} \tag{2.59}$$

where θ is the receiver gain defined by $\theta \triangleq \mathbf{w}_{opt}^T(A_1\mathbf{s}_1)$ which specifies the scaling of $\mathbf{w}_{opt}$ (the optimal filter coefficients in terms of the adaptive algorithm's cost function) relative to the biased MMSE filter coefficients. The biased MMSE filter coefficients are given by,

$$\mathbf{w}_{MMSE} = \mathbf{C}^{-1}\mathbf{p} \tag{2.60}$$

where,

$\mathbf{C} = E\{\mathbf{r}(i)\mathbf{r}^T(i)\}$

$\mathbf{p} = E\{b_1(i)\mathbf{r}(i)\}$.

The simplification of $E\{F_c e_a\}$ and $E\{F_c^2\}$, as performed in Section 2.5, enables the derivation of the steady-state and tracking performance, as well directly leads on to $\{h_{1j}, h_{ci}\}$ which is used to quantify the transient performance.

In the derivations given below, the MOE, Sato, LCCMA based on CMA1-2, and LCDCMA are all examples of code constrained blind adaptive MUD's that exploit the canonical decomposition of the optimal filter coefficients,

$$\mathbf{w}(i) = \mathbf{s}_1 + \mathbf{w}_\perp(i). \tag{2.61}$$

Note: $G = \frac{1}{2\mu}\mathrm{Tr}(\mathbf{Q}_\perp)$ and $T = \frac{\mu}{2}\mathrm{Tr}(\mathbf{C}_\perp)$ for these algorithms.

The DD-LMS algorithm is not code-constrained, but still qualifies as a blind adaptive MUD algorithm. For the DD-LMS algorithm, $G = \frac{1}{2\mu}\mathrm{Tr}(\mathbf{Q})$ and $T = \frac{\mu}{2}\mathrm{Tr}(\mathbf{C})$. The DD-LMS algorithm also converges towards the biased MMSE filter, and this needs to be taken into account when computing the statistics of the output MAI and AWGN of the optimum filter.

2.8.1 MOE

Steady-state Analysis

A new expression for the EMSE of the MOE detector is now derived. It acts to further illustrate the feedback approach to analysing the steady-state behaviour of blind adaptive MUD's. The update step of the stochastic gradient algorithm of the MOE detector is given in [25] as

$$\mathbf{w}_{\perp}(i+1)=\mathbf{w}_{\perp}(i)-\mu\mathbf{r}_{\perp}(i)y(i). \tag{2.62}$$

Comparing this to the general formula in (2.2), the driving vector in this case is $\mathbf{r}_{\perp}$ and $F_c=-y$. The receiver gain of the optimal filter coefficients corresponding to the MOE cost function is A_1, so the same expression for y holds:

$$y=A_1b_1+M+v-e_a. \tag{2.63}$$

Starting from the simplified expression for the energy preserving equation (2.33), and substituting y:

$$\begin{aligned} E\{-ye_a\}&=T.E\{y^2\}\\ E\{-(A_1b_1+M+v-e_a)e_a\}&=T.E\{(A_1b_1+M+v-e_a)^2\}. \end{aligned} \tag{2.64}$$

This expression can be further simplified using the same set of assumptions and approximations given in Section 2.5.1,

$$\begin{aligned} E\{e_a^2\}&=T.\left(E\{e_a^2\}+A_1^2+\eta^2+\sigma_n^2\right)\\ &=\frac{T\left(A_1^2+\eta^2+\sigma_n^2\right)}{1-T}. \end{aligned} \tag{2.65}$$

The expression for the EMSE derived in [25] was given as

$$E\{e_a^2\}=\frac{T}{1-T}. \tag{2.66}$$

Comparing (2.66) to the new expression given in (2.65), it is obvious that they are the same except for the correction factor $\left(A_1^2+\eta^2+\sigma_n^2\right)$, in the new expression. It can be reasoned then, that this new expression more accurately takes into account the effects of the residual MAI and AWGN at the output of the MUD.

Tracking analysis

The tracking performance of the MOE detector is derived by starting with the simplified equation (2.41), and making the same substitution, $F_c=-y$, where y is given in (2.63) above. Then using the same set of simplifications as before,

$$E\{e_a^2\}=G+T.\left(E\{e_a^2\}+A_1^2+\eta^2+\sigma_n^2\right). \tag{2.67}$$

Solving for ζ, the EMSE of the MOE detector in a non-stationary channel is given by,

$$\zeta_{MOE}=\frac{G+T\left(A_1^2+\eta^2+\sigma_n^2\right)}{1-T}. \tag{2.68}$$

The optimum step size of the MOE detector is given by

$$\mu_a^{MOE}=\sqrt{\frac{\mathrm{Tr}(\mathbf{Q}_{\perp})}{\mathrm{Tr}(\mathbf{C}_{\perp})\left(A_1^2+\eta^2+\sigma_n^2\right)}}. \tag{2.69}$$

Substituting this value into (2.68), the lowest attainable EMSE of the MOE detector may be computed for a non-stationary channel.

Transient analysis

Expressions for $\{h_{1i}, h_{2i}\}$ can be similarly derived for the MOE cost function using the results of Section 2.5, and are

$$\begin{aligned} h_{1i} &= E\{F_c^2(i)\} \\ &= A_1^2 + \eta^2 + \sigma_n^2 + \zeta_i. \end{aligned} \tag{2.70}$$

$$\begin{aligned} h_{2i} &= \frac{E\{e_a(i)F_c(i)\}}{E\{e_a^2(i)\}} \\ &= 1 \end{aligned} \tag{2.71}$$

2.8.2 Sato

The update step of the Sato cost function is given in [59] as,

$$\mathbf{w}_\perp(i+1) = \mathbf{w}_\perp(i) - \mu \mathbf{r}_\perp(i)\big(y(i) - \text{sign}\big(y(i)\big)\big). \tag{2.72}$$

The driving vector is therefore $\mathbf{r}_\perp(i)$, $F_c(i) = \text{sign}\big(y(i)\big) - y(i)$, and $\theta = A_1$. Then,

$$\begin{aligned} E\{e_a F_c\} &= E\{e_a(\text{sign}(y) - y)\} \\ &= E\{e_a(\text{sign}(y) - A_1 b_1 - M - v + e_a)\} \\ &= E\{e_a \,\text{sign}(y) - e_a A_1 b_1 - e_a M - e_a v + e_a^2\}. \end{aligned} \tag{2.73}$$

Using the independence assumptions and the assumption that $E\{e_a \,\text{sign}(y)\} = 0$ [53], we have that $E\{e_a F_c\} = E\{e_a^2\}$. The $E\{F_c^2\}$ expression may be written as 3 separate terms,

$$\begin{aligned} E\{F_c^2\} &= E\{(\text{sign}(y) - y)^2\} \\ &= E\{(\text{sign}(y))^2 - 2y\,\text{sign}(y) + y^2\} \end{aligned} \tag{2.74}$$

where $E\{\text{sign}(y)^2\} = 1$, and $E\{\text{sign}(y)\,y\} = E\{|y|\}$. Assuming that the output of the receiver is distributed symmetrically around the transmitted signal, we have that $E\{|y|\} = E\{|A_1 b_1|\} = A_1$. Using the independence assumptions, we have that $E\{y^2\} = A^2 + \eta^2 + \sigma^2 + \zeta$ as before, since $\theta = A_1$ for the Sato cost function. Combining these 3 results,

$$\begin{aligned} E\{F_c^2\} &= 1 - 2A_1 + A_1^2 + \eta^2 + \sigma^2 + \zeta \\ &= (A_1 - 1)^2 + \eta^2 + \sigma^2 + \zeta. \end{aligned} \tag{2.75}$$

The steady-state and tracking EMSE is then given by,

$$\begin{aligned} E\{e_a F_c\} &= G + T.E\{F_c^2\} \\ \zeta &= G + T.\big((A_1 - 1)^2 + \eta^2 + \sigma^2 + \zeta\big) \\ \zeta &= G + \frac{T}{1-T}\big((1 - A_1)^2 + \eta^2 + \sigma^2\big) \end{aligned} \tag{2.76}$$

The transient analysis may be computed using,

$$\begin{aligned} h_{ij} &= E\left\{F_e^2(i)\right\} \\ &= (A_1 - 1)^2 + \eta^2 + \sigma_n^2 + \zeta_i. \end{aligned} \tag{2.77}$$

$$\begin{aligned} h_{ij} &= \frac{E\left\{e_a(i)F_e(i)\right\}}{E\left\{e_a^2(i)\right\}} \\ &= 1. \end{aligned} \tag{2.78}$$

2.8.3 LCCMA (CMA1-2)

It is possible to employ the CMA1-2 cost function, as opposed to the CMA2-2 cost function in the LCCMA. The CMA1-2 cost function is given by,

$$J(\mathbf{w}) = E\left\{\left(|\mathbf{y}| - R_1\right)^2\right\} \tag{2.79}$$

where the dispersion factor is defined as $E\left\{\left|A_1 b_1\right|^2\right\} / E\left\{\left|A_1 b_1\right|\right\}$ which is equal to A_1 in this case. The update step of the adaptive algorithm is given by,

$$\mathbf{w}_\perp(i+1) = \mathbf{w}_\perp(i) + \mu \mathbf{r}_\perp(i)\left(R_1 \frac{y(i)}{|y(i)|} - y(i)\right). \tag{2.80}$$

The driving vector is therefore $\mathbf{r}_\perp(i)$, $F_e(i) = R_1 \operatorname{sign}\left(y(i)\right) - y(i)$, and $\theta = A_1$. In a similar fashion to the Sato cost function,

$$\begin{aligned} E\{e_a F_e\} &= E\left\{e_a\left(R_1 \operatorname{sign}(y) - y\right)\right\} \\ &= E\left\{e_a\left(R_1 \operatorname{sign}(y) - \left(A_1 b_1 + M + v - e_a\right)\right)\right\} \\ &= E\left\{e_a R_1 \operatorname{sign}(y) - e_a A_1 b_1 - e_a M - e_a v + e_a^2\right\} \\ &= \zeta. \end{aligned} \tag{2.81}$$

$$\begin{aligned} E\left\{F_e^2\right\} &= E\left\{\left(R_1 \operatorname{sign}(y) - y\right)^2\right\} \\ &= E\left\{\left(R_1^2 \operatorname{sign}(y)\right)^2 - 2R_1 y \operatorname{sign}(y) + y^2\right\} \\ &= R_1^2 - 2R_1 A_1 + A_1^2 + \eta^2 + \sigma^2 + \zeta \\ &= (R_1 - A_1)^2 + \eta^2 + \sigma^2 + \zeta \end{aligned} \tag{2.82}$$

This leads on to the steady-state and tracking analysis being quantified with,

$$\begin{aligned} E\{e_a F_e\} &= G + T.E\left\{F_e^2\right\} \\ \zeta &= G + T.\left((R_1 - A_1)^2 + \eta^2 + \sigma^2 + \zeta\right). \end{aligned} \tag{2.83}$$

and the transient performance computed using,

$$\begin{aligned} h_{ij} &= E\left\{F_e^2(i)\right\} \\ &= (R_1 - A_1)^2 + \eta^2 + \sigma_n^2 + \zeta_i. \end{aligned} \tag{2.84}$$

$$h_{G_i} = \frac{E\{e_a(i)F_c(i)\}}{E\{e_a^2(i)\}} = 1. \tag{2.85}$$

2.8.4 LCDCMA

The update step of the LCDCMA cost function is given by,

$$\mathbf{w}_\perp(i+1) = \mathbf{w}_\perp(i) + \mu \mathbf{r}_\perp(i)\big(y(i-1) - y(i)\big)\Big(|y(i)|^2 - |y(i-1)|^2\Big). \tag{2.86}$$

The driving vector is therefore $\mathbf{r}_\perp(i)$, $F_c(i) = \big(y(i-1) - y(i)\big)\Big(|y(i)|^2 - |y(i-1)|^2\Big)$, and $\theta = A_1$. F_c is firstly expanded using,

$$y(i) = A_1 b_1(i) + M(i) + v(i) - e_a(i) \tag{2.87}$$

$$y(i-1) = A_1 b_1(i-1) + M(i-1) + v(i-1) - e_a(i-1) \tag{2.88}$$

and then substituted into the fundamental equations, which are subsequently simplified to yield,

$$\begin{aligned} E\{e_a F_c\} &= E\Big\{e_a\big(y(i-1) - y(i)\big)\Big(|y(i)|^2 - |y(i-1)|^2\Big)\Big\} \\ &= J_2\zeta^2 + J_1\zeta \end{aligned} \tag{2.89}$$

$$\begin{aligned} E\{F_c^2\} &= E\left\{\Big(\big(y(i-1) - y(i)\big)\Big(|y(i)|^2 - |y(i-1)|^2\Big)\Big)^2\right\} \\ &= K_3\zeta^3 + K_2\zeta^2 + K_1\zeta + K_0. \end{aligned} \tag{2.90}$$

The coefficients $\{K_3, K_2, K_1, K_0, J_1\}$ are summarized in Table 2.3. The following additional assumption was used to simplify (2.89) and (2.90):

i. $E\{e_a(i)e_a(i-1)\} = 0$, this in turn yields $E\{y(i)y(i-1)\} = 0$, since the data bits and the AWGN are uncorrelated between successive bit epochs.

The coefficients $\{K_3, K_2, K_1, K_0, J_1\}$ were simplified using similar rules as before, as the random variables $\{b_1(i), M(i), v(i), e_a(i), b_1(i-1), M(i-1), v(i-1), e_a(i-1)\}$ are mutually independent, which in turn causes any of those variables with an odd power to drop out of $\{K_3, K_2, K_1, K_0, J_1\}$, after applying the expectation operation. Also, the statistics of the MAI and AWGN do not change between successive bit epochs, and therefore simplifications of the form:

$E\{M^2(i)\} = E\{M^2(i-1)\} = \eta^2$

$E\{M^2(i)M^2(i-1)\} = \eta^4$

$E\{M^4(i)\} = 3\eta^4$

were made.

Table 2.3. Coefficients for LCDCMA EMSE Expressions.

Coefficient	Value
J_2	2
J_1	$2\left(A_1^2+\eta^2+\sigma^2\right)$
K_3	24
K_2	$72\left(A_1^2+\eta^2+\sigma^2\right)$
K_1	$16A_1^4+144A_1^2\eta^2+144A_1^2\sigma^2+72\eta^4+432\eta^2\sigma^2+72\sigma^4$
K_0	$16A_1^4\eta^2+16A_1^4\sigma^2+72A_1^2\eta^4+432A_1^2\eta^2\sigma^2+72A_1^2\sigma^4+24\eta^6+360\eta^4\sigma^2+360\eta^2\sigma^4+24\sigma^6$

Filtered noise variance: $\sigma_n^2=E\left\{v^2\right\}$

Residual MAI variance: $\eta^2=E\left\{M^2\right\}$

The steady-state and tracking performance is then computed as the smallest positive root of the third order polynomial,

$$\begin{aligned} E\left\{e_a F_e\right\} &= G+T.E\left\{F_e^2\right\} \\ J_2\zeta^2+J_1\zeta &= G+T.\left(K_3\zeta^3+K_2\zeta^2+K_1\zeta+K_0\right) \end{aligned} \tag{2.91}$$

where reduced order solutions may also be considered as per the LCCMA case. The transient analysis may be computed using,

$$\begin{aligned} h_{0,i} &= E\left\{F_e^2(i)\right\} \\ &= K_3\zeta_i^3+K_2\zeta_i^2+K_1\zeta_i+K_0 \end{aligned} \tag{2.92}$$

$$\begin{aligned} h_{1,i} &= \frac{E\left\{e_a(i)F_e(i)\right\}}{E\left\{e_a^2(i)\right\}} \\ &= 2\zeta_i+J_1 \end{aligned} \tag{2.93}$$

and the coefficients $\left\{K_3,K_2,K_1,K_0,J_1\right\}$ are once again given in Table 2.3.

2.8.5 DD-LMS

The DD-LMS cost function is given by,

$$J_{DD}=E\left\{\frac{1}{2}\left|\operatorname{sign}(y)-y\right|^2\right\} \tag{2.94}$$

and the update step of the adaptive algorithm is given by,

$$\mathbf{w}(i+1)=\mathbf{w}(i)+\mu\left(\operatorname{sign}\left(y(i)\right)-y(i)\right)\mathbf{r}(i). \tag{2.95}$$

The driving vector is therefore $\mathbf{r}(i)$, $F_e(i)=\operatorname{sign}\left(y(i)\right)-y(i)$, and the receiver gain corresponds to the receiver gain of the biased MMSE filter denoted by θ_M. The necessary terms to perform the steady-state and tracking analysis are derived in a similar fashion to the Sato cost function,

$$E\{e_a F_c\} = E\{e_a(\text{sign}(y) - y)\} = \zeta. \tag{2.96}$$

$$E\{F_c^2\} = E\{(\text{sign}(y) - y)^2\} = (1 - A_1)^2 + \eta^2 + \sigma^2 + \zeta. \tag{2.97}$$

The steady-state and tracking EMSE is thus given by,

$$E\{e_a F_c\} = G + T.E\{F_c^2\}$$
$$\zeta = G + T.\left((1 - A_1)^2 + \eta^2 + \sigma^2 + \zeta\right). \tag{2.98}$$

where $G = \frac{1}{2\mu}\text{Tr}(\mathbf{Q})$ and $T = \frac{\mu}{2}\text{Tr}(\mathbf{C})$. The transient performance is computed using,

$$h_{0i} = E\{F_c^2(i)\} = (1 - A_1)^2 + \eta^2 + \sigma_n^2. \tag{2.99}$$

$$h_{Ci} = \frac{E\{e_a(i)F_c(i)\}}{E\{e_a^2(i)\}} = 1. \tag{2.100}$$

2.8.6 Normalised algorithms

It is possible to derive normalised versions of the above algorithms (if they have not already been defined) if the substitution is made,

$$\mu(i) = \frac{\mu}{\|\mathbf{u}(i)\|^2}. \tag{2.101}$$

These types of algorithms could be particularly useful considering the fading nature of the wireless communications systems that causes the signal levels to fluctuate over a large dynamic range. Normalised algorithms are inherently more stable in such scenarios since the step size is dynamically adjusted as per (2.101). This modification can easily be incorporated into the steady-state and tracking analysis if F_c is expressed in terms of the original (non-normalised) cost function F_c' and $1/\|\mathbf{u}(i)\|$ via the relationship,

$$F_c = \frac{F_c'}{\|\mathbf{u}(i)\|^2}. \tag{2.102}$$

The simplified energy preserving equation (2.41) can then be further simplified:

$$
\begin{aligned}
E\{e_a F_c\} &= G + E\left\{\tfrac{\mu}{2}\left\|\mathbf{u}(i)\right\|^2 F_c^2\right\} \\
E\left\{e_a \frac{F_c'}{\left\|\mathbf{u}(i)\right\|^2}\right\} &= G + \tfrac{\mu}{2} E\left\{\left\|\mathbf{u}(i)\right\|^2 \left(\frac{F_c'}{\left\|\mathbf{u}(i)\right\|^2}\right)^2\right\} \\
E\{\bar{\mu}\} E\{e_a F_c'\} &= G + \tfrac{\mu}{2} E\{\bar{\mu}\} E\left\{(F_c')^2\right\} \\
E\{e_a F_c'\} &= \mathrm{Tr}(\mathbf{R}) G + \tfrac{\mu}{2} E\left\{(F_c')^2\right\}
\end{aligned}
\tag{2.103}
$$

where $\mathrm{Tr}(\mathbf{R}) = 1/E\{\bar{\mu}\}$ and the expressions $E\{e_a F_c'\}$, and $E\left\{(F_c')^2\right\}$ have already been simplified in the non-normalised case. The steady-state performance of the normalised version of the adaptive algorithm therefore corresponds to the conventional algorithm (non-normalised) when $T = \frac{\mu}{2}$ is used. Similarly, the tracking performance of the normalised version of an adaptive algorithm can be calculated via the formula for the conventional algorithm if the additional substitution $G = \frac{1}{2\mu}\mathrm{Tr}(\mathbf{R})\mathrm{Tr}(\mathbf{Q})$ is made.

2.8.7 Summary

A summary of the EMSE expressions derived for the various blind adaptive MUD's in this chapter is given in Table 2.4.

Table 2.4. Summary of expressions quantifying the adaptive performance of various blind adaptive MUD's.

Algorithm	Cost Function	F_e	EMSE (ζ) expression	h_C	h_G	$E\|\mathbf{u}(i)\|^2$	θ
LCCMA (CMA2-2, Canonical)	$E\left\{\left(\|y(i)\|^2 - R_2\right)^2\right\}$	$y(i)\left(y^2(i) - R_2\right)$	$J_2\zeta^2 + J_1\zeta = G + T.\left(K_3\zeta^3 + K_2\zeta^2 + K_1\zeta + K_0\right)$	$K_3\zeta_i^3 + K_2\zeta_i^2 + K_1\zeta_i + K_0$	$3\zeta_i + J_1$	$\mathrm{Tr}(\mathbf{C}_\perp)$	A_1
LCCMA (CMA2-2, Non-canonical)	$E\left\{\left(\|y(i)\|^2 - 1\right)^2\right\}$	$y(i)\left(y^2(i) - 1\right)$	$J_2\zeta^2 + J_1\zeta = G + T.\left(K_3\zeta^3 + K_2\zeta^2 + K_1\zeta + K_0\right)$	$K_3\zeta_i^3 + K_2\zeta_i^2 + K_1\zeta_i + K_0$	$3\zeta_i + J_1$	$\mathrm{Tr}(\mathbf{C}_\perp)$	1
LCCMA (CMA1-2)	$E\left\{\left(\|y(i)\| - R_1\right)^2\right\}$	$R_1 \mathrm{sign}\left(y(i)\right) - y(i)$	$G + \frac{T}{1-T}\left(\left(R_1 - A_1\right)^2 + \eta^2 + \sigma_n^2\right)$	$\left(R_1 - A_1\right)^2 + \eta^2 + \sigma_n^2 + \zeta_i$	1	$\mathrm{Tr}(\mathbf{C}_\perp)$	A_1
Sato	$E\left\{\left(y(i) - \mathrm{sign}\left(y(i)\right)\right)^2\right\}$	$\mathrm{sign}\left(y(i)\right) - y(i)$	$G + \frac{T}{1-T}\left(\left(1 - A_1\right)^2 + \eta^2 + \sigma_n^2\right)$	$\left(1 - A_1\right)^2 + \eta^2 + \sigma_n^2 + \zeta_i$	1	$\mathrm{Tr}(\mathbf{C}_\perp)$	A_1
MOE	$E\left\{\|y(i)\|^2\right\}$	$-y(i)$	$G + \frac{T}{1-T}\left(A_1^2 + \eta^2 + \sigma_n^2\right)$	$A_1^2 + \eta^2 + \sigma_n^2 + \zeta_i$	1	$\mathrm{Tr}(\mathbf{C}_\perp)$	A_1
LCDCMA	$E\left\{\left(\|y(i)\|^2 - \|y(i-1)\|^2\right)^2\right\}$	$\left(y(i-1) - y(i)\right)\left(\|y(i)\|^2 - \|y(i-1)\|^2\right)$	$J_2\zeta^2 + J_1\zeta = G + T.\left(K_3\zeta^3 + K_2\zeta^2 + K_1\zeta + K_0\right)$	$K_3\zeta_i^3 + K_2\zeta_i^2 + K_1\zeta_i + K_0$	$2\zeta_i + J_1$	$\mathrm{Tr}(\mathbf{C}_\perp)$	A_1
DD-LMS	$E\left\{\frac{1}{2}\|\mathrm{sign}(y) - y\|^2\right\}$	$\mathrm{sign}\left(y(i)\right) - y(i)$	$G + T.\left(\left(1 - A_1\right)^2 + \eta^2 + \sigma^2\right)$	$\left(1 - A_1\right)^2 + \eta^2 + \sigma_n^2 + \zeta_i$	1	$\mathrm{Tr}(\mathbf{C})$	θ_M

Notes:

$T = (\mu/2)\mathrm{Tr}(\mathbf{R}), \quad \mathbf{R} = E\left\{\mathbf{u}(i)\mathbf{u}^H(i)\right\}$

$G = \mathrm{Tr}(\mathbf{Q})/2\mu$, for the code constrained algorithms the adaptive algorithm only tracks $\mathbf{w}_{opt}$.

$\eta^2 = E\left\{M^2(i)\right\} = \mathbf{w}_{opt}\mathbf{C}^*\mathbf{w}_{opt}$

$\sigma^2 = E\left\{v^2(i)\right\} = \mathbf{w}^H\left(\sigma^2\mathbf{I}\right)\mathbf{w}_{opt}$

For Normalised versions of the above algorithms use $T = (\mu/2)$ and $G = (1/2\mu)\mathrm{Tr}(\mathbf{R})\mathrm{Tr}(\mathbf{Q})$.

2.9 Results

2.9.1 Steady-state performance

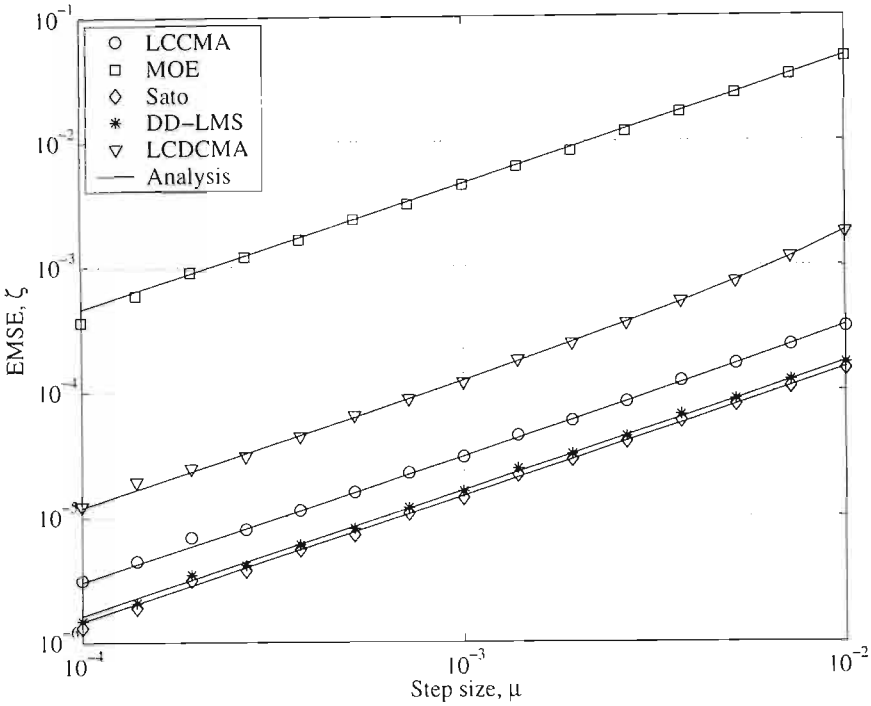

Fig. 2.13. Steady-state performance for various adaptive MUD's as a function of step size. A 10 users system with 25dB SNR for all users is considered.

A comparison between the steady-state EMSE of the LCCMA, MOE, Sato, DD-LMS, and LCDCMA cost functions for a range of step size values, is made in Fig. 2.13. A 10 user system is considered where the SNR of all the users is 25dB. The solid lines represent the theoretical steady-state EMSE of the different cost functions. The data markers correspond to the EMSE calculated from the simulation where the EMSE at each data point is taken from the average of 10^6 iterations. The different algorithms have different rates of convergence for a given step size and therefore it is better to compare speeds with which two adaptive algorithms reach the same EMSE level (as is done in the transient analysis section). The steady-state EMSE study presented in this section is still of use because the rate of convergence between algorithms does not generally differ by orders of magnitude. The fact that the EMSE of the MOE cost function is nearly 3 orders of magnitude higher than the DD-LMS and Sato cost functions for a given step size it is possible to conclude that the MOE cost function suffers from poor steady-state performance in comparison. It also appears as though the LCCMA has better steady-state performance compared to the LCDCMA. The Sato cost function has a slight edge over the DD-LMS algorithm as the Sato cost function is an orthogonally anchored algorithm, and thus only the smaller adaptive component of the filter coefficients contributes to the steady-state EMSE of the Sato cost function. The steady-state analysis is also of use as certain characteristics of a particular cost function may also be identified, and these in turn can hint at the appropriateness

or inappropriateness of a particular algorithm. One such characteristic of the MOE cost function is identified in Fig. 2.14 below.

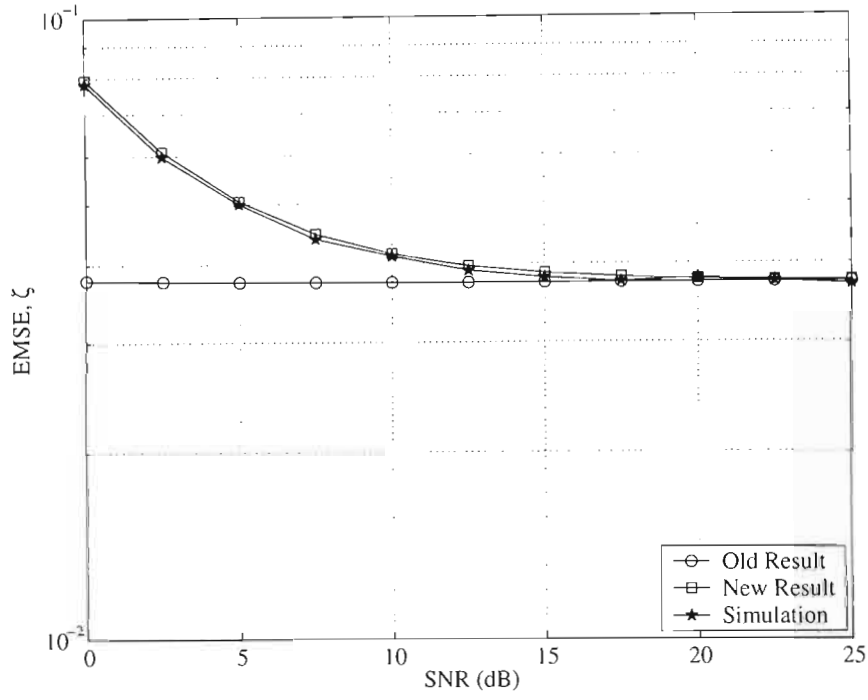

Fig. 2.14. Theoretical and simulated steady-state EMSE values for the MOE detector as a function of SNR for a 10 user system. "Old result" refers to the EMSE predicted by [25].

Fig. 2.14 demonstrates the inaccuracy of the expression for the MOE detector's EMSE given in [25], compared to the new expression (2.65) derived in this thesis. The EMSE is expressed as a function of SNR for a 25 user system with a MAI ratio of 10dB's, and $\mu = 3\times10^{-5}$. Fig. 2.14 also illustrates that the previous EMSE analysis underestimates the EMSE as the SNR decreases. The simulation results concur with the new expression closely which indicates the higher accuracy of the new expression. The old expression for the EMSE only becomes accurate as the SNR becomes very high (>20dB's in this example), due to the types of assumptions made in [25] to arrive at the EMSE expression therein. It is observed that unlike the LCCMA, the MOE's steady-state EMSE does not go to zero as the SNR increases; this is a severe disadvantage that is characteristic of the MOE cost function.

2.9.2 Tracking performance

The time varying channel was simulated in the same manner as described in Section 2.6.3. The average value of $\mathrm{Tr}(\mathbf{Q}_\perp)$ was calculated from the simulation using the definition $\mathbf{q}_\perp(i) \triangleq \mathbf{w}_\perp^{opt}(i+1) - \mathbf{w}_\perp^{opt}(i)$, and was used in the analysis.

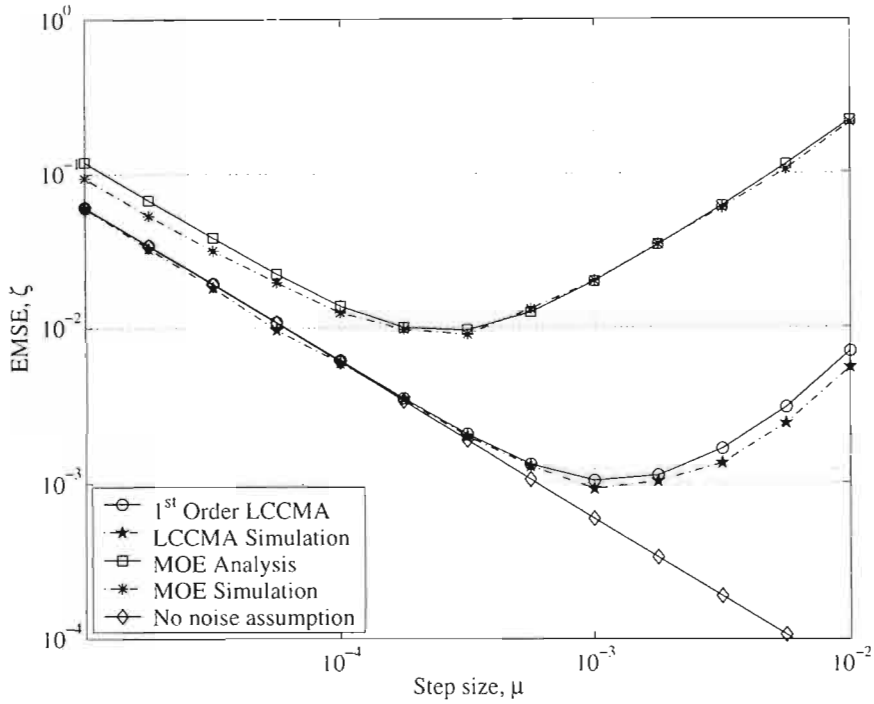

Fig. 2.15. Theoretical and simulated EMSE values for LCCMA and MOE as a function of step size, in a non-stationary channel. The "no noise" assumption was made in [54].

The MOE and canonically constrained LCCMA are plotted together in Fig. 2.15. A 10 user system with 20dB SNR and MAI level of 3dB's was considered, where $\mathrm{Tr}(\mathbf{Q}_\perp) = 2.4\times10^{-6}$. The optimum value for μ is correctly predicted by the analysis for both the MOE and LCCMA receivers. The superior performance of the LCCMA MUD is clearly evident under these operating conditions, as it achieves a lower minimum EMSE level. The inapplicability of the assumption in [54], for this system, that AWGN may be neglected, is also illustrated in this figure as the EMSE analysis using this assumption, given in (2.44), is plotted along side the correct analysis.

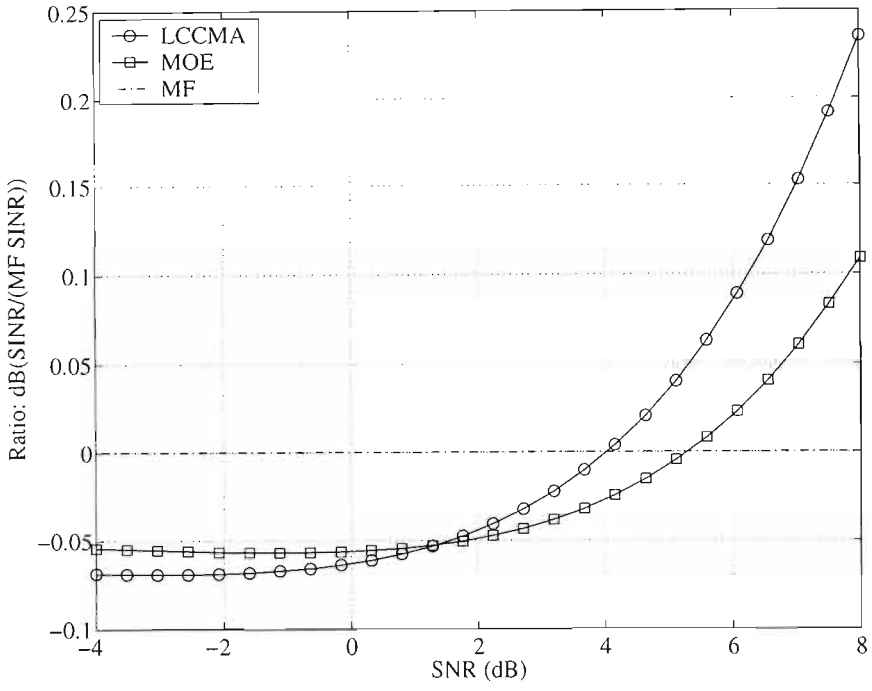

Fig. 2.16. The highest attainable SINR at the output of the LCCMA and MOE detector, relative to the single user matched filter, as a function of SNR, expressed in decibels.

Under different operating conditions it is possible that some blind adaptive MUD algorithms may perform better than others. This phenomenon can be investigated by comparing the output SINR at the lowest attainable EMSE for the adaptive algorithms, which occurs when the optimum choice of μ is used in each algorithm. For example, when the SNR decreases it is possible that the MOE detector might offer better performance than the LCCMA. Fig. 2.16 shows a system with 21 equal power users and $\mathrm{Tr}(\mathbf{Q}_{\perp}) = 3.5\times10^{-6}$. The maximum achievable output SINR of the MOE and LCCMA detector, relative to the single user matched filter (MF), is plotted. It can be seen that MOE never offers better performance than the LCCMA in the region where the LCCMA offers an improvement over the MF. The knowledge of the location of the MF/LCCMA crossover point is also a useful result.

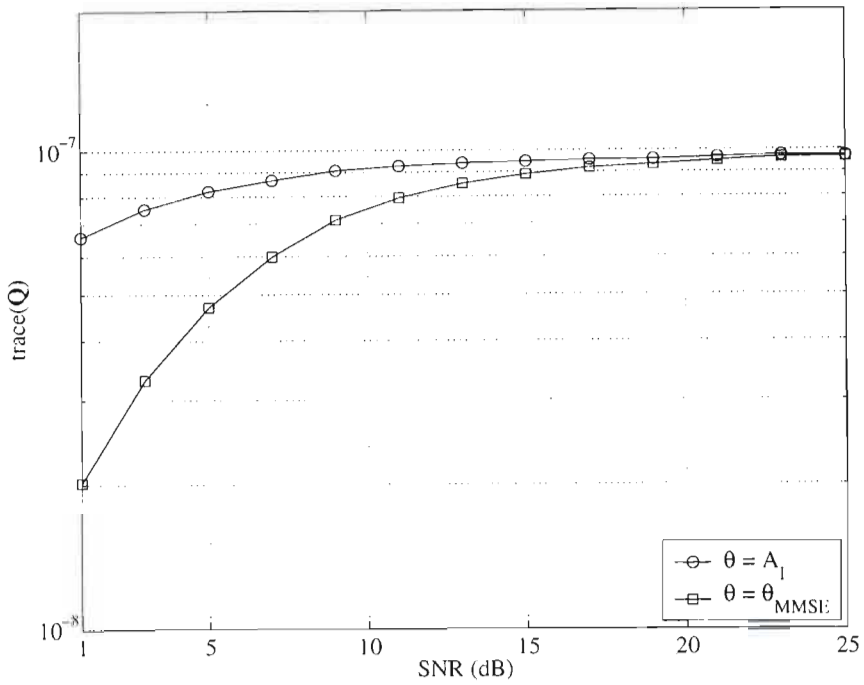

Fig. 2.17. Plot of trace($\mathbf{Q}$) as a function of SNR for canonically constrained filter coefficients and biased MMSE filter. 10 user system with a 3dB MAI ratio.

The effect that the constraint has on the tracking requirements of the adaptive algorithms is illustrated graphically in Fig. 2.17. A 10 user system with a 3dB MAI ratio was considered for the purposes of this study. The time varying channel model, as described in Section 2.6.3, does not affect the value of A_1, which is set to 1 for this system. The curve $\theta = A_1$ therefore corresponds to both canonically and non-canonically constrained filter coefficients. The value of $\mathrm{Tr}(\mathbf{Q})$ is observed to decrease as the SNR decreases because as the SNR tends to zero (minus infinity on the dB scale), the MMSE filter approaches the single user matched filter, which is not tracked by the adaptive filter. The value of $\mathrm{Tr}(\mathbf{Q})$ for the biased MMSE filter coefficients, as given in (2.60), decreases at a faster rate because the magnitude of the filter coefficients, $\|\mathbf{w}_{MMSE}\|$, also tends to zero as the SNR approaches zero. The difference in tracking requirements of the canonically and non-canonically constrained filter becomes apparent when the amplitude of the desired user is time varying. This phenomenon is studied in more detail in Section 4.5. The canonically and non-canonically constrained LCCMA therefore have equivalent performance levels for the time varying channel under consideration in this section.

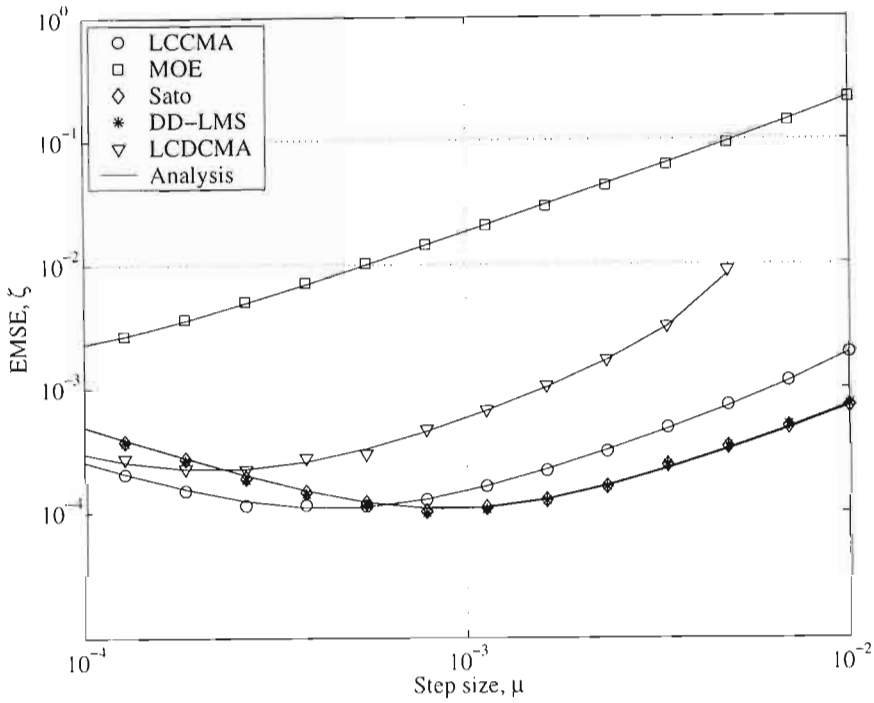

Fig. 2.18. Theoretical and simulated EMSE values for various blind adaptive MUD schemes as a function of step size, in a non-stationary channel. 10 users, 3dB MAI ratio, with desired user SNR=25dB.

The relative tracking ability of the LCCMA, MOE, Sato, DD-LMS, and LCDCMA cost functions is examined in Fig. 2.18. A 10 user system with an MAI ratio of 3dB's is considered where the SNR of the desired user is 25dB. The time varying channel was configured such that $\mathrm{Tr}(\mathbf{Q}) = 9.6\times10^{-8}$ for the DD-LMS algorithm and $\mathrm{Tr}(\mathbf{Q}) = 9.7\times10^{-8}$ for the other algorithms. The data markers represent the EMSE computed from the simulation data where an average from 10^5 iterations was used for each point. It can be seen in Fig. 2.18 that the Sato and DD-LMS algorithms have nearly equivalent performance levels. The LCCMA achieves a nearly identical minimum EMSE value but at a lower step size value. This clearly illustrates the usefulness of the tracking analysis as a tool for quantifying the relative ability of the adaptive algorithms, as it is possible to use Fig. 2.18 to show that the LCCMA has nearly the same adaptive performance as the benchmark DD-LMS and Sato algorithms. This is something that could not be shown using the steady-state analysis alone. Fig. 2.18 also shows that the LCDCMA algorithm has worse performance compared to LCCMA. A phenomenon of LCDCMA that is accurately captured by the analysis is that as the step size increases, the EMSE of LCDCMA increases more rapidly than any of the other algorithms. The poor performance of the MOE cost function is again evident in Fig. 2.18, lending credibility to the statement that constant modulus based MUD's are a very suitable choice.

2.9.3 Transient performance

The relative convergence speed of the various blind adaptive MUD algorithms is considered in Fig. 2.19 to Fig. 2.22. In those figures a 15 user system with a MAI ratio of 0dB and SNR of

20dB's is considered. All the MUD's are initialised to the single user matched filter. The theoretical learning curves are represented again with "dash-dot" lines and steady-state levels as predicted with the steady-state analysis have also been superimposed. The ensemble average of 100 independent simulation runs is used for all the simulation results. The time evolution of the EMSE when the step size of all the algorithms is set to 10^{-2} is given in Fig. 2.19. The time evolution of the output SINR of the same system is plotted in Fig. 2.20. The EMSE of MOE cost function actually increases above the level associated with the single user matched filter. This indicates a much smaller step size, and subsequent longer convergence time is required to the MOE MUD to yield a performance gain relative to the single user matched filter. This is evident in Fig. 2.20 as the steady-state SINR of the MOE MUD is approximately 5.5dB's lower than its initialisation point. From Fig. 2.19 the LCDCMA clearly has worse performance than the LCCMA as the LCCMA converges to a lower steady-state EMSE level and at a faster rate. This is manifested in Fig. 2.20 as the output SINR of the LCCMA is always higher than the LCDCMA. The situation regarding the relative performance of LCCMA, Sato and DD-LMS is less clear. The Sato cost function and DD-LMS have equivalent performance levels, but the LCCMA converges faster than these algorithms. The Sato and DD-LMS cost functions however converge towards a lower steady-state EMSE.

To resolve this uncertainty, the same system is considered in Fig. 2.21 and Fig. 2.22 but the step size of the Sato and DD-LMS cost functions is increased to 2×10^{-2}. This increase in step size causes the adaptive algorithms to converge faster and be encumbered with a higher steady-state EMSE. Examining Fig. 2.22 the learning curves of the output SINR of the LCCMA, Sato and DD-LMS cost functions are nearly indistinguishable, indicating that these algorithms have nearly equivalent adaptive performance levels. This property was also established in Fig. 2.18. This result also reinforces the importance of evaluating the time evolution of the SINR as opposed to just the EMSE. The absolute EMSE levels are not directly comparable because the different adaptive algorithms converge to differently scaled optimal filter coefficients. This is evident in Fig. 2.21 and Fig. 2.22 as both the EMSE learning curves and steady-state EMSE levels of LCCMA, Sato and DD-LMS are much further apart in Fig. 2.21 than the corresponding SINR learning curves and steady-state levels in Fig. 2.22.

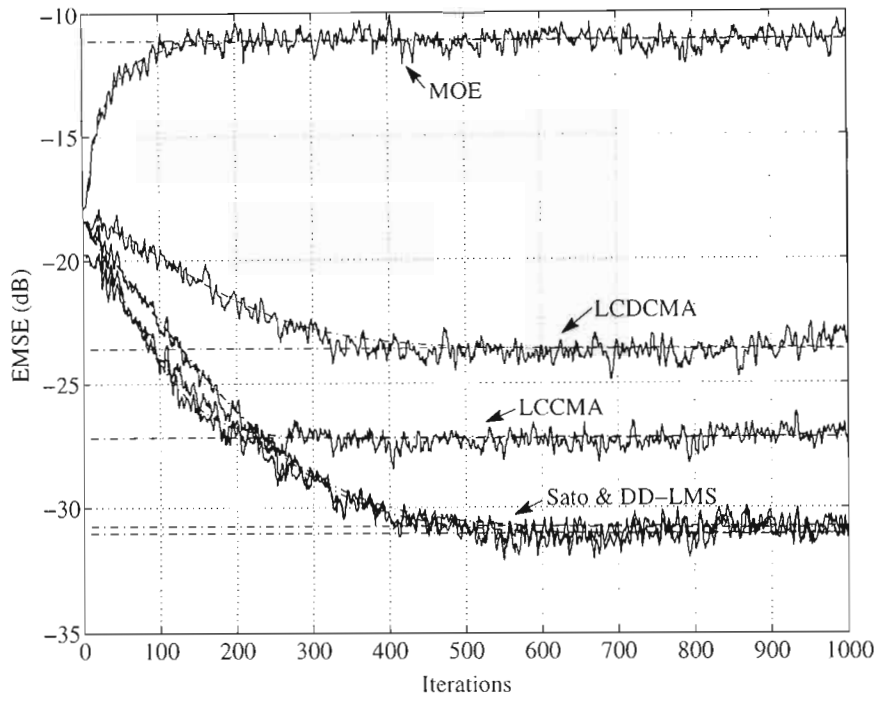

Fig. 2.19. Theoretical and simulated transient behaviour of the EMSE where the step size of all the algorithms is set to 10^{-2}. Theoretical steady-state levels are also shown.

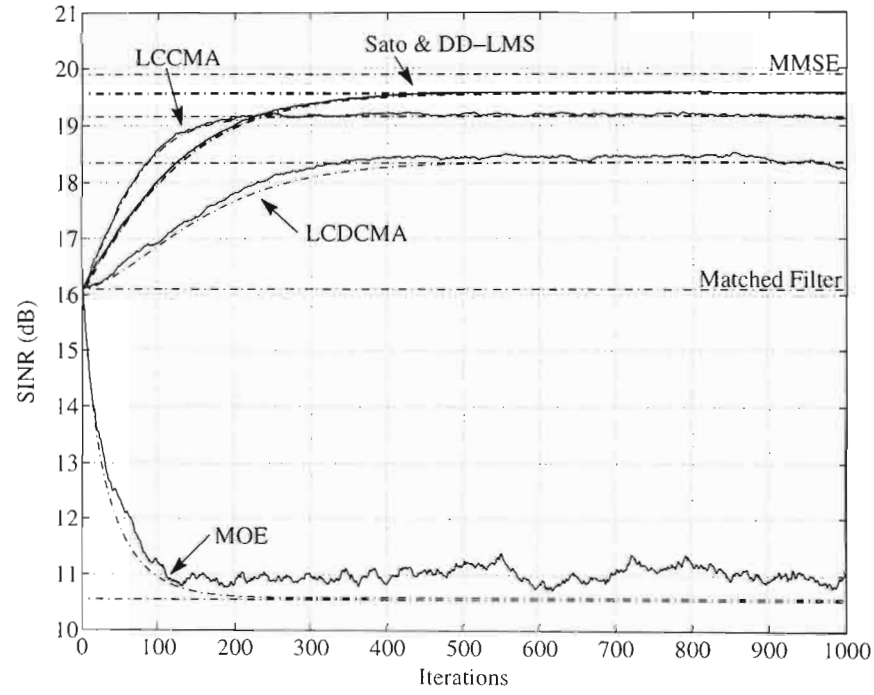

Fig. 2.20 Theoretical and simulated transient behaviour of the SINR where the step size of all the algorithms is set to 10^{-2}. Theoretical steady-state levels are also shown.

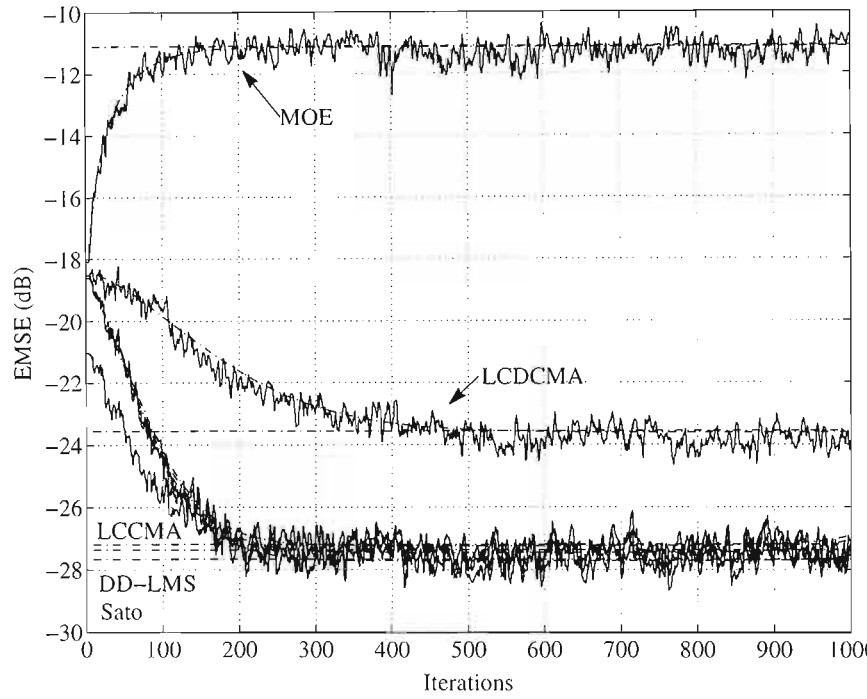

Fig. 2.21 Theoretical and simulated transient behaviour of the EMSE where the step size of MOE, LCDCMA and LCCMA is 10^{-2}, and the DD-LMS and Sato cost functions are 2×10^{-2}. Theoretical steady-state levels are also shown.

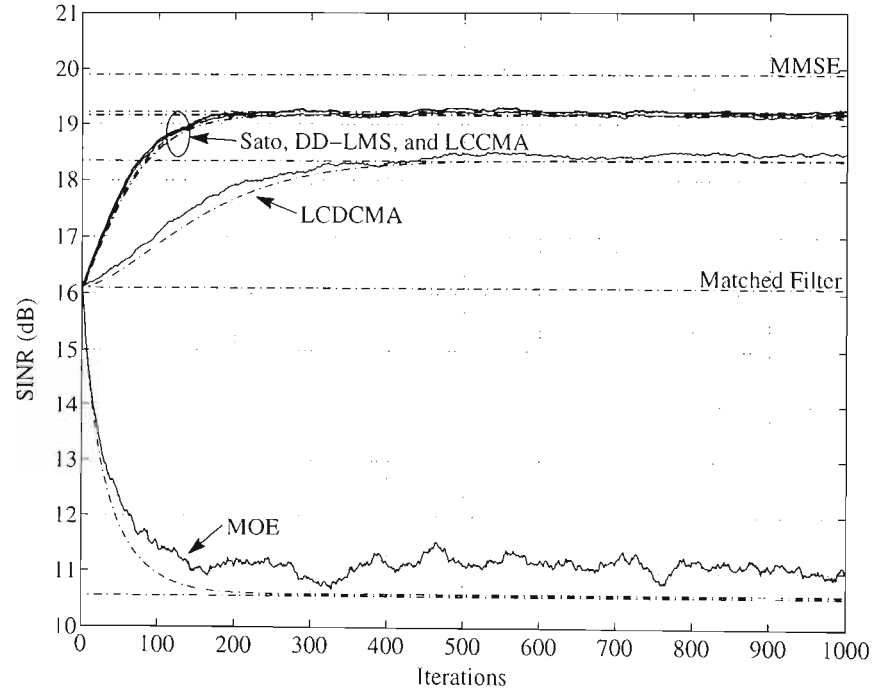

Fig. 2.22. Theoretical and simulated transient behaviour of the SINR where the step size of the MOE, LCDCMA and LCCMA is 10^{-2}, and the DD-LMS and Sato cost functions are 2×10^{-2}. Theoretical steady-state levels are also shown.

2.10 Summary

This chapter considered the steady-state, tracking, and transient performance of the LCCMA and other blind adaptive MUD's for DS-CDMA systems. New closed form expressions were derived for these detectors using the feedback approach. The algorithms that were explicitly analysed were: LCCMA (both canonical and non-canonical, and CMA2-2 and CMA1-2 cost functions), LCDCMA, Sato, MOE, and DD-LMS. The expressions that were derived accurately predicted the transient and misadjustment performance, in terms of EMSE and SINR, for both stationary and non-stationary channels. These results have not been previously published for other blind adaptive MUD's. A methodology has been presented in this chapter that enables the application of the feedback approach and energy conservation arguments to other DS-CDMA blind adaptive MUD's that can be made to fit the correct generic class of algorithm.

The accuracy of the analyses was verified using computer simulations. The equivalence between the formulas governing steady-state performance presented in [52]–[54] and those of [58] was also shown in this chapter. This equivalency was also borne out in the results as the transient analysis showed convergence to the same level predicted by the steady-state analysis.

The analysis enabled a comparative study between the MOE and LCCMA cost functions, and the results showed the superior stead-state, tracking, and convergence properties of the LCCMA. The LCCMA also demonstrated superior performance relative to the LCDCMA algorithm. The LCDCMA has the advantage, however, in that it does not require an estimate of the desired user's amplitude. A popular approach is to switch over to DD-LMS after initial convergence by more robust algorithms [25], [76] since DD-LMS closely approximates the trained LMS performance levels. This chapter showed that the adaptive performance of LCCMA was comparable with DD-LMS, the benchmark scheme for blind adaptive algorithms. The DD-LMS algorithm relies on the feedback of correct bit decision, and feedback of incorrect bit decision can lead to complete failure of the receiver, and thus its use is only recommended in reliable communications channels. This is not an issue with LCCMA as its convergence can be guaranteed. The performance levels of the Sato and similar LCCMA (CMA1-2) cost functions were also comparable with DD-LMS, and they are also more robust compared to DD-LMS. It should be noted, however, that rigorous mathematical proofs of their convergence do not exist, and so a concern is raised over their reliability and robustness. With performance levels of LCCMA approaching that of the fully trained systems, indications are that it is possible to omit pilot channels and training sequences and not suffer from a perceptible drop in performance. The applicability of constant modulus based blind adaptive MUD's is thus proved.

Chapter 3

Constant Modulus Based Cyclic MUD

3.1 Introduction

Future generation wireless communications systems based on DS-CDMA will be characterized by their flexibility to offer various services such as voice, data, and multimedia over the same air interface [8]. These heterogeneous services are characterized by their differing quality of service (QoS) and data rate requirements. Multi-rate DS-CDMA has been suggested to provide such flexibility [8]. When multi-rate DS-CDMA is used in combination with short spreading codes, it is possible to exploit the cyclostationary statistics of the received signal to greatly enhance the reliability of the communications link. Narrowband interference (NBI) sources, which arise in overlay systems, may also be efficiently suppressed by exploiting their cyclostationarity.

Cyclic multiuser detection (MUD) is one such technique that has been suggested to exploit the cyclostationary signal statistics and suppress multi-rate multiple access interference (MAI) and NBI [77] as it offers superior performance compared to conventional MUD techniques. Recently, cyclic decorrelating and MMSE receivers were defined for synchronous variable spread length (VSL) multi-rate DS-CDMA systems in [78] and [79] respectively. This concept was expanded to include an asynchronous multi-rate DS-CDMA system in [60], and specialised in [80] for the case where binary phase-shift keying (BPSK) modulation is used. Adaptive implementations were proposed in [80] based on a decision aided (trained) recursive least squares (RLS) procedure. A blind (non-adaptive) implementation of the receiver was also proposed in [80] whereby an off-line estimate of the correlation properties of data was used. A blind adaptive receiver was proposed in [60] based on a new cyclic RLS algorithm which minimised the minimum output energy (MOE) cost function (as defined in [25]). The convergence of this algorithm can be guaranteed, but it suffers from poor steady-state performance compared to (for example) the decision-directed (DD) mode of operation. The computational complexity of the algorithm in [60] was reduced by making use of the block circulant structure of the associated covariance matrices, nevertheless the computational complexity is still high. Noting these points, a lower complexity cyclic MUD algorithm based on iterative cyclic subspace tracking was developed in [81]. However, as acknowledged by the authors in [81], even this algorithm may prove to be too computationally complex for high dimension systems, and thus there is a need to develop low complexity, cyclic MUD.

The suppression of NBI in an asynchronous DS-CDMA overlay system that undergoes frequency selective fading was addressed in [82], through the use of off-line batch processing (i.e. non-adaptive detection). A comprehensive overview of the topic of NBI suppression in DS-

CDMA overlay systems is contained in [77], where it is shown how NBI can be modelled using a VSL multi-rate DS-CDMA system model. The equivalence between the two problems, NBI and multi-rate MAI suppression, is thus established.

The essential difference between cyclic MUD and conventional MUD is that cyclic MUD employs a periodically time varying (PTV) filter to the received vector of samples. A direct implementation of a PTV filter would consist of a bank of time invariant filters that are selected sequentially. This architecture is referred to as the filter bank. A frequency domain implementation of a PTV filter was proposed in [83] and is referred to as the frequency shift (FRESH) filter implementation. FRESH filters have some desirable characteristics. Firstly, they offer some computational efficiencies over the filter bank implementation [83]. Secondly, they have the ability to be implemented in a flexible or suboptimal manner whereby complexity may be reduced at the expense of performance. Exploiting this feature to enable lower complexity cyclic MUD's has been suggested in [77], [60] and [80]. It has not, however, been established in the literature on which architecture (filter bank or FRESH) an adaptive filter would operate best.

The first major contribution of this chapter is a new, low complexity, blind adaptive cyclic MUD based on a FRESH filter which is adapted via a modified version of the linearly constrained constant modulus algorithm (LCCMA) [30]. This technique offers the flexibility of the FRESH architecture combined with the low complexity of a stochastic gradient algorithm for adaptation, which has a significantly lower computational complexity as compared with the previously suggested cyclic recursive least squares (RLS) and subspace tracking algorithm of [60] and [81] respectively. The LCCMA algorithm was chosen due to its proven convergence ability in DS-CDMA, and its superior adaptive performance compared to the MOE cost function, as ascertained in Chapter 2. A proof of the global convergence of the new algorithm (referred to as FRESH-LCCMA) is also given in this chapter, and constitutes a second original contribution made in this chapter. This proof is given in order to ensure the robustness of the new algorithm. The excellent performance of this new algorithm relative to its computational complexity is shown via a performance comparison with the algorithms given in [60] and [81].

The third contribution of this chapter is an investigation into the relative performance of the different suboptimal FRESH filters, in the context of cyclic MMSE MUD. Given the dimension of a particular suboptimal FRESH filter, there exists a multitude of possible cyclic MMSE filters that it can implement. No theory or investigation exists, to the best of the author's knowledge, into determining the optimal MMSE filter given only the dimension of the suboptimal FRESH filter and system statistics.

The fourth contribution of this chapter is the derivation of the steady-state, tracking and transient performance of FRESH-LCCMA, using an extension of theory developed in Chapter 2. The performance of the new algorithm is thus fully quantified. Alternate cost functions to LCCMA are also considered in this chapter to perform low complexity SGD based cyclic MUD

using the FRESH architecture. The new algorithms that are proposed are based on the: MOE, Sato, LCDCMA, and DD-LMS cost functions. The relative adaptive performance of FRESH-LCCMA is compared to these alternate cost functions, both analytically and through computer simulation, in order to prove the suitability of the constant modulus cost function to blind adaptive cyclic MUD. The relative adaptive performance of the new algorithms on suboptimal FRESH architectures is also investigated. In addition, a recursive update procedure for the FRESH-LCCMA is given which yields an algorithm that is directly comparable (in terms of computational complexity) to [60]; it is shown in this chapter that the resulting receiver has superior performance owing to the superiority of the LCCMA cost function over the MOE cost function.

Using the feedback approach, this chapter also presents the first analytical framework in which the adaptive performance of filter bank and FRESH implementations may be directly compared. Previously, no conclusions could be drawn as to which architecture is superior in terms of the tracking capability and convergence speed of an adaptive algorithm, and thus this study constitutes the fifth significant contribution of this chapter.

The rest of this chapter is organized as follows: firstly a preliminary review of pertinent cyclostationary definitions is given. This is followed by an outline of the system model where multi-rate DS-CDMA systems are discussed as well as PTV filtering architectures. The relationship between the time and frequency domain filters is then established when the outputs of the filters are sampled at the bit rate, as opposed to the rate that samples are clocked into the filters. The next section, 3.4, details the cyclic MMSE filter equations. A novel study of the different suboptimal-FRESH MMSE receivers is conducted in this section. The new cyclic MUD algorithms are devised in Section 3.5. The performance analysis of these algorithms is carried out in Section 3.6, where a proof of the global convergence of the new FRESH-LCCMA is given as well as the adaptive performance quantified using an extension of the theory developed in Chapter 2. The performance of the new algorithms is investigated in the results Section 3.7, and finally a summary of the chapter is given in Section 3.8.

3.2 Cyclostationarity

A discrete time stochastic process $x(n)$ is said to be cyclostationary in the wide sense, if its mean and autocorrelation are periodic with some period T, i.e.

$$E\{x(n)\} = \mu_x(n) = \mu_x(n+T) \tag{3.1}$$

$$E\{x(n_1)x(n_2)\} = R_{xx}(n_1,n_2) = R_{xx}(n_1+T,n_2+T) \tag{3.2}$$

for all n_1 and n_2. The Fourier expansion of $\mu_x(n)$ and $R_{xx}(n_1,n_2)$ at fixed frequency α are denoted by

$$\mu_x^{\alpha}$$

$$R_{xx}^{\alpha}(n_1 - n_2).$$

These are the *cyclic mean* and *cyclic autocorrelation* functions of $x(n)$. Formal definitions:

$$\begin{aligned} \mu_x^{\alpha} &= \lim_{N\to\infty} \left\langle \mu_x(n)\exp(-j2\pi\alpha n)\right\rangle_N \\ &\triangleq \lim_{N\to\infty} \frac{1}{N}\sum_{n=1}^{N} E\{x(n)\}\exp(-j2\pi\alpha n) \end{aligned} \tag{3.3}$$

$$\begin{aligned} R_{xx}^{\alpha}(k) &= \lim_{N\to\infty} \left\langle R_{xx}(n,k)\exp(-j2\pi\alpha n)\right\rangle_N \\ &\triangleq \lim_{N\to\infty} \frac{1}{N}\sum_{n=1}^{N} E\{x(n+k)x(n)\}\exp(-j2\pi\alpha n) \end{aligned} \tag{3.4}$$

where $\langle\cdot\rangle_N$ denotes time average over N samples. The set of α for which $R_{xx}^{\alpha} \not\equiv 0$ is called the *cycle spectrum*, and α is called a *cycle frequency*. Note, the Fourier *transform* (as opposed to the Fourier series representation) applies to systems that are *almost* cyclostationary (e.g. measured noisy data).

3.3 System model

3.3.1 Multi-rate CDMA and overlay systems

There are four major types of multi-rate access schemes associated with DS-CDMA communications systems, these are: multi-code [84], variable spread length (VSL) [8], variable chip-rate (VCR) [85], and variable chip-rate with frequency shift (VCRFS) [86]. The multi-code technique enables a particular user to transmit on multiple spreading codes simultaneously, thereby increasing the net data rate. In the VSL scheme the chip duration for all data rates is constant but the number of chips per code differs between the high rate and low rate users, and hence the VSL designation. In a VSL system shorter spreading codes correspond to higher data rates. In a VCR scheme, the different data rates are assigned different chip durations or rates. The higher data rates are assigned higher chipping rates to boost the data throughput. The VCRFS scheme exploits the fact that in a VCR system, the low rate users occupy a smaller bandwidth compared to the high rate users, and it is therefore possible to shift the carrier frequency of the low rate users away from the carrier frequency of the high rate users to improve system performance. This is performed in VCRFS, and hence the VCRFS designation.

It was found in [87] and [88] that the VSL scheme offers better performance compared to the multi-code access scheme. It was also shown in [60] that the VSL scheme favours the low rate users and the VCR scheme favours the high rate users, and that the VCRFS scheme outperforms both the VSL and VCR for both high and low rate users.

The modelling of NBI as virtual-users in a VSL multi-rate DS-CDMA system is dealt with extensively in [77]. Suffice it to say then that an analysis of the ability of a blind adaptive MUD to suppress VSL multi-rate MAI is indicative of its ability to suppress NBI arising in overlay

systems. This is one of the motivating reasons behind considering a VSL multi-rate access scheme in this chapter.

There is a large choice of codes to choose from when considering the implementation of a VSL multi-rate access scheme for theoretical performance evaluations via computer simulation. The choice includes: random codes, Gold codes, Gold codes expanded with Walsh codes, and orthogonal Gold codes. Random codes are useful from a theoretical point of view, but would require extensive simulations to average over possible code choices. Cross correlations are relatively high between random codes and performance levels of the system will thus not be indicative of realistic systems either. Different length Gold codes are not integer multiples of one another, and thus do not provide convenient ratios of data rates. Gold codes expanded with Walsh codes preserves the orthogonality between the multi-rate codes. This is useful for real systems, but from a simulation point of view obviates the need for PTV interference suppression. Cross correlation between multi-rate codes inevitably occurs due to propagation through an imperfect communications channel, and is the reason why interference suppression is required in the first place. Orthogonal Gold codes are thus chosen as the different lengths of the codes are integer multiples of one another. Codes of the same length are orthogonal but significant cross correlation levels occur between codes of different lengths.

3.3.2 Received vector of samples

The complex baseband representation of the received signal of an asynchronous multirate DS-CDMA system at time t may be expressed by,

$$r(t)=\sum_{k=0}^{K-1}A_k\sum_{i=0}^{\infty}b_k(i)s_k\left(t-\tau_k-iT_{b,k}\right)+n(t) \tag{3.5}$$

where K is the number of users, A_k is the amplitude of the kth user, and $b_k(i)\in\{\pm 1\}$ is the kth user's ith transmitted data symbol. The unit energy signature waveform of the kth user is denoted by $s_k(t)$, τ_k is the time offset, and $T_{b,k}$ is the bit duration of the kth user. The additive white Gaussian noise (AWGN) term $n(t)$ has power spectral density σ^2.

A variable spread length (VSL) dual-rate access scheme is considered in this chapter to illustrate the effectiveness of the new cyclic-algorithms. In this system the high rate user transmit data at a rate L times faster than the low rate users, and are thus assigned spreading sequences that are shorter by a factor $1/L$ to ensure that spread signals of both rates occupy the same amount of bandwidth. The signature waveforms are given by,

$$s_k^{HR}(t)=\frac{1}{\sqrt{N}}\sum_{n=0}^{N-1}c_k^{HR}(n)\,\mathrm{rect}_{T_c}\left(t-nT_c\right) \tag{3.6}$$

$$s_k^{LR}(t)=\frac{1}{\sqrt{LN}}\sum_{n=0}^{LN-1}c_k^{LR}(n)\,\mathrm{rect}_{T_c}\left(t-nT_c\right) \tag{3.7}$$

where HR and LR specify high rate and low rate respectively, N is the number of chips in the HR spreading sequence, $c_k^{(\cdot)}(n)$ is the nth chip of the spreading code assigned to user k, and

$\text{rect}_T(.)$ is the unit-height rectangular pulse supported on $[0,T]$. From here on let the desired user be user 1, and be assigned a HR spreading code.

The receiver samples the output of a chip-matched filter to convert the received signal into discrete samples. The samples within processing window i are stacked to form a vector $\mathbf{r}(i)$, which is used to detect $b_1(i)$, which is the ith bit of the desired user. This chapter considers the case where processing window i spans bit interval i of the desired user, and the detector operates on a symbol-by-symbol basis. For the sake of brevity only, this thesis also only considers the case of rectangular shaped chip pulses and a sample rate equal to that of the chip rate.

3.3.3 PTV filtering

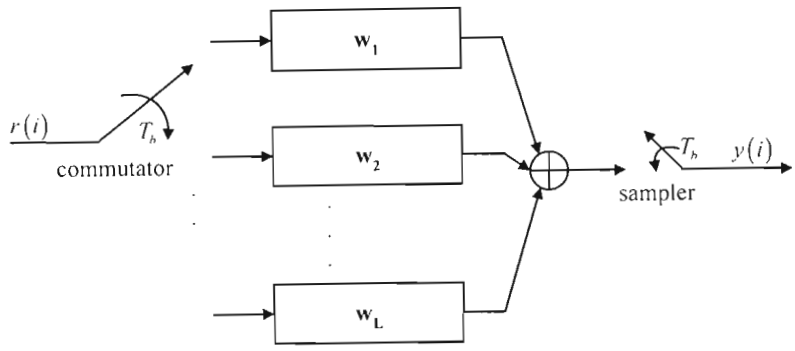

Fig. 3.1. Filter bank implementation of a PTV filter.

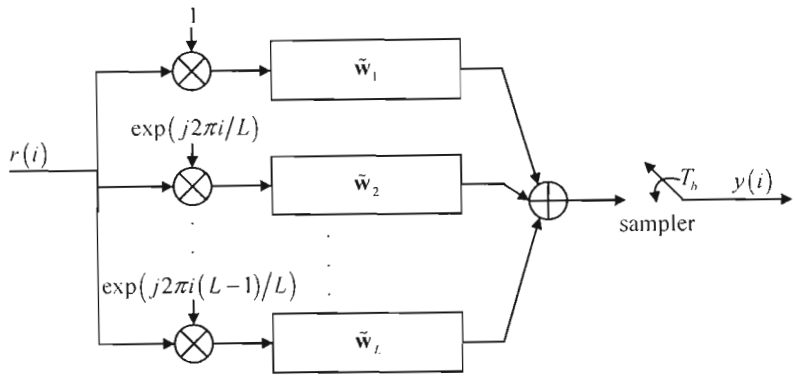

Fig. 3.2. FRESH filter implementation of a PTV filter.

A time domain implementation of a PTV filter is illustrated in Fig. 3.1. The commutator selects the individual filters $\{\mathbf{w}(1),\mathbf{w}(2),\ldots,\mathbf{w}(L)\}$ in the bank sequentially to produce a PTV filter of period L. The frequency domain implementation of this filter is given in Fig. 3.2. The FRESH architecture filters L frequency shifted versions of the input signal simultaneously and combines the output of each of these L branches. With the proper selection of the FRESH filter coefficients $\{\tilde{\mathbf{w}}_1,\tilde{\mathbf{w}}_2,\ldots,\tilde{\mathbf{w}}_L\}$, the two architectures are exactly equivalent. This equivalence is established below for the case where the outputs of the filters is sampled at the bit rate. This derivation follows along the same lines as that in [83] but is slightly modified since in [83] the output of the filters are sampled at the same rate at which samples are clocked in, which is equivalent to the chip-rate for the system under consideration.

Assume there are M filters of length N each. The operation of the sampler on the mth filter is mathematically equivalent to multiplying its output by

$$\delta_m(n)=\begin{cases}1, & \text{if } n=m,\ m\pm M,\ m\pm 2M,\ldots,\\ 0, & \text{otherwise,}\end{cases} \tag{3.8}$$

where n indexes the bit epoch. This function may in turn be represented mathematically by,

$$\tilde{\delta}_m(p)=\frac{1}{MN}\sum_{i=0}^{MN-1} e^{\frac{j2\pi i(p-mN)}{MN}} \tag{3.9}$$

or

$$\delta_m(n)=\frac{1}{M}\sum_{i=0}^{M-1} e^{\frac{j2\pi i(n-m)}{M}} \tag{3.10}$$

where p indexes the received samples. Since the filters are sampled every $p=nN$ samples, then the output of the filter may be written as,

$$\begin{aligned} y(n)&=\sum_{m=0}^{M-1}\left(\left\{x(p)*h_m(p)\right\}\cdot\tilde{\delta}_m(p)\right)\\ &=\sum_{m=0}^{M-1}\left(\left\{x(nN)*h_m(nN)\right\}\cdot\tilde{\delta}_m(nN)\right)\\ &=\sum_{m=0}^{M-1}\left(\left\{x(nN)*h_m(nN)\right\}\cdot\frac{1}{M}\sum_{i=0}^{M-1} e^{\frac{j2\pi i(n-m)}{M}}\right) \end{aligned} \tag{3.11}$$

where $x(p)$ is the input sequence to the filter, $*$ denotes the convolution operator, and $h_m(p)$ is the impulse response of the mth filter. The z-transform of this term is given by,

$$\begin{aligned} Y(z)&=\sum_{n=-\infty}^{\infty} y(n)z^{-n}\\ &=\sum_{n=-\infty}^{\infty}\sum_{m=0}^{M-1}\left(\left\{x(nN)*h_m(nN)\right\}\cdot\frac{1}{M}\sum_{i=0}^{M-1} e^{\frac{j2\pi i(n-m)}{M}}\right)z^{-n}\\ &=\sum_{n=-\infty}^{\infty}\sum_{m=0}^{M-1}\left(\left\{x(nN)*h_m(nN)\right\}\cdot\frac{1}{M}\sum_{i=0}^{M-1} e^{\frac{j2\pi in}{M}}e^{\frac{-j2\pi im}{M}}\right)z^{-n}. \end{aligned} \tag{3.12}$$

Denote the z-transform of $x(n)$ using the notation,

$$Z\left[x(n)\right]=X(z). \tag{3.13}$$

By using the modulation rule $Z\left[\exp(-an)x(n)\right]=X\left(\exp(a)z\right)$ inside the convolution rule $Z\left[x(n)*h_m(n)\right]=X(z)H(z)$ in (3.12), and letting $\tilde{x}(n)=x(nN)$, such that $Z\left[x(nN)\right]=Z\left[\tilde{x}(n)\right]=\tilde{X}(z)$ then the z-transform of $y(n)$ may be expressed as,

$$\begin{aligned} Y(z) &= \sum_{n=-\infty}^{\infty}\sum_{m=0}^{M-1}\left(\left\{x(nN)*h_m(nN)\right\}\cdot\frac{1}{M}\sum_{i=0}^{M-1}e^{\frac{j2\pi m}{M}}e^{\frac{-j2\pi im}{M}}\right)z^{-n} \\ &= \frac{1}{M}\sum_{i=0}^{M-1}\sum_{m=0}^{M-1}e^{\frac{-j2\pi im}{M}}\tilde{X}\left(ze^{-\frac{j2\pi i}{M}}\right)\tilde{H}_m\left(ze^{-\frac{j2\pi i}{M}}\right) \\ &= \sum_{i=0}^{M-1}\tilde{X}\left(ze^{-\frac{j2\pi i}{M}}\right)\frac{1}{M}\sum_{m=0}^{M-1}\tilde{H}_m\left(ze^{-\frac{j2\pi i}{M}}\right)e^{\frac{-j2\pi im}{M}} \end{aligned} \tag{3.14}$$

since there is no "m" term in $\tilde{X}\left(ze^{-\frac{j2\pi i}{M}}\right)$ it may be taken outside the inner summation in line 2 of the above equation. Now taking the inverse z-transform:

$$\begin{aligned} y(n) &= \sum_{i=0}^{M-1}\left\{x(nN)e^{\frac{j2\pi in}{M}}\right\}*\left\{\frac{1}{M}\sum_{m=0}^{M-1}h_m(nN)e^{\frac{j2\pi in}{M}}e^{\frac{-j2\pi im}{M}}\right\} \\ &= \sum_{i=0}^{M-1}\left\{x(nN)e^{\frac{j2\pi in}{M}}\right\}*\left\{\frac{1}{M}\sum_{m=0}^{M-1}h_m(nN)e^{\frac{j2\pi i(n-m)}{M}}\right\} \end{aligned} \tag{3.15}$$

Let

$$w_i(nN) = \frac{1}{M}\sum_{m=0}^{M}h_m(nN)e^{\frac{j2\pi i(n-m)}{M}} \tag{3.16}$$

such that,

$$y(n) = \sum_{i=0}^{M-1}\left\{x(nN)e^{\frac{j2\pi in}{M}}\right\}*w_i(nN) \tag{3.17}$$

which is recognised as the FRESH filter implementation, where $w_i(nN)$ is the nth filter coefficient of the ith branch of the FRESH filter. The output of the FRESH filter is thus the sum of M different frequency shifted version of the received vector of samples filtered by its corresponding filter. The M different frequencies are $\{0, 1/M, 2/M, \ldots, (M-1)/M\}$.

Equations (3.16) and (3.17) may be expressed more concisely if the following vector notation is used,

$$\mathbf{h}_m(n) = \left[h_m(1), h_m(2), \ldots, h_m(N)\right]^T \tag{3.18}$$

$$\tilde{\mathbf{w}}_i(n) = \left[w_i(1), w_i(2), \ldots, w_i(N)\right]^T. \tag{3.19}$$

Then,

$$\tilde{\mathbf{w}}_i(n) = \frac{1}{M}\sum_{m=0}^{M-1}\mathbf{h}_m(n)e^{\frac{-j2\pi im}{M}} \tag{3.20}$$

$$y(n) = \sum_{i=0}^{M-1}\left\{\mathbf{x}(n)e^{\frac{j2\pi in}{M}}\right\}*\mathbf{w}_i(n). \tag{3.21}$$

3.4 Cyclic linear multiuser detection

3.4.1 Filter bank formulas

Consider the problem of detecting desired user 1 (a high rate user), then the well known linear MMSE filter is given by,

$$\mathbf{w} = \mathbf{C}^{-1}\mathbf{p} \tag{3.22}$$

$$\mathbf{C} = E\left\{\mathbf{r}(i)\mathbf{r}(i)^T\right\}$$

$$\mathbf{p} = E\left\{b_1\mathbf{r}(i)\right\}.$$

The spreading waveforms of the low-rate users are PTV in the processing window, this causes the sequence of covariance matrices conditioned on temporal index l to also be PTV,

$$\begin{aligned}\mathbf{C}(l) &= E\left\{\mathbf{r}(l)\mathbf{r}(l)^T \middle| l\right\} \\ &= \mathbf{C}_{HR} + \mathbf{C}_{LR}(l) + \sigma^2\mathbf{I}\end{aligned} \tag{3.23}$$

since $\mathbf{C}_{LR}(l)$, the covariance matrix of the low-rate MAI, is periodic in l with period L. (The covariance matrix of the signal component associated with the HR users is denoted by $\mathbf{C}_{HR}$.) The unconditioned MMSE receiver defined in (3.22) is therefore not optimal for any particular bit epoch and would suffer worse performance compared to the PTV filter defined by,

$$\mathbf{w}(l) = \mathbf{C}^{-1}(l)\mathbf{p}. \tag{3.24}$$

3.4.2 FRESH filter coefficients

The implementation of PTV filters is a mature topic. The simplest implementation of which is the filter bank where L parallel filters defined by (3.24) are selected sequentially. The FRESH implementation [83] makes use of the Fourier series representation of the periodic sequence of the filter coefficients $\{\mathbf{w}(l)\}$, and by doing so confines the time varying component of the PTV-filter to a bank of complex oscillators.

Define the stacked vector of L frequency shifted versions of the received vector of samples as,

$$\tilde{\mathbf{r}}(i) = \left[\mathbf{r}^T(i), \mathbf{r}^T(i)e^{j2\pi i/L}, \ldots, \mathbf{r}^T(i)e^{j2\pi i(L-1)/L}\right]^T \tag{3.25}$$

then the stacked vector of (time invariant) FRESH filter coefficients is given by,

$$\tilde{\mathbf{w}} = \tilde{\mathbf{C}}^{-1}\tilde{\mathbf{p}} \tag{3.26}$$

where,

$$\tilde{\mathbf{p}} = E\left\{b_1(i)\tilde{\mathbf{r}}(i)\right\}, \tag{3.27}$$

$$\tilde{\mathbf{C}} = E\left\{\tilde{\mathbf{r}}(i)\tilde{\mathbf{r}}^H(i)\right\} = \begin{bmatrix} \mathbf{C}^{(0)} & \mathbf{C}^{(1)} & \cdots & \mathbf{C}^{(L-1)} \\ \mathbf{C}^{(L-1)} & \mathbf{C}^{(0)} & \cdots & \mathbf{C}^{(L-2)} \\ \vdots & \vdots & \ddots & \vdots \\ \mathbf{C}^{(1)} & \mathbf{C}^{(2)} & \cdots & \mathbf{C}^{(0)} \end{bmatrix}, \tag{3.28}$$

and $\mathbf{C}^{(l)} = E\left\{\mathbf{r}(i)\mathbf{r}^H(i)e^{j2\pi li/L}\right\}$, which is the mth matrix of Fourier coefficients of the Fourier series representation (FSR) of the sequence of matrices $\left\{\mathbf{C}(l)\right\}$.

3.4.3 Suboptimal FRESH

The suboptimal FRESH filter is defined by the subset of the L frequency shifts that are employed; denote this subset $\Omega \subset \{0,\ldots,L-1\}$. Let L' represent the number of elements in the set Ω, where $1 < L' < L$, then L' represents the dimension of the suboptimal FRESH receiver architecture, and the ratio L'/L is indicative of the complexity saving relative to the full FRESH filter. The optimal (MMSE) filter coefficients, given Ω, are defined as,

$$\tilde{\mathbf{w}}_{opt,\Omega} = \tilde{\mathbf{C}}_{\Omega}^{-1}\tilde{\mathbf{p}}_{\Omega} \tag{3.29}$$

$$\tilde{\mathbf{p}}_{\Omega} = E\left\{b_1(i)\tilde{\mathbf{r}}_{\Omega}(i)\right\}$$

$$\tilde{\mathbf{C}}_{\bar{\Omega}} = E\left\{\tilde{\mathbf{r}}_{\Omega}(i)\tilde{\mathbf{r}}_{\Omega}^H(i)\right\} = \begin{bmatrix} \mathbf{C}^{(0)} & \mathbf{C}^{(\Omega(1)-\Omega(2))} & \cdots & \mathbf{C}^{(\Omega(1)-\Omega(L'))} \\ \mathbf{C}^{(\Omega(2)-\Omega(1))} & \mathbf{C}^{(0)} & \cdots & \mathbf{C}^{(\Omega(2)-\Omega(L'))} \\ \vdots & \vdots & \ddots & \vdots \\ \mathbf{C}^{(\Omega(L')-\Omega(1))} & \mathbf{C}^{(\Omega(L')-\Omega(2))} & \cdots & \mathbf{C}^{(0)} \end{bmatrix}.$$

where $\mathbf{C}^{(\Omega(m)-\Omega(n))} = \mathbf{C}^{(l)}$ and $l = \mathrm{mod}\left(\Omega(m)-\Omega(n), L\right)$.

There have been no studies to date to indicate the relationship between $\tilde{\mathbf{C}}$ and the choice of Ω that maximizes the output SINR, for a particular dimension L'. As a preliminary to this investigation (which is beyond the scope of this thesis) one particular choice, $\bar{\Omega}$, is compared to the optimal choice Ω_{opt}, and the worst possible choice Ω_{worst}, for a particular system setup. Let $\bar{\Omega}$ indicate the set $\{0,\ldots,L'-1\}$. The SINR is employed as a metric as the SINR enables an accurate estimate of the bit error rate (BER) [21] or quality of service that a network subscriber experiences. The SINR of the FRESH and filter bank receivers are defined over one complete period of the system (8 data symbols in this case) and is computed using,

$$SINR_{FRESH} = \frac{\tilde{\mathbf{w}}_{opt}^H \tilde{\mathbf{U}} \tilde{\mathbf{w}}_{opt}}{\tilde{\mathbf{w}}_{opt}^H \left(\tilde{\mathbf{C}} - \tilde{\mathbf{U}}\right)\tilde{\mathbf{w}}_{opt}}. \tag{3.30}$$

$$SINR_{FilterBank} = \frac{\sum_{l=0}^{L-1} \mathbf{w}_{opt}^T(L-l)\mathbf{U}\mathbf{w}_{opt}(L-l)}{\sum_{l=0}^{L-1} \mathbf{w}_{opt}^T(L-l)\left(\mathbf{C}(L-l)-\mathbf{U}\right)\mathbf{w}_{opt}(L-l)} \tag{3.31}$$

for the FRESH and filter bank receivers respectively. In (3.30) and (3.31) $\tilde{\mathbf{U}}$ and $\mathbf{U}$ represent the covariance matrix of the desired user's signal at the input to the FRESH filter and filter bank respectively, therefore $\mathbf{U} = A_1^2 \mathbf{s}_1 \mathbf{s}_1^T$, and $\tilde{\mathbf{U}}$ is the block diagonal matrix with $\mathbf{U}$ along its main block diagonal.

The situation that is considered comprises 3 HR users and 3 LR users with orthogonal Gold codes of length 16 and 128 respectively. The desired user has a signal to noise ratio (SNR) of 25dB, and all the other users transmit with an amplitude 3dB higher than the desired user. The SINR levels corresponding to $\bar{\Omega}$, Ω_{opt}, and Ω_{worst} are plotted in Fig. 3.3 as a function of L', where Ω_{opt} and Ω_{worst} are found through an exhaustive search. $L'=1$ and $L'=8$ correspond to the conventional non-PTV MMSE MUD and full/optimal dimension PTV MMSE MUD respectively. For the filter bank implementation, L' indicates the number of parallel filters present. From Fig. 3.3 it can be seen that the filter bank receiver is obviously only effective when the number of parallel filters is a submultiple of L (for this example when $L'=2$ or $L'=4$) as it is only under these conditions that the individual filters in the bank are exposed to a subset of the interference patterns. For the FRESH filter, Fig. 3.3 shows that the output SINR is more sensitive to the value of L' than it is to the choice of Ω, also as L' increases towards the full receiver the particular Ω selection becomes less significant. These are both desirable characteristics that vindicate the use of $\bar{\Omega}$ in systems with little or no channel state information, which is generally the case in blind MUD.

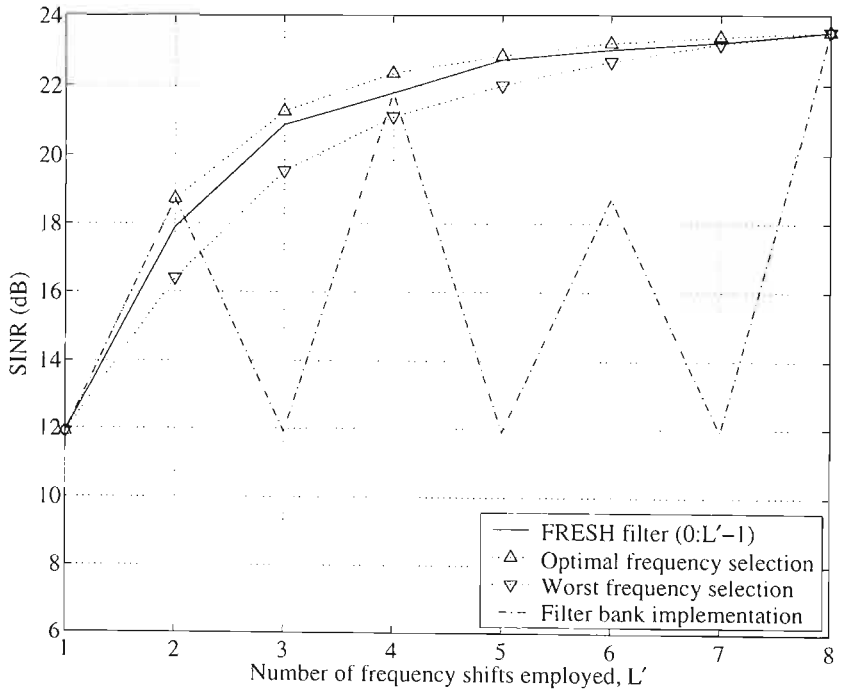

Fig. 3.3. SINR of increasing dimension MMSE filters on FRESH and filter bank architectures. Optimum, worst and $\bar{\Omega}$ frequency selections are shown for the FRESH architecture. For the filter bank receiver L' indicates the number of parallel filters present.

3.5 Cyclic adaptive algorithms

3.5.1 Filter bank LCCMA

The filter bank implementation merely runs independent versions of the LCCMA on each filter branch. Each algorithm is only activated when its branch is selected.

3.5.2 FRESH-LCCMA

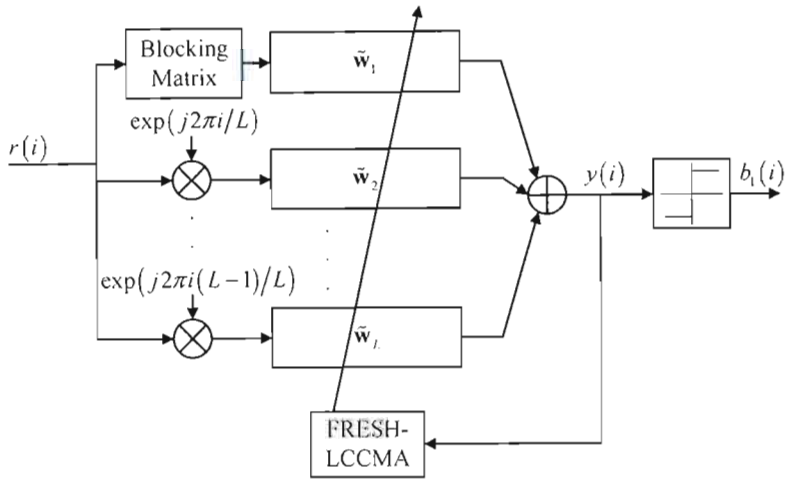

Fig. 3.4. The operation of FRESH-LCCMA on the FRESH architecture.

The FRESH-LCCMA operates directly on the stacked frequency shifted vector $\tilde{\mathbf{r}}(i)$, and thus jointly optimizes each filter bank. Based on LCCMA, FRESH-LCCMA exploits the canonical representation of the optimum FRESH filter coefficients,

$$\tilde{\mathbf{w}}_{opt} = \mathbf{s}_1' + \tilde{\mathbf{w}}_{\perp}^{opt} \tag{3.32}$$

and thereby splits the filter coefficients into the two orthogonal components above. The $\mathbf{s}_1'$ component is fixed or non-adaptive and can be computed *a priori*, the $\tilde{\mathbf{w}}_{\perp}^{opt}$ component is unknown by the receiver at start-up and is found adaptively. The $\mathbf{s}_1'$ component is given by,

$$\mathbf{s}_1' = \begin{bmatrix} \mathbf{s}_1^T & \mathbf{0}_{(L-1)N} \end{bmatrix}^T \tag{3.33}$$

where $\mathbf{0}_N$ is the zero vector of length N, and is the optimum choice at start-up when there is no channel state information: it is the single user matched filter since it corresponds to the stacked FSR of the sequence of vectors $\{\mathbf{s}_1,\ldots,\mathbf{s}_1\}$. It is also used as a linear constraint on the cost function to ensure that the desired user is captured by the receiver, as is proved in Section 3.6.1.

The FRESH-LCCMA cost function is then given by,

$$J(\tilde{\mathbf{w}}(i)) = E\left\{\left(|y(i)|^2 - R_2\right)^2\right\}, \quad \text{subject to } \tilde{\mathbf{w}}^H \mathbf{s}_1' = 1, \tag{3.34}$$

where $y(i) = \tilde{\mathbf{w}}^H(i)\tilde{\mathbf{r}}(i)$, and the dispersion factor R_2 is set to A_1^2. The update step of the stochastic gradient algorithm used to minimize this cost function is given by,

$$\tilde{\mathbf{w}}_{\perp}(i+1) = \tilde{\mathbf{w}}_{\perp}(i) + \mu y(i) F_c(i) \tilde{\mathbf{r}}_{\perp}(i) \tag{3.35}$$

where

$$F_c(i) = y(i)\left(|y(i)|^2 - R_2\right),$$

$$\tilde{\mathbf{w}}(i) = \mathbf{s}_1' + \tilde{\mathbf{w}}_\perp(i),$$

and $\tilde{\mathbf{r}}_\perp(i) = \mathbf{B}\tilde{\mathbf{r}}(i)$, $\mathbf{B} = \mathbf{I} - \mathbf{s}_1'\mathbf{s}_1'^T$, such that $\tilde{\mathbf{r}}_\perp^H(i)\mathbf{s}_1' = 0$, which ensures that $\tilde{\mathbf{w}}_\perp(i)$ remains orthogonal to $\mathbf{s}_1'$, which in turn ensures the linear constraint $\tilde{\mathbf{w}}^H(i)\mathbf{s}_1' = 1$ is always met. The operation of this algorithm on the FRESH architecture is depicted in Fig. 3.4.

The FRESH-LCCMA adaptive algorithm on the suboptimal structure is similarly defined using,

$$\mathbf{s}_1' = \begin{bmatrix} \mathbf{s}_1^T & \mathbf{0}_{(L'-1)N} \end{bmatrix}^T \tag{3.36}$$

and,

$$\tilde{\mathbf{r}}_\Omega(i) = \left[\mathbf{r}^T(i)e^{j2\pi i(\Omega(1))/L}, \ldots, \mathbf{r}^T(i)e^{j2\pi i(\Omega(L'))/L}\right]^T. \tag{3.37}$$

3.5.3 Alternate cost functions

It is possible to employ alternate code-aided adaptive algorithms that exploit the canonical representation of the optimum FRESH filter coefficients given in (3.32). The algorithms and their associated cost functions that are considered in this chapter are summarised in Table 3.1.

Table 3.1. Adaptive cyclic-MUD Cost Functions

Algorithm	Cost Function	$F_c(i)$
LCCMA	$\min J(\tilde{\mathbf{w}}(i)) = E\left\{\left(|y(i)|^2 - R_2\right)^2\right\}$, $\tilde{\mathbf{w}}^H\mathbf{s}_1' = 1$	$F_c(i) = y(i)\left(R_2 - |y(i)|^2\right)$
LCDCMA	$\min J(\tilde{\mathbf{w}}(i)) = E\left\{\left(|y(i)|^2 - |y(i-1)|^2\right)^2\right\}$, $\tilde{\mathbf{w}}^H\mathbf{s}_1' = 1$	$F_c(i) = \left(y(i-1) - y(i)\right)\left(|y(i)|^2 - |y(i-1)|^2\right)$
MOE	$\min J(\tilde{\mathbf{w}}(i)) = E\left\{|y(i)|^2\right\}$, $\tilde{\mathbf{w}}^H\mathbf{s}_1' = 1$	$F_c(i) = -y(i)$
Sato	$\min J(\tilde{\mathbf{w}}(i)) = E\left\{\left(\text{sign}(y(i)) - |y(i)|\right)^2\right\}$, $\tilde{\mathbf{w}}^H\mathbf{s}_1' = 1$	$F_c(i) = y(i)\left(\text{sign}(y(i)) - 1\right)$
DD-LMS	$\min J(\tilde{\mathbf{w}}) = E\left\{\frac{1}{2}\left\|\text{sign}(y) - y\right\|^2\right\}$	$F_c(i) = \text{sign}(y(i)) - y(i)$
LMS (data aided)	$\min J(\tilde{\mathbf{w}}(i)) = E\left\{\left(y(i) - b_1(i)\right)^2\right\}$	$F_c(i) = b_1(i) - y(i)$

3.5.4 RLS implementation

The adaptive performance of the blind adaptive cyclic MUD under consideration may be boosted if a higher computational complexity is acceptable. The RLS procedure is one such technique that could then be considered. A cyclic RLS procedure was developed in [60] for blind adaptive cyclic MUD based on the MOE cost function which exploits the block circulant structure of covariance matrix $\tilde{\mathbf{C}}$. A new algorithm can similarly be developed based on the LCCMA algorithm which has an equivalent computational complexity. Using the same derivation as in [39], a recursive update procedure for solving (3.34) is given by

$$y(i) = \tilde{\mathbf{w}}(i)\tilde{\mathbf{r}}(i)$$
$$\tilde{\mathbf{C}}(i) = \lambda\tilde{\mathbf{C}}(i-1) + \tilde{\mathbf{r}}(i)\tilde{\mathbf{r}}^H(i)$$
$$\mathbf{g}(i) = \lambda\mathbf{g}(i-1) + \tilde{\mathbf{r}}(i)\frac{y^*(i)}{|y(i)|}$$
$$\mathbf{e}(i) = \tilde{\mathbf{C}}(i)\tilde{\mathbf{w}}(i) - R_2\mathbf{g}(i)$$
$$k(i) = \frac{\mathbf{e}^H(i)\mathbf{B}\mathbf{e}(i)}{\mathbf{e}^H(i)\mathbf{B}\tilde{\mathbf{C}}(i)\mathbf{B}\mathbf{e}(i)}$$
$$\tilde{\mathbf{w}}(i) = \mathbf{B}\left(\tilde{\mathbf{w}}(i-1) - k(i)\mathbf{e}(i)\right) + \mathbf{s}_1.$$

The "forget factor" λ is set slightly smaller than unity to enable the tracking of a time-varying channel. It is also possible to minimize the suboptimal FRESH-LCCMA cost function using the above procedure.

3.5.5 Comments on complexity

The relative complexity of various blind adaptive MUD schemes is presented in Table 3.2. These algorithms are representative of three categories of blind adaptive MUD algorithm: stochastic gradient (LCCMA [30]), recursive least squares (MOE-RLS [60]), and subspace tracking (PASTd [81]). Cyclic MOE-RLS and FRESH-LCCMA (RLS) scale linearly in complexity with the periodicity of the system (which is desirable), but it can be seen that their overall complexity is far higher than the stochastic gradient based FRESH-LCCMA. Reference [81] argues that usually $L < (NM)$ and $r \ll NM$ (where M is the number of samples per chip, and r is the dimension of the signal subspace), and therefore the cyclic PASTd algorithm has a lower computational complexity than the cyclic MOE-RLS algorithm. It can be seen that the complexity of FRESH-LCCMA is lower than cyclic PASTd, and that as the periodicity of the system increases so the relative complexity of cyclic PASTd increases over FRESH LCCMA. The suboptimal FRESH schemes enable a complete scaling in complexity from the non-cyclic

Table 3.2. Complexity Comparison of Cyclic- and Non-cyclic MUD's

Algorithm	Complexity
LCCMA	$\mathcal{O}(NM)$
MOE-RLS	$\mathcal{O}\left((NM)^2\right)$
PASTd	$\mathcal{O}(NMr)$
FRESH-LCCMA	$\mathcal{O}(LMN)$
Cyclic MOE-RLS	$\mathcal{O}\left(L(MN)^{2.3}\right)$
Suboptimal FRESH-LCCMA	$\mathcal{O}(L'MN)$
Cyclic PASTd	$\mathcal{O}\left(rL^2\right) + \mathcal{O}(LMNr)$
FRESH-LCCMA (RLS)	$\mathcal{O}\left(L(MN)^2\right)$

Where: r - dimension of signal subspace, N - number of chips in processing window, M - samples per chip, L - period of system, L' - suboptimal FRESH dimension. Source: [67], [60], [81].

up to the full cyclic receiver.

3.6 Performance analysis

3.6.1 Proof of convergence

Convergence is proved for the case where there is no AWGN, as is customary [40], [30]. Firstly, a unique stationary point is shown to exist using the first derivative of the cost function with respect to the filter coefficients. This stationary point is then shown to coincide with the decorrelating detector. On inspection of the associated Hessian matrix, it is shown that this stationary point on the cost surface is a global minimum, which completes the analysis. The minimum condition required for convergence is then given.

The signal associated with user k at the input to FRESH filter $\tilde{\mathbf{w}}(i)$ is given by $A_k b_k(i)\tilde{\mathbf{s}}_k(i)$ where,

$$\tilde{\mathbf{s}}_k(i) = \left[\mathbf{s}_k^T(i), \mathbf{s}_k^T(i)e^{j2\pi i/L}, \ldots, \mathbf{s}_k^T(i)e^{j2\pi i(L-1)/L}\right]^T. \tag{3.38}$$

In a similar fashion to [40] and [30], define the (PTV) signal from user k at the output of the filter as,

$$u_k(i) = A_k \tilde{\mathbf{w}}^H \tilde{\mathbf{s}}_k(i). \tag{3.39}$$

This sequence only takes on L distinct values, denote this sequence by $\{u_k(1), \ldots, u_k(L)\}$. By making use of the property of the periodic sequence:

$$E\left\{\left(u_k(i)\right)^x\right\} = \frac{1}{L}\sum_{l=1}^{L}\left(u_k(l)\right)^x, \tag{3.40}$$

the expanded cost function (3.34),

$$\begin{aligned}\min_{\tilde{\mathbf{w}}^H \mathbf{s}_1'=1} J(\tilde{\mathbf{w}}(i)) &= E\left\{\left(\left|y(i)\right|^2 - R_2\right)^2\right\} \\ &= \left|y(i)\right|^4 - 2\left|y(i)\right|^2 R_2 + R_2^2 \\ &= \left|\tilde{\mathbf{w}}^H(i)\tilde{\mathbf{r}}(i)\right|^4 - 2\left|\tilde{\mathbf{w}}^H(i)\tilde{\mathbf{r}}(i)\right|^2 R_2 + R_2^2,\end{aligned} \tag{3.41}$$

may be expressed in terms of $u_k(l)$ using the terms,

$$\begin{aligned}E\left\{\left|\tilde{\mathbf{w}}^H(i)\tilde{\mathbf{r}}(i)\right|^2\right\} &= E\left\{\left|\sum_{k=1}^{K} A_k b_k(i)\tilde{\mathbf{w}}^H(i)\tilde{\mathbf{s}}_k(i)\right|^2\right\} \\ &= E\left\{\left|\sum_{k=1}^{K} b_k(i)u_k(i)\right|^2\right\} \\ &= E\left\{\sum_{k=1}^{K} u_k(i)u_k^*(i)\right\} \\ &= \frac{1}{L}\sum_{k=1}^{K}\sum_{l=1}^{L} u_k(l)u_k^*(l),\end{aligned} \tag{3.42}$$

$$
\begin{aligned}
E\left\{\left|\tilde{\mathbf{w}}^H(i)\tilde{\mathbf{r}}(i)\right|^4\right\} &= E\left\{\left|\sum_{k=1}^{K} b_k(i)u_k(i)\right|^4\right\} \\
&= E\left\{\sum_{k=1}^{K}\left(u_k(i)u_k^*(i)\right)^2 + 6\sum_{m=1}^{K}\sum_{\substack{n=1\\ n\neq m}}^{K} u_m(i)u_m^*(i)u_n(i)u_n^*(i)\right\} \\
&= \frac{1}{L}\sum_{k=1}^{K}\sum_{l=1}^{L}\left(u_k(l)u_k^*(l)\right)^2 + \frac{6}{L}\sum_{m=1}^{K}\sum_{\substack{n=1\\ n\neq m}}^{K}\sum_{l=1}^{L} u_m(l)u_m^*(l)u_n(l)u_n^*(l).
\end{aligned}
\tag{3.43}
$$

Define the vector,

$$
\mathbf{u} = \left[\mathbf{u}_1^T, \ldots, \mathbf{u}_K^T\right]^T \tag{3.44}
$$

where $\mathbf{u}_k = \left[u_k(1), \ldots, u_k(L)\right]^T$, then the cost function may now be expressed as $\phi(\mathbf{u})$,

$$
\begin{aligned}
\min_{|u_1(l)|\geq A_1} \phi(\mathbf{u}) = \frac{1}{L}\sum_{k=1}^{K}\sum_{l=1}^{L}\left(u_k(l)u_k^*(l)\right)^2 + \frac{6}{L}\sum_{m=1}^{K}\sum_{\substack{n=1\\ n\neq m}}^{K}\sum_{l=1}^{L} u_m(l)u_m^*(l)u_n(l)u_n^*(l) \\
-2R_2\frac{1}{L}\sum_{k=1}^{K}\sum_{l=1}^{L} u_k(l)u_k^*(l) + R_2^2.
\end{aligned}
\tag{3.45}
$$

Proposition: The linear constraint $\tilde{\mathbf{w}}^H\mathbf{s}_1' = 1$ ensures $|u_1(l)| \geq A_1$.

Proof:

$$
\begin{aligned}
\left|u_1(l)\right|^2 &= A_1^2\left|\tilde{\mathbf{w}}^H(i)\tilde{\mathbf{s}}_1(l)\right|^2 \\
&= A_1^2\left|\tilde{\mathbf{w}}^H(i)\left(\mathbf{s}_1' + \tilde{\mathbf{s}}_r(l)\right)\right|^2
\end{aligned}
$$

where $\mathbf{s}_1' = \left[\mathbf{s}_1^T, \mathbf{0}_{(L-1)N}^T\right]^T$, and $\mathbf{s}_r(l)$ is defined as

$$
\mathbf{s}_r(l) = \left[\mathbf{0}_N^T, \mathbf{s}_1^T e^{j2\pi i/L}, \ldots, \mathbf{s}_1^T e^{j2\pi i(L-1)/L}\right]^T, \tag{3.46}
$$

then $\mathbf{s}_1' \perp \tilde{\mathbf{s}}_r(l)$, and therefore,

$$
\begin{aligned}
\left|u_1(l)\right|^2 &= A_1^2\left(\left|\tilde{\mathbf{w}}^H(i)\mathbf{s}_1'\right|^2 + \left|\tilde{\mathbf{w}}^H(i)\tilde{\mathbf{s}}_r(l)\right|^2\right) \\
&= A_1^2 + \left|\delta(l)\right|^2 \\
&\geq A_1^2
\end{aligned}
$$

where $\delta(l) = A_1\tilde{\mathbf{w}}(i)^H\tilde{\mathbf{s}}_r(l)$, and therefore $|u_1(l)| \geq A_1$. ■

The $u_k(l)$ terms are complex and therefore the first partial derivative of the cost function is given with respect to the real and imaginary components of $u_k(l)$, where $u_k(l) = x_k(l) + jy_k(l)$, using the block vector notation,

$$
\frac{\partial\phi(\mathbf{u})}{\partial\mathbf{u}} = \begin{bmatrix} \dfrac{\partial\phi(\mathbf{u})}{\partial\mathbf{x}} \\ \dfrac{\partial\phi(\mathbf{u})}{\partial\mathbf{y}} \end{bmatrix} \tag{3.47}
$$

where $\mathbf{x}=\left[\mathbf{x}_1^T,\ldots,\mathbf{x}_K^T\right]^T$ and $\mathbf{x}_k=\left[x_k^T(1),\ldots,x_k^T(L)\right]^T$, and $\mathbf{y}$ is similarly defined. The above expression can then be further expanded into the terms,

$$\frac{\partial\phi(\mathbf{u})}{\partial\mathbf{x}}=\begin{bmatrix}\dfrac{\partial\phi(\mathbf{u})}{\partial\mathbf{x}_1}\\ \vdots \\ \dfrac{\partial\phi(\mathbf{u})}{\partial\mathbf{x}_K}\end{bmatrix} \tag{3.48}$$

where,

$$\frac{\partial\phi(\mathbf{u})}{\partial\mathbf{x}_k}=\begin{bmatrix}\dfrac{\partial\phi(\mathbf{u})}{\partial x_k(1)}\\ \vdots \\ \dfrac{\partial\phi(\mathbf{u})}{\partial x_k(L)}\end{bmatrix} \tag{3.49}$$

and $\partial\phi(\mathbf{u})/\partial\mathbf{y}$, $\partial\phi(\mathbf{u})/\partial\mathbf{y}_k$ are similarly defined. The partial derivatives that constitute (3.49) are in turn given by,

$$\begin{aligned}\frac{\partial\phi(\mathbf{u})}{\partial x_k(l)}&=\frac{4}{L}x_k(l)\left(x_k^2(l)+y_k^2(l)\right)+\frac{12}{L}x_k(l)\sum_{\substack{m=1\\m\neq k}}^{K}\left(x_m^2(l)+y_m^2(l)\right)-\frac{4}{L}R_2x_k(l)\\&=x_k(l)\frac{4}{L}\left(\left(x_k^2(l)+y_k^2(l)\right)+3\sum_{\substack{m=1\\m\neq k}}^{K}\left(x_m^2(l)+y_m^2(l)\right)-R_2\right)\\&=x_k(l)\frac{4}{L}\left(\left(3u_1(l)u_1^*(l)-R_2\right)+\left(x_k^2(l)+y_k^2(l)\right)+3\sum_{\substack{m=2\\m\neq k}}^{K}\left(x_m^2(l)+y_m^2(l)\right)\right)\end{aligned} \tag{3.50}$$

and similarly,

$$\frac{\partial\phi(\mathbf{u})}{\partial y_k(l)}=y_k(l)\frac{4}{L}\left(\left(3u_1(l)u_1^*(l)-R_2\right)+\left(x_k^2(l)+y_k^2(l)\right)+3\sum_{\substack{m=2\\m\neq k}}^{K}\left(x_m^2(l)+y_m^2(l)\right)\right). \tag{3.51}$$

From (3.50) and (3.51), when $\left(3u_1(l)u_1^*(l)-R_2\right)>0$ the only stationary point of the cost function is when $u_k=0$, which corresponds to the decorrelating detector. It was proved above that $\left|u_1(l)\right|^2\geq A_1^2$, and therefore a sufficient condition for the existence of the decorrelating stationary point on the cost surface is $3A_1^2-R_2>0$. This is the same condition arrived at in [40] and [30].

The Hessian matrix, or second partial derivative, of the cost function is given in the block matrix form,

$$\frac{\partial^2\phi(\mathbf{u})}{\partial\mathbf{u}^2}=\begin{bmatrix}\dfrac{\partial^2\phi(\mathbf{u})}{\partial^2\mathbf{x}} & \dfrac{\partial^2\phi(\mathbf{u})}{\partial\mathbf{x}\mathbf{y}}\\ \dfrac{\partial^2\phi(\mathbf{u})}{\partial\mathbf{y}\mathbf{x}} & \dfrac{\partial^2\phi(\mathbf{u})}{\partial^2\mathbf{y}}\end{bmatrix} \tag{3.52}$$

where

$$\frac{\partial^2\phi(\mathbf{u})}{\partial^2\mathbf{x}}=\begin{bmatrix}\dfrac{\partial^2\phi(\mathbf{u})}{\partial^2\mathbf{x}_1} & \cdots & \dfrac{\partial^2\phi(\mathbf{u})}{\partial\mathbf{x}_1\mathbf{x}_K}\\ \vdots & \ddots & \vdots\\ \dfrac{\partial^2\phi(\mathbf{u})}{\partial\mathbf{x}_K\mathbf{x}_1} & \cdots & \dfrac{\partial^2\phi(\mathbf{u})}{\partial^2\mathbf{x}_K}\end{bmatrix}, \tag{3.53}$$

$$\frac{\partial^2\phi(\mathbf{u})}{\partial\mathbf{x}\mathbf{y}}=\begin{bmatrix}\dfrac{\partial^2\phi(\mathbf{u})}{\partial\mathbf{x}_1\mathbf{y}_1} & \cdots & \dfrac{\partial^2\phi(\mathbf{u})}{\partial\mathbf{x}_1\mathbf{y}_K}\\ \vdots & \ddots & \vdots\\ \dfrac{\partial^2\phi(\mathbf{u})}{\partial\mathbf{x}_K\mathbf{y}_1} & \cdots & \dfrac{\partial^2\phi(\mathbf{u})}{\partial\mathbf{x}_K\mathbf{y}_k}\end{bmatrix}, \tag{3.54}$$

and $\partial^2\phi(\mathbf{u})/\partial\mathbf{y}\mathbf{x}$, $\partial^2\phi(\mathbf{u})/\partial^2\mathbf{y}$ are similarly defined. Then

$$\frac{\partial^2\phi(\mathbf{u})}{\partial^2\mathbf{x}_k}=\begin{bmatrix}\dfrac{\partial^2\phi(\mathbf{u})}{\partial^2x_k(1)} & \cdots & \dfrac{\partial^2\phi(\mathbf{u})}{\partial x_k(1)x_k(L)}\\ \vdots & \ddots & \vdots\\ \dfrac{\partial^2\phi(\mathbf{u})}{\partial x_k(L)x_k(1)} & \cdots & \dfrac{\partial^2\phi(\mathbf{u})}{\partial^2x_k(L)}\end{bmatrix} \tag{3.55}$$

$$\frac{\partial^2\phi(\mathbf{u})}{\partial\mathbf{x}_k\mathbf{y}_{k'}}=\begin{bmatrix}\dfrac{\partial^2\phi(\mathbf{u})}{\partial x_k(1)y_{k'}(1)} & \cdots & \dfrac{\partial^2\phi(\mathbf{u})}{\partial x_k(1)y_{k'}(L)}\\ \vdots & \ddots & \vdots\\ \dfrac{\partial^2\phi(\mathbf{u})}{\partial x_k(L)y_{k'}(1)} & \cdots & \dfrac{\partial^2\phi(\mathbf{u})}{\partial x_k(L)y_{k'}(L)}\end{bmatrix} \tag{3.56}$$

and the other sub-matrices associated with $\partial^2\phi(\mathbf{u})/\partial^2\mathbf{y}_k$ and $\partial^2\phi(\mathbf{u})/\partial\mathbf{y}_k\mathbf{x}_{k'}$ are similarly defined. The elements of the Hessian matrix are then given by,

$$\frac{\partial\phi(\mathbf{u})}{\partial x_k(l)\partial x_{k'}(l')}=\begin{cases}\dfrac{4}{L}\left(\left(3x_k^2(l)+y_k^2(l)\right)+3\sum\limits_{\substack{m=1\\ m\neq k}}^{K}\left(x_m^2(l)+y_m^2(l)\right)-R_2\right), & k'=k,l'=l\\ \dfrac{24}{L}x_{k'}(l), & k'\neq k,l'=l\\ 0, & \text{otherwise.}\end{cases} \tag{3.57}$$

$$\frac{\partial\phi(\mathbf{u})}{\partial x_k(l)\partial y_{k'}(l')}=\begin{cases}\frac{8}{L}y_k(l), & k'=k,l'=l\\ \frac{24}{L}y_{k'}(l), & k'\neq k,l'=l\\ 0 & \text{otherwise.}\end{cases} \tag{3.58}$$

$$\frac{\partial\phi(\mathbf{u})}{\partial y_k(l)\partial x_{k'}(l')}=\begin{cases}\frac{8}{L}x_k(l), & k'=k,l'=l\\ \frac{24}{L}x_{k'}(l), & k'\neq k,l'=l\\ 0 & \text{otherwise.}\end{cases} \tag{3.59}$$

$$\frac{\partial\phi(\mathbf{u})}{\partial y_k(l)\partial y_{k'}(l')}=\begin{cases}\frac{4}{L}\left(\left(x_k^2(l)+3y_k^2(l)\right)+3\sum_{\substack{m=1\\m\neq k}}^{K}\left(x_m^2(l)+y_m^2(l)\right)-R_2\right), & k'=k,l'=l\\ \frac{24}{L}y_{k'}(l), & k'\neq k,l'=l\\ 0, & \text{otherwise.}\end{cases} \tag{3.60}$$

from (3.57)–(3.60), it can be seen that the off-diagonal elements of the Hessian matrix at the stationary point are zero. The main diagonal of the Hessian matrix is fully determined by $\partial\phi(\mathbf{u})/\partial^2 x_k(l)$, $\partial\phi(\mathbf{u})/\partial^2 y_k(l)$, $\partial\phi(\mathbf{u})/\partial^2 x_1(l)$, and $\partial\phi(\mathbf{u})/\partial^2 y_1(l)$. These terms are in turn guaranteed to be positive if the following corresponding constraints are met,

$$3u_1(l)u_1^*(l)-R_2\geq 0 \tag{3.61}$$

$$3u_1(l)u_1^*(l)-R_2\geq 0 \tag{3.62}$$

$$3x_1^2(l)+y_1^2(l)-R_2\geq 0 \tag{3.63}$$

$$x_1^2(l)+3y_1^2(l)-R_2\geq 0. \tag{3.64}$$

Constraints (3.61) and (3.62) are the same and are automatically satisfied when the stricter constraints (3.63) and (3.64) are met. It has already been proved that $x_1^2(l)+y_1^2(l)\geq A_1^2$, and therefore a sufficient condition to ensure constraints (3.63) and (3.64) are satified is

$$A_1^2-R_2\geq 0 \tag{3.65}$$

thus ensuring that the Hessian matrix is positive definite. Under this condition the stationary point is a minimum point on the cost surface, thus completing the convergence proof of the FRESH-LCCMA algorithm.

It is worth noting at this point that $x_1^2(l)\gg y_1^2(l)$, since the vast majority of the energy at the output of the filter associated with the desired user lies in the real domain as BPSK signalling and phase synchronisation is assumed. This leads to the conclusion that $x_1^2(l)+3y_1^2(l)\cong A_1^2$, and therefore the constraint imposed in (3.65) is not overly loose, which indicates that the constraint for convergence of the FRESH-LCCMA is in fact more sensitive to A_1^2 overestimation than the LCCMA is, where it was proved in [40] that a sufficient condition for LCCMA convergence is $3A_1^2-R_2\geq 0$.

The same conjectures made in [30] with regard to the convergence of the LCCMA in an AWGN channel apply in this case, and it is thus assumed that by properly selecting the value of R_2 the FRESH-LCCMA cost function is strictly convex in an AWGN channel. With Regard to the convergence analysis for the suboptimal LCCMA-FRESH algorithm, it follows in the same manner as above where (3.38) is replaced by,

$$\tilde{\mathbf{s}}_k(i) = \left[\mathbf{s}_k^T e^{j2\pi i(\Omega(1))/L}, \ldots, \mathbf{s}_k^T e^{j2\pi i(\Omega(L))/L}\right]^T. \tag{3.66}$$

3.6.2 Adaptive performance

This section extends the theory developed in Chapter 2 to the study of the relative performance of an adaptive algorithm implemented on either the filter bank or FRESH filter architecture. This section therefore details: how the output of the filters may be described in terms of deterministic quantities, new assumptions, and the definitions of the optimum filters in a non-stationary channel.

The steady-state, tracking and transient analyses derive closed form expressions of the excess mean square error (EMSE), defined in this section as

$$\zeta_{FRESH} = E\left\{\left(\left(\tilde{\mathbf{w}}_{opt} - \tilde{\mathbf{w}}(i)\right)^H \tilde{\mathbf{r}}(i)\right)^2\right\} \tag{3.67}$$

$$\zeta_{FilterBank}(l) = E\left\{\left(\left(\mathbf{w}_{opt}(l) - \mathbf{w}(i)\right)^T \mathbf{r}(i)\right)^2 \delta_l(i)\right\} \tag{3.68}$$

for the FRESH filter and (lth filter of) the filter bank respectively. The EMSE of the FRESH filter is compared to the filter bank architecture by comparing the EMSE defined in (3.67) with the average EMSE of all the filters in the filter bank architecture. The analysis of the filter bank architecture thus amounts to the analysis of L independent adaptive algorithms.

The steady-state analysis requires the output of the filters to be written in terms of deterministic quantities. The same approach as used in Section 2.5 is applied here where the output of the filters is described in terms of the optimal filter coefficients and the *a priori* estimation error. The *a priori* estimation error is defined as, $e_a(i) = \left(\mathbf{w}_{opt} - \mathbf{w}(i)\right)^T \mathbf{r}(i)$ and $e_a(i) = \left(\tilde{\mathbf{w}}_{opt} - \tilde{\mathbf{w}}(i)\right)^H \tilde{\mathbf{r}}(i)$ for the filter bank and FRESH architectures respectively. The output of the lth filter in the filter bank receiver may then be expressed using,

$$\begin{aligned} y(i) &= \mathbf{w}^T(i)\mathbf{r}(i)\delta_l(i) \\ &= \left[\left(\mathbf{w}_{opt}(l) - \Delta\mathbf{w}_\perp(i)\right)^T \mathbf{r}(i)\right]\delta_l(i) \\ &= \left[\left(\mathbf{w}_{opt}^T(l)\mathbf{u}(i)\right) + v(i) - e_{a,\perp}(i)\right]\delta_l(i). \end{aligned} \tag{3.69}$$

where $\Delta\mathbf{w}_\perp$ is the error in the adaptive component of the filter coefficients, $\mathbf{u}(i)$ is the component of the received vector of samples, within processing window i, containing energy from $b_1(i)$, and v is the MAI plus filtered AWGN lumped into a single term. The *a priori*

error is denoted by $e_{a,\perp}$ (as opposed to e_a) because only error in the adaptive component of the filter coefficients is present. The signal associated with the desired user's bit at the input to one of the filters in the bank is given by,

$$\mathbf{u}(i) = A_1 b_1(i)\mathbf{s}_1. \tag{3.70}$$

The output of the FRESH filter may be similarly expressed,

$$\begin{aligned} y(i) &= \tilde{\mathbf{w}}^H(i)\tilde{\mathbf{r}}(i) \\ &= \left(\tilde{\mathbf{w}}_{opt}^H \tilde{\mathbf{u}}(i)\right) + v(i) - e_{a,\perp}(i) \end{aligned} \tag{3.71}$$

where

$$\tilde{\mathbf{u}}(i) = \left[\mathbf{u}(i), \mathbf{u}(i)e^{j2\pi i/L}, \ldots, \mathbf{u}(i)e^{j2\pi i(L-1)/L}\right]^T. \tag{3.72}$$

The $\mathbf{w}_{opt}^T(l)\mathbf{u}(i)$ and $\tilde{\mathbf{w}}_{opt}^H\tilde{\mathbf{u}}(i)$ terms are zero mean and due to the orthogonal projection operation are uncorrelated with the associated $\{v, e_{a,\perp}\}$ terms, as shown in Section 2.5.1. It can also be easily shown that,

$$E\left\{\left(\mathbf{w}_{opt}^T(l)\mathbf{u}(i)\right)^{2k}\right\} = \left(\mathbf{w}_{opt}^T(l)\mathbf{U}\mathbf{w}_{opt}(l)\right)^k \tag{3.73}$$

$$E\left\{\left(\tilde{\mathbf{w}}_{opt}^H\tilde{\mathbf{u}}(i)\right)^{2k}\right\} = \left(\tilde{\mathbf{w}}_{opt}^H\tilde{\mathbf{U}}\tilde{\mathbf{w}}_{opt}\right)^k \tag{3.74}$$

where,

$$\begin{aligned} \mathbf{U} &= E\left\{\mathbf{u}(i)\mathbf{u}^T(i)\right\} \\ &= A_1^2\mathbf{s}_1\mathbf{s}_1^T. \end{aligned} \tag{3.75}$$

and $\tilde{\mathbf{U}}$ is the block diagonal matrix with $\mathbf{U}$ along the main block-diagonal. The filtered MAI plus AWGN associated with the optimum filter is assumed to have a Gaussian distribution, which was assumed previously in Section 2.5.1, the variance of which is given by,

$$\eta_{FilterBank}^2(l) = \mathbf{w}_{opt}^T(l)\left(\mathbf{C}(l) - \mathbf{U}\right)\mathbf{w}_{opt}(l). \tag{3.76}$$

$$\eta_{FRESH}^2 = \tilde{\mathbf{w}}_{opt}^H\left(\tilde{\mathbf{C}} - \tilde{\mathbf{U}}\right)\tilde{\mathbf{w}}_{opt}. \tag{3.77}$$

for the lth filter in the bank and the FRESH architecture respectively. The required elements have been presented and the rest of the steady-state analysis follows as per the procedure laid out in Section 2.5.

The transient analysis for both architectures may now also be performed as per Section 2.7, where the time evolution of $\zeta_{FRESH}(i)$ is compared to the time evolution of the average EMSE in a sliding window of length L, which is given by,

$$\overline{\zeta}_{FilterBank}(i) = \sum_{l=0}^{L-1}\zeta_{FilterBank}(i-l). \tag{3.78}$$

The time evolution of the output SINR may then be computed via,

$$SINR_{FRESH}(i)=\frac{\tilde{\mathbf{w}}_{opt}^{H}\tilde{\mathbf{U}}\tilde{\mathbf{w}}_{opt}}{\tilde{\mathbf{w}}_{opt}^{H}\left(\tilde{\mathbf{C}}-\tilde{\mathbf{U}}\right)\tilde{\mathbf{w}}_{opt}+\zeta_{FRESH}(i)}. \tag{3.79}$$

$$SINR_{FilterBank}(i)=\frac{\sum_{l=0}^{L-1}\mathbf{w}_{opt}^{T}(L-l)\mathbf{U}\mathbf{w}_{opt}(L-l)}{\sum_{l=0}^{L-1}\mathbf{w}_{opt}^{T}(L-l)\left(\mathbf{C}(L-l)-\mathbf{U}\right)\mathbf{w}_{opt}(L-l)+\bar{\zeta}_{FB}(i)} \tag{3.80}$$

for the FRESH and filter bank architectures respectively.

The relative tracking capabilities of the filter bank and FRESH architecture are compared by assuming that the FRESH filter tracks the PTV optimal filter defined in a length L sliding window given by,

$$\tilde{\mathbf{w}}_{opt}(i)=\tilde{\mathbf{C}}^{-1}(i)\tilde{\mathbf{p}} \tag{3.81}$$

where $\tilde{\mathbf{C}}(i)$ is defined in (3.28) and $\left\{\mathbf{C}^{(l)}(i)\right\}$ is the FSR of the matrix sequence,

$$\left\{\mathbf{C}\left(\left\lfloor\frac{i+(L-2)}{L}\right\rfloor L+1\right),\mathbf{C}\left(\left\lfloor\frac{i+(L-3)}{L}\right\rfloor L+2\right),\ldots,\mathbf{C}\left(\left\lfloor\frac{i-1}{L}\right\rfloor L+L\right)\right\} \tag{3.82}$$

at time step i. The point definition of the covariance matrices, as given in (3.23), are used in (3.82). As an example, if $L = 4$, then sets of covariance matrices for time steps 1...6 is given by,

i	$\{\mathbf{C}(i)\}$
1	$\{\mathbf{C}(1),\mathbf{C}(2),\mathbf{C}(3),\mathbf{C}(4)\}$
2	$\{\mathbf{C}(5),\mathbf{C}(2),\mathbf{C}(3),\mathbf{C}(4)\}$
3	$\{\mathbf{C}(5),\mathbf{C}(6),\mathbf{C}(3),\mathbf{C}(4)\}$
4	$\{\mathbf{C}(5),\mathbf{C}(6),\mathbf{C}(7),\mathbf{C}(4)\}$
5	$\{\mathbf{C}(5),\mathbf{C}(6),\mathbf{C}(7),\mathbf{C}(8)\}$
6	$\{\mathbf{C}(9),\mathbf{C}(6),\mathbf{C}(7),\mathbf{C}(8)\}$.

The relationship between tracking requirements of the FRESH and filter bank implementations, in terms of $\text{trace}(\mathbf{Q})$ where $\mathbf{Q}$ is the covariance matrix of $\left(\mathbf{w}_{opt}(i)-\mathbf{w}_{opt}(i-1)\right)$, is given in the following section. The tracking performance of the non-PTV filter in a PTV system is performed using the assumption that it tracks the optimal filter defined over a length L sliding window,

$$\mathbf{w}_{opt,non-PTV}(i)=\left(\frac{1}{L}\sum_{l=0}^{L-1}\mathbf{C}(i-l)\right)^{-1}\mathbf{p}. \tag{3.83}$$

3.6.3 Comparative tracking requirements imposed on PTV filters

This section relates the tracking requirements imposed by a time varying channel on an adaptive algorithm implemented on the FRESH and filter bank architectures. In a single rate DS-CDMA

system with a non-stationary channel, it is assumed that the channel varies according to the model,

$$\mathbf{w}_{opt}(i+1)=\mathbf{w}_{opt}(i)+\mathbf{q}(i). \tag{3.84}$$

The value of $\text{trace}(\mathbf{Q})$, where

$$\mathbf{Q}=E\{\mathbf{q}(i)\mathbf{q}^{H}(i)\}, \tag{3.85}$$

is used in the tracking analysis and is a measure of the non-stationarity of the channel. For a PTV system that becomes non-stationary it is assumed that the channel seen by each filter in the bank varies according to the model,

$$\mathbf{w}_{opt}(i+L)=\mathbf{w}_{opt}(i)+\sum_{l=0}^{L-1}\mathbf{q}(i-l) \tag{3.86}$$

where L is the periodicity of the stationary PTV system. The measure of the time variability for each of the filters in the bank is then given by,

$$\begin{aligned}\mathbf{Q}_{FB}&=E\left\{\sum_{l=1}^{L}\mathbf{q}(l)\sum_{l=1}^{L}\mathbf{q}^{H}(l)\right\}\\&=L\mathbf{Q}.\end{aligned} \tag{3.87}$$

By using the linearity property of the FSR, the time-variability of the FRESH filter may be expressed in terms of $\mathbf{Q}$:

$$\begin{aligned}\tilde{\mathbf{q}}&=\tilde{\mathbf{w}}_{opt}(i+1)-\tilde{\mathbf{w}}_{opt}(i)\\&=\text{FSR}\{\mathbf{w}_{opt}(i+L),\mathbf{w}_{opt}(i+2),\ldots,\mathbf{w}_{opt}(i+L-1),\}-\text{FSR}\{\mathbf{w}_{opt}(i),\ldots,\mathbf{w}_{opt}(i+L-1)\}\\&=\text{FSR}\{\mathbf{w}_{opt}(i+L)-\mathbf{w}_{opt}(i),0,\ldots,0\}\\&=\text{FSR}\left\{\sum_{l=0}^{L-1}\mathbf{q}(i-l),0,\ldots,0\right\}\end{aligned} \tag{3.88}$$

where $\mathbf{w}_{opt}(i+L)-\mathbf{w}_{opt}(i)$ is given in (3.86), and the notation $\text{FSR}\{\mathbf{w}(1),\ldots,\mathbf{w}(L)\}$ denotes the vertically stacked Fourier series representation of the vector sequence $\{\mathbf{w}(1),\ldots,\mathbf{w}(L)\}$. The $\text{FSR}\{.\}$ is formally defined as,

$$\{c_0,c_1,\ldots,c_{N-1}\}=\text{FSR}\{x(0),x(1),\ldots,x(N-1)\} \tag{3.89}$$

where,

$$c_k=\frac{1}{N}\sum_{n=0}^{N-1}x(n)\exp\left(\frac{j2\pi kn}{N}\right). \tag{3.90}$$

From the definition of the FSR, it can then easily be shown that,

$$\begin{aligned}\tilde{\mathbf{Q}}&=E\{\tilde{\mathbf{q}}(i)\tilde{\mathbf{q}}^{H}(i)\}\\&=\frac{1}{L^2}\begin{bmatrix}L\mathbf{Q} & \cdots & L\mathbf{Q}\\ \vdots & \ddots & \vdots\\ L\mathbf{Q} & \cdots & L\mathbf{Q}\end{bmatrix}\end{aligned} \tag{3.91}$$

and therefore $\text{trace}\left(\tilde{\mathbf{Q}}\right) = \text{trace}\left(\mathbf{Q}_{FB}\right)/L$.

For a non-PTV filter that tracks a sliding window version of the filter, its tracking requirements are quantified by,

$$\mathbf{q}_{non}(i) = \bar{\mathbf{w}}(i) - \bar{\mathbf{w}}(i-1) \tag{3.92}$$

where,

$$\bar{\mathbf{w}}(i) = \left(\frac{1}{L}\sum_{l=0}^{L-1}\mathbf{C}(i-l)\right)^{-1}\mathbf{p}. \tag{3.93}$$

The relationship between $\mathbf{Q}$ and $\mathbf{Q}_{non} = \left\{\mathbf{q}_{non}(i)\mathbf{q}_{non}^{H}(i)\right\}$, is not obvious as,

$$\left(\frac{1}{L}\sum_{l=0}^{L-1}\mathbf{C}(i-l)\right)^{-1} \neq \frac{1}{L}\sum_{l=0}^{L-1}\mathbf{C}^{-1}(i-l) \tag{3.94}$$

and thus expressing $\mathbf{Q}_{non}$ in terms of $\mathbf{Q}$ is not tractable.

3.7 Results

To demonstrate the performance of the new algorithms derived in this chapter, a VSL dual-rate access scheme is considered. Unless otherwise stated, orthogonal Gold codes of length 16 and 64 were assigned to the high-rate and low-rate users respectively. Orthogonal Gold codes enabled the LR code to be an integer multiple of the HR code; they are constructed from conventional Gold codes (length 15 and 63 respectively) by adding a "-1" to the end of each conventional Gold code. The MAI ratio is defined again as A_k/A_1, $k \neq 1$, where all the interfering users transmit at the same amplitude. Unless otherwise stated, there are 3 LR users and 3 HR users present in all simulations. A synchronous CDMA system is considered in order to reduce the simulation time.

Extensive use is made of plots of the output SINR versus iteration number in this section to compare the relative performance of the different architectures and algorithms. The output SINR at bit epoch i of the FRESH filter is defined as,

$$SINR_{FRESH}(i) = \frac{\tilde{\mathbf{w}}^{H}(i)\tilde{\mathbf{U}}\tilde{\mathbf{w}}(i)}{\tilde{\mathbf{w}}^{H}(i)\left(\tilde{\mathbf{C}} - \tilde{\mathbf{U}}\right)\tilde{\mathbf{w}}(i)}. \tag{3.95}$$

The SINR value given above is equivalent to the mean SINR over one complete period of the system, and is a more useful metric to quantify the performance of a PTV filter. This is because the output SINR at each bit epoch of a PTV filter is cyclic in nature, and thus plots of the SINR versus time would yield a broad area instead of a line, which is unsatisfactory. A length L sliding window is thus used to equivalently define the SINR of the filter bank receiver at bit epoch i,

$$SINR_{FilterBank}(i) = \frac{\sum_{l=0}^{L-1} \mathbf{w}^T(i-l)\mathbf{U}\mathbf{w}(i-l)}{\sum_{l=0}^{L-1} \mathbf{w}^T(i-l)\left(\mathbf{C}(i-l)-\mathbf{U}\right)\mathbf{w}(i-l)} \tag{3.96}$$

and thus enables a direct comparison between the two realisations of the PTV filter.

Fig. 3.5 shows the convergence dynamics of the SINR for the different MUD architectures all updated with the LCCMA. The curves are an average of 100 independent simulation runs, and the step size was set to 10^{-2}, except for the filter bank implementation where it was set to 4×10^{-2}. A MAI ratio of 0dB was considered and the SNR was 25dB. Visual inspection of Fig. 3.5 reveals that the full dimension FRESH filter is observed to have identical performance to the filter bank implementation. The operation of two suboptimal FRESH filters of differing computational complexity ($L'=2$ and $L'=3$) are observed to offer substantially better performance than the non-PTV filter, as they converge towards their respective MMSE SINR levels.

The performance of the new FRESH-LCCMA is compared to existing cyclic-MUD algorithms: the cyclic-RLS algorithm [60], and the cyclic subspace tracking algorithm [81], in Fig. 3.6. In [81] the performance of the cyclic subspace tracking algorithm, referred to as "cyclic-PASTd", was directly compared to the algorithm presented in [60] by comparing the convergence dynamic of the output SINR for both algorithms via simulation. The same system configuration as used in [81] is considered in Fig. 3.6 in order to make a direct comparison of the new algorithm with the results of [81]. The system that is considered then consists of 2 LR users and 1 HR user, using random spreading codes of length 45 and 15 respectively. The SNR of the desired user is 20dB's and the MAI ratio is 2.5dB's. The forget factor for both the cyclic-PASTd and cyclic-RLS algorithms is 0.995. The step size of the FRESH-LCCMA is set to 5×10^{-3}, and the conventional LCCMA's is 10^{-3}. The initial estimates of the dominant eigenvalues, used by the cyclic PASTd algorithm, were obtained through batch eigendecomposition of the first 60 data vectors, in keeping with [81]. The results shown are the average of 100 independent simulation runs.

In Fig. 3.6 the cyclic-PASTd algorithm is observed to offer nearly a 6dB improvement in the steady-state SINR over the cyclic-RLS algorithm. The new FRESH-LCCMA is observed to offer a further 3dB improvement over the cyclic-PASTd algorithm. This is a significant margin, especially considering that it comes with a reduction in computational complexity over the cyclic-PASTd and cyclic-RLS algorithms, as discussed in Section 3.5.5. The superior performance of the FRESH-LCCMA may be attributed to the poor steady-state characteristics of the MOE cost function relative to the CMA cost function. This point was highlighted in Fig. 2.14 and Section 2.8.1, where it was shown analytically that the EMSE associated with the MOE cost function does not tend to zero as the SNR increases, whereas it does for the CMA cost function. It is also important to note that the FRESH-LCCMA achieves this higher steady-

state SINR level without penalty in convergence rate compared to the RLS procedure, and in fact reaches its steady-state of operation before the cyclic-PASTd algorithm too. The non-PTV LCCMA is superimposed in this figure, where it too is observed to reach a higher steady-state SINR than the existing cyclic algorithms of [60] and [81], but at a slower convergence rate.

The convergence dynamics of the new FRESH-LCCMA relative to the cyclic algorithms of [60], [81] are further investigated in the sequence Fig. 3.7 (a)–(c), for other system configurations of greater interest. The simulation results shown are again the average of 100 independent simulation runs. This sequence of figures is intended to illustrate the performance of the new FRESH-LCCMA algorithm relative to the recently proposed cyclic-RLS algorithm [60], the cyclic subspace tracking algorithm [81], and the conventional non-cyclic LCCMA [30], as a function of MAI level. The sequence of figures thus models an increasing level of severity of the near-far problem which is one of the fundamental problems or limitations of DS-CDMA systems, and which signal processing schemes such as MUD hope to circumvent. The MAI ratio is 0dB, 3dB, and 10dB for Fig. 3.7 (a), (b), and (c) respectively. The cyclic MOE-RLS forget factor was set to 0.9995, and the cyclic PASTd forget factor was set to 0.99 for Fig. 3.7 (a)–(c). The step sizes for the other adaptive algorithms, given in sequence for Fig. 3.7 (a)–(c) are, FRESH-LCCMA: 5×10^{-3}, 10^{-3}, 2×10^{-5}, LCCMA: 10^{-2}, 5×10^{-3}, 10^{-5}.

In those figures the advantage that cyclic MUD has over non-cyclic MUD is apparent as the optimal (MMSE) SINR that cyclic MUD gains over conventional linear MUD is 2.62dB, 5.47dB, and 9.29dB for Fig. 3.7 (a), (b), and (c) respectively. This inherent advantage is evident when comparing the relative performance of FRESH-LCCMA and LCCMA in Fig. 3.7 (a)–(c), where the superior performance (in terms of both convergence speed and steady-state SINR) is evident.

The performance of FRESH-LCCMA is seen to compare favourably with the existing cyclic MUD schemes. The cyclic MOE-RLS has the advantage of a rapid convergence rate due to the use of the RLS update scheme, however the MOE cost function causes poor steady-state performance as compared to FRESH-LCCMA. As the near-far problem increases, the FRESH-LCCMA algorithm requires a smaller step size to ensure stability of the algorithm, and this in turn reduces its convergence speed. The cyclic MOE-RLS algorithm does not suffer from this effect; however its worse steady-state performance is clearly evident in Fig. 3.7 (c). The cyclic subspace tracking algorithm suffers from poorer convergence speed as the near-far ratio increases, as was found in [81]. FRESH-LCCMA appears to have superior performance to the cyclic subspace tracking algorithm for the given scenarios.

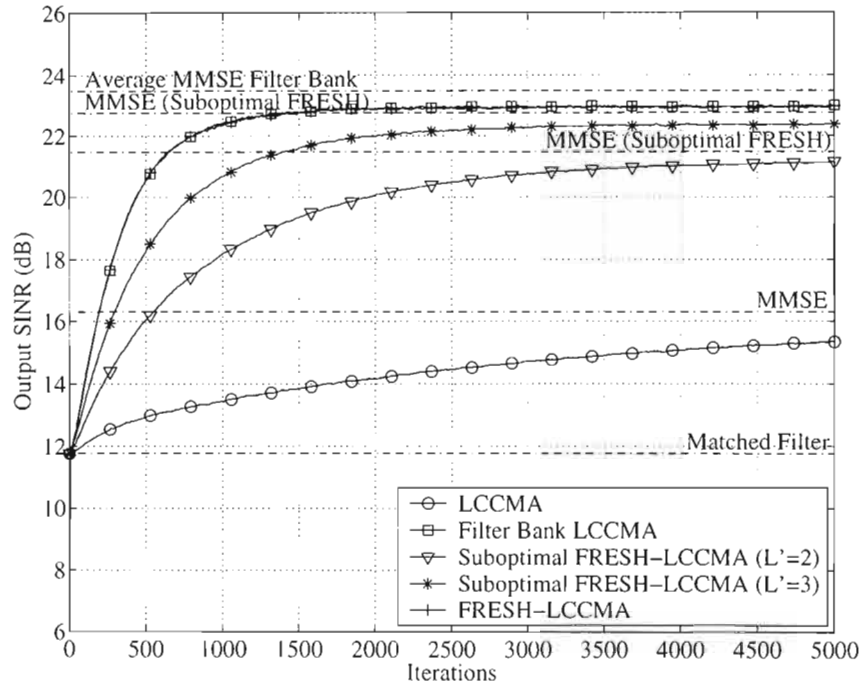

Fig. 3.5. Convergence dynamics of the different MUD architectures based on the LCCMA.

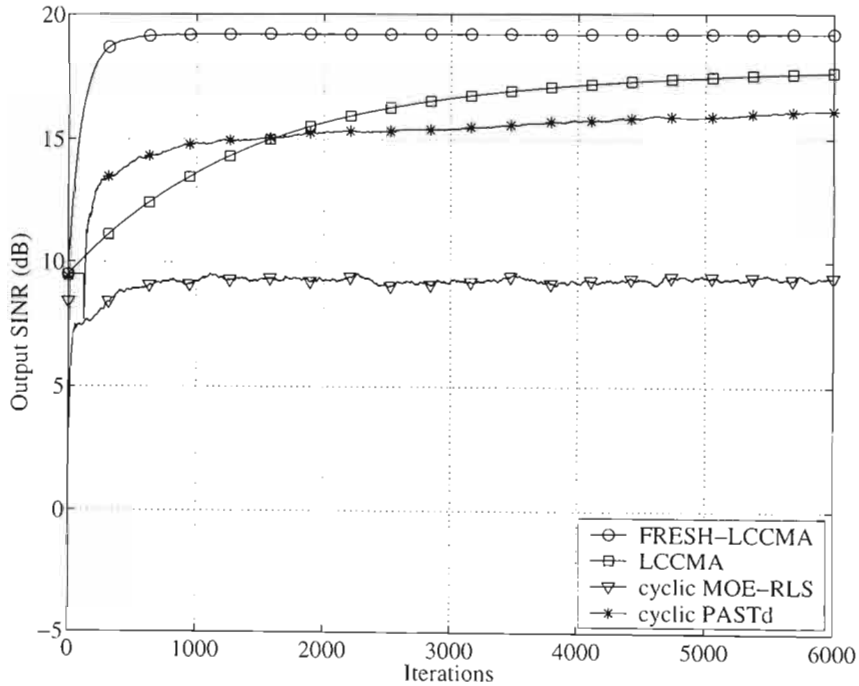

Fig. 3.6. Convergence dynamics of new FRESH-LCCMA compared with existing cyclic algorithms as per simulation setup of [81].

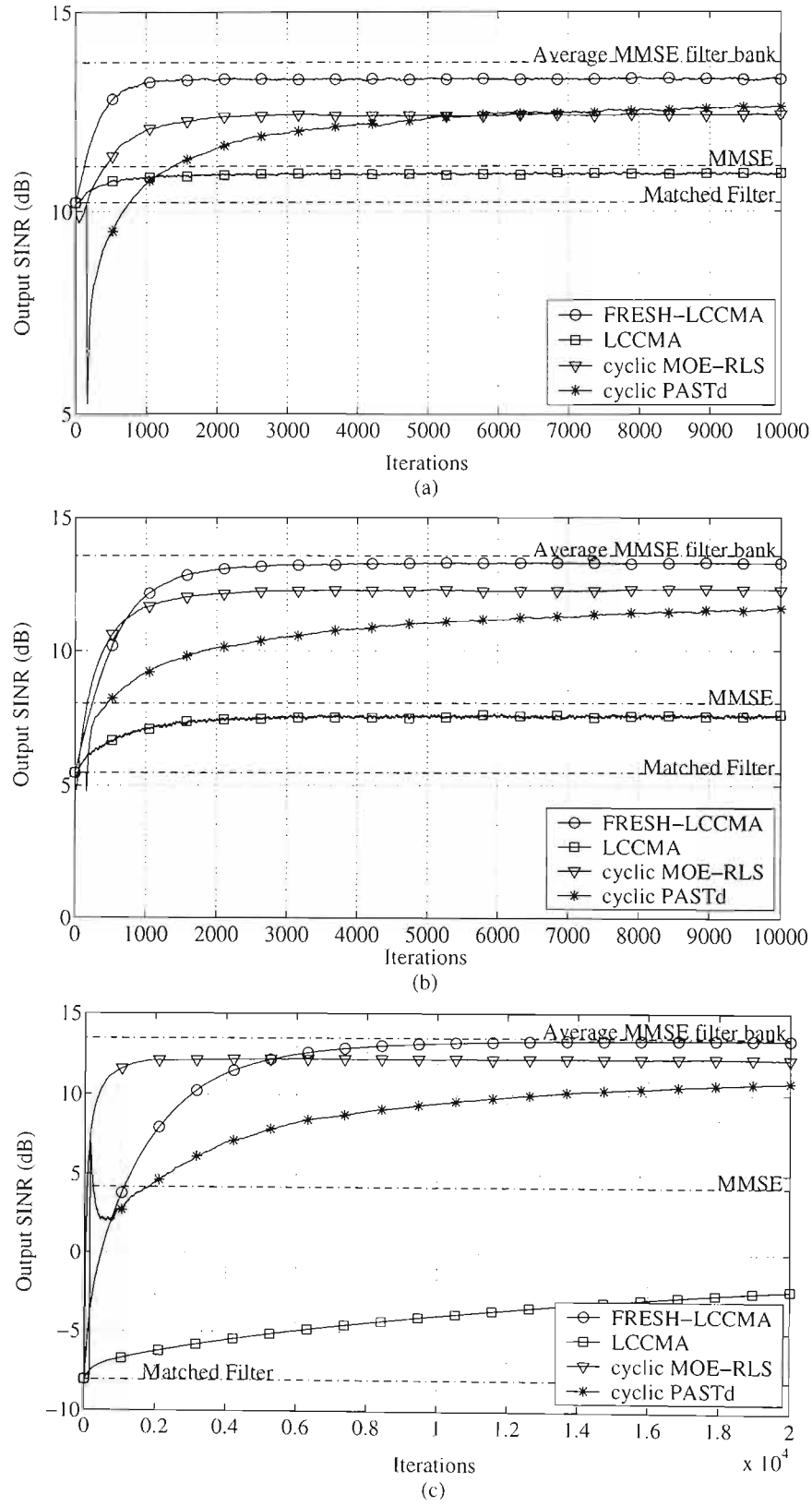

Fig. 3.7. Convergence dynamics of the new FRESH-LCCMA compared with existing cyclic algorithms with increasing MAI ratios: Figs. (a)–(c) correspond to MAI ratios of 0dB, 3dB, and 10dB respectively.

The increased convergence speed of the RLS procedure applied to the FRESH-LCCMA and suboptimal FRESH-LCCMA cost functions is explored in Fig. 3.8, where a MAI ratio of 3dB is

also considered. The forget factor was set to 0.9999 and 0.999 for the FRESH and suboptimal FRESH RLS implementations. The convergence dynamics of other existing cyclic-MUD schemes are also plotted for comparative purposes: these were the cyclic RLS-MOE [60] with forget factor set to 0.999, and cyclic subspace tracking MUD [81] with forget factor set to 0.99 and the initial subspace estimate made after 120 iterations. Under the given operating conditions the stochastic gradient algorithm (step size 10^{-2}) is once again observed to offer superior performance to the RLS-MOE and cyclic subspace tracking algorithm at a substantially lower computational complexity. The RLS based FRESH-LCCMA offers the fastest convergence with very low misadjustment (EMSE) in the steady-state. The RLS based FRESH-LCCMA has the same computational complexity as the RLS-MOE algorithm but the CMA base cost function yields vastly superior performance compared to the MOE based algorithm of [60]. The suboptimal FRESH filter based on the RLS update procedure for the LCCMA also exhibits excellent convergence characteristics, albeit towards a slightly lower optimal SINR.

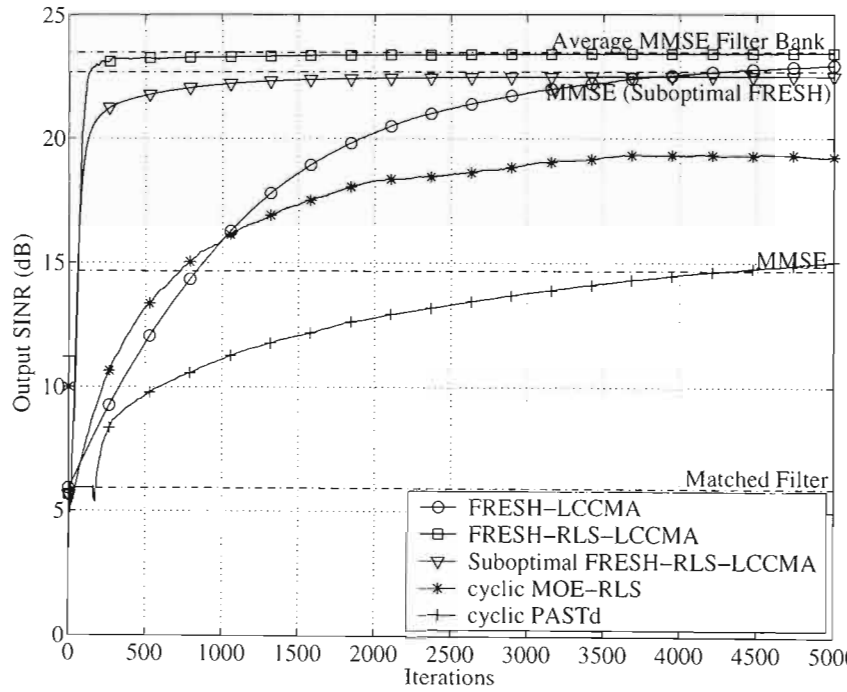

Fig. 3.8. Convergence dynamics of FRESH-LCCMA updated with the RLS procedure compared to other blind adaptive cyclic MUD's.

Fig. 3.9 (a)–(d) illustrate the operation of alternate cost functions performing SGD based cyclic MUD on differing dimension suboptimal FRESH architectures. The complexity of the receiver is varied from the full FRESH architecture in Fig. 3.9 (a) through to the conventional non-cyclic detector in Fig. 3.9 (d). The reduction in system performance, evident in this sequence, is expected as this is traded-off with receiver complexity. The results presented in Fig. 3.9 (a)–(d) are the average of 10 independent simulations for each algorithm where the SNR was set to 25dB's for all the users in the system (3 HR and 3 LR), and a common step size of 10^{-2} was used for all the algorithms.

The optimal SINR levels corresponding to the single user matched filter, and the MMSE receiver on the conventional non-PTV structure ($L'=1$), suboptimal FRESH ($L'=2$), ($L'=3$), and the full FRESH architectures ($L'=4$) are superimposed in the figures, as these levels correspond to the maximum levels that the adaptive algorithms could attain. The performance gain of the cyclic MUD strategies over the conventional MMSE MUD is once more shown to be significant. The relative gains for this particular system configuration are summarized in Table 3.3. It is interesting to note the diminishing returns as the complexity of the receiver is increased up to the full FRESH architecture, this phenomenon was also evident in Fig. 3.3. This indicates that the suboptimal FRESH architecture could provide very useful performance gains for a moderate increase in complexity (over non-cyclic MUD) for systems where the periodicity is very high.

Table 3.3. Optimal SINR values for different dimension PTV receivers of Fig. 3.9.

Receiver	SINR level (dB's)	Advantage over conventional MMSE filter (dB's)
Single user matched filter	11.76	-4.53
MMSE ($L'=1$)	16.29	0.0
MMSE Suboptimal FRESH ($L'=2$)	21.46	5.17
MMSE Suboptimal FRESH ($L'=3$)	22.75	6.46
MMSE FRESH ($L'=4$)	23.49	7.2

The relative performance of the different cost functions are compared in Fig. 3.9 by analysing the relative convergence speeds of the output SINR and the misadjustment level at steady-state. The MOE cost function has the worst performance, as its misadjustment level is so high it barely enhances performance beyond that of the single user matched filter. For reasonable performance gains from the MOE cost function the step size needs to be appreciably smaller which in turn would cause very slow convergence. The LCCMA has slightly better performance compared to the LCDCMA. The LCCMA and LCDCMA converge faster than the data aided LMS but suffer from slightly higher misadjustment levels. These simulation results also confirm that the DD-LMS and Sato cost functions have very similar performance levels to the data aided LMS algorithm.

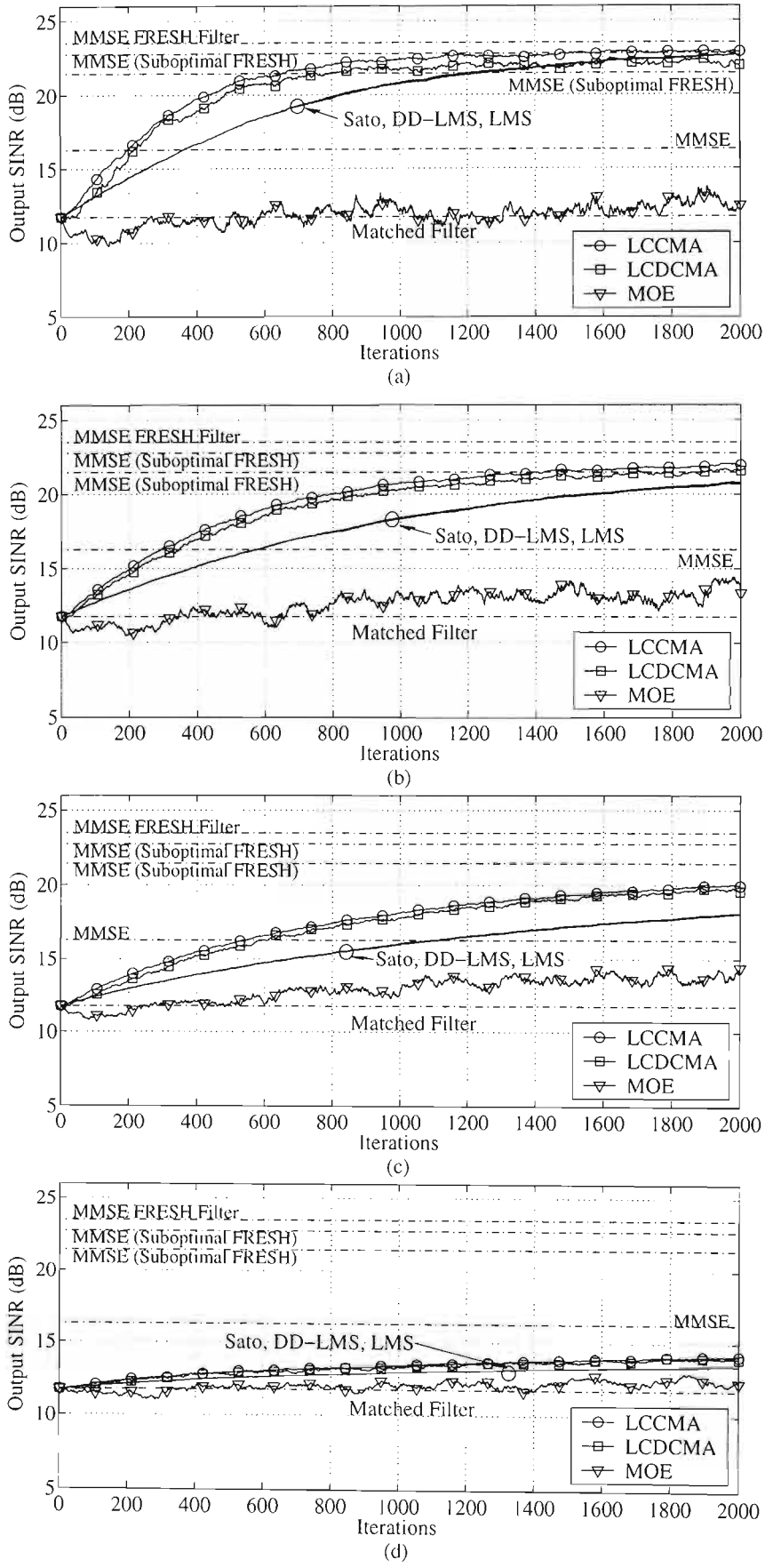

Fig. 3.9. Convergence dynamics of various code-aided (SGD based) blind adaptive cyclic MUD's implemented on the FRESH architecture where $L' = 4,3,2,1$ for Figs. (a)–(d) respectively.

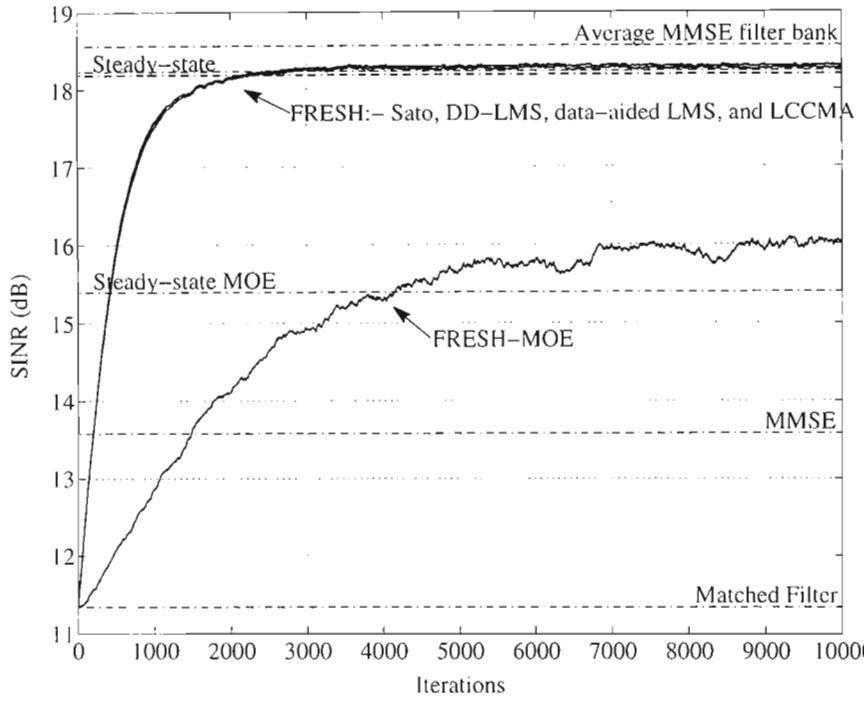

Fig. 3.10. Convergence dynamics of various code-aided (SGD based) blind adaptive cyclic MUD's showing the similarity in performance between the FRESH:- LCCMA, Sato, DD-LMS, and data-aided LMS algorithms.

The benchmark algorithms: Sato, DD-LMS, and (data-aided) LMS are observed to converge at a slower rate and to a higher steady-state SINR than the constant modulus based algorithms in Fig. 3.9 (a)–(d). To better compare the performance of FRESH-LCCMA to these algorithms, the step size of FRESH-LCCMA was modified such that it had equivalent steady-state performance to the Sato, DD-LMS, and (data-aided) LMS algorithms in Fig. 3.10. A 20db SNR system was considered and the ensemble average of 100 independent simulation runs was taken as indicative of the algorithm's performance. The step size of FRESH-LCCMA was set to 5×10^{-3}, FRESH-MOE used 2×10^{-3}, and the other algorithms' step size was set to 10^{-2}. The individual learning curves in Fig. 3.10 are nearly indistinguishable for the FRESH-: LCCMA, Sato, DD-LMS, and (data-aided) LMS algorithms, thus indicating the excellent adaptive performance levels of FRESH-LCCMA relative to these benchmark algorithms.

The accuracy of the steady-state and convergence analyses applied to the FRESH-LCCMA and filter bank implementations of LCCMA are verified via computer simulation in Fig. 3.11 and Fig. 3.12. The ensemble average EMSE and output SINR of 100 independent simulation runs are plotted in Fig. 3.11 and Fig. 3.12 respectively. A 20dB SNR system with 3 HR and 3 LR users and a 0dB MAI ratio was considered for the purposes of this comparison. The filter bank implementation of LCCMA used a step size of 4×10^{-2}, the FRESH-LCCMA was set to 2.5×10^{-3} and the non-PTV conventional LCCMA used a step size of 10^{-2}. The sliding window definition of the EMSE of the filter bank architecture, given in (3.78), is observed to accurately describe the average transient behaviour of the EMSE of the filter bank from initialisation to the steady-state region of operation. The transient behaviour of the FRESH-LCCMA and non-PTV

LCCMA are also accurately described by the analysis. Similarly, the transient behaviour of output SINR of the three differing architectures is accurately predicted by the analysis. The utility of the sliding window definition of the quantities associated with PTV filtering is thus evident in Fig. 3.11 and Fig. 3.12 as they allow a direct comparison between the performance levels associated with the three differing architectures: FRESH, filter bank, and non-PTV.

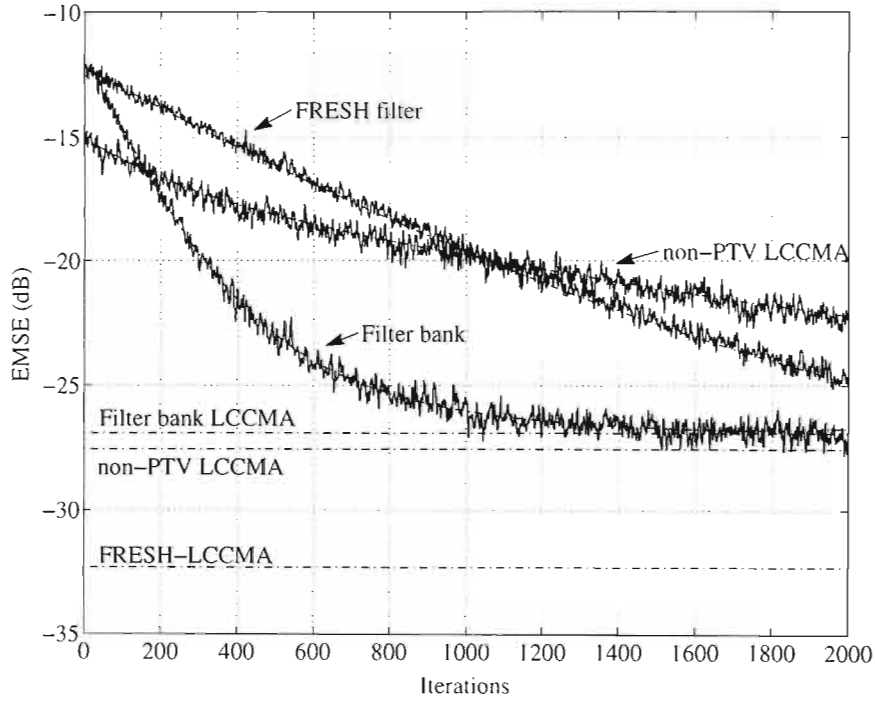

Fig. 3.11. Validation of theoretical time-evolution of the EMSE in a multi-rate DS-CDMA system. "Dash-dot" line corresponds to analysis.

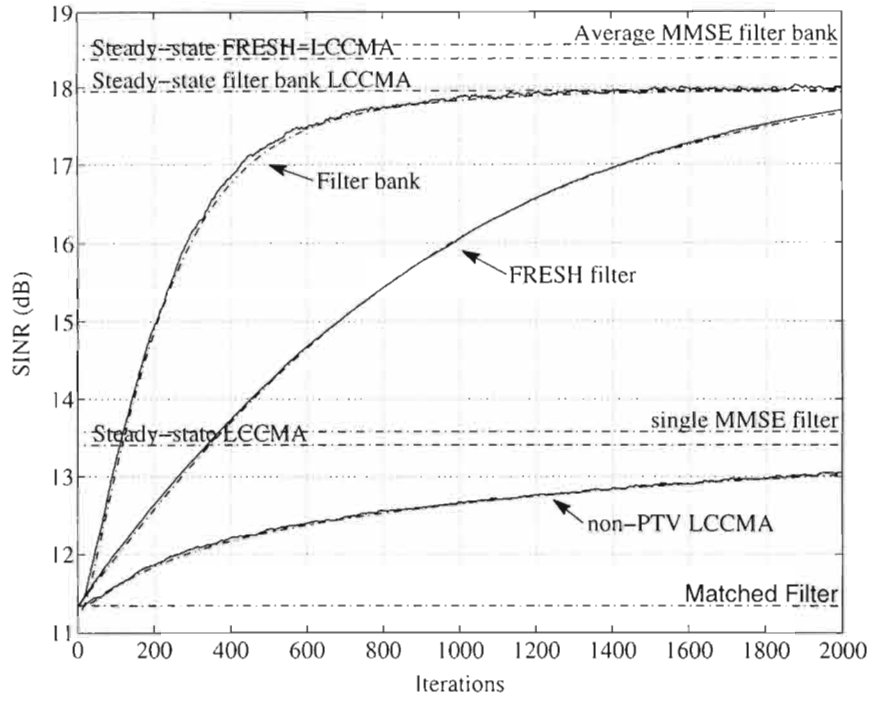

Fig. 3.12. Validation of theoretical time-evolution of the SINR in a multi-rate DS-CDMA system. "Dash-dot" line corresponds to analysis.

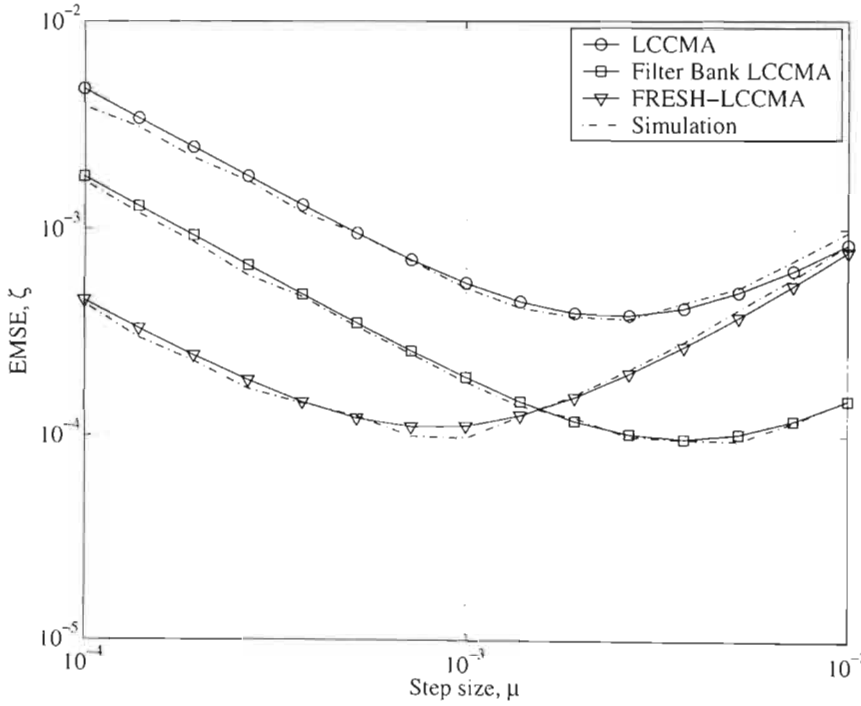

Fig. 3.13. Tracking analysis showing slight advantage of filter bank architecture.

The tracking analyses of the filter bank, FRESH filter, and non-PTV implementation of the LCCMA in a multi-rate DS-CDMA system are compared in Fig. 3.13 with EMSE values garnered from the computer simulation for various choices of step size. The value of $\mathrm{Tr}(\mathbf{Q})$ was 1.8×10^{-7} and each simulated EMSE value was taken as the average of 4×10^{5} iterations. A system with a 25dB SNR and 0dB MAI ratio was considered. Fig. 3.13 demonstrates the

accuracy of the tracking analysis and the resulting analytical framework that is developed in order to analyse the relative adaptive performance of algorithms on either filter bank or FRESH architectures. From Fig. 3.13 it can also be seen that for the system under consideration the filter bank architecture has an almost negligible performance advantage over the FRESH filter as the minimum values of EMSE for both architectures are almost the same, although they do occur at different step size values.

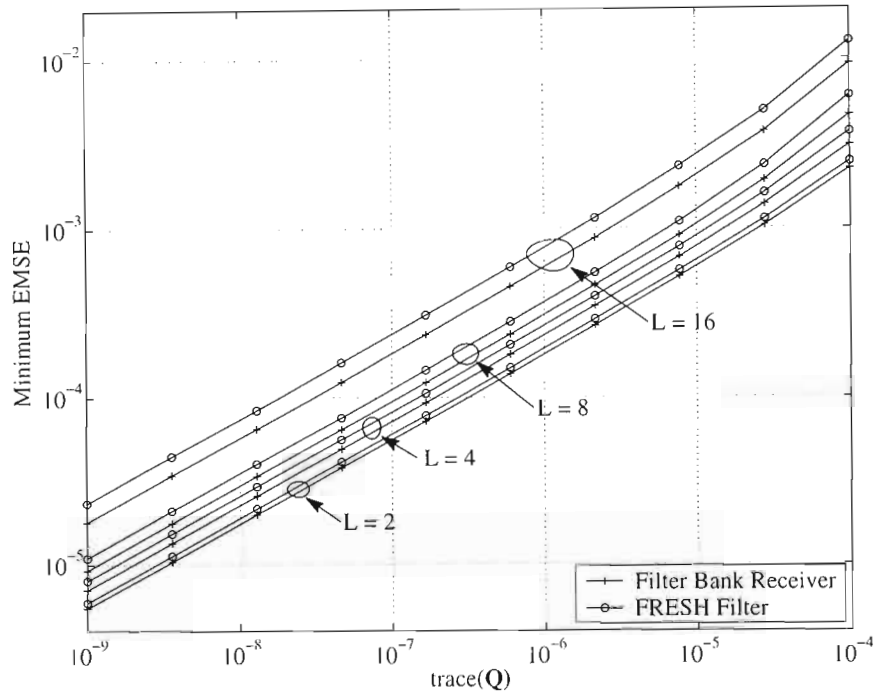

Fig. 3.14. Optimal EMSE as a function of the time-variability of the channel for the LCCMA implemented on both the filter bank and FRESH architecture.

To gain better insight into the relative performance of the filter bank and FRESH architecture, the tracking analysis is used to compute the minimum EMSE attainable by each algorithm, in a non-stationary channel, for various system configurations. The minimum EMSE occurs at the optimum choice for the step size and is found via a first order approximation for the EMSE function, as given in (2.45). The relative performance of the two techniques is explored in Fig. 3.14 for differing dimension receivers as a function of $\mathrm{Tr}(\mathbf{Q})$. The parameter L corresponds to the factor by which the LR spreading codes are longer than the HR codes and thus L also corresponds to the number of parallel branches and number of frequency shifts in the filter bank and FRESH architectures respectively. For $L=2,4,8$ the HR code length is 16, and for $L=16$ the HR code length is 8, where orthogonal Gold codes were used. In all scenarios there are 3 HR users and 3 LR users and a MAI ratio of 0dB. Fig. 3.14 shows that the relationship between the minimum EMSE for both architectures is not affected by the variability of the channel as the filter bank architecture always yields a marginally lower minimum EMSE over a large dynamic range of $\mathrm{Tr}(\mathbf{Q})$. It can also be seen from Fig. 3.14 that this relationship is maintained as the period of the interference (and thus the dimension of the receivers) increases.

3.8 Summary

This chapter considered the development and analysis of new blind adaptive cyclic MUD algorithms based on the CMA. These algorithms are important for the suppression of PTV interference sources such as MAI in multi-rate DS-CDMA systems or NBI arising in DS-CDMA overlay systems since they exploit the cyclostationary property of the interference sources. The system model presented in Section 3.3 covered the basics of multi-rate DS-CDMA systems and discussed relevant PTV filtering architectures. The equivalence of the filter bank and FRESH architecture was also established in this section for completeness. The FRESH architecture was chosen as it is a more flexible architecture for the implementation of PTV filters (in terms of computational complexity) as suboptimal structures may be derived.

The filter bank, FRESH, and suboptimal FRESH MMSE receivers were defined in Section 3.4. A novel study into the relative performance of the different suboptimal FRESH receivers was performed since no theory exists to predict the optimal set of frequency shifts for a given dimension of receiver. This novel study also served to illustrate the flexibility of the FRESH architecture relative to the filter bank receiver, and was also useful as it corroborated the particular choice of suboptimal FRESH receiver that was employed used in this thesis.

In Section 3.5 the problem of low complexity, robust, fast converging blind adaptive cyclic MUD was dealt with by proposing the use of the LCCMA algorithm on the FRESH and suboptimal FRESH receiver architectures. This section also showed how conventional code-aided blind adaptive MUD algorithms may be modified such that they can also operate on the FRESH architecture, thereby creating new blind adaptive cyclic MUD techniques. An RLS update procedure for the FRESH-LCCMA was also given in this section.

The proof of the convergence of FRESH-LCCMA was given in Section 3.6 thus ensuring the robustness of the new scheme. An extension of the adaptive performance analysis presented in Chapter 2 was also performed in this section and it was shown how this work could be used to analyse the relative adaptive performance of algorithms implemented on either the FRESH architecture or the filter bank architecture. Prior to this work, no conclusions could be drawn as to which architecture would yield superior performance.

A thorough investigation into the performance of the new algorithms was made in Section 3.7 via computer simulation and also through the adaptive performance analysis, that was developed in this chapter. The operation of the adaptive algorithms on the different suboptimal architectures was shown. The performance of the FRESH-LCCMA was evaluated by comparing its transient and steady-state behaviour with existing blind adaptive algorithms that were also explicitly developed for cyclic MUD. It was established that new FRESH-LCCMA has excellent adaptive performance characteristics relative to the existing schemes and at a substantially lower computational complexity. The performance of the different code-aided blind adaptive cyclic algorithms was compared to non-blind adaptive schemes and it was shown

that the constant modulus based schemes compared favourably with them in terms of convergence speed and steady-state performance. The FRESH-LCCMA adapted via a RLS procedure was shown to have superior performance compared with previously proposed cyclic MUD schemes, owing to the superiority of the constant modulus cost function over the MOE cost function. The results section also demonstrated the analytical framework in which the relative performance of the two approaches for the implementation of PTV filters, the FRESH filter and filter bank, may be compared. The adaptive performance of the FRESH-LCCMA and the filter bank implementation were compared using the tracking analysis and it was shown that the filter bank architecture has only a marginal performance advantage over the FRESH architecture, but obviously lacks the flexibility of the FRESH architecture.

Chapter 4

Impact of Channel and Implementation Impairments

4.1 Introduction

This chapter is concerned with the performance analysis of constant modulus based blind adaptive MUD's whilst considering the effects of realistic channel conditions, implementation limitations, and other non-ideal aspects associated with realistic systems. This chapter therefore extends the analytical framework developed in Chapter 2 and applies it to pertinent issues associated with both conventional blind adaptive MUD as well as the cyclic MUD algorithms developed in Chapter 3. The issues dealt with in this chapter have thus never previously been considered using the aforementioned analytical approach. If they have been considered at all, it is generally via computer simulation only.

The first set of issues is related to limitations in the estimation hardware at the receiver and the resulting impacts they have on the adaptive performance of the receiver. The first estimation issue that is considered is that of the estimation of the desired user's amplitude. It was shown in [31], [40], and [30] that LCCMA is only ensured to lock onto the desired user if $3A_1^2 \geq R_2$. Also, for optimum adaptive performance, ideally $R_2 \cong A_1^2$, and therefore a fairly accurate estimation of the desired user's amplitude is required. The effects that amplitude estimation error has on the adaptive performance of LCCMA are quantified in this chapter using the steady-state and convergence analysis of Chapter 2. The second issue related to estimation error that is dealt with in this chapter is the effects that mismatch have on the adaptive performance of blind adaptive MUD's. Mismatch is deemed to have occurred when the desired user's signature sequence expected at the receiver is different to that which is actually received. Multipath propagation through the wireless communications channel (as well as other non-ideal characteristics) results in distortions to the desired user's effective signature sequence. Optimum reception of the desired user is only possible using the code-aided blind adaptive MUD algorithms if this effective spreading code is accurately estimated. The effects that mismatch have on the steady-state, tracking, and transient performance of the code-aided blind adaptive MUD's are studied in this chapter.

The next issue associated with realistic implementations that is considered in this chapter is that of timing jitter at the receiver. The high data rates that characterize future generation wireless communications systems, leads to inevitable timing jitter when sampling the received baseband signal. The question of the robustness of the cyclic MUD's to timing jitter, especially when implemented using frequency shift (FRESH) filters, was raised in [77], as it is an important design consideration. This chapter extends the work of Chapters 2 and 3 by considering the impacts of timing jitter on the adaptive algorithms, using the steady-state and transient analyses,

and thus predicts the reduction in performance that the adaptive filters incur, relative to the optimal filters, as a function of jitter variance. Modifications to the LCCMA are also made in order to improve the robustness of the algorithm to timing jitter. The analytical framework developed in Chapter 3 is thus used to show the different sensitivities that the filter bank and FRESH architectures have to timing jitter.

Another important issue associated with realistic implementations is the effects of fixed point implementation. The feedback approach was explicitly applied to the analysis of fixed point implementations in [89] and [90], and consequently these issues are not revisited in this chapter.

The relative adaptive performance of the canonically and non-canonically constrained LCCMA in a Rayleigh fading channel is also considered in this chapter. Rayleigh fading is characteristic of wireless communications channels. Computer simulation results are used to illustrate the differing tracking requirements that are imposed by the differing constraints. An illustrative example is then used to verify the different adaptive performance levels of the two algorithms in a Rayleigh fading channel.

The final set of issues that is dealt with in this chapter is related to particular characteristics of DS-CDMA system implementations. These include the operation of the LCCMA in an asynchronous DS-CDMA system. The proof of convergence of the LCCMA in an asynchronous DS-CDMA is explicitly derived in this chapter, as previous analyses only considered synchronous systems. The trade-off between increasing the window size and the reduction in performance associated with the reduced tracking capability of a longer filter is examined using the adaptive performance theory developed in Chapter 2. DS-CDMA systems overlaid with pre-existing narrow band services can be greatly enhanced through interference suppression techniques, as discussed in Chapter 3. It is possible to employ non-PTV techniques to simultaneously suppress NBI and MAI [76]. However, there is a high level of correlation between successive received samples of NBI, which are not conducive to stochastic gradient based techniques. This phenomenon, as well as the exact adaptive performance of LCCMA in suppressing NBI, is considered in this chapter via an extension of the theory developed in Chapter 2.

4.2 Amplitude estimation error

Correct amplitude estimation is vital for optimum performance of the LCCMA since the steady-state performance and convergence speed of LCCMA are both affected if A_1 is incorrectly estimated. The accuracy of the steady-state and convergence analysis of the LCCMA to predict these effects is verified in Fig. 4.1 via a comparison to the ensemble average of 100 independent simulation runs. A 10 user system was considered where the MAI ratio was 3dB's, SNR was 20dB's, and all the users transmitted synchronously using length 31 Gold codes. The step size was fixed at 10^{-3}.

In Fig. 4.1, both the steady-state and the transient analysis are observed to correctly capture the effects of incorrectly estimating the desired user's amplitude. The desired user's amplitude A_1 is held constant at 1, while R_2 is varied from 1 to 0, which models correct estimation to complete underestimation respectively. As A_1 is increasingly underestimated, the convergence speed slightly increases, but the steady-state EMSE also increases, resulting in a drop in output SINR. The performance loss is thus fully quantified as a function of estimation error. The effects of underestimation are important as it is common practice to underestimate the value of A_1 to ensure stability of the LCCMA [30].

The LCDCMA has the advantage that it does not require any amplitude estimation of the desired user. The steady-state and transient analysis are thus useful to predict how accurately the amplitude needs to be estimated in order for the LCCMA to yield a performance gain over LCDCMA. An illustrative example is provided in Fig. 4.2 where a 10 user system with a 20dB SNR and 3dB MAI ratio is considered. The step size of both the LCCMA and LCDCMA is set to 10^{-3} and $R_2 = 1.4$, which corresponds to an overestimation of 18% by the LCCMA (if it normally sets $R_2 = A_1^2$) since A_1 actually equals 1). For the system configuration under consideration, the learning curves of both algorithms are nearly indistinguishable while they converge to approximately the same steady-state SINR level. This analysis therefore shows that it would be advantageous to employ the LCDCMA if it is known that the estimation error will be more than 18% in such a system. The accuracy of this theoretical cross over point is verified in Fig. 4.2 via the superimposition of the average learning curve of the SINR of 100 independent simulation runs, for both algorithms.

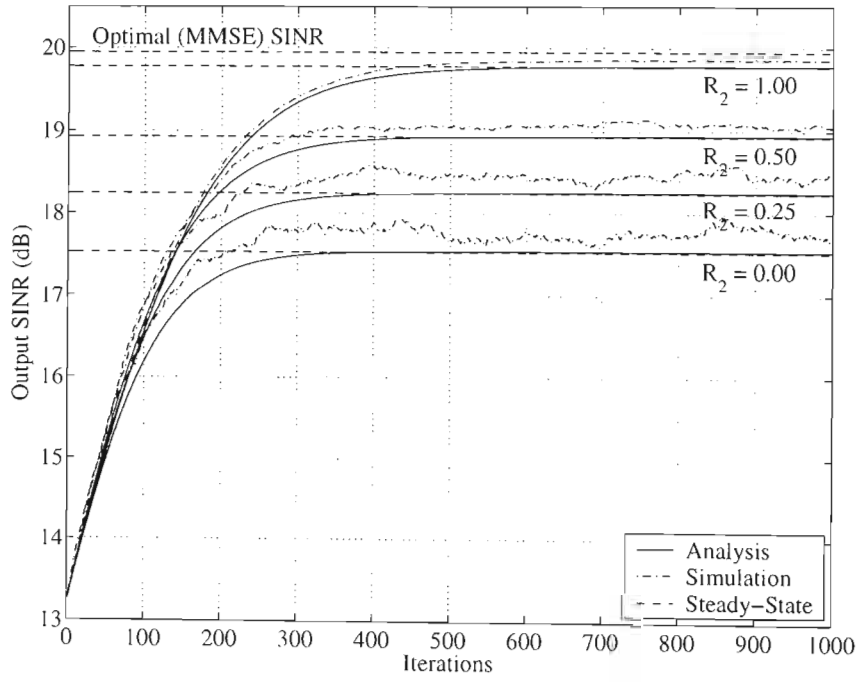

Fig. 4.1. Theoretical and simulated transient SINR behaviour of the LCCMA detector at different levels of the desired user's amplitude's underestimation.

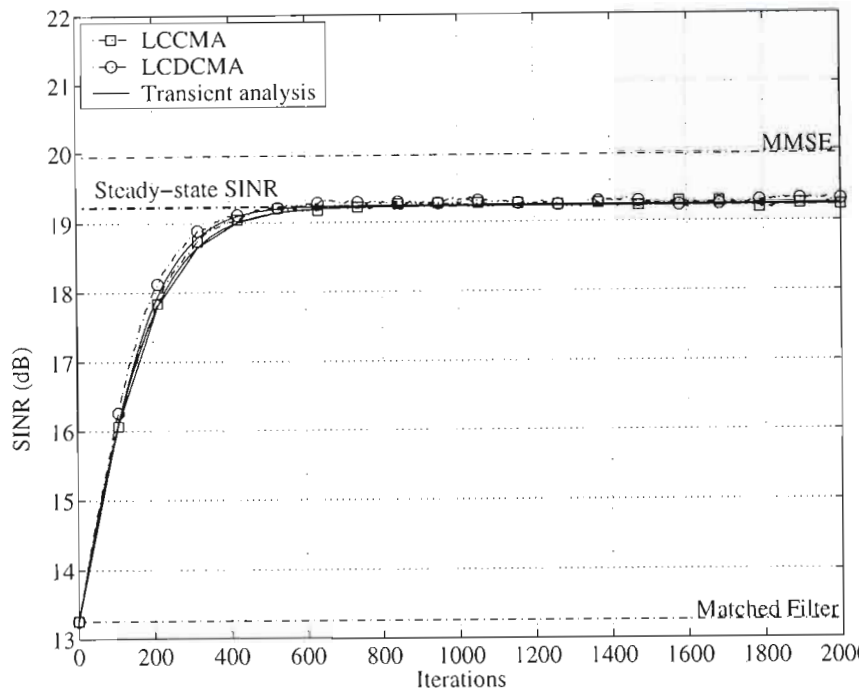

Fig. 4.2. Theoretical and simulated learning curves for the SINR of LCCMA and LCDCMA when $R_2 = 1.4$ and $A_1 = 1$.

The estimation of the desired user's amplitude is even more critical to the effective operation of the FRESH-LCCMA. The sufficient condition for convergence of FRESH-LCCMA was derived in Section 3.6.1, and it was shown there that this condition is stricter than the conventional LCCMA. Assuming that the receiver sets,

$$R_2 = (A_1')^2 \tag{4.1}$$

where A_1' is the receiver's estimate of the desired user's amplitude, then the LCCMA will converge in the mean if the receiver overestimates A_1 by no more than 73.2% (since $3A_1^2 \geq R_2$ for convergence). The FRESH-LCCMA is more sensitive since A_1 may not be overestimated at all. This increased sensitivity is illustrated in Fig. 4.3 where the FRESH, filter bank, and non-PTV versions of the LCCMA are run concurrently with $R_2 = 1.2$ (for all the algorithms) and $A_1 = 1$, which corresponds to an overestimation of approximately 10%. A 25dB SNR system, with 3 HR and 3LR users (as per the standard system setup in Chapter 3) with a MAI ratio of 0dB was considered. A step size of 10^{-2} was used for the FRESH-LCCMA and non-PTV LCCMA, and 4×10^{-2} for the filter bank implementation of LCCMA. In Fig. 4.3 the FRESH-LCCMA is observed to initially converge towards the MMSE receiver, but after approximately 12000 iterations, diverges due to the presence of alternate local minima on the FRESH-LCCMA cost surface. The non-PTV LCCMA and filter bank implementations are observed to operate without such incident due to their greater tolerance to amplitude overestimation.

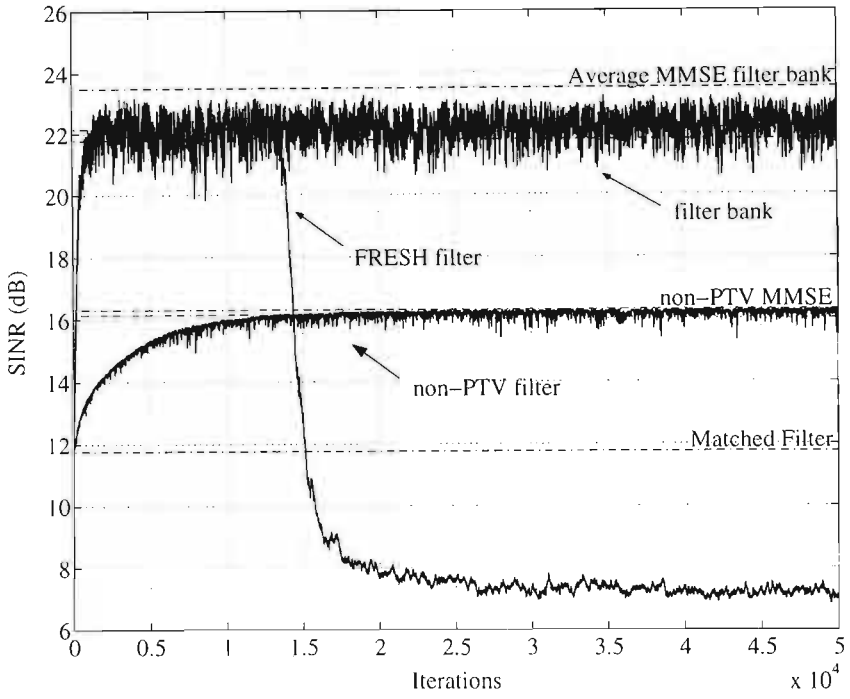

Fig. 4.3. Increased sensitivity of FRESH-LCCMA to amplitude overestimation.

4.3 Mismatch

4.3.1 Adaptive performance analysis

In a non-stationary or multipath channel, the effective spreading code received within the observation window of the receiver needs to be estimated. It is assumed that the spreading code estimator produces a non-biased estimate of the desired user's spreading code with finite precision. The finite precision causes mismatch between the actual received spreading code and that expected at the receiver. The finite precision effects are modelled by adding a Gaussian random vector to the actual received spreading code such that the estimate of the desired user's spreading code is given by,

$$\mathbf{s}_m(i) = \mathbf{s}_1(i) + \mathbf{n}_m(i) \tag{4.2}$$

where $\mathbf{n}_m$ has covariance matrix $\sigma_m^2\mathbf{I}$. To compute the effects of mismatch on the EMSE, the formula for the output of the adaptive filter given in (2.59) is modified using the canonical representation of the optimal (MMSE) filter and the receiver gain θ,

$$\mathbf{w}_{opt}(i) = \frac{\theta}{A_1}\left(\mathbf{s}_1(i) + \mathbf{w}_\perp^{opt}(i)\right) \tag{4.3}$$

where $\mathbf{w}_\perp^{opt}$ is the component of the optimal filter orthogonal to $\mathbf{s}_1$. The code constrained adaptive receivers compute the tap weights using $\mathbf{w}(i) = \mathbf{s}_m(i) + \mathbf{w}_\perp(i)$ as they only adapt the filter component orthogonal to the desired users spreading code. The output of the filter may now be expressed as,

$$\begin{aligned} y(i) &= \tfrac{\theta}{A_1}\left(\mathbf{s}_1(i)+\mathbf{n}_m(i)+\mathbf{w}_\perp(i)\right)^T \mathbf{r}(i) \\ &= \tfrac{\theta}{A_1}\left(\mathbf{w}_{opt}(i)+\mathbf{n}_m(i)-\Delta\mathbf{w}_\perp(i)\right)^T \mathbf{r}(i) \\ &= \theta b_1 + M(i)+v(i)+t(i)-e_a^\perp(i) \end{aligned} \tag{4.4}$$

where $t(i)=\frac{\theta}{A_1}\mathbf{n}_m^T(i)\mathbf{r}(i)$ and is the mismatch energy at the output of the filter, and $e_a^\perp(i)$ is the *a priori* estimation error associated with $\mathbf{w}_\perp(i)$. To simplify the EMSE expression, the output MAI plus noise is lumped with the output mismatch energy to create a new term $\tilde{v}(i)=M(i)+v(i)+t(i)$. This new term has a Gaussian distribution $\tilde{v}\sim\mathcal{N}(0,\tilde{\eta})$ where $\tilde{\eta}^2=\mathbf{w}_{opt}^T\mathbf{C}^+\mathbf{w}_{opt}+\frac{\theta}{A_1}\sigma_m^2\mathrm{Tr}(\mathbf{C})$ and $\mathbf{C}^+$ is the covariance matrix of the received vector of samples without the component from user 1. The EMSE can then be split into two terms:

$$\begin{aligned} E\left\{e_a^2(i)\right\} &= E\left\{\left(\Delta\mathbf{w}^T(i)\mathbf{r}(i)\right)^2\right\} \\ &= E\left\{\left(\left(\Delta\mathbf{w}_\perp^{opt}(i)-\mathbf{n}_m(i)\right)^T\mathbf{r}(i)\right)^2\right\} \\ &= E\left\{\left(e_a^\perp(i)\right)^2\right\}+\sigma_m^2\,\mathrm{Tr}(\mathbf{C}) \end{aligned} \tag{4.5}$$

since $\mathbf{n}_m(i)$ and $\mathbf{r}(i)$ are independent. The quantity $E\left\{\left(e_a^\perp(i)\right)^2\right\}$ is computed as before using the feedback approach, and $\sigma_m^2\,\mathrm{Tr}(\mathbf{C})$ is an irreducible term associated with the mismatch.

Under mismatch conditions (2.35) no longer closely approximates the true value of $\mathrm{Tr}(\mathbf{C}_\perp)$, which is now computed using the expression given for $\mathbf{C}_\perp$ in (4.6). The simplified fundamental energy preserving equation, given in (2.41) is now expanded using the expression for y given in (4.4) substituted into the formula for F_e as before. The resulting expression may be greatly simplified considering the mutual independence of $\{b_1,M,v,t,e_a\}$. A summary of the results of these simplifications for various algorithms are given in Table 4.1. For all the algorithms considered in Table 4.1 the receiver gain $\theta=A_1$. For the case of the non-canonical LCCMA [30], the results are the same as for the canonical LCCMA except $R_2=1$, and the receiver gain θ is 1.

The transient analysis requires the covariance matrix of the driving vector. Since the driving vector may also be written as $\mathbf{r}_\perp(i)=\mathbf{B}\mathbf{r}(i)$, where $\mathbf{B}=\mathbf{I}-\mathbf{s}_m\mathbf{s}_m^T$ and $\mathbf{B}$ is now random, it can be shown that,

$$\begin{aligned} \mathbf{C}_\perp &= E\left\{\mathbf{B}\mathbf{r}\mathbf{r}^T\mathbf{B}^T\right\} \\ &= E\left\{\left(\mathbf{I}-\mathbf{s}_m\mathbf{s}_m^T\right)\mathbf{C}\left(\mathbf{I}-\mathbf{s}_m\mathbf{s}_m^T\right)^T\right\} \\ &= \mathbf{C}-\mathbf{C}E\left\{\mathbf{s}_m\mathbf{s}_m^T\right\}-E\left\{\mathbf{s}_m\mathbf{s}_m^T\right\}\mathbf{C}+E\left\{\mathbf{s}_m\mathbf{s}_m^T\mathbf{C}\mathbf{s}_m\mathbf{s}_m^T\right\} \end{aligned} \tag{4.6}$$

where,

$$E\left\{\mathbf{s}_m\mathbf{s}_m^T\right\}=\mathbf{s}_1\mathbf{s}_1^T+\sigma_m^2\mathbf{I}$$

$$E\left\{\mathbf{s}_m\mathbf{s}_m^T\mathbf{C}\mathbf{s}_m\mathbf{s}_m^T\right\} = 2\left(\sigma_m^2\mathbf{I}+\mathbf{s}_1\mathbf{s}_1^T\right)\mathbf{C}\left(\sigma_m^2\mathbf{I}+\mathbf{s}_1\mathbf{s}_1^T\right)$$
$$+\mathbf{s}_1^T\mathbf{C}\mathbf{s}_1\left(\sigma_m^2\mathbf{I}-\mathbf{s}_1\mathbf{s}_1^T\right)+\sigma_m^2\,\mathrm{Tr}(\mathbf{C})\left(\sigma_m^2\mathbf{I}+\mathbf{s}_1\mathbf{s}_1^T\right)$$

$$\mathbf{C} = E\left\{\mathbf{r}\mathbf{r}^T\right\} = \mathbf{S}\mathbf{A}\mathbf{A}\mathbf{S}^T+\sigma^2\mathbf{I}.$$

A summary of the expressions for h_{ci} and h_{li} are given in Table 4.3. Closed form expressions have been given for $\mathbf{C}_\perp$, h_{ci}, and h_{li} and thus the transient performance may be computed using (2.49). The EMSE is assumed to be Gaussian and thus the theoretical learning curve for the output SINR may be constructed using,

$$SINR(i) = \frac{\theta^2}{\tilde{\eta}^2+\zeta(i)}. \tag{4.7}$$

It is assumed that the receiver is correctly initialised to the single user matched filter, and so the starting point of the state-space recursion is deterministic, with $\mathcal{W}_0$ computed using $\Delta\mathbf{w}_\perp(0) = \mathbf{w}_{opt}-\mathbf{s}_1$.

Table 4.1. EMSE formulas for a non-stationary channel with mismatch.

Algorithm	F_e	EMSE expression
LCCMA* (CMA2-2, Canonical)	$y\left(y^2-R_2\right)$	$J_2\zeta^2+J_1\zeta = G+T.\left(K_3\zeta^3+K_2\zeta^2+K_1\zeta+K_0\right)$
LCCMA (CMA1-2)	$R_1\,\mathrm{sign}(y)-y$	$G+\frac{T}{1-T}\left(\left(R_1-A_1\right)^2+\tilde{\eta}^2\right)$
Sato	$\mathrm{sign}(y)-y$	$G+\frac{T}{1-T}\left(\left(1-A_1\right)^2+\tilde{\eta}^2\right)$
MOE	$-y$	$G+\frac{T}{1-T}\left(A_1^2+\tilde{\eta}^2\right)$

Where $T = (\mu/2)\mathrm{Tr}(\mathbf{C}_\perp)$ (for normalised versions $T = \mu/2$)

$G = \mathrm{Tr}(\mathbf{Q})/2\mu$

$\tilde{\eta}^2$ is the output MAI plus noise plus mismatch variance.

* See Table 4.2 for $\{J_2, J_1, K_3, K_2, K_1, K_0\}$

Table 4.2. Coefficients for LCCMA EMSE expression with mismatch.

Coefficient	Value
J_2	3
J_1	$3\tilde{\eta}^2+3A_1^2-R_2$
K_3	15
K_2	$45A_1^2+45\tilde{\eta}^2-6R_2$
K_1	$R_2^2-12A_1^2R_2+45\tilde{\eta}^4+15A_1^4+90A_1^2\tilde{\eta}^2-12\tilde{\eta}^2R_2$
K_0	$A_1^6+A_1^2R_2^2+\tilde{\eta}^2R_2^2+15A_1^4\tilde{\eta}^2-6\tilde{\eta}^2R_2-12A_1^2\tilde{\eta}^2R_2-2A_1^4R_2+45A_1^2\tilde{\eta}^4+15\tilde{\eta}^6$

Table 4.3. h_G and h_G for transient analysis with mismatch.

Algorithm	$h_G = \dfrac{E\{e_a(i)F_c(i)\}}{E\{e_a^2(i)\}}$	$h_U = E\{F_c^2(i)\}$
LCCMA* (CMA2-2, Canonical)	$J_2\zeta^2(i) + J_1$	$K_3\zeta^3(i) + K_2\zeta^2(i) + K_1\zeta(i) + K_0$
LCCMA (CMA1-2)	1	$(R_1 - A_1)^2 + \tilde{\eta}^2 + \zeta(i)$
Sato	1	$(A_1 - 1)^2 + \tilde{\eta}^2 + \zeta(i)$
MOE	1	$A_1^2 + \tilde{\eta}^2 + \zeta(i)$

* See Table 4.2 for $\{J_2, J_1, K_3, K_2, K_1, K_0\}$

4.3.2 Results

The accuracy of the mismatch analysis is confirmed via simulation. The EMSE for the tracking results (Fig. 4.4–Fig. 4.6) were obtained once the algorithm had reached the tracking phase, and calculated as the mean square value of $e_a(i) \triangleq \Delta\mathbf{w}^T(i)\mathbf{r}(i)$ over 10^5 iterations.

Fig. 4.4 compares the EMSE of the LCCMA, MOE and Sato cost functions when there is no mismatch. A 10 user system with a 20 dB SNR, and a 3 dB MAI ratio was considered. It was found from the simulation that $\mathrm{Tr}(\mathbf{Q}) \cong 2.4\times10^{-6}$. This figure is provided as a reference for the situation considered below it, Fig. 4.5, where a mismatch level of $\sigma_m^2 = 10^{-4}$ is considered. From Fig. 4.5 it is evident that the presence of mismatch does not affect the value of the optimum choice of μ to a noticeable extent, but the increase in EMSE is fully accounted for by the analysis. This phenomenon is more clearly evident in Fig. 4.6 where the tracking performance of the LCCMA is plotted for different amounts of mismatch. The same system configuration as Fig. 4.4 and Fig. 4.5 is used in Fig. 4.6. The accuracy of the analyses in Fig. 4.4–Fig. 4.6 validates the assumptions used therein.

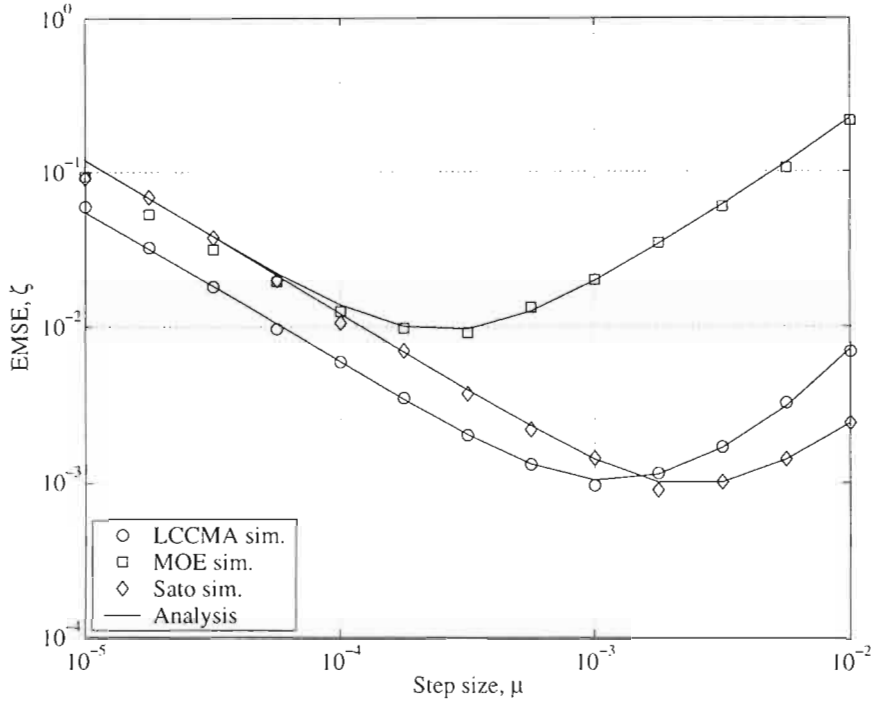

Fig. 4.4. Tracking performance of different algorithms with no mismatch present.

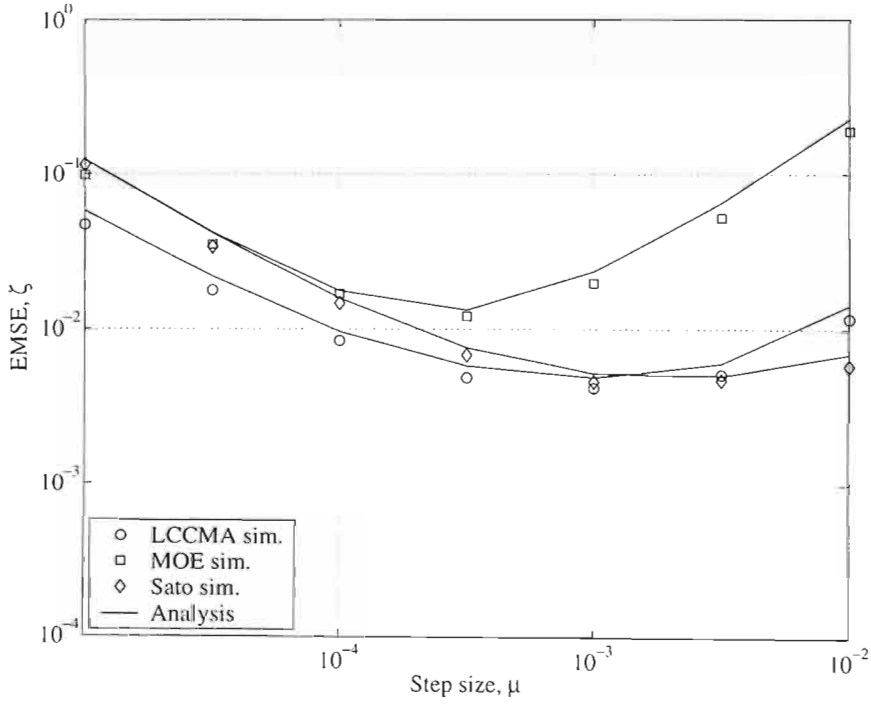

Fig. 4.5. Tracking performance of different algorithms with mismatch: $\sigma_m^2 = 10^{-4}$.

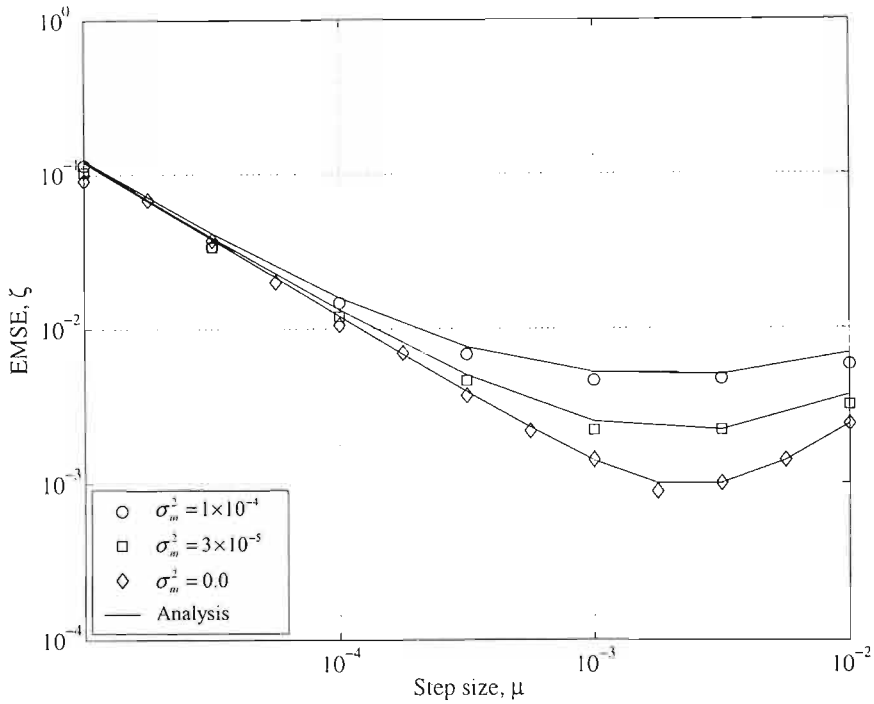

Fig. 4.6. Tracking performance of LCCMA for different amounts of mismatch.

The transient analysis is verified in Fig. 4.8, where the effects of mismatch are clearly evident by comparing this figure to the case where there is no mismatch given in Fig. 4.7. The transient simulation results were computed from the average output SINR from 100 independent simulations. For each simulation the receiver was initialised to the single user matched filter and then adapted at the bit rate for 1000 bits. The same system as defined for the tracking analysis above is considered, where the mismatch is $\sigma_m^2 = 10^{-4}$. The step size of each algorithm was set to 10^{-3}. The time evolution of the output SINR for the three different algorithms (under mismatch) is accurately predicted by the analysis. The LCCMA is still seen to be the fastest converging of the three algorithms for a given step size. Comparing Fig. 4.7 and Fig. 4.8 it can be seen that the convergence speed and steady-state SINR of the algorithms is affected by the presence of mismatch. Mismatch causes the steady-state MOE SINR to drop by a further 0.55dB and the steady-state LCCMA and Sato SINR by approximately 1.4dB's. These are significant margins thus illustrating the importance in quantifying the EMSE of the adaptive receivers under mismatch.

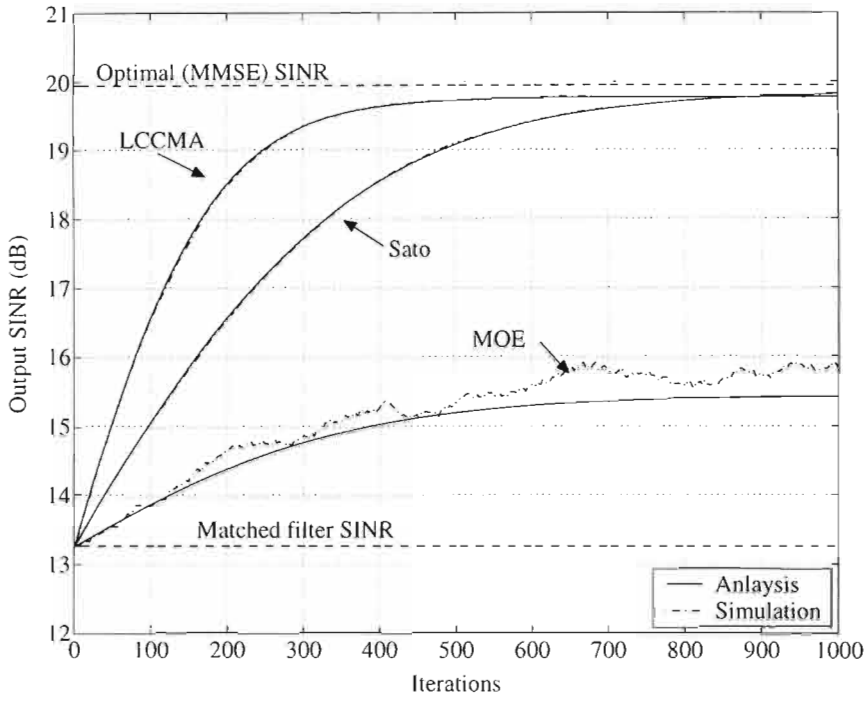

Fig. 4.7. Transient performance showing time evolution of SINR when there is no mismatch present. Receivers all initialized to the single user matched filter.

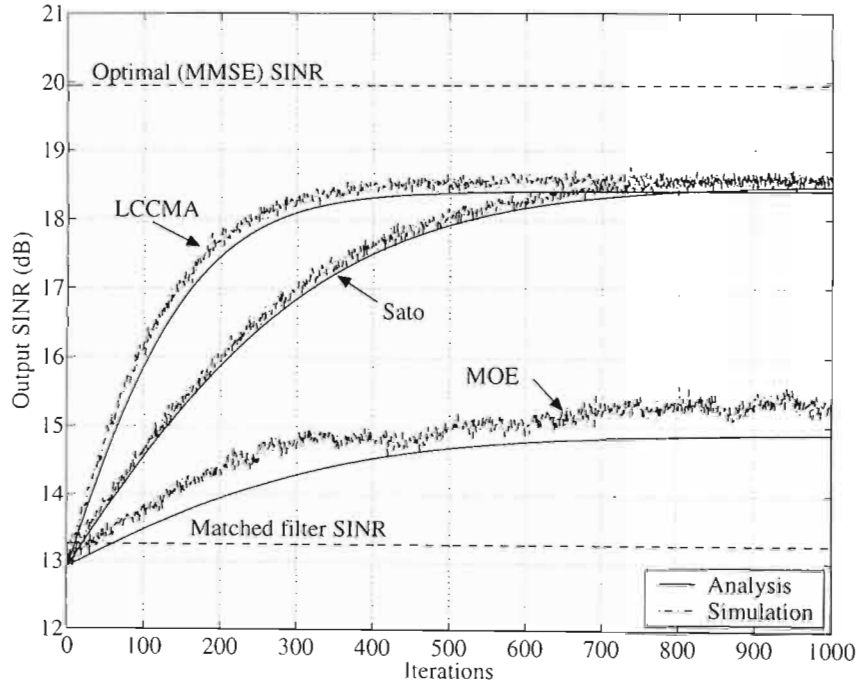

Fig. 4.8. Transient performance showing time evolution of SINR when mismatch is present where $\sigma_m^2 = 10^{-1}$. Receivers all initialized to the single user matched filter.

4.4 Receiver timing jitter

4.4.1 System model

Timing jitter at the receiver causes a misalignment between the processing window at the receiver and the bit epoch of the desired user. The same receiver model as given in Chapters 2 and 3 is considered here: the receiver samples the output of a chip-matched filter, the samples within processing window i are stacked to form vector $\mathbf{r}(i)$, which is used to detect $b_1(i)$, which is the ith bit of the desired user. This section considers the case where processing window i spans bit interval i of the desired user, and the detector operates on a symbol-by-symbol basis. For the sake of brevity only, this section considers the case of rectangular shaped chip pulses and a sample rate equal to that of the chip rate. Given timing jitter $\varepsilon(i)$, which falls in the interval $\left[-T_{c,1}/2, T_{c,1}/2\right]$ with a particular statistical distribution which is dealt with later, the set of observables within processing window i may be recast as

$$r_i(t) = r(t)\,\mathrm{rect}_{T_{b,1}}\left(t - iT_{b,1} - \varepsilon(i)\right) \tag{4.8}$$

Under the conditions outlined above, the nth sample of $r_i(t)$ may be expressed as,

$$\left[\mathbf{r}(i)\right]_n = \frac{1}{\sqrt{T_c}} \int_{nT_c+\varepsilon(i)}^{(n+1)T_c+\varepsilon(i)} r_i(t)\,dt \quad \text{for } n = 0,1,\ldots,N-1. \tag{4.9}$$

N of which are then concatenated into the received vector of samples,

$$\mathbf{r}(i) = A_1 b_1(i)\mathbf{s}_1^{HR}(i) + \sum_{k=1}^{K} \mathbf{z}_k(i) + \mathbf{n}(i) \tag{4.10}$$

where $\mathbf{s}_1(i), \mathbf{z}_k(i)$, and $\mathbf{n}(i)$ are the discrete-time representations of: the desired user's signature waveform, the MAI component attributed to user k, and the noise vector respectively. The intersymbol interference (ISI) from user k due to jitter is modelled as another source of MAI and hence there is a $\mathbf{z}_1(i)$ term in (4.10). The desired user's effective signature waveform during bit epoch i is given by

$$\mathbf{s}_1^{HR}(i) = \left(1 - \left|\varepsilon(i)\right|\right)\hat{\mathbf{s}}_1^{HR} + \boldsymbol{\varphi}_1(i) \tag{4.11}$$

where $\hat{\mathbf{s}}_1$ is the discrete representation of the spreading waveform under zero-jitter conditions and is time invariant, $\boldsymbol{\varphi}_1(i)$ is the inter-chip interference (ICI) due to jitter given by,

$$\boldsymbol{\varphi}_1(i) = \begin{cases} \left|\varepsilon(i)\right|\hat{\mathbf{s}}_1^{HR}[+1] & \text{if } \varepsilon(i) \geq 0 \\ \left|\varepsilon(i)\right|\hat{\mathbf{s}}_1^{HR}[-1] & \text{if } \varepsilon(i) < 0 \end{cases} \tag{4.12}$$

where $\mathbf{s}_k[n]$ indicates a downward shift of the elements of vector $\mathbf{s}_k$ by n elements, with replacement by zero. Let $\boldsymbol{\chi}_1(i)$ be the ISI due to jitter given by

$$\boldsymbol{\chi}_1(i) = \begin{cases} A_1 b_1(i-1)\left|\varepsilon(i)\right|\hat{\mathbf{s}}_1^{HR}[1-N] & \text{if } \varepsilon(i) \geq 0 \\ A_1 b_1(i+1)\left|\varepsilon(i)\right|\hat{\mathbf{s}}_1^{HR}[N-1] & \text{if } \varepsilon(i) < 0, \end{cases} \tag{4.13}$$

and so $z_1(i) = \chi_1(i)$. The discrete MAI samples corresponding to the other HR users are similarly composed of ICI corrupted signature sequences and ISI components,

$$\mathbf{z}_k^{HR}(i) = A_k b_k(i)\mathbf{s}_k^{HR}(i) + \chi_k(i) \tag{4.14}$$

Let $\hat{\mathbf{s}}_k^{LR}(i)$ be the effective spreading sequence of the kth LR user within processing window i under zero-jitter conditions, then clearly $\hat{\mathbf{s}}_k^{LR}(i)$ is PTV in i with period L. Taking this into account, the MAI from the other LR users may be similarly constructed as per (4.14).

The timing jitter (or error) $\varepsilon(i)$ of processing window i is given by

$$\varepsilon(i) = iT_{b,1} - T'_{b,1}(i) \tag{4.15}$$

where $T'_{b,1}(i)$ is the receiver's estimate of the start time of the desired user's ith bit. The timing error distribution is derived from the phase error distribution of a phase locked loop (PLL) which is modelled using a von Mises/Tikhonov distribution [91], the probability distribution function (PDF) of which is given by,

$$p(\theta) = \frac{1}{2\pi I_0(\kappa)} \exp(\kappa \cos(\theta - \alpha)) \tag{4.16}$$

where $I_0(.)$ is the modified Bessel function of the first kind of order 0, κ is the concentration parameter (large κ corresponds to very small phase error) and α shifts the position of the peak by α radians. It is assumed that the timing error is unbiased and thus $\alpha = 0$. The von Mises/Tikhonov distribution distributes the bit timing phase $\theta(i)$ error between $[-\pi, \pi]$ radians, which maps the timing error $\varepsilon(i)$ into the interval $[-T_{c,1}/2, T_{c,1}/2]$. A histogram of a von Mises/Tikhonov distribution is given in Fig. 4.9 for illustrative purposes. For the scale of the timing jitter under consideration in this thesis, it is possible for the von Mises/Tikhonov distribution of θ to be approximated with a zero-mean Gaussian distribution with variance $1/\kappa$.

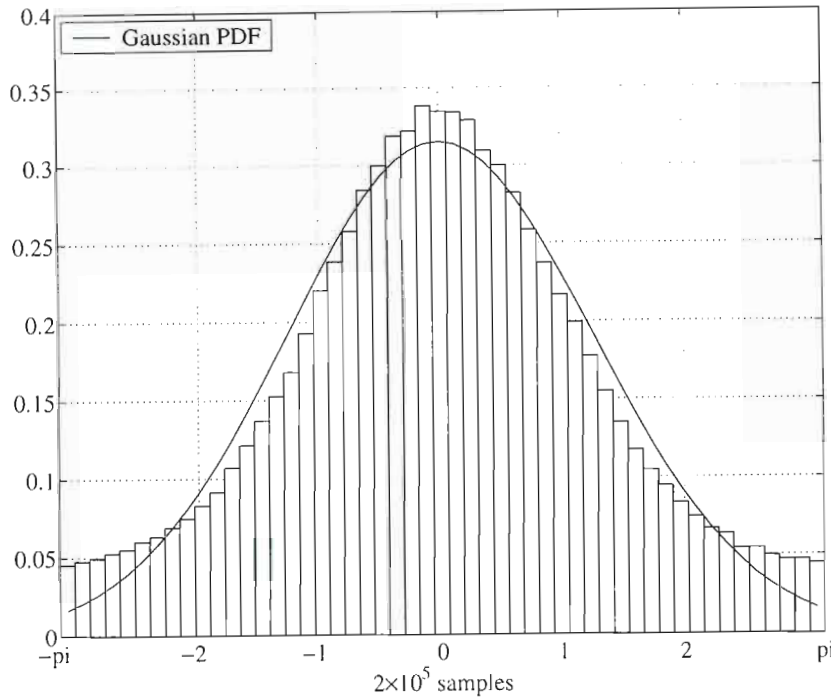

Fig. 4.9. Sample von Mises histogram ($\kappa = 1$, $\alpha = 0$) compared to a Gaussian PDF whose variance parameter was set to the same variance as the sample von Mises data.

4.4.2 MMSE detection

When jitter is present, the periodicity of $\mathbf{C}(l)$ is destroyed, and thus the advantages of PTV filtering are lost. To restore the periodicity, the *point* MMSE filter, as given in (3.23), is not used, but rather $\mathbf{C}(l)$ is redefined as the time-average:

$$\mathbf{C}(l) \triangleq E\left\{\mathbf{r}(i)\mathbf{r}^{T}(i)\delta_{l}(i)\right\} \tag{4.17}$$

where,

$$\delta_{l}(i) = \begin{cases} 1, & \text{if } i = l,\ l \pm L, l \pm 2L,\ \ldots \\ 0, & \text{otherwise.} \end{cases} \tag{4.18}$$

An exponentially time-windowed version of (4.17) may also be employed in order for a slowly time varying channel to be tracked. Also, it is not realistic to assume that a stochastic gradient algorithm could track the uncorrelated jitter from bit epoch to bit epoch, and therefore the time-average MMSE receiver defined using (4.17) is applicable.

This time averaged covariance matrix may be split into fixed and PTV components that correspond to the HR users plus noise, and the LR users respectively,

$$\mathbf{C}(l) = \mathbf{C}_{HR} + \mathbf{C}_{LR}(l) + \sigma^{2}\mathbf{I} \tag{4.19}$$

Denote the number of HR users by K' and the number of LR users by K'', then by defining the matrix notation,

$$\mathbf{S}_{HR}[n] = \left[\hat{\mathbf{s}}_{1}[n], \hat{\mathbf{s}}_{2}[n], \ldots, \hat{\mathbf{s}}_{K'}[n]\right] \tag{4.20}$$

$$\mathbf{A}_{HR} = \mathrm{diag}\left(\left[A_1,\ldots,A_{K'}\right]\right) \tag{4.21}$$

it is possible to express $\mathbf{C}_{HR}$ with,

$$\begin{aligned}\mathbf{C}_{HR} &= \left(1-2E\left\{|\varepsilon|\right\}+E\left\{\varepsilon^2\right\}\right)\left(\mathbf{S}_{HR}[0]\mathbf{A}_{HR}\mathbf{A}_{HR}^T\mathbf{S}_{HR}^T[0]\right)\\ &+\frac{1}{2}E\left\{\varepsilon^2\right\}\left(\mathbf{S}_{HR}[+1]\mathbf{A}_{HR}\mathbf{A}_{HR}^T\mathbf{S}_{HR}^T[+1]+\mathbf{S}_{HR}[-1]\mathbf{A}_{HR}\mathbf{A}_{HR}^T\mathbf{S}_{HR}^T[-1]\right)\\ &+\frac{1}{2}\left(E\left\{|\varepsilon|\right\}-E\left\{\varepsilon^2\right\}\right)\left(\mathbf{S}_{HR}\mathbf{A}_{HR}\mathbf{A}_{HR}^T\mathbf{S}_{HR}^T[+1]+\mathbf{S}_{HR}[+1]\mathbf{A}_{HR}\mathbf{A}_{HR}^T\mathbf{S}_{HR}^T\right.\\ &\left.+\mathbf{S}_{HR}\mathbf{A}_{HR}\mathbf{A}_{HR}^T\mathbf{S}_{HR}^T[-1]+\mathbf{S}_{HR}\mathbf{A}_{HR}\mathbf{A}_{HR}^T[-1]\mathbf{S}_{HR}^T\right)\\ &+\frac{1}{2}E\left\{\varepsilon^2\right\}\left(\mathbf{S}_{HR}[N-1]\mathbf{A}_{HR}\mathbf{A}_{HR}^T\mathbf{S}_{HR}^T[N-1]+\mathbf{S}_{HR}[1-N]\mathbf{A}_{HR}\mathbf{A}_{HR}^T\mathbf{S}_{HR}^T[1-N]\right)\end{aligned} \tag{4.22}$$

which is made up of terms from the current bit epoch ($\mathbf{S}_{HR}[0]$), the ICI ($\mathbf{S}_{HR}[+1]$, $\mathbf{S}_{HR}[-1]$), the cross terms between the current bit epoch and ICI, and finally the ISI components ($\mathbf{S}_{HR}[N-1]$, $\mathbf{S}_{HR}[1-N]$), as given in (4.11)–(4.14). The above expression is derived by making use of the fact that 50% of the time $\varepsilon \geq 0$ and the other 50% of the time $\varepsilon < 0$, and also using the fact that $E\left\{b_k(i)b_k(i-1)\right\}=0$, and $E\left\{b_k(i)b_k(i+1)\right\}=0$.

For a similar expression for the PTV component $\mathbf{C}_{I,R}(l)$ of the covariance matrix define,

$$\mathbf{S}_{I,R}[n] = \left[\hat{\mathbf{s}}_{K'+1}[n],\hat{\mathbf{s}}_2[n],\ldots,\hat{\mathbf{s}}_{K''}[n]\right] \tag{4.23}$$

$$\mathbf{A}_{I,R} = \mathrm{diag}\left(\left[A_{K'+1},\ldots,A_{K''}\right]\right) \tag{4.24}$$

and define the partitioning of $\mathbf{S}_{I,R}[n]$ into L blocks each having the same dimension $(N\times K'')$ with,

$$\mathbf{S}_{I,R}[n] = \begin{bmatrix}\mathbf{S}_{I,R}^1[n]\\ \vdots \\ \mathbf{S}_{I,R}^L[n]\end{bmatrix}. \tag{4.25}$$

$\mathbf{C}_{I,R}(l)$ is then given by a similar expression to (4.22) where $\mathbf{S}_{HR}[n]$ is replaced by $\mathbf{S}_{I,R}^l[n]$ and $\mathbf{A}_{HR}$ is replaced by $\mathbf{A}_{I,R}$.

The values $E\left\{|\varepsilon|\right\}$ and $E\left\{\varepsilon^2\right\}$, as appears in (4.22), may be approximated by $T_c/\sqrt{2\kappa\pi^3}$ and $T_c^2/(4\kappa\pi^2)$ respectively, using the Gaussian approximation for the von Mises distribution. When the jitter becomes more severe (smaller κ) the Gaussian approximation becomes less accurate and more accurate values should be used which may be computed via numerical integration over the von Mises PDF. Numerical integration is required as it is not possible to express $E\left\{|\varepsilon|\right\}$ and $E\left\{\varepsilon^2\right\}$ with closed form solutions.

4.4.3 Adaptive performance in the presence of jitter

The impacts of timing jitter at the receiver on the adaptive algorithms are explored in this section. The relative effectiveness of the filter bank and FRESH architectures under jitter

conditions is evaluated via the steady-state and transient analysis of the adaptive algorithms. This section details the new elements required to extend the analysis of Chapters 2 and 3 to account for the presence of timing jitter at the receiver. This section therefore details: how the output of the filters may be described in terms of deterministic quantities, and some new assumptions that are required to compute the EMSE.

To express the output of the filters in terms of deterministic quantities, the same approach as used Chapters 2 and 3 is applied here where the output of the filters is described in terms of the optimal filter coefficients and the *a priori* estimation error. The output of the *l*th filter in the filter bank receiver may then be expressed using,

$$y(i)=\left[\left(\mathbf{w}_{opt}^{T}(l)\mathbf{u}(i)\right)+v(i)-e_{a,\perp}(i)\right]\delta_{l}(i). \tag{4.26}$$

where v is the MAI (containing ISI and ICI components) plus AWGN at the output of the optimal filter. The signal associated with the desired user's data symbol within the current processing window is given by,

$$\mathbf{u}(i)=A_{1}b_{1}(i)\left(\left(1-\left|\varepsilon(i)\right|\right)\hat{\mathbf{s}}_{1}+\boldsymbol{\varphi}_{1}(i)\right). \tag{4.27}$$

The output of the FRESH filter may be similarly expressed,

$$y(i)=\left(\tilde{\mathbf{w}}_{opt}^{H}\tilde{\mathbf{u}}(i)\right)+v(i)-e_{a,\perp}(i) \tag{4.28}$$

where $\tilde{\mathbf{u}}(i)$ is given in (3.72). It is assumed that $\mathbf{w}_{opt}^{T}(l)\mathbf{u}(i)$ and $\tilde{\mathbf{w}}_{opt}^{H}\tilde{\mathbf{u}}(i)$ are zero mean and uncorrelated with the associated $\{v,e_{a,\perp}\}$ terms. This may not hold in general but leads to a good match between theoretical and simulation results. It is also assumed that the higher moments of $\mathbf{w}_{opt}^{T}(l)\mathbf{u}(i)$ and $\tilde{\mathbf{w}}_{opt}^{H}\tilde{\mathbf{u}}(i)$ are not significantly affected by the presence of jitter and thus,

$$E\left\{\left(\mathbf{w}_{opt}^{T}(l)\mathbf{u}(i)\right)^{2k}\right\}=\left(\mathbf{w}_{opt}^{T}(l)\mathbf{U}\mathbf{w}_{opt}(l)\right)^{k} \tag{4.29}$$

$$E\left\{\left(\tilde{\mathbf{w}}_{opt}^{H}\tilde{\mathbf{u}}(i)\right)^{2k}\right\}=\left(\tilde{\mathbf{w}}_{opt}^{H}\tilde{\mathbf{U}}\tilde{\mathbf{w}}_{opt}\right)^{k}. \tag{4.30}$$

This assumption is confirmed in Table 4.4 where the approximation is observed to hold closely even under severe jitter conditions ($\kappa=2.3$).The approximation is observed to hold more closely as the amount of jitter decreases ($\kappa=23$) as expected.

The covariance matrix of the component of the received vector of samples associated with the desired user is given by,

$$\begin{aligned}\mathbf{U}&=E\left\{\mathbf{u}(i)\mathbf{u}^{T}(i)\right\}\\&=A_{1}^{2}\left[\left(1-2E\left\{|\varepsilon|\right\}+E\left\{\varepsilon^{2}\right\}\right)\left(\hat{\mathbf{s}}_{1}\hat{\mathbf{s}}_{1}^{T}\right)+\frac{1}{2}E\left\{\varepsilon^{2}\right\}\left(\hat{\mathbf{s}}_{1}[+1]\hat{\mathbf{s}}_{1}^{T}[+1]+\hat{\mathbf{s}}_{1}[-1]\hat{\mathbf{s}}_{1}^{T}[-1]\right)+\right.\\&\left.\frac{1}{2}\left(E\left\{|\varepsilon|\right\}-E\left\{\varepsilon^{2}\right\}\right)\left(\hat{\mathbf{s}}_{1}\hat{\mathbf{s}}_{1}^{T}[+1]+\hat{\mathbf{s}}_{1}[+1]\hat{\mathbf{s}}_{1}^{T}+\hat{\mathbf{s}}_{1}\hat{\mathbf{s}}_{1}^{T}[-1]+\hat{\mathbf{s}}_{1}[-1]\hat{\mathbf{s}}_{1}^{T}\right)\right],\end{aligned} \tag{4.31}$$

Table 4.4. Confirmation of higher order moments of $\mathbf{w}_{opt}^{T}\mathbf{u}(i)$ not being affect by jitter.

κ Parameter	Term	Simulation	Theory
2.3	$E\left\{\left(\mathbf{w}_{opt}^{T}\mathbf{u}(i)\right)^{2}\right\}$	0.870	0.867
	$E\left\{\left(\mathbf{w}_{opt}^{T}\mathbf{u}(i)\right)^{4}\right\}$	0.767	0.757
	$E\left\{\left(\mathbf{w}_{opt}^{T}\mathbf{u}(i)\right)^{6}\right\}$	0.685	0.658
23	$E\left\{\left(\mathbf{w}_{opt}^{T}\mathbf{u}(i)\right)^{2}\right\}$	0.951	0.951
	$E\left\{\left(\mathbf{w}_{opt}^{T}\mathbf{u}(i)\right)^{4}\right\}$	0.905	0.904
	$E\left\{\left(\mathbf{w}_{opt}^{T}\mathbf{u}(i)\right)^{6}\right\}$	0.863	0.860

Simulation setup: 25dB SNR, 0dB MAI, 15 users all using length 31 Gold codes. Average from 10^5 iterations.

and $\tilde{\mathbf{U}}$ is the block diagonal matrix with $\mathbf{U}$ along the main block-diagonal. The filtered MAI (containing ISI and ICI components) plus AWGN at the output of the optimum filter is again assumed to have a Gaussian distribution, the variance of which is given by (3.76) and (3.77) for the lth filter in the bank and the FRESH architecture respectively.

The required elements have been presented and the rest of the steady-state and transient analysis follows as per the procedure laid out in Chapters 2 and 3.

4.4.4 A note on the convergence of LCCMA in the presence of jitter

When there is significant timing jitter at the receiver the average effective spreading code of the desired user may differ significantly from the non-jitter affected spreading code that is expected at the receiver. Although the LCCMA is significantly more robust to signature sequence mismatch compared to the MOE algorithm [27], convergence towards the MMSE filters as defined in (3.22), (3.24), and (3.26) cannot be guaranteed. A similar situation arises in an unknown multipath channel where the LCCMA tends to suppress multipaths as opposed to combine them. This ill-convergence associated with timing jitter is avoided in this thesis by modifying the update step of the adaptive algorithm in the same way that the constrained MOE algorithm is in [25], thereby creating a jitter resilient LCCMA. This is achieved by adding a small proportion (ν_1) of the adaptive component of the filter coefficients to the projection of the gradient of the cost surface orthogonal to the fixed component of the filter coefficients. The update step of the FRESH-LCCMA (for example) now becomes,

$$\tilde{\mathbf{w}}_{\perp}(i+1)=(1-\mu\nu_1)\tilde{\mathbf{w}}_{\perp}(i)+\mu y(i)F_c(i)\tilde{\mathbf{r}}_{\perp}(i). \tag{4.32}$$

The parameter ν_1 thus counteracts the effects of jitter and enables convergence to a point much closer to the true MMSE solution, as is corroborated by simulation results. The optimal filter coefficients of the constrained MOE cost function are given in [25]. This chapter therefore

assumes that the optimal constrained LCCMA filter coefficients are closely approximated by the true MMSE filter coefficients.

4.4.5 Results

In Fig. 4.10 the convergence dynamics of the LCCMA on the three architectures is compared in the presence of timing jitter at the receiver. The jitter parameter κ was set to 2.3 which corresponds to a standard deviation in the timing error ε of 12% of T_c. The constraint parameter ν_1 was set to 0.01. The SINR curves are the ensemble average of 100 independent simulation runs. The same system settings as Fig. 3.5 were used: 25dB SNR, 0dB MAI ratio, 3 HR and 3 LR users, a step size of 10^{-2} for the FRESH-LCCMA and non-PTV LCCMA, and a step size of 4×10^{-2} for the filter bank implementation of the LCCMA. Unlike Fig. 3.5, the filter bank and FRESH architectures no longer have equivalent performance levels, rather the filter bank architecture is observed to be more resilient to timing jitter, as it converges to a higher SINR level faster. The constrained versions of the FRESH-LCCMA and filter bank LCCMA are observed to enhance the SINR. This enhancement becomes more obvious (as well as for the non-PTV filter) after more iterations as the SINR levels of the unconstrained algorithms continue to drop. From Fig. 4.10 the reduction in the maximum attainable SINR level due to timing jitter can also be seen as the SINR levels of the PTV and non-PTV MMSE filters are reduced by 3.6dB and 2.1dB respectively, relative to the non-jitter affected system. The difference between the MMSE SINR levels and those achieved by the adaptive algorithms, as well as the convergence curves, are readily predicted via the steady-state and transient analysis respectively.

In order to illustrate the accuracy of the steady-state analysis, the EMSE is plotted in Fig. 4.11 as a function of the jitter parameter κ. The step sizes of the adaptive algorithms were fixed at 10^{-3}, 8×10^{-3}, and 2×10^{-3} for the non-PTV, filter bank, and FRESH filter implementations of the LCCMA respectively. The constraint parameter ν_1 was set to 10^{-3}. The EMSE level computed from the simulation was the average from 10000 iterations (once steady-state was reached), then this value was averaged using 100 independent simulation runs. The analysis is observed to correctly predict the rise in EMSE as the severity of the jitter increases (small κ values). The combination of step size values for the FRESH-LCCMA and filter bank implementation of the LCCMA was chosen such that the algorithms would have equivalent performance levels in the zero jitter situation, as seen in Fig. 3.5. This enables a direct comparison between the EMSE levels of the two architectures. Fig. 4.11 shows that the FRESH-LCCMA is more susceptible to jitter since it has a higher steady-state EMSE level for a given amount of jitter.

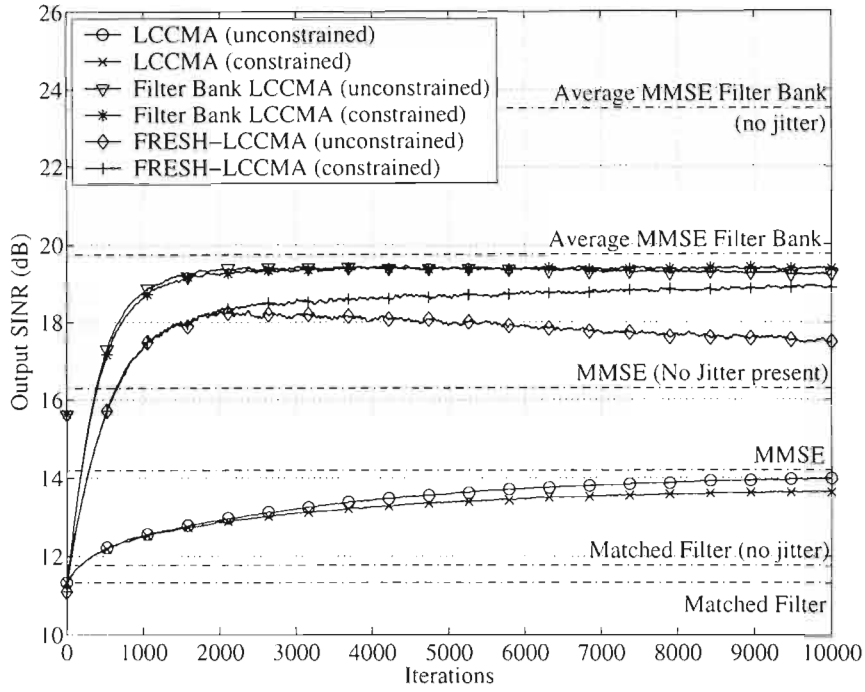

Fig. 4.10. LCCMA Convergence dynamics of constrained and unconstrained LCCMA with timing jitter at the receiver.

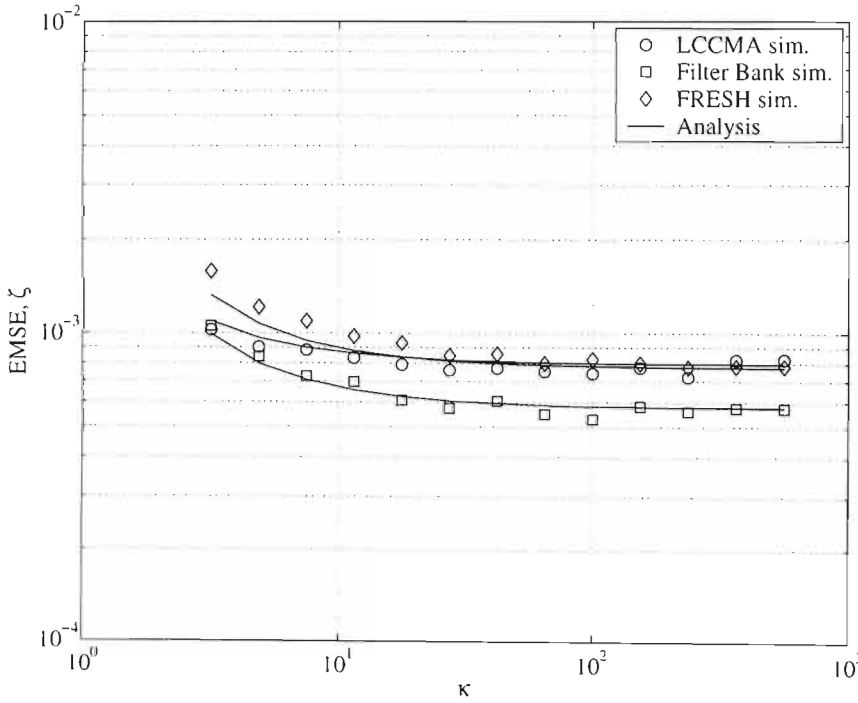

Fig. 4.11. EMSE of LCCMA as a function of jitter parameter κ.

4.5 Rayleigh fading

Wireless communications channels are subjected to Rayleigh fading when there is no line of sight between the transmitter and the receiver, which is often the case. The increased tracking requirements of the non-canonically constrained LCCMA in a fading channel, was discussed in

Section 2.6.2. This phenomenon is illustrated in Fig. 4.12 for a Rayleigh fading channel via a plot of $\mathrm{Tr}(\mathbf{Q}_\perp)$ as a function of SNR. The value of $\mathrm{Tr}(\mathbf{Q}_\perp)$ was computed via simulation by using the average from 60000 bits in a correlated Rayleigh fading channel, with correlation function given by,

$$\phi_{\ell'}(\Delta t) = J_0(2\pi f_m \Delta t) \tag{4.33}$$

as defined by Jakes model [91]. The normalised maximum Doppler frequency was set to 10^{-4}. Such a value for the normalised Doppler frequency would, for example, translate to a vehicular speed of 15m/s (or 54km/h, 33.5 miles/h) if a user was transmitting at a bit rate of 1Mbits/sec at a carrier frequency of 2GHz. The number of users was set to 10, and a MAI of 3dB was used. As the SNR decreases, the optimal LCCMA filter converges towards the MF, and hence the value of $\mathrm{Tr}(\mathbf{Q}_\perp)$ decreases in this direction as the single user matched filter has zero variability as a function of MAI as the SNR tends to $-\infty$. Over the SNR range illustrated in Fig. 4.12, the non-canonically constrained LCCMA's $\mathrm{Tr}(\mathbf{Q}_\perp)$ is typically 4 orders of magnitude higher than the canonically constrained LCCMA for the same channel. This is due to the greater dynamic range that the orthogonal component $\mathbf{w}_\perp$ of the non-canonically constrained LCCMA uses, as discussed in Section 2.6.2.

This massive disparity of the two algorithms in a fading channel is illustrated graphically in Fig. 4.13 by comparing the average performance of the two algorithms in a correlated Rayleigh fading channel. The ensemble average SINR from 500 simulation runs over the same set of fading terms is plotted where the time correlation function is the same as that defined for Fig. 4.12. A 5 user system with a 3dB MAI level, $\mu = 2\times10^{-3}$, and mean SNR of 10dB was considered. The average value of $\mathrm{Tr}(\mathbf{Q}_\perp)$ over the simulation was 2.2×10^{-5}. It was assumed that both algorithms have perfect knowledge of the amplitude of the desired user. The output SINR of the canonically constrained LCCMA is lower bounded by the analytical expression, computed at each bit epoch for the set of amplitudes at that point and the average value of $\mathrm{Tr}(\mathbf{Q}_\perp)$. The inferior performance of the non-canonically constrained LCCMA is evident, offering only a slight improvement over the single user matched filter.

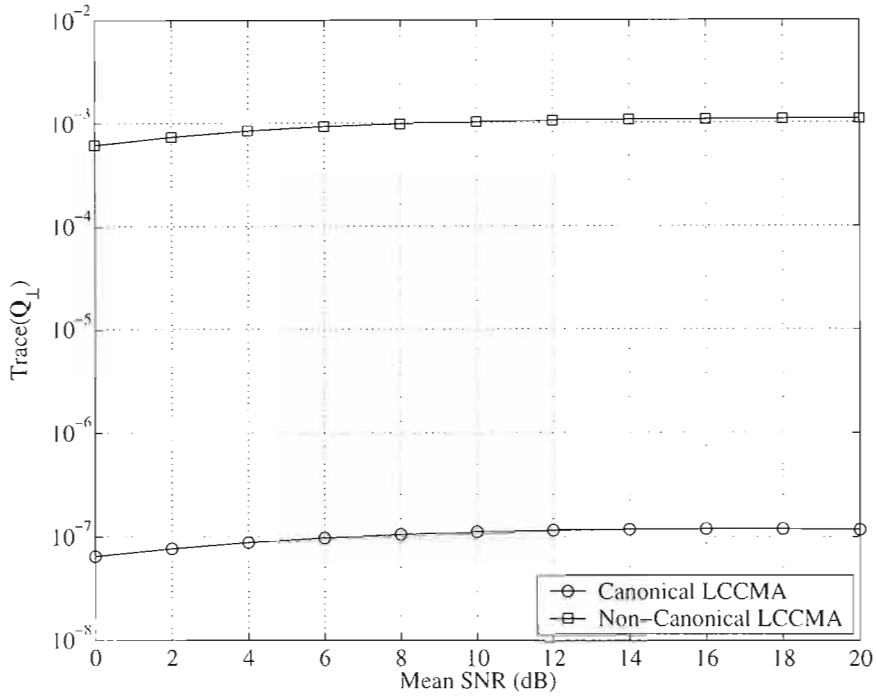

Fig. 4.12. The value of $\mathrm{Tr}(\mathbf{Q}_\perp)$ for the canonically and the non-canonically constrained LCCMA for the same time-correlated Rayleigh fading channel, at different SNR's.

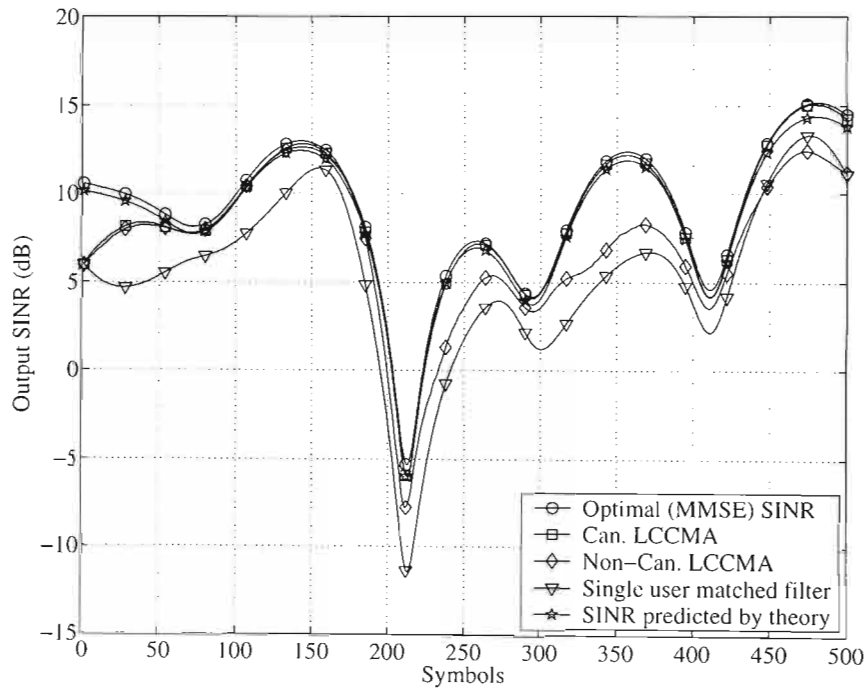

Fig. 4.13. The ensemble average SINR showing the inferior performance of the non-canonically constrained LCCMA compared to the canonically constrained LCCMA in a fading channel.

4.6 Operation of LCCMA in asynchronous DS-CDMA systems

This section formally presents the proof of global convergence of the LCCMA in an asynchronous DS-CDMA communications system. The technique used to prove the global convergence property of the LCCMA in an asynchronous DS-CDMA system follows the same

technique as that presented in [40]. The derivation presented in this section differs from that presented in [40] in the definition of the $\mathbf{u}$ and $\bar{\mathbf{u}}$ vectors, as well as the block matrix notation used for the first and second derivatives of the LCCMA cost function, in order to accommodate the asynchronous data transmission of the various users. In an asynchronous DS-CDMA system, a performance gain may be had if the size of the processing window at the receiver is increased. This section also details the application of the tracking analysis to the optimization of the processing window size in a non-stationary channel.

4.6.1 System model

An asynchronous DS-CDMA transmitter model for the uplink of a mobile radio network is considered. The baseband representation of the *k*th user's transmitted signal is given by

$$x_k(t) = A_k \sum_{i=-\infty}^{\infty} b_k(i) s_k(t - iT - \tau_k) \tag{4.34}$$

where A_k and s_k denote the amplitude and normalised spreading waveform of the *k*th user respectively, and T is the data symbol duration. The relative offset of the *k*th user's asynchronous signal is given by τ_k, which takes on integer values in the range $[0, N)$. The *k*th user's *i*th transmitted symbol $b_k(i)$ takes on the values $\{+1, -1\}$ with equal probability. The spreading waveform takes the form

$$s_k(t) = \sum_{n=0}^{N-1} c_k(n) \psi(t - nT_c), \quad t \in [0, T] \tag{4.35}$$

where N is the processing gain and c_k is the *k*th user's spreading code sequence of ± 1's, $\psi(t)$ is the chip pulse shape of duration $T_c = T/N$. It is noted that $s_k(t)$ only takes on values in the interval [0, *T*].

The received signal is passed through a chip-matched filter and sampled at the chip-rate. These samples are concatenated into a length N vector of received samples. Let $\mathbf{s}_k[\tau_k] = [0, \ldots, 0, s_k(0), \ldots s_k(N - \tau_k - 1)]^T$ be the down shifted (by amount τ_k) version of discrete signature sequence vector $\mathbf{s}_K$, of length N. Define,

$$\mathbf{s}_k = (1/\sqrt{N})[c_k(1), \ldots, c_k(N)]^T \tag{4.36}$$

$$\mathbf{S}[0] = [\mathbf{s}_1[0], \mathbf{s}_2[\tau_2], \ldots, \mathbf{s}_K[\tau_K]] \tag{4.37}$$

$$\mathbf{S}[1] = [\mathbf{0}, \mathbf{s}_2[-(N - \tau_2)], \ldots, \mathbf{s}_K[-(N - \tau_K)]] \tag{4.38}$$

where $\mathbf{s}_k[-(N - \tau_k)]$ is the up shifted version of $\mathbf{s}_k$, also padded with zeros. The first entry in (4.38) is the zero vector as the receiver is bit synchronized to the desired user ($\tau_1 = 0$). Using this notation, the received vector of samples from the chip-matched filter is given by,

$$\mathbf{r} = \mathbf{S}[0]\mathbf{A}\mathbf{b}(i) + \mathbf{S}[1]\mathbf{A}\mathbf{b}(i+1) + \mathbf{n} \tag{4.39}$$

$\mathbf{b}(i) = [b_1(i), \ldots, b_K(i)]^T$, $\mathbf{A} = \mathrm{diag}([A_1, \ldots, A_K])$, and $\mathbf{n}(i)$ is an AWGN vector with covariance matrix $\sigma^2 \mathbf{I}_N$. The vector $\mathbf{r}(i)$ is filtered by a FIR filter structure, whose coefficients

form the vector $\mathbf{w}(i)=\left[w_1(i),\ldots,w_N(i)\right]^T$. The desired user, from here on, will be user 1. The output of the filter, which constitutes the decision statistic, is given by

$$y(i)=\mathbf{w}(i)^T\mathbf{r}(i). \tag{4.40}$$

Reference [30] showed that the LCCMA converges to a scaled version of the MMSE filter, which is given by,

$$\mathbf{w}_{opt}=\frac{\mathbf{C}^{-1}\mathbf{s}_1}{A_1\mathbf{s}_1^T\mathbf{C}^{-1}\mathbf{s}_1} \tag{4.41}$$

$$\begin{aligned}\mathbf{C}&=E\left\{\mathbf{r}(i)\mathbf{r}(i)^T\right\}\\&=\mathbf{S}[0]\mathbf{A}\mathbf{A}^T\mathbf{S}^T[0]+\mathbf{S}[1]\mathbf{A}\mathbf{A}^T\mathbf{S}^T[1]+\sigma^2\mathbf{I}.\end{aligned} \tag{4.42}$$

4.6.2 Proof of convergence

Define vectors $\mathbf{u}_0$ and $\mathbf{u}_1$ whose elements correspond to the contribution at the output of the filter of the users' current and successive transmitted bits,

$$\mathbf{u}_0=\left(\mathbf{S}[0]\mathbf{A}\right)^T\mathbf{w} \quad \text{and} \quad \mathbf{u}_1=\left(\mathbf{S}[1]\mathbf{A}\right)^T\mathbf{w}. \tag{4.43}$$

The kth element of $\mathbf{u}_0$ and $\mathbf{u}_1$ are given by respectively,

$$u_{0,k}=A_k\left(\mathbf{w}^T\mathbf{s}_k[\tau_k]\right) \quad \text{and} \quad u_{1,k}=A_k\left(\mathbf{w}^T\mathbf{s}_k\left[-(N-\tau_k)\right]\right). \tag{4.44}$$

The output of the chip-matched matched filter may now be written as

$$\mathbf{w}^T\mathbf{r}=\mathbf{b}_0^T\mathbf{u}_0+\mathbf{b}_1^T\mathbf{u}_1. \tag{4.45}$$

Expanding the cost function in (2.22), we have

$$J(\mathbf{w})=E\left\{\left(\mathbf{w}^T\mathbf{r}\right)^4-2\left(\mathbf{w}^T\mathbf{r}\right)^2+R_2^2\right\}. \tag{4.46}$$

Using the relationship in (4.45), the cost function $J(\mathbf{w})$ may be expressed in terms of $\mathbf{u}_0$ and $\mathbf{u}_1$ using,

$$E\left\{\left(\mathbf{w}^T\mathbf{r}\right)^2\right\}=\mathbf{u}_0^T\mathbf{u}_0+\mathbf{u}_1^T\mathbf{u}_1, \tag{4.47}$$

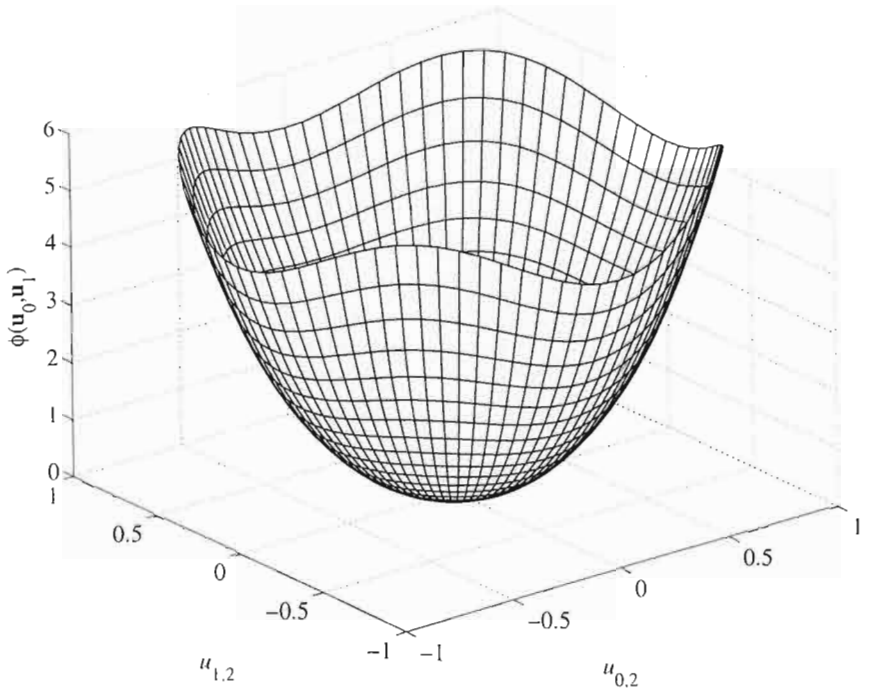

Fig. 1. Surface Plot of LCCMA cost function (4.49) for a two user asynchronous system.

$$\begin{aligned} E\left\{\left(\mathbf{w}^T\mathbf{r}\right)^4\right\} &= E\left\{\left(\mathbf{b}_0^T\mathbf{u}_0\mathbf{b}_0^T\mathbf{u}_0 + 2\mathbf{u}_1^T\mathbf{b}_1\mathbf{b}_0^T\mathbf{u}_0 + \mathbf{u}_1^T\mathbf{b}_1\mathbf{b}_1^T\mathbf{u}_1\right)^2\right\} \\ &= 3\left(\mathbf{u}_0^T\mathbf{u}_0\right)^2 - 2\sum_{k=1}^{K}\left(u_{0,k}\right)^4 \\ &\quad +3\left(\mathbf{u}_1^T\mathbf{u}_1\right)^2 - 2\sum_{k=1}^{K}\left(u_{2,k}\right)^4 + 6\left(\mathbf{u}_0^T\mathbf{u}_0\right)\left(\mathbf{u}_1^T\mathbf{u}_1\right), \end{aligned} \tag{4.48}$$

since the linear constraint in (2.22) is equivalent to $u_{0,1}=1$, the cost function in (4.46) can be written as,

$$\begin{aligned} \min_{u_{0,1}=1}\phi(\mathbf{u}_0,\mathbf{u}_1) &= 3\left(\mathbf{u}_0^T\mathbf{u}_0\right)^2 - 2\sum_{k=1}^{K}\left(u_{0,k}\right)^4 + 3\left(\mathbf{u}_1^T\mathbf{u}_1\right)^2 \\ &\quad -2\sum_{k=1}^{K}\left(u_{1,k}\right)^4 + 6\left(\mathbf{u}_0^T\mathbf{u}_0\right)\left(\mathbf{u}_1^T\mathbf{u}_1\right) \\ &\quad -2\left(\mathbf{u}_0^T\mathbf{u}_0 + \mathbf{u}_1^T\mathbf{u}_1\right) + R_2^2. \end{aligned} \tag{4.49}$$

The stationary points of the cost function are found by defining a new column vector

$$\bar{\mathbf{u}} = \begin{bmatrix} \bar{\mathbf{u}}_0 \\ \bar{\mathbf{u}}_1 \end{bmatrix} \tag{4.50}$$

where $\bar{\mathbf{u}}_0 = \left[u_{0,2},\ldots,u_{0,K}\right]^T$, and $\bar{\mathbf{u}}_1 = \left[u_{1,2},\ldots,u_{1,K}\right]^T$. A new cost function may then be defined in terms of $\bar{\mathbf{u}}$, which is equivalent to (4.49),

$$\bar{\phi}\left(\bar{\mathbf{u}}\right) = \phi\left(\mathbf{u}_0,\mathbf{u}_1\right). \tag{4.51}$$

Using block matrix notation, the first derivative takes the form,

$$\frac{\partial \bar{\phi}(\bar{\mathbf{u}})}{\partial \bar{\mathbf{u}}} = \begin{bmatrix} \dfrac{\partial \bar{\phi}(\bar{\mathbf{u}})}{\partial \bar{\mathbf{u}}_0} \\ \dfrac{\partial \bar{\phi}(\bar{\mathbf{u}})}{\partial \bar{\mathbf{u}}_1} \end{bmatrix} \tag{4.52}$$

where the elements of $\partial \bar{\phi}(\bar{\mathbf{u}})/\partial \bar{\mathbf{u}}_0$ are given by,

$$\begin{aligned} \frac{\partial \bar{\phi}(\bar{\mathbf{u}})}{\partial u_{0,k}} &= 4u_{0,k}\left(3\left(\mathbf{u}_0^T\mathbf{u}_0\right) - R_2^2 - 2u_{0,k}^2\right) + 12u_{0,k}\left(\mathbf{u}_1^T\mathbf{u}_1\right) \\ &= 4u_{0,k}\left(3\left(\mathbf{u}_0^T\mathbf{u}_0\right) - R_2^2 - 2u_{0,k}^2 + 3\left(\mathbf{u}_1^T\mathbf{u}_1\right)\right) \\ &= 4u_{0,k}\left(\left(3A_1^2 - R_2^2\right) + u_{0,k}^2 + 3\sum_{\substack{j=2 \\ j\neq k}}^{K} u_{0,j}^2 + 3\sum_{j=2}^{K} u_{1,j}^2\right), \end{aligned} \tag{4.53}$$

and similarly for $\partial \bar{\phi}(\bar{\mathbf{u}})/\partial \bar{\mathbf{u}}_1$:

$$\frac{\partial \bar{\phi}(\bar{\mathbf{u}})}{\partial u_{1,k}} = 4u_{1,k}\left(\left(3A_1 - R_2^2\right) + u_{1,k}^2 + 3\sum_{\substack{j=2 \\ j\neq k}}^{K} u_{1,j}^2 + 3\sum_{j=2}^{K} u_{0,j}^2\right) \tag{4.54}$$

for $2 \le k \le K$.

From (4.53) and (4.54), clearly if $\left(3A_1^2 - R_2^2\right) \ge 0$, then the only stationary point is when

$$\bar{\mathbf{u}}_0 = \bar{\mathbf{u}}_1 = \mathbf{0}, \tag{4.55}$$

which corresponds to the decorrelating detector, since the MAI has been completely removed. The global convexity of the cost function can be assured by analysing the Hessian matrix of $\bar{\phi}(\bar{\mathbf{u}})$. Using block matrix notation, the Hessian matrix takes the form

$$\frac{\partial^2 \bar{\phi}(\bar{\mathbf{u}})}{\partial \bar{\mathbf{u}}^2} = \begin{bmatrix} \dfrac{\partial^2 \bar{\phi}(\bar{\mathbf{u}})}{\partial^2 \bar{\mathbf{u}}_0} & \dfrac{\partial^2 \bar{\phi}(\bar{\mathbf{u}})}{\partial \bar{\mathbf{u}}_0 \bar{\mathbf{u}}_1} \\ \dfrac{\partial^2 \bar{\phi}(\bar{\mathbf{u}})}{\partial \bar{\mathbf{u}}_1 \bar{\mathbf{u}}_0} & \dfrac{\partial^2 \bar{\phi}(\bar{\mathbf{u}})}{\partial^2 \bar{\mathbf{u}}_1} \end{bmatrix}. \tag{4.56}$$

Where the elements of the sub matrices are given by

$$\frac{\partial \bar{\phi}(\bar{\mathbf{u}})}{\partial u_{0,k}\partial u_{0,l}} = \begin{cases} 4\left(3\left(\mathbf{u}_0^T\mathbf{u}_0\right) - R_2^2 + 3\left(\mathbf{u}_1^T\mathbf{u}_1\right)\right) & l = k \\ 24u_{0,k}u_{0,l} & l \neq k \end{cases} \tag{4.57}$$

$$\frac{\partial \bar{\phi}(\bar{\mathbf{u}})}{\partial u_{0,k}\partial u_{1,l}} = 24u_{1,l}u_{0,k} \tag{4.58}$$

and similarly for,

$$\frac{\partial \bar{\phi}(\bar{\mathbf{u}})}{\partial u_{1,k}\partial u_{1,l}} = \begin{cases} 4\left(3\left(\mathbf{u}_1^T\mathbf{u}_1\right) - R_2^2 + 3\left(\mathbf{u}_0^T\mathbf{u}_0\right)\right) & l = k \\ 24u_{1,k}u_{1,l} & l \neq k \end{cases} \tag{4.59}$$

$$\frac{\partial \overline{\phi}(\overline{\mathbf{u}})}{\partial u_{1,k}\partial u_{0,l}} = 24u_{0,l}u_{1,k}. \tag{4.60}$$

When $3A_1^2 - R_2^2 \geq 0$, and thus $\overline{\mathbf{u}} = \mathbf{0}$, then the main diagonal of the Hessian matrix equals $4\left(3A_1^2 - R_2^2\right)$ and the off diagonal elements equal 0. Clearly under this condition the Hessian matrix is positive definite, the decorrelating detector is the only stationary point, which is also the global minimum, and thus global convergence is guaranteed. This is the same condition which applies to the synchronous system, which was proved in [40].

The cost function as given in (4.49) is plotted in Fig. 1 for a two user asynchronous system. In this case $u_{0,1} = 1$ and $u_{1,1} = 0$, as it is assumed that the spreading code and timing of the desired user is known perfectly. The height of the surface in Fig. 1 is equal to the cost function of the remaining two degrees of freedom $u_{0,2}$ and $u_{1,2}$. It can be seen that although the curvature of the cost surface is not constant, there does exist a unique global minimum, corresponding to $u_{0,2} = u_{1,2} = 0$, which is the decorrelating receiver.

4.6.3 Processing window size optimisation

The performance of the MMSE receiver can be greatly enhanced if the size of the processing window is increased from one bit epoch to two [60]. However, the tracking ability of an adaptive filter updated with a stochastic gradient algorithm is inversely proportional to the length of the filter. The tracking analysis enables a novel study of the optimisation of the processing window size in a non-stationary channel, since performance gained by the increasing size of the processing window is tempered by the reduction in performance incurred due to the reduced tracking ability of a longer filter. Increasing the size of the processing window comes at the expense of increased computational complexity, thus it is not worth increasing the processing window size if an appreciable increase in performance is not realised.

A plot of the mean SINR attainable with a stochastic gradient algorithm as a function of window size would not follow the same trajectory as the optimal MMSE filter's SINR. The tracking analysis enables the computation of the optimal filter length, or point at which any increase in the filter length yields diminishing returns. As an illustrative example of such a study a 10 user asynchronous DS-CDMA system is considered. All the users transmit using length 31 Gold codes and the interfering users transmit at a level 3dB's higher than the desired user. The desired user is received at a SNR ratio of 20dB's. The receiver resolves 2 multipaths per user where the second multipath is 3dB's lower in amplitude relative to the main multipath. The receiver estimates the effective spreading code of the desired user with a mismatch variance of $\sigma_m^2 = 10^{-5}$. A value of 10^{-6} was used for $\mathrm{Tr}(\mathbf{Q})$ when the processing window is of length 31, and it was conservatively estimated that the value of $\mathrm{Tr}(\mathbf{Q})$ grows by 1% every time the processing window size is increased by one extra sample. The theoretical EMSE of the LCCMA running with a step size of 10^{-4} is plotted as a function of window size in Fig. 4.14. The EMSE at each choice of window size is computed as the average theoretical EMSE over 10^5 random

combinations of relative timing offsets of the asynchronous users, in order to average over the different cross-correlations between the Gold codes. As expected, the EMSE level is observed to increase as a function of window size due to the increased tracking requirements imposed by an increasing filter length. In Fig. 4.15 the mean SINR attainable by LCCMA in the same system is computed using the different realisations of timing offsets and corresponding theoretical EMSE levels. The diminishing returns are clearly evident, showing the utility of such a study.

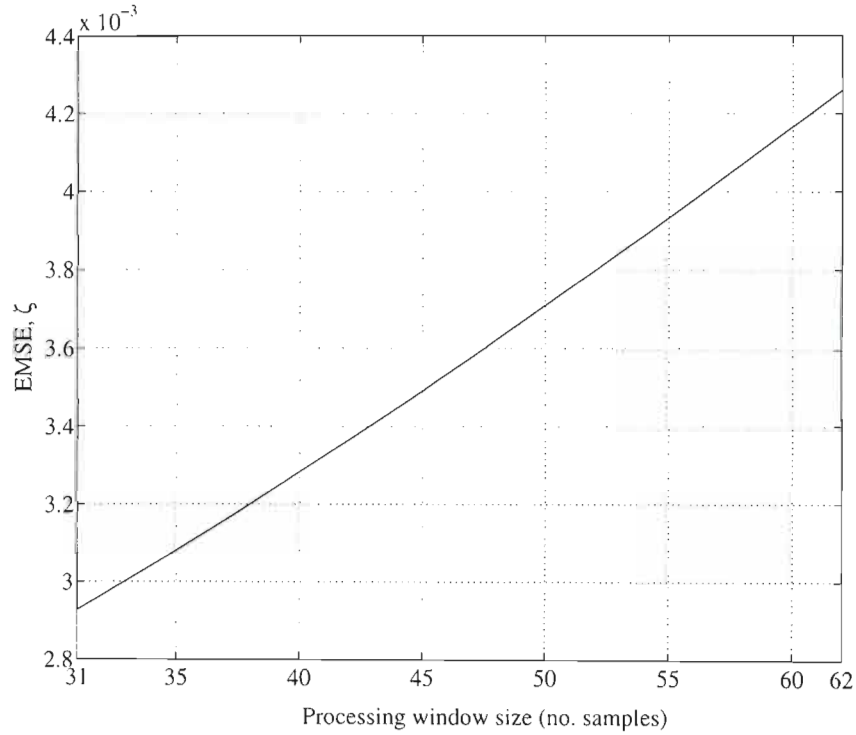

Fig. 4.14. EMSE of the LCCMA as a function of window size in a non-stationary asynchronous multipath channel.

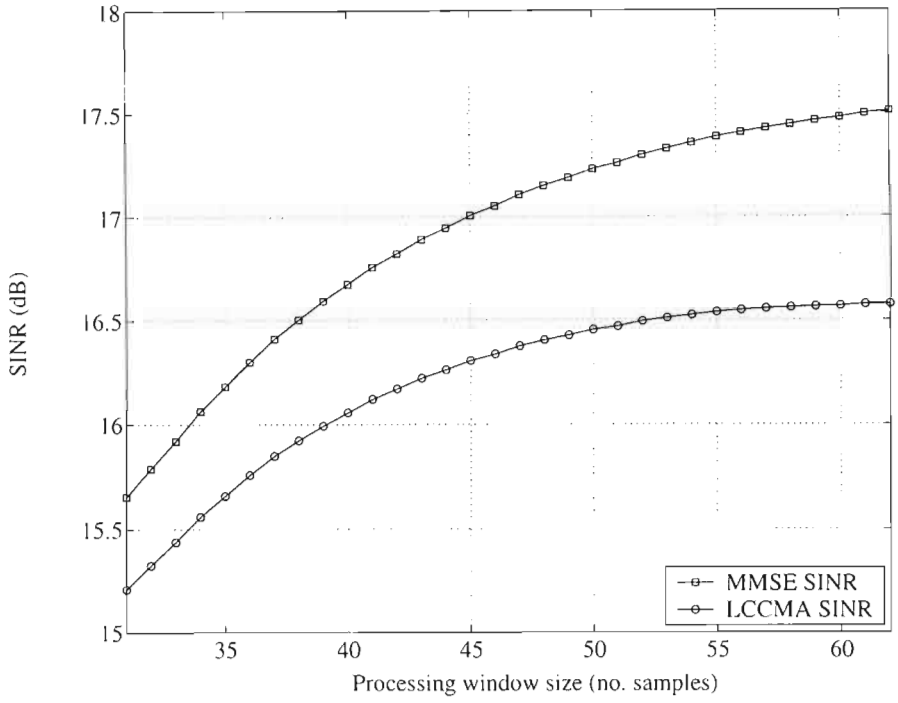

Fig. 4.15. Comparison between the SINR of the optimum MMSE filter and the LCCMA adapted filter as a function of window size in a non-stationary asynchronous multipath channel.

4.7 Narrowband interference suppression analysis

Simultaneous MAI and NBI suppression is an important research topic for future generation wireless communications systems, as outlined in detail in previous sections of this thesis. There are situations where non-PTV techniques may be considered: when they provide sufficient levels of performance e.g. [76] and [92], or when it is not possible to employ PTV techniques due to complexity constraints. The analysis of the LCCMA's capability to concurrently suppress NBI and MAI is thus important if the suitability of LCCMA to future generation wireless communications systems is to be established. The steady-state and transient analysis presented in Chapter 2 is therefore extended in this chapter to account for the presence of NBI.

4.7.1 System model

The familiar received vector of samples model given in (2.20) is modified to include the NBI component and is given by,

$$\mathbf{r}(i) = \mathbf{SAb}(i) + \mathbf{i}(i) + \mathbf{n}(i) \tag{4.61}$$

where $\mathbf{i}(i)$ is the vector of NBI samples which is assumed to be wide sense stationary, with zero mean, and covariance matrix $\mathbf{R}_i$. The narrow band nature of this interference imposes a high level of correlation between the successive samples in $\mathbf{i}(i)$. The model for these samples is the same as that used in [76] and [92] where it is assumed that they are generated from a second order autoregressive process with both poles at 0.99.

The samples of $\mathbf{i}(i)$ are therefore generated by filtering white Gaussian noise $v(n)$ through a second order IIR filter whose transfer function is given by,

$$\begin{aligned} h_{G_i}(z) &= \frac{1}{\left(1-0.99z^{-1}\right)^2} \\ &= \frac{1}{1-1.98z^{-1}+0.9801z^{-2}}. \end{aligned} \tag{4.62}$$

The output of this filter is given by,

$$u(n) = v(n) - a_1^* u(n-1) - a_2^* u(n-2) \tag{4.63}$$

where $a_1 = -1.98$ and $a_2 = 0.9801$, and $E\{v^2(n)\} = \sigma_v^2$, and $E\{u^2(n)\} = \sigma_u^2$. The autocorrelation function of $u(n)$ is then given recursively by,

$$r(m) + a_1 r(m-1) + a_2 r(m-2) = 0 \tag{4.64}$$

and then $\mathbf{R}_i$ is given by the Toeplitz matrix,

$$\mathbf{R}_i = \begin{bmatrix} r(0) & r(1) & \dots & r(N) \\ r(1) & r(0) & \dots & r(N-1) \\ \vdots & \vdots & \ddots & \vdots \\ r(N) & r(N-1) & \dots & r(0) \end{bmatrix}. \tag{4.65}$$

It is possible to solve for $r(0)$ and $r(1)$ in terms of the system parameters $\{a_1, a_2, \sigma_v\}$ using the Yule-Walker equations [67] to yield,

$$\begin{aligned} r(0) &= \sigma_u^2 \\ &= \left(\frac{1+a_2}{1-a_2}\right)\frac{\sigma_v^2}{\left[(1+a_2)^2 - a_1^2\right]} \end{aligned} \tag{4.66}$$

and,

$$r(1) = \frac{-a_1}{1+a_2}\sigma_u^2 \tag{4.67}$$

The NBI power level is defined in this thesis as,

$$P_{NBI} = 10\log_{10}\left(\frac{\sigma_u^2}{A_1^2}\right) \tag{4.68}$$

which is in dB's relative to the desired user's signal power.

4.7.2 Adaptive performance analysis

The adaptive performance analysis of Chapter 2 is extended to include the effects of NBI by modifying the expression given in (2.31) that describes the output of the filter in terms of the optimal filter and the *a priori* estimation error,

$$\begin{aligned} y(i) &= \left(\mathbf{w}_{opt} - \Delta\mathbf{w}(i)\right)^T \mathbf{r}(i) \\ &= A_1 b_1(i) + M(i) + v(i) + t(i) + l(i) - e_a(i) \end{aligned} \tag{4.69}$$

to include the new term $l(i) = \mathbf{w}_{opt}^{T}\mathbf{i}(i)$ which represents the NBI at the output of the optimum filter. The task of solving the simplified fundamental energy preserving equation given in (2.32) is greatly simplified by exploiting the fact that the terms $\{M(i), v(i), t(i), l(i)\}$ are mutually independent and may be lumped into the new term,

$$\tilde{v}(i) = M(i) + v(i) + t(i) + l(i). \tag{4.70}$$

This new term is accurately approximated by a zero mean Gaussian distribution, whose variance is given by,

$$\begin{aligned} E\left\{\tilde{v}(i)^2\right\} &= \mathbf{w}_{opt}^{T}\left(\mathbf{C} - A_1^2\mathbf{s}_1\mathbf{s}_1^{T}\right)\mathbf{w}_{opt} + \sigma_m^2\,\mathrm{Tr}(\mathbf{C}) \\ &= \tilde{\eta}^2 + \sigma_m^2\,\mathrm{Tr}(\mathbf{C}) \end{aligned} \tag{4.71}$$

where σ_m^2 is the mismatch variance, and the covariance matrix of the received vector of samples is given by,

$$\mathbf{C} = \mathbf{SAAS}^{T} + \mathbf{R}_{i} + \sigma^2\mathbf{I}, \tag{4.72}$$

where a closed form expression for $\mathbf{R}_{i}$ was given in (4.64)–(4.67).

4.7.3 Results

The accuracy of the steady-state and transient analysis to capture the adaptive performance of LCCMA when suppressing both MAI and NBI is verified using computer simulation. A 10 user synchronous DS-CDMA system based on length 31 Gold codes is considered. The desired user is received at a SNR of 15dB, there is a 3dB MAI ratio, and the step size of LCCMA is set to 10^{-3}. The ensemble average SINR learning curves are plotted from 200 independent simulation runs for various NBI power levels in Fig. 4.16. The theoretical learning curves are observed to correspond closely with the simulation results. The matched filter and optimal MMSE SINR levels are also displayed in Fig. 4.16 for the different NBI levels. The same simulation is plotted over a longer time scale in Fig. 4.17 to show that the LCCMA does eventually reach the steady-state level predicted by the analysis. Fig. 4.17 also illustrates the slowing in convergence rate as the level of NBI increases.

It is known that the convergence rate of stochastic gradient descent techniques (such as the LCCMA) is very sensitive to the eigen-spread of the received vector covariance matrix $\mathbf{C}$. High eigen-spreads correspond to slow convergence rates. The higher the correlation between the successive samples in $\mathbf{i}(i)$ the larger the eigen-spread in $\mathbf{R}_{i}$ which in turn increases the eigen-spread of $\mathbf{C}$. (The eigen-spread of a matrix is defined as the ratio between the highest and lowest eigenvalues of that matrix.) As an example, the eigen-spread of $\mathbf{C}$ for the above system when there is no NBI is approximately 131, with a -3dB NBI source the eigen-spread increases to approximately 527, which is slightly more than a four fold increase. The reduced convergence rate of LCCMA is exactly predicted by the transient analysis performed in this section.

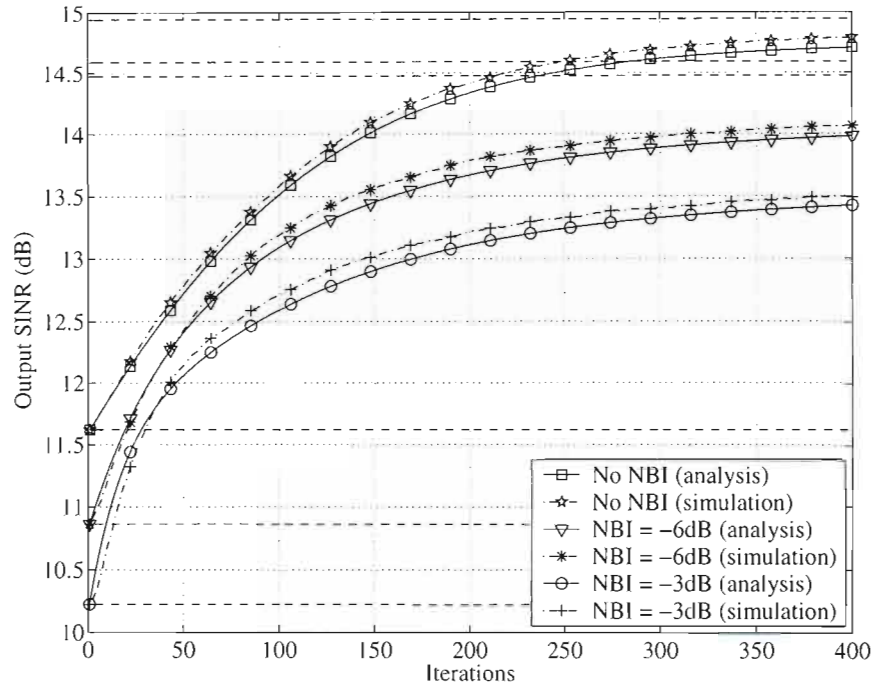

Fig. 4.16. Transient performance of LCCMA for differing strengths of NBI. Matched filter and optimal MMSE SINR levels displayed for the different NBI levels.

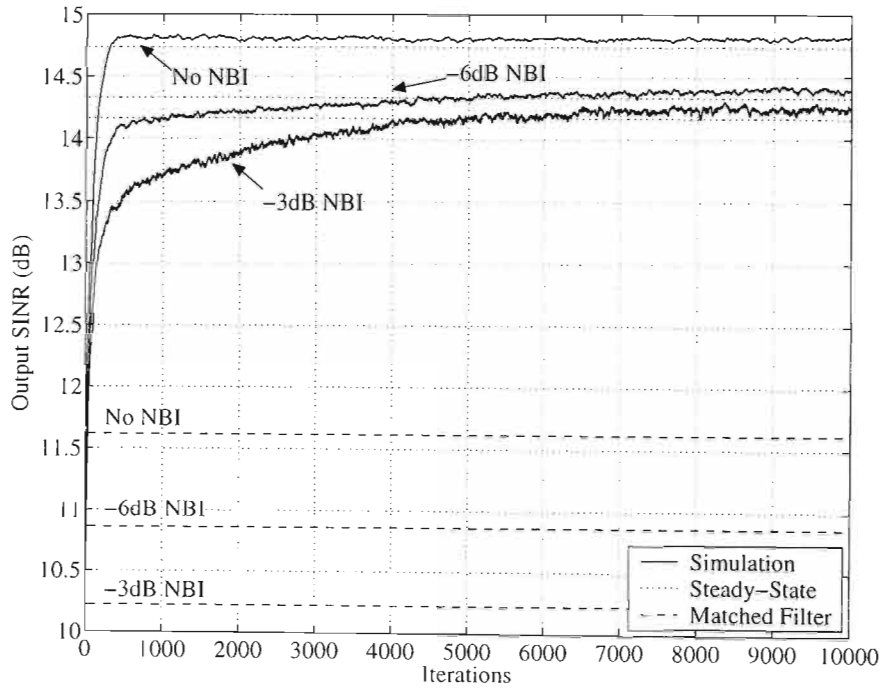

Fig. 4.17. Transient performance of LCCMA for differing strengths of NBI showing eventual attainment of theoretical steady-state levels of operation.

4.8 Summary

This chapter has examined the impact that pertinent channel and implementation issues have on the performance of constant modulus based blind adaptive MUD's via extensions to the

adaptive performance analysis and through performance comparisons with alternate cost functions.

The impact that the finite accuracy characteristic of the channel estimation circuitry has on the adaptive performance on LCCMA was studied first. It was found that as the desired user's amplitude was increasingly underestimated the steady-state analysis accurately predicted the increase in steady-state EMSE and the transient analysis accurately predicted the new learning curve of the output SINR. This theoretical analysis also proved to be useful in predicting how accurately the desired user's amplitude needed to be estimated in order for the LCCMA to yield a performance gain over the LCDCMA. The effects of signature sequence mismatch at the receiver were also studied in this chapter. The finite accuracy of the channel estimator also introduces mismatch. The steady-state, tracking and transient analysis was thus extended in this chapter to include the effects of mismatch. This is important as the analysis and simulation results show that mismatch can severely decrease the performance of the adaptive algorithms.

The impact that timing jitter at the receiver has on the adaptive algorithms' performance were also analysed via an extension of the steady-state and transient analysis. This chapter showed that the FRESH architecture is more susceptible to jitter than the filter bank implementation. This is contra to the results of Chapter 3 that showed that adaptive algorithms implemented on both architectures have equivalent performance levels, and thus an important result. A modification to the LCCMA was also presented which increases the stability of the LCCMA in the presence of jitter. The value of such a modification was illustrated via computer simulations.

The operation of the LCCMA in a Rayleigh fading channel was also examined. It was found that the canonically constrained LCCMA offers superior tracking performance in a Rayleigh fading channel compared to the non-canonically constrained LCCMA. The operation of the LCCMA in an asynchronous DS-CDMA system was also studied. The proof of the global convergence of the LCCMA in an asynchronous DS-CDMA system was given, and a novel application of the tracking analysis was applied to the optimisation of the processing window size for an asynchronous multipath DS-CDMA system. Finally, the ability of a non-PTV implementation of the LCCMA to NBI suppression was investigated via an extension of the steady-state and transient analysis.

Chapter 5

Conclusion

The central premise of this thesis: that constant modulus based blind adaptive multiuser detectors provide low complexity, robust, and reliable signal processing techniques for the enhancement of future generation personal communications systems based on DS-CDMA, was verified in this thesis. This was achieved via: novel performance analyses of blind adaptive MUD's, the derivation of novel constant modulus based cyclic algorithms, the rigorous mathematical analysis of the convergence of the new cyclic algorithms, and by considering the impacts that realistic channel and implementation impairments have on the performance of these algorithms.

5.1 Thesis summary

The argument for constant modulus based MUD was made in Chapter 1. The main argument was that the CMA has been widely deployed in actual blind equalisation applications (and therefore has a reputable track record in real implementations), and its theory of operation in such applications is well established. Also, the application of MAI suppression in DS-CDMA systems is very similar to the blind equalisation problem. Chapter 1 also showed that constant modulus based MUD has also received much attention from the research community lately, and that the SGD based techniques offer good performance versus complexity ratios. These schemes also have a well established theoretical framework in which their performance may be evaluated and are therefore an important focal point of this thesis. Chapter 1 then went on to show that the adaptive performance of such schemes, such as the LCCMA, has not been dealt with formally in the literature, and that the suitability of constant modulus based schemes can only be properly established via a rigorous analysis of their adaptive performance. Another outstanding issue that was highlighted in Chapter 1 was the need for new constant modulus based algorithms that are suitable for the suppression of cyclostationary interference sources, since the presence of cyclostationary interference sources is a trait of future generation wireless communication systems, e.g. multi-rate MAI and NBI in DS-CDMA overlay systems. Finally, Chapter 1 also discussed how the suitability of constant modulus based MUD's can only be fully evaluated if realistic channel and implementation impairments are considered in the adaptive performance analyses of the new and existing algorithms.

The first major contribution of this thesis was made in Chapter 2 when the steady-state, tracking, and transient performance of the LCCMA and other code-aided blind adaptive MUD's were derived for the first time. Closed form expression for the EMSE for these three phases were explicitly derived for the LCCMA (based on CMA2-2 and CMA1-2 cost functions, and for

both canonical and non-canonical constraints), MOE, Sato, and LCDCMA using the recently proposed feedback approach [52]–[54], and energy conservation arguments of [58]. Similar expressions for other blind adaptive MUD's do not exist in the literature to the best of the author's knowledge, except for the steady-state EMSE of the MOE detector in [25]. This chapter derived a new more accurate expression of the EMSE of the MOE detector, and in a much simpler manner than was done in [25]. It was also shown that these EMSE values may be used to accurately describe output SINR of the MUD in all phases of the adaptive algorithms, and thus the performance penalty incurred by the adaptive algorithms relative to the optimal MMSE filter was fully quantified.

The results of Chapter 2 were that the LCCMA incurs very little performance penalty relative to the benchmark DD-LMS algorithm, and that the adaptive performance of the MOE cost function is vastly inferior to the LCCMA cost function. It was also shown that the LCCMA has better performance than the LCDCMA when a perfect estimate of the desired user's amplitude is known. Since convergence of the DD-LMS algorithm cannot be ensured, and the exact proof of convergence of the Sato/LCCMA-CMA1-2 cost functions remains an open problem, it was concluded in Chapter 2 that LCCMA (based on CMA2-2) is a very suitable algorithm for blind adaptive MUD due to its proven convergence capability and excellent adaptive performance.

The major original contribution of Chapter 3 was the development and analysis of new blind adaptive cyclic MUD algorithms based on the CMA suitable for the suppression of PTV/cyclostationary interference sources. The new algorithms were the results of an original modification that was made to the LCCMA to enable it to operate directly on the FRESH and suboptimal FRESH filter architectures. The FRESH architecture was chosen as suboptimal implementations are possible which enable performance and complexity to be traded-off. A novel study was also conducted into the different MMSE receivers that are possible on the suboptimal FRESH architectures. This study showed that suboptimal FRESH filters are in fact suitable and flexible alternatives to the filter bank implementation. The new FRESH-LCCMA algorithm was shown to exhibit superior performance compared to existing algorithms and at a substantially lower computational complexity. The operation of alternate cost functions on the suboptimal FRESH architectures was also demonstrated as well as the operation of an RLS update procedure for the FRESH-LCCMA for a further performance increase. When updated with the RLS procedure, the FRESH-LCCMA was shown to have vastly superior performance when compared to the previously proposed cyclic MUD schemes.

The robustness and adaptive performance of the FRESH-LCCMA was also dealt with analytically in this chapter. Robustness of the FRESH-LCCMA was proven via a proof of the global convergence of the algorithm. The adaptive performance of this algorithm was quantified via an extension of the theory developed in Chapter 2. Another contribution of Chapter 3 was the analytical framework in which the relative performance of the two approaches to the

implementation of PTV filters, the FRESH filter and filter bank, may be compared. It was shown that the filter bank architecture has only a marginal performance advantage over the FRESH architecture for the LCCMA. Prior to this work no conclusions could be drawn as to which architecture would yield superior performance from the adaptive algorithm.

The main concern of Chapter 4 was the impact that realistic channel and implementation impairments have on the adaptive performance of constant modulus based blind adaptive MUD's. The main original contributions of Chapter 4 were thus the study of: the sensitivity of LCCMA to the error in the estimation of the desired user's amplitude, the effects of signature waveform mismatch, timing jitter at the receiver, operation in a Rayleigh fading channel, operation in an asynchronous DS-CDMA system, and the ability of a non-PTV implementation of LCCMA to suppress NBI.

The study of the sensitivity of LCCMA to the error in the estimation of the desired user's amplitude was performed using the steady-state and transient analysis. It was found that the analysis was useful for predicting when it would be more advantageous to switch to LCDCMA (which does not require knowledge of the desired user's amplitude). The analysis of the effects of signature waveform mismatch was achieved via an extension of the steady-state, tracking, and transient analysis. It was shown that even moderate amounts of mismatch may severely effect the adaptive performance of the algorithms. An aligned problem with FRESH filters is the performance of the adaptive algorithm under jitter conditions. An extension of the steady-state analysis of FRESH-LCCMA, to account for timing jitter at the receiver, was performed to this end. It quantified the performance reduction as a function of the jitter variance accurately. A useful result of this analysis was the proof that the FRESH filter is indeed more sensitive to timing jitter than the filter bank implementation. The convergence of the LCCMA under severe jitter conditions was also improved via a modification to the algorithm which made it more jitter resilient.

5.2 Future work

Some interesting extensions of the work performed in this thesis are possible:

- The application of the feedback approach to schemes that have been proposed to enhance the speed of convergence of SGD algorithms, e.g. adaptive step size algorithms [93], and stochastic gradient averaging schemes [94]. The actual benefit of these schemes could then be quantified.
- No theory exists which will predict the optimal set of the frequency shifts for a given dimension of suboptimal FRESH filter. Reference [60] did mention that this was an object under current investigation but no papers, to the best of the author's knowledge, have been published in this regard.

- The application of constant modulus based MUD to OFDM signalling schemes could also be considered. Such schemes have been proposed to offer data rates of up to 100Mb/s for 4G systems. Practical MUD/interference suppression at such high data rates is challenging due to the processing power requirements. Thus new ideas for interference suppression on these systems could be developed.

References

[1] J. Korhonen, *Introduction to 3G mobile communications*, 2nd ed., Artech House mobile communications series, 2003.

[2] G. Jenkins, "Brilliant Past, Bright Future," *GSM White Paper*, Deutsche Bank, 18 Feb. 2004.

[3] GSM Association Press Release, Cannes, France, 22 Feb. 2004.

[4] K. Tachikawa, "A perspective on the evolution of mobile communications," *IEEE Commun. Mag.*, pp. 66–73, Oct. 2003.

[5] B. Meyerson, "Smart phones finally more than just talk," *Business Report*, Independent News and Media (Publ.), pp. 2, 26 March 2004.

[6] T. Ojanperä, R. Prasad, "An Overview of Air Interface Multiple Access for IMT-2000/UMTS," *IEEE Comms. Mag.*, pp. 82–95, Sept. 1998.

[7] R. Prasad, W. Konhauser, W. Mohr, *Third Generation Mobile Radio Systems*. Reading, MA: Artech House, 2000.

[8] E. Dahlman, B. Gudmundson, M. Nilsson, J. Sköld, "UMTS/IMT-2000 based on wideband CDMA," IEEE Personal Commun. Mag., vol. 36, pp. 70–80, Sept. 1998.

[9] W. W. Lu, "4G Mobile research in Asia," *IEEE Commun. Mag. (Guest Editorial)*, pp. 104–106, March 2003.

[10] Y. Kim, B. J. Jeong, J. Chung, C. Hwang, *et al*, "Beyond 3G: vision, requirements and enabling technologies," *IEEE Commun. Mag.*, pp 120–124, March 2003.

[11] M. LeFevre, P. Okrah, "Making the Leap to 4G Wireless," *Communications Systems Design Magazine*, pp. 26–32, July 2001.

[12] V. Torokh, N. Seshadri, A. R. Calderbank, "Space-time codes for high data rate wireless communication: performance criterion and code construction," *IEEE Trans. Inform. Theory*, vol. 44, no. 2, pp. 744–765, March 1998.

[13] A. J. Paulraj, C. B. Papadias, "Space-Time Processing for Wireless Communications," *IEEE Signal Proc. Mag.*, pp. 49–83, Nov. 1997.

[14] X. Wang, H. V. Poor, "Space-Time Multiuser Detection in Multipath CDMA Channels," *IEEE Trans. On Signal Processing*, vol. 47, no. 9, pp. 2356–2374, September 1999.

[15] K. Yen, L. Hanzo, "Antenna-diversity-assisted genetic-algorithm-based multiuser detection schemes for synchronous CDMA systems," *IEEE Trans. Commun.*, vol. 51, no. 3, pp. 366–370, March 2003.

[16] P. Peng, "An efficient multiuser detection algorithm for direct sequence code division multiple access by using neural networks," *Proc. IEEE Int. Conf. Commun. (ICC'01)*, vol. 1, pp. 36–40.

[17] J. Luo, K. Pattipati, K. Willett, F. Hasegawa, "A PDA approach to CDMA multiuser detection," *Proc. IEEE Globecom Conf.*, vol. 2, pp. 763–766, 2001.

[18] H. Lim, M. Rao, A. Tan, H. Chuah, "Multiuser detection for DS-CDMA systems using evolutionary programming," *IEEE Commun. Letters*, vol. 7, issue 3, pp. 101–103, March 2003.

[19] M. Ghotbi, M. R. Soleymani, "Multiuser detection of DS-CDMA signals using partial parallel interference cancellation in satellite communications," *IEEE J. Selec. Areas Commun.*, vol. 22, no. 3, pp. 584–593, Apr. 2004.

[20] D. Reynolds, X. Wang, "Adaptive group-blind multiuser detection based on a new subspace tracking algorithm," *IEEE Trans. on Commun.*, vol. 49, no. 7, pp.1135–1141, July 2001.

[21] S. Verdú, *Multiuser Detection*, Cambridge University Press, 1998.

[22] S. Chen, A. K. Samingan, B. Mulgrew, L. Hanzo, "Adaptive minimum-BER linear multiuser detection for DS-CDMA signals in multipath channels," *IEEE Trans. Signal Processing*, vol. 49, no. 6, pp. 1240–1247, June 2001.

[23] U. Madhow, "Blind adapive interference suppression for direct-sequence CDMA," *Proc. of IEEE*, vol. 86, no. 10, pp. 2049–2069, Oct. 1998.

[24] G. Woodward, B. S. Vucetic, "Adaptive detection for DS-CDMA," *Proc. of IEEE*, vol. 86, no. 7, pp. 1413–1434, July 1998.

[25] M. Honig, U. Madhow, S. Verdú, "Blind adaptive multiuser detection," *IEEE Trans. On Inform. Theory*, vol. 41, no. 4, pp. 944–960, July 1995.

[26] D. N. Godard, "Self-recovering equalization and carrier tracking in two dimensional data communications system," *IEEE Trans. Commun.*, vol. 28, no. 11, pp. 1867–1875, Nov. 1980.

[27] J. Miguez, L. Castedo, "A linearly constrained constant modulus approach to blind adaptive multiuser interference suppression," *IEEE Commun. Letters*, vol. 2, no. 8, pp. 217–219, Aug. 1998.

[28] Z. Tang, Z. Yang, Y. Yao, "Closed-form analysis of linearly constrained CMA-based blind multiuser detector," *IEEE Commun. Lett.*, vol. 4, no. 9, pp. 273–276, Sept. 2000.

[29] X. M. Wang, "A constant-modulus algorithm for blind multiuser detection in DS-CDMA systems with antenna array," *Proc. IEEE Pacific Rim Conf. on computers and signal processing (PACRIM. 2001)*, vol. 1, pp. 234–237, 2001.

[30] Changjiang Xu, Guangzeng Feng, Kyung Sup Kwak, "A modified constrained constant modulus approach to blind adaptive multiuser detection," *IEEE Trans. Commun.*, vol. 49, no. 9, pp. 1642–1648, Sep. 2001.

[31] Changjiang Xu, Guangzeng Feng, "Non-canonically constrained CMA for blind multiuser detection," *IEE Electronics Letters*, pp. 171–172, Jan. 2000.

[32] W. Lee, B. R. Vojcic, R. L. Pickholtz, "Constant modulus algorithm for blind multiuser detection," in *IEEE Proc. Int. Symp. Spread SpectrumTech. Appl. ISSSTA 96*, Mainz, Germany, pp. 1262–1266, May 1996.

[33] N. Zecevic, J. H. Reed, "Blind CDMA interference rejection in multipath channels," in *Proc. IEEE Veh. Technol. Conf.*, Phoenix, AZ, pp. 21–25, 1997.

[34] N. R. Mangalvedhe, J. H. Reed, "Blind adaptation algorithms for direct-sequence spread-spectrum CDMA single-user detection," in *Proc. IEEE Veh. Technol. Conf.*, Phoenix, AZ, 1997, pp. 2133–2137.

[35] P. He, T. T. Tjhung, L. K. Rasmussen, "Constant modulus algorithm (CMA) for CDMA communications systems," in *Proc. IEEE Veh. Technol. Conf.*, Ottawa, Canada, 1998, pp. 949–953.

[36] T. E. Biedka, W. H. Tranter, J. H. Reed, "Convergence Analysis of the Least Squares Constant Modulus Algorithm in Interference Cancellation Applications," *IEEE Trans. Comms.*, pp. 491–501, vol. 48, no. 3, March 2000.

[37] C. Xu, K. S. Kwak, "Comments on "Closed-form analysis of linearly constrained CMA-based blind multiuser detector"," *IEEE Commun. Lett.*, vol. 5, no. 7, pp. 290–291, July 2001.

[38] X. M. Wang, W. S. Lu, A. Antoniou, "Blind adaptive multiuser detection using a vector constant-modulus approach," *Proc. of Asilomar Conf. on Signals, Systems and Computers*, vol. 1, pp. 36–40, 2001.

[39] Zhimin Du, Sheng Zhou, Peng Wan, Weiling Wu, "Novel variable step size constant modulus algorithms for blind multiuser detection," *Proc. IEEE Vehicular Technology Conference, VTC Fall 2001,* vol. 2 , pp. 673–677, 2001.

[40] C. Xu, G. Feng, "Comments on "A linearly constrained constant modulus approach to blind adaptive multiuser interference suppression," *IEEE Commun. Letters*, vol. 4, no. 9, pp. 280–282, Sept. 2000.

[41] Q. Xue, X. Jiang, W. Wu, "A new CMA-based blind adaptive multiuser detection," *Proc. of IEEE Vehic. Techn. Conf. (VTC 2001)*, Spring, vol. 3, pp. 1775–1778, 2001.

[42] C. B. Papadias, A. J. Paulraj, "A constant modulus algorithm for multiuser signal separation in presence of delay spread using antenna arrays," *IEEE Sign. Proc. Lett.*, vol. 4, no. 6, pp. 178–181, May 1997.

[43] P. Arasaratnam, S. Zhu and A. G. Constantinides, "Fast convergent multiuser constant modulus algorithm for use in multiuser DS/CDMA environments," *IEEE Proc. Int. Conf. Acoust., Speech, Signal Process. (ICASSP 2002)*, Orlando, Florida, pp. 2761–2764, May 2002.

[44] J. K. Tugnait, Tongtong Li, "Blind asynchronous multiuser CDMA receivers for ISI channels using code-aided CMA," *IEEE JSAC*, vol. 19, no. 8, pp. 1520–1530, Aug. 2001.

[45] T.Miyajima, "Blind adaptive detection using differential CMA for CDMA systems," *Trans IEICE.*, Vol.J83-A, no. 11, pp. 1318–1329, Nov. 2000.

[46] Z. Xu, P. Liu, "Code-constrained blind detection of CDMA signals in multipath channels," *IEEE Sign. Process. Lett.*, vol. 9, no. 12, pp. 389–392, Dec. 2002.

[47] P. Arasaratnam, S. Zhu, A. G. Constantinides, "Robust and fast convergent blind multi-user detectors for DS-CDMA systems in nonstationary multipath environments," *Proc. of 14th Int. Conf. Digital Signal Processing*, vol. 2, pp. 627–630, 2002.

[48] H. Jiang, K. S. Kwak, "A non-canonical linearly constrained constant modulus algorithm for a blind multiuser detector," *ETRI Journal*, vol. 24, no. 3, pp. 239–246, June 2002.

[49] C. R. Johnson, Jr., P. Schinter, I. Fijalkow, L. Tong, *et al*, "The core of FSE-CMA behavior theory," *Unsupervised Adaptive Filtering* (S. Haykin, ed.), vol. 2, chapter 2, Wiley, 2000.

[50] R. W. Lucky, "Techniques for adaptive equalization of digital communication systems," *Bell System Tech. J.*, vol. 45, pp. 255–286, 1966.

[51] Y. Sato, "Two extensional applications of the zero-forcing equalization method," *IEEE Trans. Commun.*, vol. COM-23, pp. 684–687, 1975.

[52] N. R. Yousef, A. H. Sayed, "A unified approach to the steady-state and tracking analyses of adaptive filtering algorithms," *Proc. 4th IEEE-EURASIP workshop On Nonlinear Signal And Image Processing*, vol. 2, pp. 699–703, Antalya, Turkey, June 1999.

[53] J. Mai, A. H. Sayed, "A feedback approach to the steady-state performance of fractionally spaced blind adaptive equalizers," *IEEE Trans. Sig. Proc.*, vol. 48, no. 1, pp. 80–91, Jan. 2000.

[54] N. R. Yousef, A. H. Sayed, "A unified approach to the steady-state and tracking analyses of adaptive filters," *IEEE Trans. Sig. Proc.*, vol. 49, no. 2, pp. 314–324, Feb. 2001.

[55] N. R. Yousef, A. H. Sayed, "Ability of adaptive filters to track carrier offsets and random channel non-stationarities," *IEEE Trans. Signal Processing*, vol. 50, pp.1533–1544, July 2002.

[56] N. R. Yousef, A. H. Sayed, "A feedback analysis of the tracking performance of blind adaptive equalization algorithms," in *Proc. CD Conf.*, vol. 1, pp.174–179. 1999.

[57] T. Y. Al-Naffouri, A. H. Sayed, "Transient analysis of data-normalized adaptive filters," *IEEE Trans. Sign. Proc.*, vol. 51, pp. 639–652, March 2003.

[58] T. Y. Al-Naffouri, A. H. Sayed, "Transient analysis of adaptive filters with error nonlinearities," *IEEE Trans. Sign. Proc.*, vol. 51, pp. 653–663, March 2003.

[59] M. Honig, "Orthogonally anchored blind interference suppression using the Sato cost criterion," *Proc. IEEE Int. Symposium on Inform. Theor.*, pp. 314, 1995.

[60] S. Buzzi, M. Lops, A. Tulino, "Blind adaptive multiuser detection for asynchronous dual-rate DS/CDMA systems," *IEEE J. Select. Areas Commun.*, vol. 19, pp. 233–224, Feb. 2001.

[61] X. Wang, H. V. Poor, "Blind adaptive multiuser detection in multipath CDMA channels based on subspace tracking," *IEEE Trans. Sig. Proc.*, vol. 46, no. 11, pp. 3030–3044, Nov. 1998.

[62] H. H. Zeng, Lang Tong, C. Richard Johnson, "Relationships between the constant modulus and Wiener receivers," *IEEE Trans. Inform. Theor.*, vol. 44, no. 4, pp. 1523–1538, July 1998.

[63] D. G. Luenberger, *Optimization by vector space methods*, 2nd ed., New York, Wiley, 1990.

[64] I. Fijalkow, C. E. Manlove, C. R. Johnson, Jr., "Adaptive fractionally spaced blind CMA equalization: excess MSE," *IEEE Trans. Signal Processing*, vol. 46, no. 1, pp. 227–231, Jan. 1998.

[65] A. Touzni, I. Fijalkow, "Does fractionally-spaced CMA converge faster than LMS?" *Proc. European Signal Processing Conference*, Trieste, Italy, pp. 1227–1230, Sept. 1996.

[66] Teng Joon Lim, Yu Gong, B. Farhang-Boroujeny, "Convergence analysis of chip- and fractionally spaced LMS adaptive multiuser CDMA detectors," *IEEE Trans. Sig. Proc.*, vol. 48. no. 8, pp. 2219–2228, Aug. 2000.

[67] S. Haykin, *Adaptive Filter Theory*, Englewood Cliffs, NJ: Prentice-Hall, 1996.

[68] P. S. R. Diniz, *Adaptive filtering: algorithms and practical implementation*, Kluwer Academic Publishers, 1997.

[69] D. G. Manoloakis, V. K. Ingle, S. M. Kogon, *Statistical and adaptive signal processing: spectral estimation, signal modeling, adaptive filtering and array processing*, McGraw-Hill, 2000.

[70] A. H. Sayed, M. Rupp, "A time-domain feedback analysis of adaptive algorithms via the small gain theorem," *Proc. SPIE*, vol. 2563, pp. 458–469, 1995.

[71] M. Rupp and A. H. Sayed, "A time-domain feedback analysis of filtered error adaptive gradient algorithms," *IEEE Trans. Signal Processing*, vol. 44, pp. 1428–1439, June 1996.

[72] A. H. Sayed and M. Rupp, "Robustness issues in adaptive filtering," in *DSP Handbook*. Boca Raton, FL: CRC, 1998, ch. 20.

[73] M. Rupp and A. H. Sayed, "On the convergence of blind adaptive equalizers for constant-modulus signals," *IEEE Trans. Commun.*, vol. 48, pp. 795–803, May 2000.

[74] A. H. Sayed and M. Rupp, "An l_2-stable feedback structure for nonlinear adaptive filtering and identification," *Automatica*, vol. 33, no. 1, pp. 13–30, Jan. 1997.

[75] J. Zhang, E.K. P. Chong, D. N. C. Tse, "Output MAI distributions of linear mmse multiuser receivers in DS-CDMA systems," *IEEE Trans. Inform. Theory*, vol. 47, pp. 1128–1144, March 2001.

[76] H. V. Poor, X. Wang, "Code-aided interference suppression for DS/CDMA communications—Part II: Parallel blind adaptive implementations," *IEEE Trans. Commun.* vol. 45, no. 9, pp. 1112–1122, Sept. 1997.

[77] S. Buzzi, M. Lops, H. Vincent Poor, "Code-aided interference suppression for DS/CDMA overlay systems," *Proc. IEEE*, vol. 90, pp. 394–435, March 2002.

[78] M. Saquib, R. Yates, N. Mandayam, "Decorrelating detectors for dual rate synchronous DS/CDMA channel," *Wireless Pers. Commun.*, vol. 9, pp. 197–216, May 1999.

[79] J. Chen, U. Mitra, "MMSE receivers for dual-rate DS/CDMA signals: Random signature sequence analysis," presented at the Globecom, Phoenix, AZ, Nov. 1997.

[80] S. Buzzi, M. Lops, A. Tulino, "A new family of MMSE multiuser receivers for interference suppression in DS/CDMA systems employing BPSK modulation," *IEEE Trans. Commun.*, vol. 49, pp. 154–167, Jan. 2001.

[81] S. Buzzi, M. Lops, A. Pauciullo, "Iterative cyclic subspace tracking for blind adaptive multiuser detection in multirate CDMA systems," *IEEE Trans. Veh. Technol.*, vol. 52, pp. 1463–1475, Nov. 2003.

[82] S. Buzzi, M. Lops, A. Tulino, "Time-varying narrow-band interference rejection in asynchronous multiuser DS/CDMA systems over frequency selective fading channels," *IEEE Trans. Commun.*, vol. 47, pp. 1523–1536, Oct. 1999.

[83] E. Ferrara, "Frequency-domain implementations of periodically time-varying filters," *IEEE Trans. Acoust., Speech, Signal Processing.*, vol. ASSP-33, pp. 883–892, Aug. 1985.

[84] C.-L. I, R. D. Gitlin, "Multi-code CDMA wireless personal communications networks," *Proc. IEEE Int. Conf. Comm.*, Seattle, WA, pp. 1060–1064, June 1995.

[85] T.-H.Wu and E. Geraniotis, "CDMA with multiple chip rates for multimedia communications," *Proc. 28th Annu. Conf. Inform. Sci. Syst.*, Princeton, NJ, Mar. 1994.

[86] S. Buzzi, M. Lops, and A. M. Tulino, "MMSE multi-user detection for asynchronous dual rate direct sequence CDMA communications," *Proc. of 9th Int. Symp. Personal Indoor Mobile Radio Commun.*, Boston, MA, Sept. 8–11, 1998.

[87] U. Mitra, "Comparative study of maximum likelihood detection for two multi-rate DS/CDMA systems," *Proc. Int. Symp. Inform. Theory*, Ulm, Germany, pp. 352, June 1997.

[88] U. Mitra, "Comparison of maximum likelihood-based detection for two multi-rate access schemes for CDMA signals," *IEEE Trans. Comm.*, vol. 47, pp. 64–77, Jan. 1999.

[89] N. R. Yousef, A. H. Sayed, "Fixed point analysis of the constant modulus algorithm" *Proc. IEEE Conf. on Acoustics, Speech, and Signal Processing*, vol.4, pp. 2177–2180, 2001.

[90] N.R. Yousef, A.H. Sayed, "Fixed-point steady-state analysis of adaptive filters," *International Journal of Adaptive Control and Signal Processing*, vol. 17, no. 3, pp. 237–258, April 2003.

[91] J. G. Proakis, *Digital Communications*, 4th Ed., McGraw-Hill, 2001.

[92] V. Krishnamurthy, G. Yin, S. Singh, "Adaptive step-size algorithms for blind interference suppression in DS/CDMA systems," *IEEE Trans. Sign. Proc.*, vol. 49, no. 1, pp. 190–201, Jan. 2001.

[93] R. Kwong, E. Johnston, "A variable step size LMS algorithm," *IEEE Trans. Sign. Proc.*, pp. 1633–1642, July 1992.

[94] V. Krishnamurthy, "Averaged stochastic gradient algorithms for adaptive blind multiuser detection in DS/CDMA systems," *IEEE Trans. Commun.*, vol. 48, pp. 125–134, Jan. 2000.